HAL
open science

Phase Transitions Theory and applications to Biophysics

Matteo Gori

To cite this version:

Matteo Gori. Phase Transitions Theory and applications to Biophysics. Physics [physics]. Aix-Marseille Université (AMU); Centre de Physique Théorique - UMR 7332, 2016. English. NNT : . tel-03598298

HAL Id: tel-03598298

https://hal.science/tel-03598298v1

Submitted on 4 Mar 2022

HAL is a multi-disciplinary open access archive for the deposit and dissemination of scientific research documents, whether they are published or not. The documents may come from teaching and research institutions in France or abroad, or from public or private research centers.

L'archive ouverte pluridisciplinaire **HAL**, est destinée au dépôt et à la diffusion de documents scientifiques de niveau recherche, publiés ou non, émanant des établissements d'enseignement et de recherche français ou étrangers, des laboratoires publics ou privés.

Université d'Aix-Marseille
Faculté des Sciences de Luminy
Ecole doctorale de Physique et Sciences de la Matiére
Centre de Physique Théorique - UMR 7332

Thése de Doctorat
Mention Physique Théorique et Mathématique

Defended by

Matteo GORI

Phase Transitions Theory and applications to Biophysics

Thesis referred by:

Prof. Cecilia CLEMENTI, Dept. of Chemistry, Rice University, Houston, USA.
Prof. Jack TUSZYNSKI, Dept. of Oncology, University of Alberta, Edmonton, Canada.

Defended on December 16th, 2016, before a jury composed of:

Prof. Marco PETTINI, Centre de Physique Théorique, Marseille, France. **Thesis Supervisor**
Prof. Cecilia CLEMENTI, Dept. of Chemistry, Rice University, Houston, USA.**Referee**
Prof. Jack TUSZYNSKI, Dept. of Oncology, University of Alberta, Edmonton, Canada **Referee**
Prof. Gerhard HUMMER, Dept. of Theoretical Biophysics, Max Planck Institute für biophysik, Frankfurt am Main, Germany
Prof. Lapo CASETTI, Dept. of Physics, Universitá di Firenze, Italy
Prof. Roberto PASSANTE, Dept. of Physics, Università di Palermo, Italy

TABLE OF CONTENTS

Introduction v

CHAPTER Introduction x

PART I Developments on Topological Theory of phase transitions **1**

CHAPTER 1 State of art on theory of phase transitions in classical systems 3

1.1 Fundamentals of statistical mechanics 3

1.1.1 Mechanical foundations of statistical mechanics and statistical ensembles 3

1.1.2 Equivalence of statistical ensembles 8

1.2 Phase Transitions (PTs) at thermodynamic equilibrium: definition and classification 11

1.2.1 General concepts on equilibrium Phase Transitions 11

1.2.2 Mechanisms at the origin of PTs: Landau's theory and Yang-Lee Theorems 13

1.3 Beyond the *thermodynamic limit dogma*: signature of PTs in microcanonical ensemble 14

1.4 The Topological Theory of phase transitions 16

1.4.1 Motivations: From the dynamics of chaotic systems to the topological hypotheisis 16

1.4.2 Necessity theorem for PTs and Pettini-Franzosi Theorem 18

1.4.3 A counterexample to Topological Theory of PTs 20

CHAPTER 2 Developments of the Topological Theory of Phase Transitions 21

2.1 Preliminary results towards a generalization of the Topological Theory 21

2.1.1 Motivations 21

2.1.2 The model: φ^4-model on lattice 23

2.1.3 Numerical simulation of Hamiltonian dynamics 23

2.1.4 Monte Carlo simulation on equipotential level sets 26

2.1.5 Discussion of the numerical results 29

2.2 Geometry of regular potential energy level sets in configuration space 30

2.2.1 Microcanonical configurational statistical mechanics from differential topology of regular equipotential level sets 30

2.3 Results of simulation on φ^4-model on 2D-lattice 39

2.3.1 From the numerical simulation to the revision of the Franzosi-Pettini necessity Theorem: outlooks and perspectives 45

2.4 Geometrization of thermodynamics through regular equipotential level sets . . . 47

2.4.1 Regular equipotential surfaces as manifolds with density 47
2.4.2 Rescaled metric in configuration space 48
2.4.3 Geometry of Riemannian Manifolds $(M^{\overline{V}_N}_{[\bar{v}_0,\bar{v}_1]}, \tilde{g})$ and $(\Sigma^{\overline{V}_N}_{\bar{v}}, \tilde{g}|_{\Sigma^{\overline{V}_N}_{\bar{v}}})$ 53
2.4.4 Geometrical interpretation of the configurational microcanonical statistical mechanics 56
2.5 Persistent homology: a method to "compute" topology 58
2.5.1 The Mean-Field XY Model. 59
2.5.2 Topological analysis 60
2.5.3 Samples of the configuration space 60
2.5.4 Persistent Homology 61
2.5.5 Simplicial Complexes in configuration space 61
2.5.6 Results 62
2.5.7 Some remarks on the application of persistent homology to Topological Theory 67

PART II Self organization and out-of-thermal equilibrium PTs in biological systems 69

CHAPTER 3 Basics facts on the theory of long range interactions among biomolecules 71
3.1 Motivations 71
3.2 Intermolecular interactions 72
3.2.1 Electrostatic interactions 72
3.2.2 Dispersive interactions 76
3.3 Electrodynamic long range interactions among biomolecules 78
3.3.1 Why electrodynamic interactions can be long range in biological systems . 78
3.3.2 Electrodynamic interactions among by biomolecules 83
3.3.3 Fröhlich condensation 84
3.3.4 Classical electrodynamic long range interactions two oscillating dipole . . 87
3.4 Developments in research of long range interactions among biomolecules 91

CHAPTER 4 From theory to experiment and return: Fröhlich condensation in classical systems 93
4.1 Looking for Fröhlich condensation in classical open systems: motivations 93
4.2 Quantum Hamiltonian to describe Fröhlich condensation: Wu and Austin model 94
4.3 Dequantization of Wu and Austin Hamiltonian by Time Dependent Variational Principle (TDVP) 97
4.4 Derivation of Fröhlich-like rate equations using Koopman-Von Neumann (KvN) formalism 101
4.4.1 General considerations concerning KvN formalism 101
4.4.2 Liouvillian operator properties of Wu-Austin-like model 104
4.4.3 Derivation of rate equations for actions expectation values J_{ω_i} 108

4.5 Discussion and properties of Fröhlich-like rate equations (4.99) 114
4.5.1 Results of numerical simulation 117
4.6 Comments and conclusions 121

CHAPTER 5 Terahertz spectroscopy experiments for the observation of collective oscillations in biomolecules out-of-thermodynamic equilbrium . 123
5.1 Terahertz spectroscopy on biomolecules: motivations and methods 123
5.1.1 Set-up of the experiments 124
5.1.2 Experimental outcomes 129
5.2 Interpretation of experimental outcomes 131
5.2.1 A premise on methodology 131
5.2.2 Interpretation of the absorption peak frequency 131
5.2.3 Spectroscopic detection of the collective mode 132
5.3 Some remarks on THz spectroscopy measures 134

CHAPTER 6 Study of experimental strategies to detect long range interactions: Feasibility study 136
6.1 Motivations 136
6.2 Model and methods 137
6.2.1 Basic equations 137
6.2.2 Model potentials 139
6.2.3 Numerical algorithms 140
6.2.4 Long-time diffusion coefficient 143
6.2.5 Self-diffusion coefficient for interacting particles 143
6.2.6 Measuring chaos in dynamical systems with noise 145
6.3 Numerical Results 147
6.3.1 Excluded volume effects 148
6.3.2 Effects of long and short range electrostatic interactions at fixed average intermolecular distance 149
6.3.3 Effects of long and short range electrostatic interactions at fixed charge value 151
6.3.4 Long range attractive dipolar effects 154
6.4 Conclusions and perspectives 158

CHAPTER 7 Validation of Fluorescence Correlation Spectroscopy measures for detection of long-range interactions 160
7.1 Motivations 160
7.2 Experimental measures of self-diffusion coefficient of biomolecules interacting by Fluorescence Correlation Spectroscopy (FCS) 160
7.2.1 A brief review on FCS 160
7.2.2 How characterize long-range interaction with FCS experiments 162
7.2.3 FCS results 163
7.3 Numerical results for validation of the experimental tehcnique 166
7.3.1 Basic dynamical equations 167

7.3.2 Model potential 168
7.3.3 Long-time diffusion coefficient 169
7.3.4 Simulation Parameters 170
7.4 Concluding remarks 171

CHAPTER A Basic facts of differential geometry and geometric measure theory 176
A.1 Brief review of Riemannian Geometry 176
A.1.1 The concept of differentiable manifold 176
A.1.2 Tangent and cotangent space 177
A.2 Tensor fields, derivations, connections and curvatures 179
A.3 Differential forms, exterior differentiations, integration of forms 181
A.4 Riemannian structure 184
A.5 Riemmanian geometry of codimension one submanifolds (regular level sets) . . . 187

CHAPTER B Details on the codes used in numerical simulations 190
B.1 A MonteCarlo code to explore regular level sets of potential energy 190
B.2 Derivatives of the Hirsch vector field as function of potential 191

CHAPTER C Basic facts of homololgy 194
C.1 Simplicial Complexes 194
C.1.1 Simplicial Homology 194
C.1.2 Persistent Homology 195

Introduction

Ce travail de thèse concerne les aspects différents de transitions de phase tant á l'équilibre thermodynamique que hors équilibre thermodynamique. Plus spé cifiquement, les études et les résultats rapportés dans ce manuscrit sont visés pour développer une compréhension plus profonde des principes à la base d'auto-organisation dans des systèmes biologiques l'échelle moléculaire qui exige un haut niveau de coordination parmi les degrés de liberté du système.
Considérons, comme un exemple paradigmatique déjà au niveau d'une molécule seule, le problème du *repliement des proteines*. Parmi tous les sequences d'acides aminés possibles de longueur finie, seulement très peu dont eux - quand introduites dans un environnement aqueux - sont capables de se replier dans les configurations précises qui donnent lieu à des protéines. Commenant "d'un bon" ordre d'acides aminés, dans un temps étonnamment court la mme conformation compacte spatiale d'une protéine est toujours atteinte. Ces ordres sont appelés de *bons replieurs*. Au contraire, un ordre aléatoirement produite rapporte un heteropolymer aléatoire qui fait une transition vitreuse (*mauvais plieurs*). La question cruciale est comment distinguer un bon replieur d'un mauvais. On le remarquait à plusieurs reprises [Pet07b] [Bac14b] qu'un mécanisme efficace de repliement est strictement lié à l'établissement de comportements coopératifs parmi les acides aminés en raison des interactions mutuelles entre eux. Cette phénoménologie partage beaucoup de caractéristiques avec les transitions de phase telles qu'elle sont caractérisés par la mécanique statistique classique. Néanmoins, selon la mécanique statistique, les transitions de phase sont rigoureusement définies et caractérisées seulement pour de très grands systèmes, en réalité seulement dans la limite d'un nombre infini de degrés de liberté, ce qui a amene à l'idée répandue que les transitions de phase exigent nécessairement *le dogme de la limite thermodynamique*. D'autre part, des problèmes comme *le repliement des protéines* exige une faon de caractériser des phénomènes coopératifs aussi dans de petits systèmes, c'est-à-dire pour lequel le nombre de particules est beaucoup plus petit que le nombre de Avogadro.
La Théorie Topologique de transitions de phase, avancées principalement pendant la décennie dernière, est une des approches possibles qui fournit une généralisation de la description standard fait par la mécanique statistique qui parte sur les transitions de phase dans des systèmes petits ou mesoscopique et fournit un aperu plus profond du mécanisme général qui provoque les transitions de phase. Une telle théorie semble de pertinence potentielle pour aborder plusieurs problèmes en Biophysique, comme il sera clarifié ci-dessous. Selon la Théorie Topologique, les singularités des potentiels thermodynamiques - surgissant dans la limite thermodynamique dans les ensembles canonique et grancanonique - seraient induites par des changements topologiques appropriés de quelques sous-varieté de l'espace des configurations. Ces mmes changements topologiques peuvent avoir lieu à n'importe quel *nombre fini* de degrés de liberté. Cette théorie, supportée par beaucoup d'évidences s'étendant de simulations numériques aux calculs analytiques exacts concernant des différents modèles statistiques, a été rigoureusement enracinée

dans deux théorèmes. Ces théorems associent les changements topologiques des ensembles du niveau potentiels dans l'espace des configurations avec la perte d'analycité de l'entropie microcanonique configurationelle. Cette dernière circonstance est assumée pour tre la signature de l'occurrence d'une transition de phase. Un contre-exemple à ce Théorème de Nécessité a été récemment trouvé; ceci semble saper, ou au moins considérablement affaiblir, la Théorie Topologique entière des transitions de phase .

La **Première Partie** de ce manuscrit est consacrée à une analyse minutieuse "du contre-exemple" pour comprendre si et comment la théorie peut tre sauvée en fournissant un raffinement et un approfondissement de notre compréhension des relations parmi la topologie et la géométrie d'espace de configuration dans un cté, et les propriétés thermodynamiques/statistiques d'un système dans l'autre cté. De plus, ce travail peut potentiellement paver la voie à une reformulation et à une généralisation de la mme théorie aux cas que on n'a pas considérés dans la formulation originale, comme, par exemple, les interactions à longue portée.

Ce dernier cas pourrait avoir une pertinence biophysique pour beaucoup d'aspects, parmi les autres nous mentionnons les interactions intermoléculaires électrodynamiques à longue portée dont on a théoriquement conjecturées qui pourrait jouer un rle important dans *l'organisation dynamique* de la machinerie biomoleculaire à l'intérieur des cellules.

Et en fait, du point de vue physique, un problème saisissant et stimulant issu de la biologie moléculaire vient de l'observation qu'un grand nombre de réactions biochimiques et de processus impliquant un nombre énorme d'acteurs (des molécules, des structures, organelles, etc.) est coordonné simultanément et efficacement séquencé à temps créant des systèmes dynamiques hautement organisés. Les dimensions spatiales de ces systèmes sont beaucoup plus grandes que les rayons d'action de réactions chimiques, des interactions électrostatiques et quasi-électrostatiques (qui sont fortement ecrantées tant par la grande valeur statique de la constante diélectrique d'eau que par les ions libres), ou des interactions dispersive (Van der Waals-London). Pourtant les interactions dans la matière vivante entre les partenaires moléculaires apparentés (les heteropolymers des acides nucléiques, les homopolymères organises en microtubules et les protéines) produisent un système biochimique spatio-temporel très spécifique et très efficace. Par conséquent l'exactitude extraordinaire de ces rencontres moléculaires semble à peine tre le résultat de la seule diffusion aléatoire.

Ceci fait le lien conceptuel avec **la Deuxième Partie** de ce manuscrit qui fait un rapport sur les contributions de l'auteur à un projet ambitieux qui a pour but de vérifier si les partenaires des reactiones biochimique apparentés sont activement recruités par des forces attractives (résonantes) sélectives de nature électrodynamique agissant a grande distance. L'activation des interactions électrodynamiques classiques à longue portée (décrit par un potentiel decroissant comme r^{-3} avec la distance intermoléculaire r) est théoriquement possible entre des grands diples electrique *résonantes* oscillant dans la gamme de fréquence $0.1 - 1$ THz. La spectroscopie à infrarouge lointain et THz à*l'équilibre thermodynamique* a montré que les biomolecules (comme les protéines ou les fragments d'acides nucléiques) ont des modes normaux dans cette gamme de fréquences. Ces modes sont généralement attribués aux oscillations collectives par conséquent, ils devraient provoquer de grandes oscillations du diple electrique associé à chaque

biomolecule. Néanmoins, à l'équilibre, les collisions avec les molécules d'eau environnantes mènent à l'equipartition de l'énergie parmi les modes normaux d'un biomolecule. Par consequence les fluctuations thermiques entrainent des oscillations de diple trop faibles qui ne peuvent pas tre responsables des interactions électrodynamiques à longue distance. Entre la fin des années 60 et les années 70, Herbert Fröhlich a proposé un modèle heuristique qui prévoit la possibilité de canaliser une grande partie de l'énergie vibratoire d'une biomolecule dans sa fréquence la plus basse de ses modes normaux. Deux conditions sont exigées pour realiser cette condensation analogue à celle de Bose; premièrement un taux d'injection d'énergie suffisamment haut[1] et deuxièmement des interactions non linéaires parmi les modes normaux obtenus grace à la médiation d'un bain thermique. Ce phénomène est un exemple d'un *transition de phase "hors-équilibre"*; la fréquence la plus basse des modes normaux est alors favorisée au detriment de l'equipartition de l'énergie (la phase symétrique).
Le modèle original de Fröhlich fournit une métaphore possible pour expliquer certains phénomènes collectifs dans des systèmes biologiques. Une métaphore plutt qu'un modèle prédictif parce que l'évaluation des paramètres de couplage qui rentre dans les équations originales de taux est trop difficile.
Dans ce manuscrit sont rapportés, les résultats d'enqutes théoriques, numériques et expérimentales sur la condensation de Fröhlich pour les modes normaux de biomolecules. En particulier la contribution originale de l'auteur du travail présent consiste dans la dérivation en ensemble des équations de taux qui décrivent un Fr "le phénomène de condensation ohlich-semblable mis au point dans un contexte classique. Le départ étant un système Hamiltonian classique qui décrit - d'une faon très idéalisée - la dynamique des modes normaux d'une protéine, du bain thermique et la source externe d'énergie. De plus, l'auteur de ce manuscrit a participé à la définition conceptuelle et à l'interprétation théorique des expériences de spectroscopie THZ sur une protéine modèle. Ces experiences ayant fourni une première observation expérimentale de la condensation de Fröhlich pour une protéine hors equilibre en solution aqueuse.

Ceci est un prérequis pour l'activation d'oscillations de diples géants dans les biomolecules qui entrane des interactions électrodynamiques à longue portée entre des molécules co-résonantes, en accord avec les premiers principes d'électrodynamique. Cependant, la question suivante surgit : la Nature exploite-t-elle ces forces intermoléculaires électrodynamiques à longue portée dans la matière vivante? Autrement dit, est-ce que ces interactions sont suffisamment fortes pour organiser la machinerie biomoleculaire à l'intérieur de la cellule? Pour répondre à cette question on doit concevoir une configuration expérimentale technologiquement faisable *in vitro* pour détecter les effets directs des interactions électrodynamiques intermoleculaires à longue portée. Comme nous verrons tout au long de cette thèse, les interactions à longue portée affectent manifestement les propriétés de diffusion des molécules en solution acqueuse. En particulier, une compétition s'établit entre les forces aleatoires créées par les collisions des biomolécules avec les molécules d'eau environnantes (le bruit thermique) et les intéractions intermoléculaires

[1] Dans des systèmes biologiques, l'approvisionnement en énergie environnemental pourrait tre attribué à la injection d'énergie métabolique, par exemple, de l'hydrolyse d'adénosine triphosphate (ATP) ou guanosine triphosphate (GTP) comme bien à partir des collisions d'ion.

mutuelles. On remarque qu'une compétition analogue entre l'énergie interne et le bruit thermique est caractéristique des transitions de phase décrites dans l'ensemble canonique. Ainsi il est raisonnable de penser que la signature de la présence d'interactions à longue portée pourrait tre un phénomène de type transition de phase pour le coefficient de diffusion. Ce dernier peut être consideré comme une fonction d'un paramètre de contrle qui est l'intensité des intéractions mutuelles parmi les biomolécules qui, à son tour, est proportionnelle à la concentration de la solution. Dans ce manuscrit une étude de faisabilité -basée sur des simulations de dynamique moléculaire- est presentée pour évaluer cette stratégie expérimentale. Des simulations analogues ont été realisées pour valider une approche expérimentale basée sur la Spectroscopie de Corrélation de Fluorescence (FCS) dans le but de trouver une telle signature dans des systèmes avec des interactions à longue portée avérées (comme dans le cas d'une solution avec deux espèces moléculaires de charge opposée dissoutes dans l'eau pure).

Organisation du manuscrit

Comme déjà mentionné, ce manuscrit est divisé en deux parties.

La **Partie I** traitant de la Théorie Topologique de transitions de phase est composée de deux chapitres:

- le Chapitre 1 est un chapitre o sont presentés les fondements de la théorie des transitions de phase dans des systèmes classiques et de la Théorie Topologique concernant l'origine des transitions de phase;
- dans le Chapitre 2 des nouveaux résultats sont rapportés concernant le raffinement de la Théorie Topologique des transitions de phase en réponse aux critiques récentes. Ces contributions incluent la définition d'un concept de difféomorphicité asymptotique des hypersurfaces equipotentielles dans l'espace des configurations, l'interprétation de la thermodynamique microcanonique en termes des propriétés géométriques des hypersurfaces equipotentielles mentionnées et l'application d'un outil informatique récemment développé dans le domaine de la topologie algébrique, appelé *homologie persistante*, à l'étude de la signature topologique des transitions de phase.

La **Partie II** présente mes contributions à la recherche sur les interactions électrodynamiques à longue portée parmi les biomolécules.

Elle est divisée en cinq chapitres:

- Le Chapitre 3 est un chapitre d'état de l'art de la recherche sur des interactions électrodynamiques à longue portée sélectives entre biomolecules. Le contexte théorique principal de la recherche en cours est présenté; en particulier quelques aspects principaux de la théorie de la condensation de *Fröhlich* sont rappelés;
- le chapitre 4 presente une démonstration inedite des équations de Fröhlich pour un système d'oscillateurs harmoniques classiques représentant les modes vibratoires d'une biomolecule

générique. Une discussion des solutions stationnaires de ces équations pour quelques cas simples est rapportée;

- le chapitre 5 présente les résultats expérimentaux nouveaux (et leur interprétation) obtenus avec des techniques alternatives de spectroscopie THz, sur une protéine "modèle"(BSA). Ces expériences fournissent une première observation de la condensation de Fröhlich dans des biomolecules en solution aqueuse;

- le chapitre 6 présente une étude numérique et théorique concernant la possibilité de détecter la présence d'interactions à longue portée entre biomolecules en étudiant leurs propriétés de diffusion dans la solution. Ceci inclut aussi l'étude des effets d'interactions mutuelles sur le chaos dynamique et l'ordre spatial dans ces systèmes;

- le chapitre 7 traite de la validation de la technique de FCS avec des simulations numériques de dynamique moléculaire. On montre que la technique FCS peut être une technique efficace pour détecter la présence des interactions à longue portée avérées (ne nécessitant pas d'activation) comme, par exemple, les interactions coulombiennes électrostatiques entre biomolecules en solution aqueuse.

Introduction

This thesis work concerns different aspects of phase transitions both at thermodynamic equilibrium and out-of-thermodynamic equilibrium. More specifically, the studies and results reported in this manuscript are aimed to develop a deeper understanding of the principles at the basis of self-organization in biological systems at the molecular scale that requires a high level of coordination among the degrees of freedom of the system.

Let us consider, as a paradigmatic example already at the level of a single molecule, the so called *protein folding* problem. Among all the possible amino-acid sequences of finite length, only a very few of them - when put in an aqueous environment - are capable of folding into precise configurations that are working proteins. Starting from a "good" sequence of amino acids, in a surprisingly short time the same spatial compact conformation of a protein is always reached. These sequences are called *good folders*. In contrast, a randomly sorted sequence yields a random heteropolymer undergoing a glassy transition (*bad folders*). The crucial question is how to distinguish a good folder from a bad one. It has been repeatedly noticed [Pet07b][Bac14b] that an efficient folding mechanism is strictly related to the establishment of cooperative behaviour among amino acids due to the mutual interactions among them. This phenomenology shares many features with phase transitions as characterized in classical statistical mechanics. Nevertheless, according to statistical mechanics, phase transitions are rigorously defined and characterized only for very large systems, actually in the limit of an infinite number of degrees of freedom, what has led to the widespread idea that phase transitions necessarily require the thermodynamic limit (*thermodynamic limit dogma*).

On the other hand, problems like *protein folding* demand a way to characterize cooperative phenomena also in small systems, i.e. for which the number of particles is much smaller than the Avogadro number.

The Topological Theory of phase transitions, put forward mainly during the last decade, is one of the possible approaches to provide a generalization of the statistical mechanical description of phase transitions in small or mesoscopic systems, and to provide a deeper insight into the general mechanism which gives rise to phase transitions. Such a theory appears of potential relevance to tackle several problems in Biophysics, as it will be clarified in the following.

According to the Topological Theory, the singularities of thermodynamic potentials - arising in the thermodynamic limit in the canonical and grancanonical ensembles - would be induced by suitable topological changes of some submanifolds of configuration space. These same topological changes can take place at any *finite number* of degrees of freedom. This theory, supported by many evidences ranging from numerical simulations to exact analytic computations carried on different statistical models, has been rigorously rooted in two theorems that associate topological changes of the equipotential level sets of configuration space with the loss of analyticity of microcanonical configuration entropy. This last circumstance is assumed to be the signature

of the occurrence of a phase transition in the microcanonical ensemble. In particular, one of these two theorems states that if all the equipotential level sets in a certain interval of specific potential energy are diffeomorphic among them, then the system cannot undergo any phase transition in the corresponding interval of temperatures.
A counterexample to this Necessity Theorem has been recently found; this seems to undermine, or at least to considerably weaken, the whole Topological Theory of phase transitions.
The **First Part** of this manuscript is devoted to a thorough investigation of the "counterexample" in order to understand if and how the theory can be saved by providing a refinement and a deepening of our understanding of the relations among topology and geometry of configuration space on the one side, and thermodynamic/statistical properties of a system on the other side. Moreover, this work can potentially pave the way to a reformulation and generalization of the same theory to cases that were not considered in the original formulation, as, for instance, long-range interactions.
This latter case could be of biophysical relevance for many aspects, among the others we mention long-range electrodynamic intermolecular interactions that have been theoretically surmised to play an important role in the *dynamical organization* of the biomolecular machinery inside the cell.
And in fact, from the physics point of view, a striking and challenging problem arising from molecular biology stems from the observation that a large number of biochemical reactions and processes involving a huge number of actors (molecules, structures, organelles, etc.) are coordinated simultaneously and efficiently sequenced in time thus giving rise to well and highly organized dynamic systems. The spatial dimensions of these systems are much larger than the "action radii" of chemical reactions, of electrostatic and quasi-electrostatic interactions (which are strongly shielded both by the large static value of water dielectric constant and by freely moving ions), or of van der Waals-London dispersion interactions. Yet the interactions between cognate molecular partners in living matter (nucleic acids heteropolymers, microtubules homopolymers, and proteins) produce a highly specific and highly efficient spatial-temporal biochemical pattern. Hence the extraordinary accuracy of these molecular encounters hardly seems to be the result of random diffusion only.
This makes the conceptual link with the **Second Part** of this manuscript which reports on the author's contribution to an ambitious project aimed to ascertain whether the encounters of distant cognate partners of biomolecular reactions are actively driven by selective (resonant) attractive forces of electrodynamic nature.
The activation of long-range classical electrodynamic interactions (described by a potential falling as r^{-3} with the intermolecular distance r) is theoretically possible between large *resonant* dipoles oscillating in the frequency range $0.1 - 1$ THz. Far-infrared and THz spectroscopy at *thermodynamic equilibrium* have shown that biomolecules (proteins and fragments of nucleic acids) have normal modes in this range of frequencies, and these modes are commonly attributed to collective oscillations, consequently, they should bring about large dipole oscillations. Nevertheless, at equilibrium, the collisions with the surrounding water molecules leads to energy equipartition among the normal modes of a biomolecule; hence, the dipole oscillations

due to thermal fluctuations would be too small to be responsible for the activation of sizeable long-range electrodynamic interactions.

Between the late '60s and the '70s, Herbert Fröhlich proposed an heuristic model that predicts the possibility to channel a large part of the vibrational energy of a biomolecule into its lowest frequency normal modes. Two conditions are required for this Bose-like condensation; a sufficiently high energy injection rate[2] and non linear interactions among the normal modes mediated by a thermal bath. This phenomenon is an example of a *out-of-thermal-equilibrium phase transition*; the equipartition of energy (symmetric phase) is broken in favour of the lowest frequency normal modes. The original Fröhlich model provides a possible metaphor to explain certain collective phenomena in biological systems. A metaphor rather than a predictive model because the estimation of the coupling parameters entering the original rate equations seems too hard a task.

In this manuscript the results of theoretical, numerical and experimental investigations on Fröhlich-like condensation for normal modes of biomolecules are reported. In particular the original contribution of the author of the present work consists in the derivation of a set of rate equations that describe a Fröhlich-like condensation phenomenon worked out in a classical context. The starting point is a classical Hamiltonian system that describes - in a very idealized way - the dynamics of the normal modes of a protein, of the thermal bath and the external source of energy. Moreover, the author of this manuscript participated in the conceptual definition and theoretical interpretation of the THz spectroscopy experiments on a model protein where a first experimental evidence of a Fröhlich-like condensation phenomenon has been observed for a protein in watery solution and out of thermal equilibrium.

This is a prerequisite for the activation of giant dipole oscillations in biomolecules which, according to the first principles of electrodynamics, entail long-range electrodynamic interactions between co-resonant molecules. However, the following question arises: does Nature exploit these long-range electrodynamic intermolecular forces in living matter? In other words, are these forces sufficiently strong to play the above surmised role of driving the organisation of the biomolecular machinery inside the cell? To answer this question one has to devise a technologically feasible experimental set-up *in vitro* - to begin with - to detect some direct physical consequence of the long-range interparticle interactions. As we shall see throughout this thesis, long-range interactions markedly affect the self-diffusion properties of molecules in solution. In particular, a competition sets in between the random forces acting on the solvated molecules due to the collisions with water molecules (thermal noise), and the mutual intermolecular interactions. It has to be remarked that an analogous competition among thermal noise and internal energy is also a feature of phase transitions when described in the canonical ensemble. Thus it is reasonable to think that the fingerprint of long-range interactions could be a "transitional" phenomenon concerning the self-diffusion coefficient as a function of a control parameter. This control parameter would naturally be the strength of the mutual interactions among the biomolecules which, in turn, is proportional to the concentration of the solution. In

[2] In biological systems, the environmental energy supply could be attributed to metabolic energy stemming, for example, from the hydrolysis of adenosine triphosphate (ATP) or guanosine triphosphate (GTP) as well as from ion collisions.

this manuscript - based on molecular dynamics simulations - a feasibility study is reported to assess this hypothesized experimental strategy. Analogous simulations have been performed to validate an experimental approach based on Fluorescence Correlation Spectroscopy aimed at finding such "fingerprint" in systems with built-in long-range interactions (like a binary solution of oppositely charged molecules solvated in pure water).

Organization of the manuscript

As already mentioned, this manuscript is divided in two parts. The **Part I** deals with Topological Theory of phase transitions and is composed of two chapters:

- chapter 1 is a review chapter where some basic facts of the theory of phase transitions (PTs) in classical systems, and of the Topological Theory of phase transitions are reported;
- chapter 2 is a chapter where original results are reported concerning the refinement of the Topological Theory of phase transitions in response to recent criticisms. These contributions included the definition of a concept of asymptotic diffeomorphicity of the equipotential level sets of configuration space (thus diffeomorphicity in the thermodynamic limit), the interpretation of microcanonical thermodynamics in terms of geometrical properties of the mentioned level sets, and the application of a recently developed computational tool in algebraic topology, called persistent homology, to the investigation of the topological counterpart of phase transitions.

The **Part II** deals with different contributions given to the research concerning the long-range electrodynamic interactions among biomolecules. It is divided into five chapters:

- chapter 3 is a review chapter where the state of the art of the research on selective long-range electrodynamic interactions among biomolecules is reported. The main theoretical background of the ongoing research is presented; in particular, some main aspects of the so called *Fröhlich condensation* are reviewed;
- chapter 4 is a chapter were an original derivation of Fröhlich-like rate equations is presented for a system of classical harmonic oscillators representing the vibrational *modes of a generic biomolecule. A discussion of the stationary solutions of these equations for some simple cases is reported;
- chapter 5 reports the original experimental results (and their interpretation) obtained with non-standard techniques of THz spectroscopy, on a "model" protein (BSA). These observations provide a first evidence of a Fröhlich-like phonon condensation phenomenon of a biomolecule in watery solution;
- chapter 6 presents a numerical and theoretical investigation concerning the possibility to detect the presence of long-range interactions among biomolecules by studying their diffusion properties in solution. This also includes the study of the effects of mutual interactions on the dynamical chaoticity and spatial ordering of the systems;

- chapter 7 deals with the validation of Fluorescence Correlation Spectroscopy by means of numerical simulations of molecular dynamics. the FCS technique is shown to be a fruitful technique to detect the presence of built-in (in the sense of non-externally activated) long-range interactions among biomolecule in watery solutions.

PART I

Developments on Topological Theory of phase transitions

CHAPTER 1 State of art on theory of phase transitions in classical systems

In this chapter some basic facts on the theory of phase transitions (PTs) in classical systems are reported. The problem concerning the definition of phase transitions in a unified framework both for large and small classical systems is far to be considered a closed problem. After a general overview on the possible approaches, we concentrate our attention on the topological theory of PTs: the deep origin of a phase transition would be related with a suitable change of topology of energy (or equipotential) level sets.

1.1 Fundamentals of statistical mechanics

1.1.1 Mechanical foundations of statistical mechanics and statistical ensembles

Classical equilibrium statistical mechanics gives prescriptions to express "macroscopic" (generally thermodynamic) observables of a system in equilibrium state as averages of some suitable function of generalized coordinates of "microscopic" systems getting rid of the details of the dynamic of the system. In particular time averages can be replaced by statistical integrals over configuration space endowed with a probability distribution compatible with physical constraints on macroscopic parameters like the number of degrees of freedom, the range of states accessible to each degree of freedom, the total energy of the system, total electric charges and so on.

Statistical mechanics allows to derive the thermodynamic (so *macroscopic*) properties of a large system of particles when the Hamiltonian equations describing their *microscopic* dynamics are known. Nevertheless statistical mechanics is not the same as thermodynamics as being meaningful also when applied to small or mesoscopic system[1].

Rigorous foundations of statistical mechanics are rooted in Hamiltonian theory of classical systems, where the problem of integrability is rigorously defined.

Let us consider an isolated Hamiltoninan system with N degrees of freedom whose state is described by the canonical conjugate variables $(p_1, ..., p_N; q_1, ..., q_N) \in \Lambda^N_{(p,q)}$, being $\Lambda^N_{(p,q)}$ the phase space[2].Let $\mathcal{H}_N : \Lambda^N_{(p,q)} \longmapsto \mathbb{R}^N$ be the Hamiltonian,then the Poisson' brackets $\{\cdot, \cdot\}$ are

[1]This almost-epistemological statement has a great importance for the development of a theory of phase transitions in finite small and mesoscopic systems

[2]In what follows we consider the canonical coordinates and the Hamiltonian of the system expressed in nondimensionalized units.

given by:

$$\{f,g\} = \sum_{i=1}^{N} \left(\frac{\partial A}{\partial q_i}\frac{\partial B}{\partial p_i} - \frac{\partial A}{\partial p_i}\frac{\partial B}{\partial q_i} \right) \qquad \forall f(\{p_i\},\{q_i\},t), g(\{p_i\},\{q_i\},t) : \Lambda^N_{(p,q)} \times \mathbb{R} \to \mathbb{R}. \quad (1.1)$$

where f, g are two arbitrary functions of conjugate canonical coordinates with an explicit time dependence. The Hamilton equations of motion for the dynamics of *microscopical* degrees of freedom are:

$$\begin{cases} \dfrac{\mathrm{d}p_i}{\mathrm{d}t} & = -\{p_i, H\} = -\dfrac{\partial \mathcal{H}}{\partial q_i} \\ \dfrac{\mathrm{d}q_i}{\mathrm{d}t} & = -\{q_i, H\} = \dfrac{\partial \mathcal{H}}{\partial p_i} \end{cases} \quad (1.2)$$

and, through the Liouville theorem, the evolution of a density function $\rho\left(\{p_i\},\{q_i\}_{i=1,\dots,N},t\right)$ is described by

$$\frac{\partial \rho}{\partial t} = -\{\rho, \mathcal{H}\} = -\frac{\partial \mathcal{H}_N}{\partial q_i}\frac{\partial \rho}{\partial p_i} + \frac{\partial \mathcal{H}_N}{\partial p_i}\frac{\partial \rho}{\partial q_i} \quad (1.3)$$

which is well suited to take into account, for instance, the case of the dynamics of a system with some incertitude on initial conditions.

The density function ρ entails information on the *statistical* behaviour of the Hamiltonian system: many different realisations of the dynamics can be taken into account with different initial conditions at the same time. The definition of the probability density ρ allows to calculate statistical averages of observables $\mathcal{O} = \mathcal{O}(\{p_i\},\{q_i\})$ that can be expressed as functions of the microscopic degrees of freedom of the system

$$\langle \mathcal{O} \rangle_\rho (t) = \int_{\Lambda^N_{(p,q)}} \rho\left(\{p_i\},\{q_i\}_{i=1,\dots,N},t\right) \mathcal{O}\, \mathrm{d}\mu \quad (1.4)$$

A dynamical system is considered at the equilibrium if

$$\frac{\partial \rho_{\mu Can}}{\partial t} = 0 \qquad \Longrightarrow \qquad \{\rho_{\mu Can}, \mathcal{H}_N\} = 0 \quad (1.5)$$

which means that the density function is a proper constant of motion.

If the dynamical system described by Equation 1.2 is *metrically indecomposable* (i.e. the only invariant subsets X of $\Lambda^N_{(p,q)}$ with respect to the flow are those for which their measure is $\langle X \rangle_\rho = 1$ or $\langle X \rangle_\rho = 0$) then the time averages calculated along the dynamics are equivalent to the statistical averages in Equation 1.4 (Birkhoff's ergodic Theorem); this can be considered the foundation of statistical mechanics.

If the total energy is the only constant of motion, the density distribution ρ at the equilibrium is only a functional of $\mathcal{H}$ and it reads:

$$\rho_{\mu\mathrm{Can}} = \frac{1}{\omega_N(E)}\, \delta(\mathcal{H}_N(\{p_i\},\{q_i\}) - E) \qquad E \in \mathrm{CoDom}(\mathcal{H}_N)\ . \quad (1.6)$$

In the previous equation, $\omega_N(E)$ is a normalization constant depending on the control parameter E and it is formally given by

$$\omega_N(E) = \int_{\Lambda_{(p,q)}} \delta\left(\mathcal{H}_N(\{p_i\},\{q_i\}) - E\right) \mathrm{d}\mu = \frac{\mathrm{d}}{\mathrm{d}E} \int_{\int_{\Lambda_{(p,q)}}} \Theta\left(\mathcal{H}_N(E - \{p_i\},\{q_i\})\right) \tag{1.7}$$

where $\mathrm{d}\mu$ is the volume form of the phase space $\Lambda_{(p,q)}$ and $\Theta\left(\mathcal{H}_N(E - \{p_i\},\{q_i\})\right)$ the Heaviside Theta function .

If the phase space is endowed with a Riemannian metric g, and *in the absence of critical points* of the Hamiltonian, the Coarea formula (see Appendix A for more details) can be applied to Equation 1.7 to give

$$\omega_N(E) = \int_{\Sigma_E^N} \frac{\mathrm{d}\sigma_{\Sigma_E^N}}{\|\mathrm{grad}_g \mathcal{H}_N\|_g} \tag{1.8}$$

where $\Sigma_E^N = \mathcal{H}_N^{-1}(E)$ is the level set of the Hamiltonian corresponding to a total energy E and grad_g and $\|\cdot\|_g$ are respectively the gradient and the vector norms.

The probability density distribution in Equation 1.6 and the level set volume in Equation 1.7 allow to calculate the statistical averages of any observables for a system with a fixed total energy E, number of degrees of freedom N, and volume V accessible to the degrees of freedom at the equilibrium: this defines the *microcanonical ensemble*.

In more realistic conditions, the total energy of isolated systems is fixed with an uncertainty ΔE. In this case the definition of microcanonical probability density is given by

$$\rho_{\mu Can}(\mathbf{p},\mathbf{q}) = \begin{cases} \dfrac{1}{\Delta\omega_N(E)} & \text{If} \quad E \leq \mathcal{H}_N(\mathbf{p},\mathbf{q}) < E + \Delta E \\ 0 & \text{elsewhere .} \end{cases} \tag{1.9}$$

Consequently the volume of the region of the phase space of microstates compatible with the fixed parameters $(N, \mathcal{V}, E)$ is given by $\Delta\omega_N(E) = (\Delta E)\,\omega_N(E)$ at the first order.

Statistical mechanics allows to connect the microscopic properties of large systems with their thermodynamic properties through the *Boltzmann principle*: the microcanonical partition function $\Delta\omega_N(E,\mathcal{V})$ is direct by related with the *(microcanonical) entropy* $S_N(E,\mathcal{V})$ by

$$S_N(E,\mathcal{V}) = k_B \log\left[C(N)\Delta\omega_N(E,\mathcal{V})\right] = k_B \log\left[a(\Delta E)\omega_N(E,\mathcal{V})\right] \tag{1.10}$$

where k_B is the Boltzmann constant and $C(N)$ is a constant to resolve paradoxes related with an overcounting of the microstates due to the indistinguishability of the particles(the so called "Gibbs Paradox"). Thermodynamic intensive observables (as temperature, pressure, specific heat for instance) are calculated as derivatives of the entropy in Equation 1.10 with respect to

the parameters $(N, \mathcal{V}, E)$[3] For instance, the *microcanonical temperature* $T_{\mu\text{Can}}$ is given by:

$$\beta_{\mu\text{Can}}(E, \mathcal{V}) = \frac{1}{k_B T_{\mu\text{Can}}} = \frac{\partial S_N(E, \mathcal{V})}{\partial E} \tag{1.12}$$

while the pressure is defined as

$$P_{\mu\text{Can}}(E, \mathcal{V}) = k_B T \frac{\partial S_N(E, \mathcal{V})}{\partial \mathcal{V}} \tag{1.13}$$

The susceptibilities are calculated as second order derivatives of the entropy, as the specific heat

$$C_{s,\mu\text{Can}} = -\frac{1}{k_B} \frac{\left(\dfrac{\partial S_N(E, \mathcal{V})}{\partial E}\right)^2}{\left(\dfrac{\partial^2 S_N(E, \mathcal{V})}{\partial E^2}\right)} \tag{1.14}$$

or the compressibility

$$B_{\mu\text{Can}} = k_B T \frac{\partial^2 S_N(E, \mathcal{V})}{\partial \mathcal{V}^2} \,. \tag{1.15}$$

We have to stress that the theory of phase transitions has been historically formulated in the framework of thermodynamics; Equation 1.10 allows to give a characterization of phase transitions in terms of the geometrical and topological properties of the energy level sets.

Although the microcanonical ensemble is the most fundamental statistical ensemble, it is very difficult to realise in practice a completely isolated system: exchanges of energy, particles, charges etc. with larger systems (resevoirs) are generally unavoidable. Moreover a rigours mathematical description of microcanonical ensemble is in general quite difficult.

For such reasons the notion of statistical equilibrium ensembles for open systems has been introduced in statistical mechanics. The equilibrium probability distribution in these cases is obtained from the second principle of thermodynamics: it is the function ρ_{eq} that maximize the Shannon entropy of the system $S_{sh}[\rho]$

$$S_{sh}[\rho] = \lambda_i \left\langle \log \rho \right\rangle_\rho = \int_{\Lambda^N_{(p,q)}} \rho \log(\rho) \, \mathrm{d}\mu \tag{1.16}$$

[3]Different definitions of the entropy lead to different expected temperatures in the microcanonical ensemble and, more in general, to a different thermodynamic description especially for systems with negative temperatures or for "small" systems (i.e. with a number of degrees of freedom much higher of the number of integrals of motion and much less than the Avogadro's number). In particular, a different definition of the microcanonical entropy has been proposed by Gibbs:

$$S_N(E, V) = k_B \log\left[\Omega_N(E, \mathcal{V})\right] = k_B \log \int_{M^N_E} \mathrm{d}\mu \,. \tag{1.11}$$

while the entropy of Equation 1.10 is usually referred to as the Boltzmann entropy. The definition of microcanonical temperature from this two different definition of entropy has been recently the subject of an intense debate (see for more details [CPV15] and references therein). Nevertheless many arguments and considerations required the Boltzmann entropy to consistently describes the thermodynamical behaviour of "small" systems and negative temperatures as argued in [Gro01] and [CPV15].

under the constraint that the averages $\langle f_i \rangle_\rho$ of some observables are fixed so that

$$\delta \left(S_{sh}[\rho] + \sum_{i=1}^{n_{cons}} \lambda_i \langle f_i \rangle_\rho \right) \Big|_{\rho_{eq}} = 0 \tag{1.17}$$

where λ_i are Langrange multipliers. These parameters λ_i are intensive fixed physical quantities that define the macrostate of the system.
For instance, in the *canonical ensemble* the *average* total energy $\langle \mathcal{H} \rangle_{\rho_{eq}}$ is fixed. It follows that the *canonical probability density* is

$$\rho_{eqCan} = \frac{e^{-\beta \mathcal{H}_N}}{Z_{N,Can}(\beta, \mathcal{V})} \tag{1.18}$$

$$Z_{N,Can}(\beta, \mathcal{V}) = \int_{\Lambda^N_{(p,q)}} e^{-\beta \mathcal{H}_N} \mathrm{d}\mu \tag{1.19}$$

where $\beta = (k_B T)^{-1}$ is proportional to the inverse of the canonical temperature T while $Z_{N,Can}$ is the *canonical partition function.*
In analogy with microcanonical ensemble, the thermodynamic observables of a given system can be calculated as derivatives of the *thermodynamic potential* that, in this case, is the *Helmholtz free energy*

$$F_N(\beta, \mathcal{V}) = -\frac{1}{\beta} \log \left[Z_{N,Can}(\beta, \mathcal{V}) \right] . \tag{1.20}$$

We immediately notice that the partition function of Equation 1.24 has a simpler mathematical form than the density of states in Equation 1.8, its analogous in microcanonical ensemble.
Another example of statistical ensemble for open systems at equilibrium is the *Grancanonical ensemble.* In this case only the average number of particle and of the energy are fixed; the total phase space is $\Lambda_{(p,q)} = \otimes_{i=n_{min}}^{+\infty} \Lambda^i_{(p,q)}$ and the statistical averages are consequently calculated using a probability density $\rho(\{p_{(k,N)}\}, \{q_{(k,N)}\}, N)$ (where (k, N) identifies the k-th degree of freedom in configuration space of dimension N)

$$\left\langle f(\{p_{(k,N)}\}, \{q_{(k,N)}\}, N) \right\rangle_\rho = \sum_{i=n_{min}}^{+\infty} \left(\int_{\Lambda^i_{(p,q)}} f(\{p_{(k,N)}\}, \{q_{(k,N)}\}, N) \rho(\{p_{(k,N)}\}, \{q_{(k,N)}\}, N) \mathrm{d}\mu_N \right) . \tag{1.21}$$

In this case the second principle of thermodynamics leads to the variational equation for ρ_{eqGCan}

$$\delta \left(S_{sh}[\rho] + \beta \left\langle \mathcal{H}(\{p_{(k,N)}\}, \{q_{(k,N)}\}, N) \right\rangle_\rho - \eta \langle N \rangle_\rho \right) \Big|_{\rho_{eq}} = 0 \tag{1.22}$$

whose solution is

$$\rho_{eqGCan} = \frac{e^{-\beta \mathcal{H}_i + \eta N}}{Z_{N,Can}(\beta, \eta)} \tag{1.23}$$

$$Z_{GCan}(\beta, \eta) = \sum_{i=N_{min}}^{+\infty} e^{\eta N} \left(\int_{\Lambda^i_{(p,q)}} e^{-\beta \mathcal{H}_N} \mathrm{d}\mu \right) \tag{1.24}$$

where η is the chemical potential. The thermodynamic potential of the grandcanonical ensemble is the grand potential $F_{GCan}(\beta,\eta)$ and it is related to the grand partition function $Z_{GCan}(\beta,\eta)$ by

$$F_{GCan}(\beta,\eta) = -\frac{1}{\beta}\log\left[Z_{GCan}(\beta,\eta)\right] \tag{1.25}$$

The grand canonical ensemble has a great relevance in studies of phase transitions as it is the statistical ensemble where the celebrated Yang-Lee theorem has been proved.

1.1.2 Equivalence of statistical ensembles

The different statistics associated to different statistical ensembles would in principle lead to different thermodynamic descriptions of a system. Nevertheless, a widely investigated topic in statistical mechanics is the relation among thermodynamic observables computed in different ensembles: in particular, if and when it is possible to find equivalence relations among thermodynamic potentials of different statistical ensembles. This problem is usually referred to as the *equivalence of statistical ensembles* and it represents a foundamental issue in statistical mechanics (see for instance [Rue99],[Ell12], [CDFR14],[Tou15] and references therein).
A detailed discussion of this problem is beyond the aims of this work, so we limit our discussion to the aspects which are relevant for definition of phase transitions at thermodynamic equilibrium in microcanonical ensemble. As previously remarked, the concept of phase transition has been historically defined and characterized in the framework of thermodynamics, especially in open systems[4]. The possibility to establish equivalences among statistical ensembles allows to understand which is the signature of PTs in the microcanonical ensemble on the basis of the standard definitions given in the statistical ensembles of open systems. As a paradigmatic case we consider here only the case of the equivalence among canonical and microcanonical ensembles. In this case, the equivalence can be established if the fluctuations of total energy in the canonical ensemble become negligible: the canonical measure "concentrates" around the energy level set corresponding to the mean energy $\Sigma_{\langle H\rangle}$ and can be approximated by the microcanonical probability density associated to such level set. As statistical fluctuations usually tends to zero with $N^{-1/2}$ in the limit of large N, the equivalence is generally established for systems with a large number of degrees of freedom. More formally, let us consider the canonical thermodynamic potential:

$$\begin{aligned} F_N(\beta,\mathcal{V}) &= -\frac{1}{\beta}\log\left[\int_{\Lambda^N_{(p,q)}} e^{-\beta\mathcal{H}_N}\mathrm{d}\mu\right] = -\frac{1}{\beta}\log\left[\int_0^{E_{max}}\mathrm{d}E\, e^{-\beta E}\int_{\Sigma^N_E}\frac{\mathrm{d}\sigma^N_E}{\|\mathrm{grad}_g\mathcal{H}_N\|_g}\right] = \\ &= -\frac{1}{\beta}\log\left[\int_0^{E_{max}}\mathrm{d}E\, e^{-\beta E}\omega_N(E,V)\right] = \frac{1}{\beta}\log\left[\int_0^{E_{max}}\mathrm{d}E\, e^{-\beta E+S_N(E,\mathcal{V})}\right] \end{aligned} \tag{1.26}$$

[4]Let us recall that with open systems we mean a system at thermal equilibrium with a heath bath, thus exchanging energy with its environment.

where the Coarea formula has been used and the formal definition of the density of states (1.7) and of the microcanonical entropy (1.10) has been used neglecting the ΔE term.
To compare the behaviour at large N, *thermodynamic limit* prescription is used; a larger systems is constructed by considering many interacting replicas of smaller systems. For a system of particles, for instance, that means to consider the limit $N \longrightarrow +\infty$ with $N/\mathcal{V} = constant$. According to this prescription, usually referred to as the thermodynamic limit, the succession of microcanonical entropy functions $\{\bar{S}_N(\bar{E},\bar{\mathcal{V}})\}_{N\in\mathbb{N}}$ is defined

$$\bar{S}_N(\bar{E},\bar{\mathcal{V}}) = \frac{1}{N} S_N(N\bar{E}, N\bar{\mathcal{V}})\,. \tag{1.27}$$

If this sequence of functions converges punctually to a function $\bar{S}_{+\infty}(\bar{E},\bar{\mathcal{V}})$ in a certain range of specific energy $\bar{E}$ and specific volumes $\bar{\mathcal{V}}$, then the entropy is an extensive quantity of the system and the thermodynamic limit exists. The existence of this limit it is non-trivial and for a systems whose Hamiltonian at fixed N is of the form

$$\mathcal{H}_N = \sum_{i=1}^{N} \frac{p_i^2}{2} + V_N(\{q_i\}_{i=1,\dots,N}) \tag{1.28}$$

that is, for systems composed by mutually interacting particles through a potential which depends only on the interparticle distances, it has been demonstrated that thermodynamic limit exists. This also requires that the potential be smooth, confining, short-range and bounded from below[5]. Analogously, it is possible to construct a succession of functions $\{\bar{F}_N(\beta,\bar{\mathcal{V}})\}_{N\in\mathbb{N}}$ substituting (1.27) in (1.26) for each fixed N

$$\bar{F}_N(\beta,\bar{\mathcal{V}}) = -\frac{1}{N\beta}\log\left[\int_0^{\bar{E}_{max}} \mathrm{d}\bar{E}\, e^{-N\left(\beta\bar{E}-\frac{1}{k_B}\bar{S}_N(\bar{E},\bar{\mathcal{V}})\right)}\right]. \tag{1.29}$$

If $\{\bar{S}_N\}_{N\in\mathbb{N}}$ converges uniformly to a continuous function [6] in thermodynamic limit, we can write an approximate expression for $F_N(\beta,\bar{\mathcal{V}})$

$$\begin{aligned}\bar{F}_N(\beta,\bar{\mathcal{V}}) &= -\frac{1}{N\beta}\log\left[\int_0^{\bar{E}_{max}} \mathrm{d}\bar{E}\, e^{-N\left(\beta\bar{E}-\frac{1}{k_B}\bar{S}_{+\infty}(\bar{E},\bar{\mathcal{V}})\right)+\frac{N}{k_B}[\bar{S}_N(\bar{E},\bar{\mathcal{V}})-\bar{S}_{+\infty}(\bar{E},\bar{\mathcal{V}}))]}\right] \approx \\ &\approx -\frac{1}{N\beta}\log\left[\int_0^{\bar{E}_{max}} \mathrm{d}\bar{E}\, e^{-N\left(\beta\bar{E}-\frac{1}{k_B}\bar{S}_{+\infty}(\bar{E},\bar{\mathcal{V}})\right)+No(1)}\right] = \\ &= -\frac{1}{N\beta}\log\left[\int_0^{\bar{E}_{max}} \mathrm{d}\bar{E}\, e^{-N\left(\beta\bar{E}-\frac{1}{k_B}\bar{S}_{+\infty}(\bar{E},\bar{\mathcal{V}})\right)}\right] + o(1)\,.\end{aligned} \tag{1.30}$$

[5] A key point in the proof is relied with the *additivity* of short-range potentials: namely if an isolated system is divided in two subsystems the interaction energy among two subsystems vanishing when compeared with the sum of the energies of the two systems *in the thermodynamic limit*(See [Rue99] for more details). This additivity does not hold in general for particle systems with long-range interactions. In this case the procedure to construct the sequence of functions $\{\bar{S}_N(\bar{E},\bar{\mathcal{V}})\}_{N\in\mathbb{N}}$ can be recovered if a prescription is given to construct a system for which the total energy is extensive (i.e. the Kac' prescription).

[6] This condition is a little bit stronger than the pointwise convergence

The integral in (1.30) can be evaluated using the Laplace approximation method for asymptotic integrals. If for a given β there exists a unique $\bar{E}_0(\beta)$ that maximizes the exponent in the integrand of (1.30) , i.e.

$$\beta - \frac{1}{k_B}\frac{\partial \bar{S}_\infty}{\partial \bar{E}}(\bar{E}_0, \bar{\mathcal{V}}) = 0 \quad \wedge \quad \frac{\partial^2 \bar{S}_\infty}{\partial \bar{E}^2}(\bar{E}_0, \bar{\mathcal{V}}) < 0 \tag{1.31}$$

then

$$\begin{aligned}\bar{F}_N(\beta, \bar{\mathcal{V}}) &\approx -\frac{1}{N\beta}\log\left[e^{-N\left[\beta\bar{E}_0(\beta,\bar{\mathcal{V}})-\frac{1}{k_B}S_N\left(\bar{E}_0(\beta,\bar{\mathcal{V}})\right)\right]}\int_0^{\bar{E}_{max}} e^{-\frac{N}{2k_B}\left(-\frac{\partial^2 S_\infty}{\partial \bar{E}^2}\right)\left(\bar{E}-\bar{E}_0(\beta)\right)^2}\mathrm{d}\bar{E}\right] \approx \\ &\approx \frac{1}{\beta}\bar{E}_0(\beta, \bar{\mathcal{V}}) - \frac{1}{k_B}S_\infty\left(\bar{E}_0\left(\beta, \bar{\mathcal{V}}\right)\right) + \frac{1}{2}\log\left[\frac{2\pi k_B}{N\left(-\frac{\partial^2 S_\infty}{\partial \bar{E}_0}\right)}\right] + o(1)\,.\end{aligned} \tag{1.32}$$

In the limit $N \longrightarrow +\infty$ the previous equation reads

$$\bar{F}_\infty(\beta, \bar{\mathcal{V}}) = \bar{E}_0(\beta) - TS_\infty(\bar{E}_0(\beta), \bar{\mathcal{V}}) = \frac{1}{\beta}\inf_{\bar{E}}\left\{\beta\bar{E} - TS_\infty(\bar{E}, \bar{\mathcal{V}})\right\} \tag{1.33}$$

where the definition of temperature $T = (\beta k_B)^{-1}$ has been used.
From the right hand side of (1.33) it follows that the specific free energy in the canonical ensemble is the Legendre transform of the specific microcanonical entropy *if it exists* or, in other words, if the specific free energy is the convex conjugate of the specific microcanonical entropy $\bar{F}_\infty(\beta, \bar{\mathcal{V}}) = \bar{E}_0 - T\bar{S}_\infty(\bar{E}_0, \bar{\mathcal{V}})$. This relation among thermodynamic potentials is fundamental in studies of classical equilibrium phase transitions as will be discussed in the following section.

Remark 1 (Concavity of microcanonical entropy)**.** *Concavity of the microcanonical entropy plays a crucial role to asses the equivalence of canonical and microcanonical ensembles. In fact, if the microcanonical entropy is a non strictly concave function, some "pathological" behaviour is expected for the function $\bar{F}_N$. In particular the Laplace approximation cannot be applied and the Laplace transform is ill-defined: this is signalled by a loss of analyticity of $\bar{F}_N$.*
This mechanism has been suggested to characterize the signature of phase transitions in the microcanonical ensemble for systems where the existence of phase transitions in canonical ensemble is known.

According to eqs.(1.31) and (1.33) we can calculate the derivatives of the canonical free

energy as a function of derivatives of the microcanonical entropy in the thermodynamic limit

$$\begin{aligned}
\frac{\mathrm{d}F_\infty(\beta)}{\mathrm{d}\beta} &= \frac{\mathrm{d}\bar{E}_0}{\mathrm{d}\beta} - \frac{1}{k_B\beta}\frac{\mathrm{d}S_\infty}{\mathrm{d}\bar{E}_0}\frac{\mathrm{d}\bar{E}_0}{\mathrm{d}\beta} + \frac{1}{k_B\beta^2}S_\infty(\bar{E}(\beta)) = \frac{1}{k_B\beta^2}S_\infty(\bar{E}(\beta)) \\
\frac{\mathrm{d}^2F_\infty(\beta)}{\mathrm{d}\beta^2} &= -\frac{2}{k_B\beta^3}S_\infty(\bar{E}_0(\beta)) + \frac{1}{k_B\beta^2}\frac{\mathrm{d}S_\infty}{\mathrm{d}\bar{E}_0}\frac{\mathrm{d}\bar{E}_0}{\mathrm{d}\beta} = \\
&= -\frac{2}{k_B\beta^3}S_\infty(\bar{E}_0(\beta)) + \frac{1}{k_B\beta}\left(\frac{\mathrm{d}^2S_\infty}{\mathrm{d}\bar{E}_0^2}(\bar{E}_0(\beta))\right)^{-1} \\
\frac{\mathrm{d}^3F_\infty(\beta)}{\mathrm{d}\beta^3} &= \frac{6}{k_B\beta^3}S_\infty(\bar{E}_0(\beta)) - \frac{3}{k_B\beta^2}\left(\frac{\mathrm{d}^2S_\infty}{\mathrm{d}\bar{E}_0^2}(\bar{E}_0(\beta))\right)^{-1} - \frac{\mathrm{d}^3S_\infty}{\mathrm{d}\bar{E}_0^3}(\bar{E}_0(\beta))\left(\frac{\mathrm{d}^2S_\infty}{\mathrm{d}\bar{E}_0^2}(\bar{E}_0(\beta))\right)^{-2}
\end{aligned} \tag{1.34}$$

where the following relations derived from the first of eqs.(1.31) has been used

$$\frac{\mathrm{d}\bar{E}_0}{\mathrm{d}\beta} = \left(\frac{\mathrm{d}^2S_\infty}{\mathrm{d}\bar{E}_0^2}(\bar{E}_0(\beta))\right)^{-1} \tag{1.35}$$

$$\frac{\mathrm{d}^2\bar{E}_0}{\mathrm{d}\beta^2} = -\frac{\mathrm{d}^3S_\infty}{\mathrm{d}\bar{E}_0^2}(\bar{E}_0(\beta))\left(\frac{\mathrm{d}^2S_\infty}{\mathrm{d}\bar{E}_0^2}(\bar{E}_0(\beta))\right)^{-3} \tag{1.36}$$

1.2 Phase Transitions (PTs) at thermodynamic equilibrium: definition and classification

1.2.1 General concepts on equilibrium Phase Transitions

The concept of phase transition is quite intuitive: a major qualitative change of the property systems (typically the establishment of collective behaviours like magnetization, crystallization, spatial order etc. etc.) in response to a small changes of some external thermodynamic parameters (total energy, pressure, temperature, external fields). Nevertheless, a formal definition and classification remains a major issue in statistical mechanics and thermodynamics.
The first attempts to give a precise characterization of phase transitions is historically related with the study of liquid-vapour transitions.
Such transitions has been studied in pressure-temperature ($P-T$) statistical ensemble whose associated thermodynamic potential is the (specific) Gibbs free energy $\bar{G}_{\infty,Gibbs}$ defined as:

$$\begin{aligned}
\bar{G}_{\infty,Gibbs} &= \lim_{N\longrightarrow+\infty}\bar{G}_{N,Gibbs}(\beta,P) = \lim_{N\longrightarrow+\infty} -\frac{1}{Nk_B}\log\left[Z_{N,Gibbs}(\beta,P)\right] = \\
&= -\frac{1}{k_B}\log\left[\int_0^{+\infty}\left(\int_{\Lambda^{N,\mathcal{V}}_{(p,q)}} e^{-\beta(\mathcal{H}_N-P\mathcal{V})}\mathrm{d}\mu\right)\mathrm{d}\mathcal{V}\right] \qquad \text{with} \quad \beta = \frac{1}{k_BT}\ .
\end{aligned} \tag{1.37}$$

For a fixed pressure, liquid-vapour phase transition is associated with the coexistence of the two phases a certain critical (inverse) temperature β_C; for $\beta < \beta_C$ ($\beta > \beta_C$) only the vapour (liquid) phase exists. The coexistence of two phases at a certain temperature is related to the fact that the energy injected/subtracted into/to the system (which corresponds to decrease/increase β) affects discontinuously the number of microstates compatible with the values of macroscopic

parameters: degrees of freedom suddenly decorrelates/correlates among them and the disappearance/appearance cooperative of phenomena (as clustering, or condensation) is observed in the real physical system. This yields to a discontinuity of the entropy, which is (proportional) to the first order derivative of the free energy of the systems respect to the (inverse) of temperature β;

$$\bar{S}_{\infty,Gibbs}(\beta, P) = k_B \beta^2 \frac{\partial \bar{G}_{\infty,Gibbs}}{\partial \beta}\Bigg)_P \tag{1.38}$$

or, in other words, the (specific) constant pressure latent heat Q_P (which measure the jump of entropy around the transition temperature) is strictly positive, i.e

$$\Delta Q_P = \lim_{\tau \longrightarrow 0} \frac{1}{k_B \beta} \left[\bar{S}_{\infty,Gibbs}(\beta - \tau, P) - \bar{S}_{\infty,Gibbs}(\beta + \tau, P) \right] > 0\,. \tag{1.39}$$

However, not all thermodynamic phase transitions show positive latent heat; such an example is provided by the He I/He II phase transition. In this case *phase coexistence is not observed* and the latent heat is zero $Q_P = 0$ so that the entropy is a continuous function of the temperature while discontinuities or singularities affects susceptibility of the systems, namely the second order derivative.
Such phenomenology suggested a possible classification of phase transitions according to the behaviour of specific heat: transitions with strictly positive latent heat has been referred to as *discontinuous* or *first order* phase transition while transitions with zero latent heat has been referred to as *continuous* phase transition.
A more refined classification based on regularity properties of thermodynamic potentials was suggested by P. Erehnfest

Definition 1.2.1 (PTs in equilibrium systems: classical definition and Ehrenfest's classification)**.** *Let be given a system $\mathcal{S}$, whose equilibrium thermodynamics is described by a general thermodynamic potential $\mathcal{F}(\mathbf{a})$ being $\boldsymbol{a} = \{a_i\}_{i\in\mathbb{N}}$ the set of external thermodynamic variables. Then the systems undergoes a phase transition at the point $\boldsymbol{a}_0$ if some derivatives of $\mathcal{F}(\mathbf{a})$:*

$$\frac{\partial^k}{\partial a_i^k} \mathcal{F}(\mathbf{a}_0) \tag{1.40}$$

is discontinuous or(weakly) diverges at $\boldsymbol{a}_0$.
The phase transition is said to be of k-order if the first non regular derivative is of order k.

Such classification has been subjected has been object both of criticisms [CZ90, WKLS90] and refinements[Hil93]. Nevertheless this remains a phenomenological classification strictly related to the thermodynamical characterization of PTs. In fact, at this level, the problem to relate PTs with some features of mutual interaction among microscopic degree of freedom remain unsolved. In the following Subsection the main results on the origin of phase transition in classical systems are resumed.

1.2.2 Mechanisms at the origin of PTs: Landau's theory and Yang-Lee Theorems

As reviewed before, PTs have been characterized in mathematical terms by the loose of analyticity of the thermodynamic potentials of open systems.
However the thermodynamic potential $\mathcal{F}(\mathbf{a})$ is a smooth or even an analytic function in the "finite-size" case (meaning both a finite number of degrees of freedom N for discrete system and/or a finite accessible range for microscopical degree of freedom) for a very large class of systems. This suggests the idea that the loose of analyticity of the thermodynamic potentials is mathematically possible only in the so called in the sense of succession of functions: a succession of analytic function does not *necessarily* converge to an analytic function. In order to accord the statistical mechanics with thermodynamic experimental evidence, this leads to the idea to take the *thermodynamic limit* where the number of degrees of freedom tends to infinity at a fixed density: the succession of function is composed, in this case, by the thermodynamic potentials at different N.
Historically, the first major evidence of this facts relies in the Onsager's exact solution for 2D-Ising model in canonical ensemble; when a finite lattice with N site is considered, the free energy for degree of freedom $F_N(T) = N^{-1}F(T, N)$ is analytic, while in the thermodynamic limit, the free energy punctually to a *piece-wise analytic function.*
A first attempt to give a deeper insight to phase transitions is due to the Landau theory (1937) which relates phase transitions with a *spontaneous symmetry breaking* phenomena. Such a theory has been developed in the contest of canonical ensemble where energy fluctuations are allowed. The main idea is that when a system undergoes a phase transition the set of sets accessible to the system is characterized by a different set of symmetries: this origin discontinuities in second order derivatives of thermodynamic potential respect to the control parameters of the systems. The maximal set of the possible symmetries that a physical system can have is represented by all the symmetries of the Hamiltonian describing it. In general, at low temperatures the accessible states of a system can lack some of the symmetries of the Hamiltonian, so that the corresponding phase is the less symmetric one, whereas at higher temperatures the thermal fluctuations allow the access to a wider range of energy states having more, and eventually all, the symmetries of the Hamiltonian. In the broken-symmetry phase, an extra variable is required to characterize the physical states belonging to it. Such a variable, of extensive nature, is called an *order parameter.* The order parameter vanishes in the more-symmetric phase and is different from zero in the less-symmetric phase. Under the hypothesis that the free energy $F(P, T, \{\eta_i\})$ has the same symmetries of the Hamiltonian and that it can be expressed as a function of order parameters $\{\eta_i\}$, the discontinuous behaviour of some order parameter at the transition point induce discontinuities in second order derivatives of free energy.
Landau's theory of phase transition and the spontaneous symmetry breaking mechanism represent a very important achievement in comprehension of phase transitions and critical phenomena giving a first theoretical tools to understand in a wide class of phenomena from condensed matter to fundamental physics. Despite of this Landau's theory is a mean-field theory, as the order parameters are averages of some quantities over the degrees of freedoms of the system,

and neglect the contribution of fluctuations around the transition point. Moreover it requires the *thermodynamic limit*, so an infinite number of degrees of freedom to be exact, as for finite systems thermal fluctuations always allow the system to explore a set of states invariant for the hamiltonian set of symmetries.
The idea that phase transition phenomena are strictly possible only in thermodynamic limit has been enforced in a rigours and mathematical sense by Yang-Lee theories, formulated in the framework of grand canonical ensemble. The main idea is that, for finite systems, the grand canonical potential $F_{GCan}(T, z, \mathcal{V})$ is an analytic function as a function of temperature and fugacity $z = e^{\eta}$ as the Grand partition function $Z_{GCan}(T, z, \mathcal{V})$ can be written as a polynome in z with not real roots.
Nevertheless in the *thermodynamic limit* it is possible that some root of the Grand partition function tend to real axes on the fugacity complex plane. If this happens, it can be rigorously argued that the succession of analytic functions $F_{GCan}(T, z, \mathcal{V})$ for $\mathcal{V} \longrightarrow +\infty$ does not converge to an analytic function on the real axes of fugacity complex plane but only to a *piecewise analytic* function $F_{GCan}(T, z)$. Such result assumes a great relevance in statistical mechanics as for some physical relevant model it is possible to calculate the distribution of roots of grand partition function in the limit $\mathcal{V} \longrightarrow +\infty$ on complex fugacity plane.
This two important rigours results lead to the idea that phase transitions intended as a loss of analyticity of the thermodynamic potentials can be take place only in *thermodynamic limit* or, in other words, in infinite systems.
Although this idea attained a strong and coherent *mathematical* description of phase transitions as usually described in thermodynamics, it is not a well suited scheme to study self-organization or transitional phenomena (as nuclear fragmentation or polymerization, i.e.) in system with a finite number of degrees of freedom far from the "thermodynamic limit".

1.3 Beyond the *thermodynamic limit dogma*: signature of PTs in microcanonical ensemble

In the last years there has been a growing interest in the emergence of cooperative behaviour in small or mesoscopic systems, where thermodynamic limit (and consequently a classical thermodynamic interpretation) is meaningless.
This enlarged view on "phase transition" in finite systems leads also to new insight in the classical "thermodynamic" theory: it would be questionable if, for instance, is there in finite systems which entails a phase transition in thermodynamic limit, a signature of the asymptotic transitional behaviour.
All the different approach that try to answer to these questions have in common the framework where the problem is set, i.e. the *microcanonical ensemble*. This choice it seems quite natural for different reasons. First of all, as largely observed before, *microcanonical ensemble* constitute the foundation of statistical mechanics as all the other statistical ensemble; classical thermodynamic observables are not required to be known *a priori* to define the ensemble.
Moreover if the presence of self-organization and cooperative phenomena are assumed to be an

essential features of phase transitions, then they are only due to the *mutual interactions among the degrees of freedom*: so the *possibility* for a system to undertake a phase transition could in principle be read in the Hamiltonian. This is coherent with the well known fact that the class of universality which a phase transition belongs to depends only on some properties of the Hamiltonian describing the "microscopic" degrees of freedom dynamics (as for instance the nature of the broken symmetries, range of the interactions and dimensionality of the system). From a statistical mechanics perspective, one of the simplest structure that encodes information on the system are the Hamiltonian level sets in phase space. The microcanonical entropy at a fixed value E is the logarithm of the volume of this level sets Σ_E and consequently encodes a global information on the level sets: it is natural to wonder how the emergence of cooperative phenomena and organization between the degrees of freedom affects the behaviour of the microcanonical entropy as a function. This problem is equivalent to a pure statistical mechanics definition of a phase transition in microcanonical ensemble.
Different approaches to this problem have been explored in the last thirty years. One of the more interesting has been proposed by D.H.E. Gross [GK05][Gro01] and it is kwown as *Microcanonical analysis*: phase transitions in microcanonical systems are signalled by the presence of convex region of (microcanonical) *entropy*[7]

$$\exists \bar{E}_c \in [E_{min}, +\infty) \quad \text{such that} \frac{\partial \bar{S}_N}{\partial \bar{E}}\bigg|_{\bar{E}=\bar{E}_c} \geq 0 \ . \tag{1.41}$$

In Gross' microcanonical characterization of phase transition the usual Erhenfest classification is abandoned in favour of a simplified scheme:

- *first order phase transitions* are characterized by a convex hull of the entropy, i.e. there is a region where $\mathrm{d}^2\bar{S}_N/\mathrm{d}\bar{E}^2 > 0$; the parameters that characterize the convex hull of the function are related with a *not null latent heat* and the presence of separation surfaces among different phases;
- *continuous phase transition* are characterized $\mathrm{d}^2\bar{S}_N/\mathrm{d}\bar{E}^2 \longrightarrow 0$ in the thermodynamic limit, characterized by diverging specific heat and/or spontaneously broken symmetries ; they can take place only in thermodynamic limit.

This characterization of phase transitions partially takes advantage of researches on statistical mechanics of systems with long-range interactions where non strictly concave microcanonical entropies are quite common. The presence of convex-hull in microcanonical entropy in these cases generally results in non-equivalence of thermodynamic ensembles and in the presence of angular points of the canonical free energy (first order phase transition).
In very recent works Bachmann et al.[SSLB11][Bac14a][Bac14b] developed the Microcanonical analysis; the inflection point of inverse microcanonical temperature (the fingerprint of phase

[7] In the original Gross' formulation, the entropy is a function of the specific energy and of the density of particle $n = N/V$, i.e. $\bar{S}_N = \bar{S}_N(\bar{E}, n)$. If $\lambda_1 > \lambda_2$ are the eigenvalues of the Hessian of the microcanonical entropy, a phase transition takes place if exists a region on the plane $\bar{E} - n$ where $\lambda_1 > 0$ (first order phase transition) or if there is a point s.t. $\lim_{N \longrightarrow +\infty} \lambda_1 = 0$ (continuous phase transition).

transition in finite and infinite system) would be the phenomenological manifestation of a*least sensitivity principle* around the transition point the microcanonical temperature is less sensitive to variation of energy.
This approach for the definition and classification of phase transitions in microcanonical ensemble has the advantage to be a very general approach that inscribe transitional phenomena for large and small systems in a common framework. Very recently it has been proposed to apply Microcanonocal analysis also for the classification of phase transitions also in finite systems *out-of-equilibrium*.
On the other side, it gives only a general criteria to characterize phase transition fingerprint at a "*phenomenological level*" as entropy (or someone of its derivatives) can not be determined *a priori* but it results from numerical simulation, experimental measures, and, only in rare cases, from analytical computations. In this sense the approach presented in this section remains on a phenomenological/thermodynamical level, as it does not associate phase transitions with some property related with the form of the interaction among the microscopic degrees of freedom.
In the same framework of microcanonical ensemble, an other approach has been developed aimed to predict if the system undertake a PTs from the information encoded in topology of level set of the Hamiltonian (or more precisely of the potential energy function for a separable Hamiltonian). Such a theory is presented in following section: it constitute the main framework where a part of this thesis work is inscribed.

1.4 The Topological Theory of phase transitions

1.4.1 Motivations: From the dynamics of chaotic systems to the topological hypotheisis

Topological Theory of phase transitions has its roots in the geometrical formulation of Hamiltonian dynamics for the characterization of chaotic systems[8].
In mid '90s, the group leaded by Prof. Pettini investigated chaos in hamiltonian systems, from a geometrical point of view. Natural motions can be read as geodesic in configuration space endowed with Jacobi metric, a local conformal rescaling of natural euclidean metric depending encoding the information of potential energy $g_{ij} = (E - V(q1, ..., q_N))\delta_{ij}\mathrm{d}q_i \otimes \mathrm{d}q_j$: this allows to describe hamiltonian chaos in terms of geodesic spread. This approach succeeded to find the origin of chaos in parametric resonances of curvature fluctuations of configuration space (with Riemannian structure induced by Jacobi metric) along the geodesic.
The study of curvature fluctuations of configuration space along natural motions was performed also in systems where continuous phase transition and critical phenomena take place. A peak of curvature fluctuations as function of total energy was observed at the critical point for different choices of configuration space metric. These results suggested that high curvature fluctuation would be the geometric signature of some *topological change* (independent by metric choice) of the topological subspace $\mathcal{M}_v = \left\{x \in \Lambda_q^N | V_N(q) = v\right\}$ when v crosses the critical energy value

[8]This section is brief summary of second part of the book [Pet07b]. The interested reader can be found there a more detailed discussion.

$N\bar{E}_c$.
Moreover a "jump" has been observed in the pattern of Largest Lyapunov Exponent as function of total energy in correspondence of critical value of energy. The stability property of geodesic flux around critical point q_c of potential energy in configuration space are related to its index, namely the number of negative eigenvalues of Hessian of potential in q_c. On the other side, critical points of a suitable class of functions on manifold and their index are strictly related to the topology of the same manifold according to *Morse theory.* An abrupt change in density of critical points or of their index passing from $\mathcal{M}_{v_0}$ to $\mathcal{M}_{v_1}$ where $v_0 < E_c < v_1$, signalling a topological change among this two manifolds, *can in principle be the origin* both of changes in chaotic behaviour of the dynamics and of phase transitions.
The topology of Morse function level sets are strictly connected with the topology of the whole configuration space: this facts allows to establish a more direct link among the topology of configuration space accessible to the system and thermodynamics. In fact, for system described by Hamiltonian of the form $\mathcal{H}_N = \sum_i^N p_N^2/2 + V_N(q_1, ..., q_N)$, *microcanonical partition function* can be written in terms of integral evaluated on equipotential level sets

$$\omega_N(E) = \int_0^E \mathrm{d}v \int_{\Sigma_v^N} \frac{\mathrm{d}\sigma_{\Sigma_v^N}}{\|\mathbf{grad}_g V_N\|} \int \mathrm{d}^N p\, \delta\left(\sum_{i=1}^N \frac{p_i^2}{2} - (E - v)\right) \tag{1.42}$$

and the same is possible for *canonical free energy*

$$F_N(\beta, \mathcal{V}) = -\frac{1}{\beta} \log\left[\int_{\Lambda_{(p,q)}^N} e^{-\beta \mathcal{H}_N} \mathrm{d}\mu\right] = -\frac{1}{\beta}\left(\frac{N}{2}\log\frac{\pi}{\beta} + \log\left[\int_0^{E_{max}} \mathrm{d}v\, e^{-\beta v} \int_{\Sigma_v^N} \frac{\mathrm{d}\sigma_{\Sigma_v^N}^N}{\|\mathbf{grad}_g V_N\|_g}\right]\right). \tag{1.43}$$

The only non trivial integral in previous expressions is the so called *structure integral*

$$\omega_N(v) = \int_{\Sigma_v^N} \frac{\mathrm{d}\sigma_{\Sigma_v^N}^N}{\|\mathrm{grad}_g V_N\|_g} \tag{1.44}$$

that can be interpreted as the *configurational microcanonical entropy.* In this framework, the Topological Hypothesis can be formulated:

Proposition 1.4.1 (Topological Hypothesis)**.** *The basic origin of phase transitions lies in a topological change of the support of the measure describing a system. This change of measure itself at the transition point.*

The peculiarity of this approach is that phase transition are characterized from the point of view of *Hamiltonian dynamics*: this allows to look for a characterization of phase transition more related to geometrical/dynamical properties (being equipotential level sets the "fundamental" objects) than to thermodynamic properties (as in the case of Microcanonical Analysis where the knowledge of microcanonical temperature is required.). This open the possibility to predict the possibility of a system to undergo a phase transition or not from the properties of potential. In this theoretical framework, two theorems, proved in late '90s, established a strong relation

among topology of configuration space and the presence of phase transitions in thermodynamic limit.

1.4.2 Necessity theorem for PTs and Pettini-Franzosi Theorem

A major leap forward of Topological Theory of phase transition is constituted by two theorems claiming that that topological changes of equipotential hypersurfaces of configuration space—and of the regions of configuration space bounded by them are a *necessary* condition for the appearance of thermodynamic phase transitions. This is obtained for a wide class of potential functions of physical relevance, and for first- and second-order phase transitions. However, long-range interactions, nonsmooth potentials, unbound configuration spaces, "exotic" and higher-order phase transitions, are not encompassed by the actual formulation of the theory and are still open problems deserving further work.

In these standard approaches, a phase transition is seen as stemming from singular properties of the statistical measures, whereas the two theorems presented below show that these singularities are not "primitive" phenomena but are induced from a deeper level, that of configuration-space topology. In other words, once the microscopic interaction potential is given, the information about the existence of a phase transition is already contained in the topology of its level sets, *prior to and independently of* the definition of any statistical measure.

Theorem 1.4.2 (Regularity under diffeomorphicity)**.** *Let $V_N(q_1, \ldots, q_N) : \mathbb{R}^N \to \mathbb{R}$, be a smooth, nonsingular, finite-range potential. Denote by $\Sigma_v := V_N^{-1}(v)$, $v \in \mathbb{R}$, its <u>level sets</u>, or <u>equipotential hypersurfaces</u>, in configuration space.*
Then let $\bar{v} = v/N$ be the potential energy per degree of freedom. If for any pair of values $\bar{v}$ and $\bar{v}'$ belonging to a given interval $I_{\bar{v}} = [\bar{v}_0, \bar{v}_1]$ and for any $N > N_0$, we have

$$\Sigma_{N\bar{v}} \approx \Sigma_{N\bar{v}'},$$

that is, $\Sigma_{N\bar{v}}$ is <u>diffeomorphic</u> to $\Sigma_{N\bar{v}'}$, then the sequence of the Helmholtz free energies $\{F_N(\beta)\}_{N\in\mathbb{N}}$—where $\beta = 1/T$ (T is the temperature) and $\beta \in I_\beta = (\beta(\bar{v}_0), \beta(\bar{v}_1))$—is <u>uniformly</u> convergent at least in $\mathcal{C}^2(I_\beta)$, so that $F_\infty \in \mathcal{C}^2(I_\beta)$ and neither first- nor second-order phase transitions can occur in the (inverse) temperature interval $(\beta(\bar{v}_0), \beta(\bar{v}_1))$.

In general, given a model described by a smooth, nonsingular, finite-range potential, it is a hard task to locate all its critical points and thus to ascertain whether Theorem **??** actually applies to it. Moreover, the requirement of the existence—at any N—of an energy density interval $[\bar{v}_0, \bar{v}_1]$ free of critical values seems rather strong. Theorem 1.4.2 is very useful and *crucial* to prove Theorem 1.4.3 which establishes that the occurrence of a phase transition is *necessarily* driven by topological changes in configuration space. To do this we have to consider what happens to the entropy when a critical value of the potential is crossed. Taking just *one* critical value v_c of the potential, and allowing an arbitrary growth with N of the number of critical points on Σ_{v_c}, one can see that it is the energy variation of the volume only in the vicinity of critical points that can entail an unbounded growth with N of the third- or fourth-order

derivative of the entropy. In other words, the breaking of uniform convergence of the entropy in $\mathcal{C}^3$ or in $\mathcal{C}^2$ can be originated *only* by a topological change of the Σ_v or, equivalently, of the M_v. To rule out any role—in the breaking of uniform convergence—of the part of configuration space volume which is free of critical points, one resorts to Theorem 1.4.2. Theorem Theorem 1.4.3 applies to all those systems whose potential is a good Morse function.[9] But are there systems with only one critical value in an interval $[\bar{v}_0, \bar{v}_1]$? At present we can conjecture that the result expressed by Theorem Theorem 1.4.3 extends at least to those potential functions for which the number of critical values $\bar{v}_c^j$ contained in $[\bar{v}_0, \bar{v}_1]$ grows at most linearly with N (thus encompassing a wide class of short-range interaction potentials). The basic case of only one critical value has a great *conceptual* meaning: it allows a direct proof of the role of critical points. Once we have proved that phase transitions can stem only from the neighbourhoods of critical points in the *ideal* case of one v_c in $[\bar{v}_0, \bar{v}_1]$, we can hardly imagine how the part of configuration space volume which is free of critical points could start playing any role when the number of critical values in the interval is let grow, although it is possible in principle. However, this possibility is ruled out by resorting to Theorem 1.4.2, though in the special case of one critical value in an interval $[\bar{v}_0, \bar{v}_1]$. Again, it seems very hard to imagine how this could change by simply allowing the existence of more critical values. As a consequence, topology changes are also *necessary* for the existence of phase transitions. Theorem 1.4.3, is enunciated as follows:

Theorem 1.4.3 (Entropy and topology)**.** *Let $V_N(q_1, \ldots, q_N) : \mathbb{R}^N \to \mathbb{R}$, be a smooth, nonsingular, finite-range potential. Denote by $M_v := V_N^{-1}((-\infty, v])$, $v \in \mathbb{R}$, the generic submanifold of configuration space bounded by Σ_v. Let $\{q_c^{(i)} \in \mathbb{R}^N\}_{i\in[1,\mathcal{N}(v)]}$ be the set of critical points of the potential, that is, such that $\nabla V_N(q_c^{(i)}) = 0$, and let $\mathcal{N}(v)$ be the number of critical points up to the potential energy value v. Let $\Gamma(q_c^{(i)}, \varepsilon_0)$ be pseudocylindrical neighborhoods of the critical points, and $\mu_i(M_v)$ the Morse indexes of M_v. Then there exist real numbers $A(N, i, \varepsilon_0)$, g_i and real smooth functions $B(N, i, v, \varepsilon_0)$ such that the following equation for the microcanonical configurational entropy $S_N^{(-)}(v) = (1/N) \log \int_{V(q)\leq v} d^N q$ holds:*

$$S_N^{(-)}(v) = \frac{1}{N} \log\Bigg[\int_{M_v \setminus \bigcup_{i=1}^{\mathcal{N}(v)} \Gamma(q_c^{(i)},\varepsilon_0)} d^N q + \sum_{i=0}^{N} A(N, i, \varepsilon_0)\ g_i\ \mu_i(M_{v-\varepsilon_0}) + \sum_{n=1}^{\mathcal{N}_{cp}^{\nu(v)+1}} B(N, i(n), v - v_c^{\nu(v)}, \varepsilon_0)\Bigg]$$

Moreover, an unbounded growth with N of one of the derivatives $|\partial^k S^{(-)}(v)/\partial v^k|$, for $k = 3, 4$, and thus the occurrence of a first- or second-order phase transition, can be entailed only by the topological term $\sum_{i=0}^{N} A(N, i, \varepsilon_0)\ g_i\ \mu_i(M_{v-\varepsilon_0})$.

Together, these two theorems imply that for a wide class of potentials that are good Morse functions, a first- or second-order phase transition can only be the consequence of a topological change of the submanifolds M_v (or equivalently of the Σ_v) of configuration space. The converse

[9] Let us keeping mind that Morse functions are dense in the space of smooth functions bounded below.

is not true: topological changes are necessary but not sufficient for the occurrence of phase transitions.

1.4.3 A counterexample to Topological Theory of PTs

The Topological Theory of phase transitions has been recently object of harsh criticism [KM11, MHK12]. In these papers it has been argued against this theory on the basis of the observation the second order phase transition of the $2D$ lattice ϕ^4-model would be a counterexemple of the Theorem.
The lattice ϕ^4 model with Periodic Boundary Conditions (PBC) is defined by the Hamiltonian

$$\mathcal{H}(p,\varphi) = \sum_{\mathbf{i}\in\mathcal{S}^{(d)}_{lact}} \left[\frac{p^2_{\mathbf{i}}}{2} + \frac{J}{2} \sum_{\mathbf{j}\in\mathcal{N}^{(d)}(\mathbf{i})} (\varphi_{\mathbf{j}} - \varphi_{\mathbf{i}})^2 - \frac{1}{2} m^2 \varphi^2_{\mathbf{i}} + \frac{\lambda}{4} \varphi^4_{\mathbf{i}} \right] \tag{1.45}$$

where $\mathbf{i}$ is an index which identifies a node of the d-dimensional lattice $\mathcal{S}^{(d)}_{lact}$, $\mathcal{N}^{(d)}(\mathbf{i})$ is the set of the nearest neighbours of the node $\mathbf{i}$ and J, m and λ parameters which define potential energy. At equilibrium and for $d \geq 2$, this model – representing a set of linearly coupled nonlinear oscillators – shows a second order phase transition with nonzero critical temperature. This phase transition consist in a spontaneous breaking of the discrete $O(1)$, or $\mathbb{Z}_2$, symmetry and it occurs at a critical value v_c of the potential energy density which belongs to a broad interval of v-values void of critical points of the potential function.
This means that the $\{\Sigma^N_{v<v_c}\}_{v\in\mathbb{R}}$ are diffeomorphic to the $\{\Sigma^N_{v>v_c}\}_{v\in\mathbb{R}}$ so that no topological change seems to correspond to the phase transition.
The authors of [KM11, MHK12] conclude that the Franzosi-Pettini Necessity Theorem for PTS is "allegedly proved" and that in the case of $2D$ lattice ϕ^4-model the phase transitions are originated by a "concentration measure" mechanism.
The object of part of the work reported in this manuscript is aimed to provide a refinement and development of Topological Theory of PTs. In particular:

- *numerical simulation* has been performed to investigate the dynamical properties of the system and geometrical properties of different diffeomorphic level sets in the region around a critical value;
- concept of *asymptotic diffeomorphicity* among level sets is delineated as a possible hypothesis to be added to the formulation of the Necessity Theorem;
- derivatives of entropy at any order in (configurational) microcanonic ensemble are interpreted in terms of *global geometry* of the foliation induced by (potential) energy level sets in (configuration) phase space, in absence of critical points;
- the application of new computational techniques in algebraic topology (*persistent homology*) for investigation of topology of (potential) energy landscape is presented.

CHAPTER 2 Developments of the Topological Theory of Phase Transitions

In this chapter some original results and contributions for the refinement of the topological theory of PTs is reported. Results of Monte Carlo simulations for the "counterxample", namely the φ^4-model on 2d lattice, are discussed and the necessity of a supplementary hypothesis (the *asymptotic diffeomorphicity among level sets*) to prevent phase transitions is conjectured.
Moreover, the derivatives of (configurational) microcanonical entropy are interpreted in terms of the geometry of configuration space with a properly rescaled metric. Finally, an application of new computational techniques in algebraic topology is given in the context of the Topological Theory of PTs.

2.1 Preliminary results towards a generalization of the Topological Theory

2.1.1 Motivations

The counterexample to the Pettini-Franzosi Necessity Theorem, briefly discussed in the previous chapter, has undermined the Topological Theory of PTs. However, since the validity of this theoretical approach relies also on some rigorous analytical results worked out for some particular models, an effort to save the theory is well justified.
Thus the work presented in this chapter is motivated by the reasonable conviction that the above mentioned counterexample does not really undermine the Topological Theory, so that, as a matter of fact, the microcanonical thermodynamic information of a physical system is actually encoded in the topological/geometrical properties of its configuration space and in the foliation induced on it by the equipotential level sets. So the question is if it is possible to fix the problem paving the way to a more general formulation of the theory itself.
Let us remark that a counterexample to a theory does not necessarily mean that it has to be discarded: to the contrary, a counterexample can stimulate a refinement of a theory. An instance, which is not out of place in the present context, is the famous counterexample that J. Milnor gave against De Rham's cohomology theory (the two manifolds $M = \mathbb{S}^2 \times \mathbb{S}^4$, product of spheres, and $N = \mathbb{C}P^3$, complex-projective space, are neither diffeomorphic nor homeomorphic yet have the same cohomology groups). The introduction of the so called "cup product" fixed the problem and saved the theory making it more powerful.
Let us remark that the two basic theorems Theorem 1.4.2 rely on the assumption of diffeomorphicity at any arbitrary *finite* $N \in \mathbb{N}$ of any pair of level sets of specific potential energy $\Sigma_{\bar{v}}^{\overline{V}_N}$, with $\bar{v} \in [\bar{v}_0, \bar{v}_1]$, but no assumption is made about the "asymptotic ($N \to \infty$) diffeomorphicity" relation among the $\Sigma_{\bar{v}}^{\overline{V}_N}$.

The concept of "asymptotic diffeomorphicity" for the leaves of foliations in ambient spaces of increasing dimension ($N \to \infty$) seems an almost-meaningless problem. In fact, it requires to define a measure of "how much" two leaves are diffeomorphic between them and to define a prescription to compare pairs of leaves defined in spaces with different dimensionality. These two operations can be defined in a quite arbitrary way: the choice as meaningful as possible has to be done on the basis of physical considerations and constraints as general as possible.
An heuristic argument in favour of the idea that asymptotic diffeomorphicity takes place in the φ^4-model on 2d lattice is suggested by the interpretation of the qualitative feature of the Hamiltonian dynamics in terms of the geometry/topology properties of configuration and phase space spaces. In this case, spontaneous $\mathbb{Z}_2$-symmetry breaking, present in the thermodynamic limit, is associated with an asymptotic ($N \to \infty$) breaking of the ergodicity of the systems whose phase space trajectories remain "confined" in a region corresponding to a non vanishing average magnetization (subsection 2.1.3). In turn, this ergodicity breaking stems from the asymptotic breaking of topological transitivity giving rise to an asymptotic ($N \longrightarrow +\infty$) "disconnection" of regions of the energy level sets corresponding to opposite signs of the total magnetization. In this framework, phenomena like concentration of microcanonical measure would not be unique on the energy level sets (what is often invoked as a possible origin of ergodicity breaking) and would result from an "asymptotic disconnection" of the *support of the measure*, i.e. of the same energy level sets $\Sigma_{\bar{\epsilon}}^{\overline{\mathcal{H}}_N}$ with $\bar{\epsilon} < \bar{\epsilon}_c$ where $\bar{\epsilon}_c$ is the specific critical energy.
A link among the topology of (specific) energy level sets and the topology of configuration space accessible to the system can be established, and this is possible as the Topological Theory of phase transitions is (in its actual formulation) restricted to systems whose microscopic dynamics is described by Hamiltonian of the form $\mathcal{H}_N(p,q) = \sum_{i=1}^{N} p_i^2/2 + V_N(q_1, ..., q_N)$ with short-range potentials bounded from below (we can suppose that $\bar{v}_{min} = 0$ for all N).
Hence, the level sets of the specific energy function $\overline{\mathcal{H}}_N = \mathcal{H}_N/N$ can be given by the disjoint union of a trivial unitary sphere bundle (representing the phase space region where the kinetic energy does not vanish) and the hypersurface in configuration space where the potential energy takes total energy value.

$$\Sigma_{\bar{\epsilon}}^{\overline{\mathcal{H}}_N} = M_{[0,\bar{\epsilon})}^{\overline{V}_N} \times \mathbb{S}^{N-1} \bigsqcup \Sigma_{\bar{\epsilon}}^{\overline{V}_N} \tag{2.1}$$

where $\mathbb{S}^n$ is the n-dimensional unitary sphere and

$$M_{\mathcal{I}}^f = \{x \in \mathrm{Dom}(f) | f(x) \in \mathcal{I}\}\,, \qquad \Sigma_c^f = \{x \in \mathrm{Dom}(f) | f(x) = c\}\,,. \tag{2.2}$$

The idea that the "asymptotic topology" of $\Sigma_{\bar{\epsilon}}^{\overline{\mathcal{H}}_N}$ is affected by the "asymptotic topology" of the accessible region of configuration space is suggested by the *Künneth formula*: if $H_k(X)$ is the k-th homological group of the topological space X on the field $\mathbb{F}$ then

$$H_k(X \times Y; \mathbb{F}) \simeq \bigoplus_{i+j=k} H_i(X; \mathbb{F}) \ \otimes \ H_j(Y; \mathbb{F})\ . \tag{2.3}$$

Moreover, as $H_k\left(\sqcup_{i=1} X_i, \mathbb{F}\right) = \bigoplus_i^N H_k(X_i, \mathbb{F})$, it follows that:

$$\begin{aligned} H_k\left(\Sigma_{\bar\epsilon}^{\overline{\mathcal{H}}_N}, \mathbb{R}\right) &\simeq \bigoplus_{i+j=k} H_i\left(M_{[0,\bar\epsilon)}^{\overline{V}_N}; \mathbb{R}\right) \otimes H_j\left(\mathbb{S}^{N-1}; \mathbb{R}\right) \oplus H_k\left(\Sigma_{\bar\epsilon}^{\overline{V}_N}; \mathbb{R}\right) \simeq \\ &\simeq H_{k-(N-1)}\left(M_{[0,\bar\epsilon)}^{\overline{V}_N}; \mathbb{R}\right) \otimes \mathbb{R} \oplus H_k\left(M_{[0,\bar\epsilon)}^{\overline{V}_N}; \mathbb{R}\right) \otimes \mathbb{R} \oplus H_k\left(\Sigma_{\bar\epsilon}^{\overline{V}_N}; \mathbb{R}\right) \quad . \end{aligned} \tag{2.4}$$

So, in that case, the topological changes of $\Sigma_{\bar\epsilon}^{\overline{\mathcal{H}}_N}$ can be derived only by topological changes in configuration space. Numerical simulations to support these hypotheses have been performed on the model claimed to be a definitive "counterexample" to the theory. The results are reported in what follows.

2.1.2 The model: φ^4-model on lattice

As mentioned in the previous chapter, the model of interest is the $d = 2$ version of the ϕ^4-model on d-dimensional lattice, with nearest neighbour interactions, defined by the Hamiltonian

$$\mathcal{H}(p, \varphi) = \sum_{\mathbf{i} \in \mathcal{S}_{lact}^{(d)}} \left[\frac{p_{\mathbf{i}}^2}{2} + \frac{J}{2} \sum_{\mathbf{j} \in \mathcal{N}^{(d)}(\mathbf{i})} (\varphi_{\mathbf{j}} - \varphi_{\mathbf{i}})^2 - \frac{1}{2} m^2 \varphi_{\mathbf{i}}^2 + \frac{\lambda}{4} \varphi_{\mathbf{i}}^4 \right] \qquad \varphi = \{\varphi_{\mathbf{i}}\}_{\mathbf{i} \in \mathcal{S}_{lact}^{(d)}} \qquad p = \{p_{\mathbf{i}}\}_{\mathbf{i} \in \mathcal{S}_{lact}^{(d)}} \tag{2.5}$$

where $\mathbf{i}$ is an index which identifies a node of the d-dimensional lattice $\mathcal{S}_{lact}^{(d)}$, $\mathcal{N}^{(d)}(\mathbf{i})$ is the set of the nearest neighbours of the node $\mathbf{i}$ and J, m and λ are parameters. This system has a discrete $\mathbb{Z}_2$-symmetry and short-range interactions; therefore, according to the Mermin–Wagner theorem, in $d = 1$ there is no phase transition whereas in $d = 2$ there is a a second order symmetry-breaking transition, with nonzero critical temperature, of the same universality class of the 2d Ising model. The thermodynamic signature of this transition is a logarithmic divergence of the specific heat in correspondence of critical energy $\bar\epsilon_c$. Also hamiltonian dynamics displays a transition at critical energy between a weak chaotic regime to a strong one (see [CCP98] for a detailed analysis of this phase transition)[1].

2.1.3 Numerical simulation of Hamiltonian dynamics

The numerical integration of the equations of motion derived from (1.45) has been performed for $d = 2$ and $d = 1$, with periodic boundary conditions, using a bilateral symplectic integration scheme [Cas95b]. The model parameters have been chosen as follows: $J = 1$, $\mu^2 = 2$, and $\lambda = 3/5$ for the whole set of numerical simulation reported in what follows.

By means of standard computations, as reported in [CCP98] and [CCC+98b], and for the chosen values of the parameters, the $2d$ system undergoes the symmetry-breaking phase transi-

[1] Chaotic properties have been shown to be related with the presence of critical points of the potential function, in fact the neighbors of critical points act as "scatterers" of the configuration space trajectories. Morse theory establishes a strong relation among critical point of (Morse) functions on manifold and the topology of the latest; this originally suggested a connection among phase transitions and topology of configuration space.

tion at a critical energy density value $\varepsilon_c = E_c/N \simeq 11.1$, correspondingly the critical potential energy density value is $v_c = \langle V \rangle_c/N \simeq 2.2$. The initial conditions were: $\varphi_i = 0$ and p_i randomly chosen and adjusted so that the initial kinetic energy value corresponds to the wanted ε value. With respect to the numerical simulations already reported in the mentioned literature we have here followed the time evolution of the order parameter ("magnetization")

$$M = \frac{1}{\mathrm{card}(\mathcal{S}^{(d)}_{lact})} \sum_{\mathbf{i} \in \mathcal{S}^{(d)}_{lact}} \varphi_{\mathbf{i}} \ . \tag{2.6}$$

This vanishes in the symmetric phase, that is for $\bar{\epsilon} > \bar{\epsilon}_c$, whereas it takes a positive or negative value in the broken symmetry phase, that is for $\bar{\epsilon} < \bar{\epsilon}_c$. However, at finite N the order parameter can flip from positive to negative and viceversa. This flipping is associated with a trapping phenomenon of the phase space trajectories alternatively in one of the two subsets of the constant energy surfaces which correspond to positive and negative magnetization, respectively. This phenomenon has been investigated by computing the average trapping time τ_{tr} for different lattice sizes, and choosing values of ε just below and just above $\bar{\epsilon}_c$. The results are displayed in Figure 2.1. Denote with $\psi^H_t : \Sigma_{\bar{\epsilon}} \to \Sigma_{\bar{\epsilon}}$ the $\mathcal{H}$-flow, with $\Sigma_{\bar{\epsilon}} = \mathcal{H}^{-1}(N\bar{\epsilon})$ a constant energy hypersurface of phase space, with $\mathcal{M}^+_{\bar{\epsilon}} \subset \Sigma_{\bar{\epsilon}}$ the set of all the phase space points for which $M \geq \eta > 0$, i-th $\mathcal{M}^-_{\bar{\epsilon}} \subset \Sigma_{\bar{\epsilon}}$ the set of all the phase space points for which $M \leq -\eta < 0$, and with $\mathcal{M}^\eta_{\bar{\epsilon}} \subset \Sigma_{\bar{\epsilon}}$ a transition region, that is, the set of all the phase space points for which $-\eta \leq M \leq \eta$, with $\eta \ll \langle |M| \rangle$. In numerical computations we used $\eta = 0.01\langle |M| \rangle$.

Thus $\Sigma_{\bar{\epsilon}} = \mathcal{M}^+_{\bar{\epsilon}} \cup \mathcal{M}^-_{\bar{\epsilon}} \cup \mathcal{M}^\eta_{\bar{\epsilon}}$. From the very regular functional dependences of $\tau_{tr}(N)$ reported in Figure Figure 2.1, we can see that:

- *at $\bar{\epsilon} < \bar{\epsilon}_c$, for any given $\tau_{tr} > 0$ there exists an $N(\tau_{tr})$ such that for any $N > N(\tau_{tr})$ and $t \in [0, \tau_{tr}]$ we have $\varphi^H_t(\mathcal{M})^\pm_{\bar{\epsilon}} = \mathcal{M}^\pm_{\bar{\epsilon}}$.*
  In other words, below the transition energy density the subsets $\mathcal{M}^\pm_{\bar{\epsilon}}$ of the constant specific energy surfaces $\Sigma^{\overline{\mathcal{H}}_N}_{\bar{\epsilon}}$ appear to be *invariant* for the $\overline{\mathcal{H}}_N$-flow on a finite time scale τ_{tr}, with the remarkable fact that $\tau_{tr} \to \infty$ in the limit[2] $N \to \infty$.
  Formally this reads as

$$\begin{aligned} &\forall A \subset \mathcal{M}^+_{\bar{\epsilon}}, \forall B \subset \mathcal{M}^-_{\bar{\epsilon}} \quad \textit{and} \quad t \in [0, \tau_{tr}(N)] \\ &\textit{is} \quad \psi^H_t(A) \cap B = \emptyset \ . \end{aligned}$$

- To the contrary *at $\bar{\epsilon} > \bar{\epsilon}_c$, there exists a $\tau^0_{tr} > 0$ such that for any N and*

$$\begin{aligned} &\forall A \subset \mathcal{M}^+_{\bar{\epsilon}}, \forall B \subset \mathcal{M}^-_{\bar{\epsilon}} \quad \textit{and} \quad t > \tau^0_{tr} \\ &\textit{is} \quad \psi^H_t(A) \cap B \neq \emptyset \ . \end{aligned}$$

Since $\Sigma_{\bar{\epsilon}} = \mathcal{M}^+_{\bar{\epsilon}} \cup \mathcal{M}^-_{\bar{\epsilon}} \cup \mathcal{M}^\eta_{\bar{\epsilon}}$, and since the residence times in the transition region are found to be very short and independent of N - so that the relative measure $meas(\mathcal{M}^\eta_{\bar{\epsilon}})/meas(\mathcal{M}^\pm_{\bar{\epsilon}})$

[2]The $N \to \infty$ extrapolation is safe because increasing N essentially amounts to gluing together identical replicas of smaller lattices.

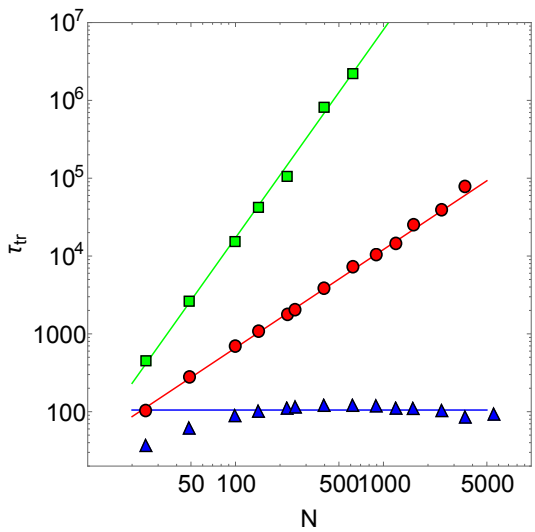

Figure 2.1: Average trapping time τ_{tr} of the magnetization vs.the number of lattice sites N for the 2d φ^4-model. Different data series refer to different values of the energy per degree of freedom $\bar{\epsilon}$: $\bar{\epsilon} = 8$ (squares), $\bar{\epsilon} = 10$ (circles), both below the transition energy $\bar{\epsilon}_c = 11.1$, and $\bar{\epsilon} = 12$ (triangles), above the transition energy.

vanishes in the limit $N \to \infty$ - Theorem 1.4.2 means that below the transition energy the *topological transitivity* of $\Sigma_{\bar{\epsilon}}$ is broken up to a time $\tau_{tr}(N)$ - which is divergent with N.

To the contrary, above the transition energy the $\Sigma_{\bar{\epsilon}}$ are *topologically transitive* [Kol][AN07]. The asymptotic breaking of topological transitivity at $\bar{\epsilon} < \bar{\epsilon}_c$, that is the divergence of $\tau_{tr}(N)$ in the limit $N \to \infty$, goes together with asymptotic ergodicity breaking due to the $\mathbb{Z}_2$-symmetry breaking. Moreover, on metric and compact topological spaces, topological transitivity is equivalent to *connectedness* of the space [Kol][AN07], so the *loss of topological transitivity entails the loss of connectedness*, that is, *a major topological change of the space.*

And if we denote by $H^0_\tau(\Sigma^N_{\bar{\epsilon}};\mathbb{R})$ the "finite time zeroth cohomology space" of $\Sigma^{\overline{\mathcal{H}}_N}_{\bar{\epsilon}}$, for $\tau < \tau_{tr}(N)$ we have $b_0 = \dim H^0_\tau(\Sigma^{\overline{\mathcal{H}}_N}_{\bar{\epsilon}};\mathbb{R}) = 2$ at $\bar{\epsilon} < \bar{\epsilon}_c$, and $b_0 = \dim H^0_\tau(\Sigma^{\overline{\mathcal{H}}_N}_{\bar{\epsilon}};\mathbb{R}) = 1$ at $\bar{\epsilon} > \bar{\epsilon}_c$. The dimension of this cohomology space (the Betti number b_0) counts the number of connected components of $\Sigma^{\overline{\mathcal{H}}_N}_{\bar{\epsilon}}$ and is invariant under diffeomorphisms of the $\Sigma^{\overline{\mathcal{H}}_N}_{\bar{\epsilon}}$. Hence the asymptotic jump of a diffeomorphism invariant across the phase transition point, which can be deduced by our numerical computations, means that the $\Sigma^{\overline{\mathcal{H}}_N}_{\bar{\epsilon}}$ undergo an *asymptotic loss of diffeomorphicity*, in the absence of critical point[3] of the potential $V(q)$. Now, the breaking of topological transitivity of the $\Sigma^{\overline{\mathcal{H}}_N}_{\bar{\epsilon}}$ implies the same phenomenon for configuration space and its submanifolds $\Sigma^{\overline{V}_N}_{\bar{v}}$ (specific potential level sets) as discussed above. These level sets are the basic objects, foliating configuration space, that enter in Theorem 1.4.2 and Theorem 1.4.3, and represents the nontrivial topological part of phase space.
The link of these geometric objects with microcanonic entropy is given by

$$\overline{S}_N(\bar{\epsilon}) = \frac{k_{\rm Bol}}{2N} \log \int_0^{\bar{\epsilon}} \mathrm{d}\bar{v} \int \prod_i^N \mathrm{d}p_i \;\; \delta\left(\frac{1}{N}\sum_{i=1}^N \frac{p_i^2}{2} - (\bar{\epsilon} - \bar{v})\right) \int_{\Sigma^{\overline{V}_N}_{N\bar{v}}} \frac{d\sigma_{\Sigma^{\overline{V}_N}_{\bar{v}}}}{\|\nabla \overline{V}_N\|} \; . \tag{2.7}$$

[3]Notice that in this case transversality is absent, see([Hir97]).

As N increases the microscopic configurations giving a relevant contribution to the entropy, and to any microcanonical average, concentrate closer and closer on the level set $\Sigma^{V_N}_{N\overline{v}}$.
Therefore, it is interesting to make a direct numerical analysis on these level sets at different N values to find out - with a purely geometric glance- how configuration space asymptotically breaks into two disjoint components. The intuitive picture is that, approaching from above ($\varepsilon > \varepsilon_c$) the transition point, some subset of each $\Sigma^{V_N}_{v}$ - a "high dimensional neck" related with $\mathcal{M}^{\eta}_{E}$ - should be formed which bridges the two regions $\mathcal{M}^{+}_{v}$ and $\mathcal{M}^{-}_{v}$. And this neck should increasingly shrink with increasing N.

2.1.4 Monte Carlo simulation on equipotential level sets

To perform the analysis prospected at the end of previous section, we resort to a Monte Carlo algorithm constrained on any given $\Sigma^{\overline{V}_N}_{\overline{v}}$ of a general specific potential function $\overline{V}_N$ of the class considered in Theorem 1.4.2 and Theorem 1.4.3.
This is obtained by generating a Markov Chain with a Metropolis importance sampling of the microcanonical configuration weight appearing in (2.7) $\overline{\chi}_N = \|\nabla \overline{V}_N\|^{-1}_{\mathbb{R}^N}$. The details of the Monte Carlo code are discussed in Appendix B.

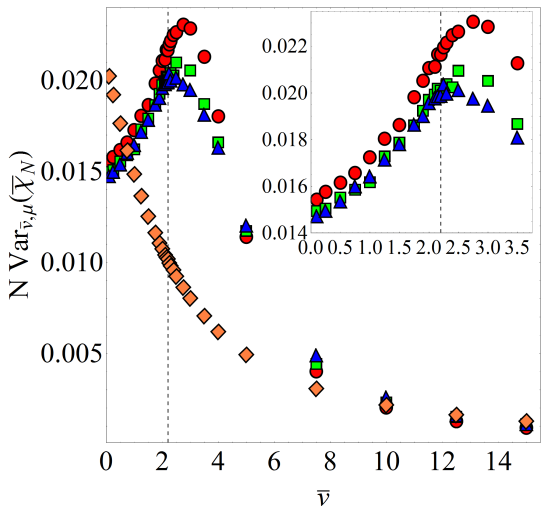

Figure 2.2: Variance of χ_N over potential level sets $\Sigma^{\overline{V}_N}_{\overline{v}}$ endowed with microcanonical measure μ vs. potential energy per degree of freedom $\overline{v}$ for 1d and 2d ϕ^4-models, and for lattice sizes: $N = 10 \times 10$ (circles), $N = 20 \times 20$ (squares), $N = 30 \times 30$ (triangles) in the 2d case, and $N = 900$ (rhombs) in the 1d case. The vertical dashed line indicates the phase transition point at $\overline{v} \simeq 2.2$.

In order to check the validity of the intuitive idea of a neck which shrinks at increasing N, we have to identify some useful geometric quantities to be numerically computed. To do this we proceed as follows.
Let us note that, in the *absence of critical points in an interval* $[a, b]$, the explicit form of the diffeomorphism $\boldsymbol{\xi}$ that maps one to the other the level sets Σ^{f}_{c}, with $c \in [a, b]$, of a function

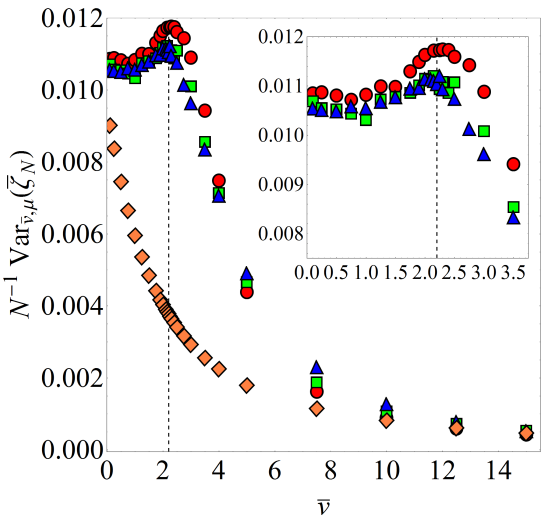

Figure 2.3: Variance of $\bar{\zeta}_N = \mathrm{div}_{\mathbb{R}^N}\bar{\boldsymbol{\xi}}_N$ on the potential level sets $\Sigma_{\bar{v}}^{\overline{V}_N}$ with microcanonical measure μ vs. potential energy per degree of freedom $\bar{v}$ for 1d and 2d ϕ^4-models, and for lattice sizes: $N = 10 \times 10$ (circles), $N = 20 \times 20$ (squares), $N = 30 \times 30$ (triangles) in the 2d case, and $N = 900$ (rhombs) in the 1d case. The vertical dashed line indicates the phase transition point at $\bar{v} \simeq 2.2$.

$f : \mathbb{R}^N \to \mathbb{R}$ is explicitly given by [Hir97]

$$\frac{dx^i}{dc} = \xi^i(x) = \frac{\nabla^i f(x)}{\|\nabla f(x)\|^2} \qquad x(c) \in \Sigma_c \tag{2.8}$$

and this applies as well to the energy level sets in phase space as to the potential level sets in configuration space. It has to be stressed that $\chi_N = \|\boldsymbol{\xi}_N\|$ for the equipotential level sets $\Sigma_v^{V_N}$. If we consider an infinitesimal change of specific potential energy $\bar{v} \to \bar{v} + \Delta\bar{v}$ with $|\Delta\bar{v}|/\bar{v} \ll 1$, and denote with $\mathrm{dist}(\varphi)$ the field of local distances between two level sets $\Sigma_{\bar{v}}^{\overline{V}_N}$ and $\Sigma_{\bar{v}+\Delta\bar{v}}^{\overline{V}_N}$, from $\varphi_{\mathbf{i}}(\bar{v}+\Delta\bar{v}) = \varphi_{\mathbf{i}}(\bar{v}) + \xi_{\mathbf{i}}\Delta\bar{v}$ and using (2.8), at first order in $\Delta\bar{v}$, we get $\mathrm{dist}(\varphi) = \Delta_{\bar{v}}/\|\nabla\overline{V}_N\|_\varphi = \Delta_{\bar{v}}\overline{\chi}_N(\varphi)$.

Moreover the divergence $\mathrm{div}_g\bar{\boldsymbol{\xi}}_N$ in euclidean configuration space can be related with the variation rate of the measure of the microcanonic area $\mathrm{d}\mu_{\Sigma_{\bar{v}}^{\overline{V}_N}} = \overline{\chi}_N \mathrm{d}\sigma_{\Sigma_{\bar{v}}^{\overline{V}_N}}$ over regular level sets $\Sigma_{\bar{v}}^{\overline{V}_N}$.

The first variation formula for the induced measure of the Riemannian area $\mathrm{d}\sigma_{\Sigma_{\bar{v}}^{\overline{V}_N}}$ along the flow $\varphi(\bar{v})$ reads [Lee09]

$$\mathrm{d}\sigma(\varphi(\bar{v}+\Delta\bar{v})) = \left(1 - \Delta\bar{v}\overline{\chi}(N-1)h_{\Sigma_{\bar{v}}^{\overline{V}_N}, g_{\mathbb{R}^N}}\right)\mathrm{d}\sigma(\varphi(\bar{v})) + o(\Delta\bar{v}) \tag{2.9}$$

here $h_{\Sigma_c^f, g}$ is the *mean curvature* of the regular hypersurface Σ_c^f respect to metric g, i.e. the sum of principal curvatures(see Appendix A for a more details), that in terms of f is given by

$$h_{\Sigma_c^f, g}(x) = -\frac{1}{N-1}\mathrm{div}_g\left(\frac{\nabla f}{\|\nabla f\|}\right)\Bigg|_x \qquad x \in \Sigma_c^f \tag{2.10}$$

Applying the Leibniz rule, the first variation formula for the measure of the microcanonic

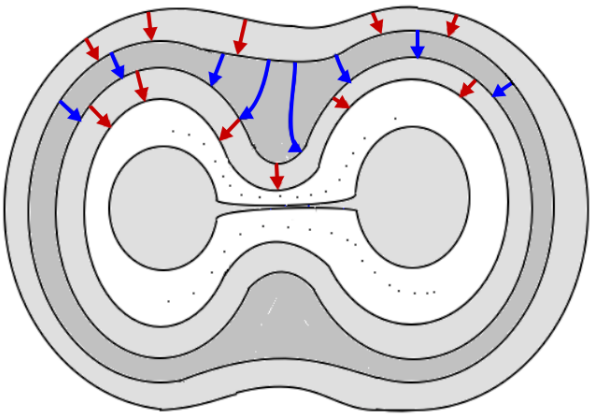

Figure 2.4: Toy model representation of the possible geometrical origin of the peaks in Figure 2.2 and Figure 2.3. The first four lines pictorially represent "level sets" separated by the same potential energy interval. The first two external lines abstractly represent level sets $\Sigma_{\bar{v}}^{\overline{V}_N}$ at $\bar{v} > \bar{v}_c$ (above the phase transition). The third and fourth lines abstractly represent level sets $\Sigma_{\bar{v}}^{\overline{V}_N}$ at $\bar{v} < \bar{v}_c$ (below the phase transition) with a neck. The variance of the length of the blue lines (corresponding to the formation of the neck) is larger than that of the red lines.

area is

$$
\begin{aligned}
&\mathrm{d}\mu(\varphi(\bar{v}+\Delta\bar{v})) = \overline{\chi}_N(\varphi(\bar{v}+\Delta\bar{v}))\mathrm{d}\sigma(\bar{v}+\Delta\bar{v}) = \\
&= \left[1 + \Delta\bar{v}\left(-\overline{\chi}_N(N-1)h_{\Sigma_{\bar{v}}^{\overline{V}_N},g_{\mathbb{R}^N}} + \frac{(\nabla^i\overline{V}_N)}{\|\nabla\overline{V}_N\|}\nabla_i\overline{\chi}_N\right)\right]\mathrm{d}\mu(\varphi(\bar{v})) = \\
&= \left(1 + \Delta\bar{v}\ \mathrm{div}\overline{\boldsymbol{\xi}}_N\right)\mathrm{d}\mu(\varphi(\bar{v}))
\end{aligned}
\tag{2.11}
$$

Then, the two following quantities have been numerically computed along the mentioned Monte Carlo Markov Chain: $\mathrm{Var}_{\Sigma_{\bar{v}}^{\overline{V}_N},\mu}(\overline{\chi}_N) = \langle\overline{\chi}_N^2\rangle_{\Sigma_{\bar{v}}^{\overline{V}_N},\mu} - \langle\overline{\chi}_N\rangle^2_{\Sigma_{\bar{v}}^{\overline{V}_N},\mu}$ and $\mathrm{Var}_{\Sigma_{\bar{v}}^{\overline{V}_N},\mu}(\mathrm{div}\overline{\boldsymbol{\xi}_N}) = \langle(\mathrm{div}\overline{\boldsymbol{\xi}}_N)^2\rangle_{\Sigma_{\bar{v}}^{\overline{V}_N},\mu} - \langle(\mathrm{div}\overline{\boldsymbol{\xi}})\rangle^2_{\Sigma_{\bar{v}}^{\overline{V}_N},\mu}$. These are functions of the specific potential energy $\bar{v} = V/N$ and are sequences labeled by N; the thermodynamic limit can be derived if the density is kept constant for $N \longrightarrow +\infty$.

In order to obtain point-wise convergent functions for the mentioned quantities, they have to be scaled by a factor depending on N. The estimation of these scale factors is a key point to compare geometrical and topological properties of objects defined in ambient spaces of different dimensionality. We proceeded heuristically in the derivation of these terms, although a rigorous derivation of their scaling would be in principle possible by taking into account the prescription to take the thermodynamic limit of systems with short range potentials.

The basic assumption is that $\partial_i V_N \sim O(1)$, i.e. these terms do not scale with N because of the short-range property of the interactions among the degrees of freedom, this fact introduces a cut-off scale: each degree of freedom does not interact with the degrees freedom outside the cut-off radius of the interaction (which is the same at any N) . It follows that the forces acting on a single degree of freedom depend on the energy density but not on N. This leads to estimate

$\partial_i \overline{V}_N \sim O(N^{-1})$ and $|\nabla \overline{V}_N\|^2 = \sum_{i=1}^{N} (\partial_i \overline{V}_N)^2 \sim O(N^{-1})$ that yields

$$\langle \overline{\chi}_N \rangle_{\Sigma^{\overline{V}_N}_{N\bar{v}},\mu} = \langle \|\overline{V}_N\|^{-1} \rangle_{\Sigma^{\overline{V}_N}_{N\bar{v}},\mu} \sim O(N^{1/2}) \ . \tag{2.12}$$

Through analogous considerations, we can derive the scaling with N for the average of $\mathrm{div}_g \overline{\boldsymbol{\xi}}_N$,

$$\langle \mathrm{div}_g \overline{\boldsymbol{\xi}}_N \rangle_{\Sigma^{\overline{V}_N}_{N\bar{v}},\mu} = \left\langle \frac{\sum_{i=1}^{N} \partial_i \overline{V}_N}{\|\nabla \overline{V}_N\|^2} \right\rangle_{\Sigma^{\overline{V}_N}_{N\bar{v}},\mu} \sim \frac{N \cdot O(N^{-1})}{O(N^{-1})} \sim O(N) \tag{2.13}$$

The variance (so the average of squared fluctuation)of these two quantities are supposed to scale as

$$\begin{aligned} &\mathrm{Var}_{\Sigma^{\overline{V}_N}_{N\bar{v}},\mu}(\overline{\chi}_N) \sim O(1) \\ &\mathrm{Var}_{\Sigma^{\overline{V}_N}_{N\bar{v}},\mu}(\mathrm{div}_g \overline{\boldsymbol{\xi}}_N) \sim O(N) \, . \end{aligned} \tag{2.14}$$

The outcomes, reported in Figure 2.2 and Figure 2.3, show very different patterns in the $1d$ and $2d$ cases: monotonic for the $1d$ case, non-monotonic displaying cuspy points at $\bar{v} = \bar{v}_c$ (the phase transition point) of $\mathrm{Var}(\overline{\chi}_N)$ and of $\mathrm{Var}_{\Sigma^{\overline{V}_N}_{N\bar{v}},\mu}(\mathrm{div}\overline{\boldsymbol{\xi}}_N)$ for the $2d$ case.
As $\overline{\chi}_N = 1/\|\nabla \overline{V}_N\|$ is locally proportional to the distance between nearby level sets, its variance is a measure of the total dishomogeneity of this distance, so that a peak of $\mathrm{Var}(\overline{\chi}_N)$ can be due to the formation of a "neck" in the $\left\{\Sigma^{\overline{V}_N}_{\bar{v}}\right\}_{\bar{v}\in\mathbb{R}}$ foliation of configuration space.
This is pictorially shown through the toy model of Figure 2.4. The same is true for $\mathrm{Var}(\mathrm{div}_g \overline{\boldsymbol{\xi}}_N)$ since $\mathrm{div}_g \overline{\boldsymbol{\xi}}_N$ is locally proportional to the variation of the area of a small surface element when a level set is transformed into a nearby one by the diffeomorphism in Eq.(2.8).

2.1.5 Discussion of the numerical results

In spite of the absence of critical points of $\overline{V}(\phi)$ of the φ^4-model [Eq.(**??**)] in correspondence with the critical potential energy density $\overline{v}_c$ at which the phase transition takes place, we have here found sufficient evidence that this transition stems from an *asymptotic change of topology* of both the $\Sigma^{\overline{\mathcal{H}}_N}_{\bar{\epsilon}}$ and $\Sigma^{\overline{\mathcal{H}_N}}_{\bar{v}}$ around the critical level. This paves the way to a more general formulation of the topological theory of phase transitions once a basic assumption of the theory is made explicit also in the $N \to \infty$ limit. This can be achieved by resorting to the explicit analytic representation (2.8) of the diffeomorphism $\overline{\boldsymbol{\xi}}_N : \Sigma^{\overline{V}_N}_{\bar{v}} \subset \mathbb{R}^{N+1} \to \Sigma^{\overline{V}_N}_{v'} \subset \mathbb{R}^{N+1}$.
Uniform convergence in N of the sequence of vector valued many-variable functions $\left\{\overline{\boldsymbol{\xi}}_N\right\}_{N\in\mathbb{N}}$ can be used to define *asymptotic diffeomorphicity* in some class $\mathcal{C}^l$ of the $\{\Sigma^{\overline{V}_N}_{\bar{v}}\}_{\bar{v}\in\mathbb{R}}$ after the introduction of a suitable norm containing all the derivatives up to $(\partial^l \overline{\boldsymbol{\xi}}_N / \partial x^{l_1}_{i_1} \dots \partial x^{l_k}_{i_k})$. Accordingly, in Theorem 1.4.2 and Theorem 1.4.3 the assumption of asymptotic diffeomorphicity of the $\left\{\Sigma^{\overline{V}_N}_{\bar{v}}\right\}_{\bar{v}\in\mathbb{R}}$ has to be added to the hypothesis of diffeomorphicity just at any finite N.
A deeper investigation of the link between the geometry and topology of the regular equipotential level sets and the thermodynamics of (configurational) microcanonical ensemble is developed

in what follows.

2.2 Geometry of regular potential energy level sets in configuration space

As prospected at the end of the previous Section, the numerical simulations therein reported suggest that a suitably defined concept of "asymptotic diffeomorphicity" among the equipotential level sets for $N \to +\infty$ can lead to a generalization of the Theorem 1.4.2 (Necessity Theorem) by adding the assumption of asymptotic diffeomorphicity to its hypotheses, thus excluding the 2d lattice φ^4 model from the domain of validity of the theorem. This will fix the problem by eliminating the counterexample.
A first encouraging step in this direction is in the possibility of expressing the microcanonical (configurational) Boltzmann entropy in terms of integrals on regular level sets $\Sigma_{\overline{\epsilon}}^{\overline{\mathcal{H}}_N}$ ($\Sigma_{\overline{v}}^{\overline{V}_N}$) of geometrical properties of the vector field that generates the diffeomorphism of eq.(2.8) among level sets.

2.2.1 Microcanonical configurational statistical mechanics from differential topology of regular equipotential level sets

We consider in what follows the configurational microcanonical ensemble[4] $(\Lambda_q, \rho_N(\mathbf{q}; \overline{v}))$ where the constraint is obtained by fixing the value of some specific potential energy function $\overline{V}_N : \Lambda_q \longrightarrow \mathbb{R}$ and the corresponding microcanonical configurational density function is given by

$$\rho_N(\mathbf{q}; \overline{v}) = \frac{\delta\left(\overline{V}_N(\mathbf{q}) - \overline{v}\right)}{\int_{\mathcal{X}^N} \delta\left(\overline{V}_N(\mathbf{q}) - \overline{v}\right) \mathrm{dVol}_g}. \tag{2.15}$$

where g is a natural metric structure in configuration space[5] and dVol_g the associated Riemannian volume form. The normalization constant in (2.15) is the microcanonical partition function according to Boltzmann's definition:

$$\Omega_{N,\mathrm{Boltz}}(\overline{v}) = \frac{\partial}{\partial \overline{v}} \Omega_{N,\mathrm{Gibbs}}(\overline{v}) = \frac{\partial}{\partial \overline{v}} \int_{\Lambda_q} \Theta(\overline{V}_N(\mathbf{q}) - \overline{v}) \mathrm{dVol}_g = \int_{\Lambda_q} \delta\left(\overline{V}_N(\mathbf{q}) - \overline{v}\right) \mathrm{dVol}_g \tag{2.16}$$

where $\Theta(x)$ is the Heaviside step function.
In analogy with the usual definitions in statistical microcanonical ensemble, the configurational microcanonical entropy density function is given by:

$$\overline{S}_{N,\mathrm{Boltz}} = \frac{1}{N} \ln \Omega_{N,\mathrm{Boltz}}(\overline{v}) \tag{2.17}$$

[4]The same considerations apply to the classical microcanonical ensemble where the specific energy is fixed, simply replacing the configuration space Λ_q with the phase space $\Lambda_{p,q}$ and the specific potential energy $\overline{V}_N$ (with fixed value $\overline{v}$) with the Hamiltonian representing the energy per degree of freedom $\overline{\mathcal{H}}_N$ (with fixed value $\overline{\epsilon}$).

[5]The introduction of a metric space is an arbitrary operation and not always the euclidean one is the best choice. For instance for a system with angular generalized coordinates $\theta_i \in [0; 2\pi)$ the torus metric could be more appropriate.

As a consequence of eq.(2.17), the microcanonical volume of the level sets of $\overline{V}_N$ as a function of $\bar{v}$ contains the whole information on the thermodynamics of the system.
In what follows, the thermodynamic properties of the configurational microcanonical ensemble are expressed as integrals of quantities associated with the vector field that generates the diffeomorphism among the level sets of $\overline{V}_N$.

Definition 2.2.1 (Equipotential level sets)**.** *We recall that the equipotential level sets $\Sigma_{\overline{v}}^{\overline{V}_N}$ are defined as*

$$\Sigma_{\overline{v}}^{\overline{V}_N} = \left\{ q \in \Lambda_q | \overline{V}_N(q) = \overline{v} \right\} \tag{2.18}$$

Remark 2 (Compactness of level sets)**.** *As $\overline{V}_N \in C^\infty(\Lambda_q)$ is a continuous function then $\overline{V}_N^{-1}(\overline{v}) \subseteq \Lambda_q$ is a compact set.*

Let the gradient vector field $\mathbf{grad}_g \overline{V}_N \in \mathfrak{X}(\Lambda_q)$ of the function $\overline{V}_N$ be

$$g(\mathbf{grad}_g \overline{V}_N, \mathbf{X}) = \mathrm{d}\overline{V}_N(X) \qquad \forall \mathbf{X} \in \mathfrak{X}(\Lambda_q) \ . \tag{2.19}$$

Remark 3 (Non critical level set)**.** *If there are no critical points of $\overline{V}_N$ on the level set $\Sigma_{\overline{v}}^{\overline{V}_N}$, i.e.:*

$$\mathbf{grad}_g \overline{V}_N \Big|_{\mathbf{q}} \neq \mathbf{0} \qquad \forall q \in \Sigma_{\overline{v}} \tag{2.20}$$

then $\Sigma_{\overline{v}}^{\overline{V}_N}$ is a regular compact hypersurface.

Let consider a configuration space subset where there is no critical point, i.e.

$$\mathcal{B}_N = \left\{ q \in \Lambda_q | \ \mathbf{grad}_g \overline{V} \Big|_q \neq \mathbf{0} \right\} . \tag{2.21}$$

and the set

$$M_{[\overline{v}_0, \overline{v}_1]}^{\overline{V}_N} = \bigcup_{\overline{v} \in [\overline{v}_0, \overline{v}_1]} \Sigma_{\overline{v}}^{\overline{V}_N} \tag{2.22}$$

and suppose that exist some $\overline{v}_0, \overline{v}_1$ such that $M_{[\overline{v}_0, \overline{v}_1]}^{\overline{V}_N} \subset B$. This means that the one-form $\mathrm{d}\overline{V}_N$ is non-degenerate over $M_{[\overline{v}_0, \overline{v}_1]}^{\overline{V}_N}$.
It follows from Froebenius' Theorem that a co-dimension one foliation can be defined on $M_{[\overline{v}_0, \overline{v}_1]}^{\overline{V}_N}$ through regular level sets of $\overline{V}_N$. Hence, it is possible to define a unit normal vector field to the equipotential hypersurfaces (the leaves of the foliation):

$$\boldsymbol{\nu}_N = \frac{\mathbf{grad}_g \overline{V}_N}{\|\mathbf{grad}_g \overline{V}_N\|_g} \tag{2.23}$$

We stress that the absence of critical points of $\overline{V}_N$ over the manifold $M_{[\overline{v}_0, \overline{v}_1]}^{\overline{V}_N}$ has important consequences on the topology of the level sets therein: in particular, we will use the following well known result in differential topology:

Theorem 2.2.1 (Regular interval theorem([Hir97], p.153)). *Let $f : M \longrightarrow [a, b]$ be a C^{r+1} map on a compact manifold $1 \leq r \leq \omega$ (where ω means analytical). Suppose f has no critical points and $f(\partial M) = \{a, b\}$. Then all level surfaces of f are diffeomorphic.*

In the proof of the same theorem in [Hir97], an explicit formulation is given for the vector field that generates the diffeomorphisms among the level sets and it is parametrized by the values taken by f on them.
If the function f is identified with $\overline{V}_N$ (as already mentioned in the previous Section) the vector field that generates the diffeomorphisms among the level sets, parametrized by $\bar{v}$, is

$$\overline{\boldsymbol{\xi}}_N = \frac{\mathbf{grad}_{\mathbb{R}^N}\overline{V}_N}{\|\mathbf{grad}_{g_{\mathbb{E}^N}}\overline{V}_N\|^2_{g_{\mathbb{E}^N}}} = \overline{\chi}_N \boldsymbol{\nu}_N \qquad \boldsymbol{\xi}_N \in \mathfrak{X}(M^N_{[v_0,v_1]})\,. \tag{2.24}$$

where we have introduced the symbol $\overline{\chi}_N$ for the norm of vector field $\overline{\boldsymbol{\xi}}_N$ in the ambient space $(\Lambda_q,\, g)$, i.e.:

$$\overline{\chi}_N = \frac{1}{\|\mathbf{grad}_g \overline{V}_N\|_g} = \|\overline{\boldsymbol{\xi}}_N\|_g\ . \tag{2.25}$$

This means that the diffeomorphic flow generated by $\overline{\boldsymbol{\xi}}_N$ is normal to the level sets and is parametrized by the differences of $\overline{V}_N$ along the flow lines

$$\mathrm{d}\overline{V}_N(\overline{\boldsymbol{\xi}}_N) = 1 \tag{2.26}$$

More in explicit, this means that there exists a diffeomorphism flow $\mathrm{Fl} : \Sigma^{\overline{V}_N}_{\bar{v}_0} \times [0; \bar{v}_1 - \bar{v}_0] \to M^{\overline{V}_N}_{[\bar{v}_0,\bar{v}_1]}$ among the level sets, s.t.

$$\begin{cases} \mathrm{Fl}_t(p) \in \Sigma^{\overline{V}_N}_{\bar{v}_0+t} \\ \dfrac{\mathrm{d}}{\mathrm{d}t}\left(f \circ \mathrm{Fl}_t\right)(p)\Big|_{t=(\bar{v}-\bar{v}_0)} = \left(\overline{\boldsymbol{\xi}}_N f\right)\left(\mathrm{Fl}_{(\bar{v}-\bar{v}_0)}(p)\right) \qquad \forall p \in \Sigma^{\overline{V}_N}_{\bar{v}_0} \text{ and } \forall \bar{v} \in [\bar{v}_0; \bar{v}_1] \end{cases} \tag{2.27}$$

where f is an arbitrary function of class C^1 defined over an open set of Λ_q containing $M^{\overline{V}_N}_{[\bar{v}_0,\bar{v}_1]}$.

In this differential topological framework it is possible to express the microcanonical entropy and its derivatives in terms of integral of quantities related only to the vector field $\overline{\boldsymbol{\xi}}_N$: this establishes a link among the property of diffeomorphicity of the level sets in $M^{\overline{V}_N}_{[\bar{v}_0,\bar{v}_1]}$ and the thermodynamic behaviour of the system. In particular the microcanonical partition function in eq.(2.16) can be rewritten in a more suitable form using the Coarea Formula [Fed14, Nic] which generalizes Fubini's theorem.

Theorem 2.2.2 (Co-Area formula ([Nic] Corllary 1.4, p.5)). *Suppose $\mathcal{M}$ is a C^1 manifold equipped with a C^1-metric g and $f : M \longrightarrow \mathbb{R}$ is a function with no critical points. Then for any measurable function $\phi : \mathcal{M} \to \mathbb{R}$ we have*

$$\int_{\mathcal{M}} \phi(p)\mathrm{dVol}_g = \int_{\mathbb{R}} \left(\int_{\Sigma^f_t} \frac{\phi(p)}{\|\mathbf{grad}_g f\|_g} \mathrm{d}\sigma_{\Sigma^f_t,g} \right) \mathrm{d}t \tag{2.28}$$

where dVol_g *is the Riemannian volume form on* $\mathcal{M}$*, and* $\mathrm{d}\sigma_{\Sigma_t^f,g_{\mathcal{M}}}$ *is its restriction over the regular level set* Σ_t^f*. In particular, by setting* $\phi = 1$ *it follows*

$$\mathrm{Vol}_g(\mathcal{M}) = \int_{\mathbb{R}} \left(\int_{\Sigma_t^f} \frac{\mathrm{d}\sigma_{\Sigma_t^f,g}}{\|\mathbf{grad}_g f\|_g} \right) \mathrm{d}t \tag{2.29}$$

We can apply the Theorem (2.2.2) to derive an useful expression for the configurational microcanonical partition function $\Omega_N(\bar{v})$ for $\bar{v} \in \mathcal{B}_N$. In fact, let us consider two values $\bar{v}_0, \bar{v}_1 \in \mathcal{B}_N$ such that $\bar{v}_0 < \bar{v} < \bar{v}_1$, then the smooth function $\overline{V}_N$ has no critical points in $M^{\overline{V}_N}_{[\bar{v}_0,\bar{v}_1]}$ and it follows

$$\begin{aligned} \Omega_{N,\mathrm{Boltz}}(\bar{v}) &= \frac{\partial}{\partial \bar{v}'} \Omega_{N,\mathrm{Gibbs}}(\bar{v}') \Big|_{\bar{v}'=\bar{v}} = \frac{\partial}{\partial \bar{v}'} \left[\Omega_{N,\mathrm{Gibbs}}(\bar{v}_0) + \int_{M^{\overline{V}_N}_{[\bar{v}_0,\bar{v}']}} \mathrm{dVol}_g \right] \Bigg|_{\bar{v}'=\bar{v}} = \\ &= \frac{\partial}{\partial \bar{v}'} \int_{\bar{v}_0}^{\bar{v}'} \left(\int_{\Sigma_t^{\overline{V}_N}} \frac{\mathrm{d}\sigma_{\Sigma_t^{\overline{V}_N},g}}{\|\mathbf{grad}_g \overline{V}_N\|_g} \right) \mathrm{d}t \Bigg|_{\bar{v}'=\bar{v}} = \int_{\Sigma_{\bar{v}}^{\overline{V}_N}} \frac{\mathrm{d}\sigma_{\Sigma_{\bar{v}}^{\overline{V}_N},g}}{\|\mathbf{grad}_g \overline{V}_N\|_g} . \end{aligned} \tag{2.30}$$

This very well known formula can be reinterpreted in order to make the vector field $\overline{\boldsymbol{\xi}}_N$ appear by simply using eq.(2.25):

$$\Omega_{N,\mathrm{Boltz}}(\bar{v}) = \int_{\Sigma_{\bar{v}}^{\overline{V}_N}} \overline{\chi}_N \, \mathrm{d}\sigma_{\Sigma_{\bar{v}}^{\overline{V}_N},g} = \int_{\Sigma_{\bar{v}}^{\overline{V}_N}} \mathrm{d}\mu_{\bar{v}}^{N-1} \tag{2.31}$$

where

$$\mathrm{d}\mu_{\bar{v}}^{N-1} = \overline{\chi}_N \mathrm{d}\sigma_{\Sigma_{\bar{v}}^{\overline{V}_N},g} \tag{2.32}$$

is the microcanonical area $(N-1)$-form for non critical energy level sets. In what follows we refer only to the Boltzmann configurational microcanonical entropy, i.e. defined through the volume $\Omega_{N,\mathrm{Boltz}}(\bar{v})$.

As we have seen, the thermodynamic behaviour of a system is described by means of response functions which depend on the derivatives of the configurational microcanonical entropy and, consequently, of the configurational microcanonical partition function (volume). So we need to calculate the derivatives of $\Omega_{N,\mathrm{Boltz}}(\bar{v})$ in eq.(2.31) with respect to the control parameter $\bar{v}$ in the configurational microcanonical ensemble that we are considering, and then express these derivatives in terms of quantities directly related with the diffeomorphisms generating vector field.

The following result allows to do this

Theorem 2.2.3 (Derivation of integral over regular level sets)**.** *Let* O *an open bounded set of a Riemannian manifold* $(\mathcal{M}^N, g)$ *with a connection* ∇*. Let* $\psi \in \mathcal{C}^{p+1}(\overline{O})$ *be constant on each connected component of the boundary* $\partial\overline{O}$ *and* $f \in \mathcal{C}^p(O)$*. Define* $M^N_{]t,t'[} = \{x \in O | t < \psi(x) < t'\}$ *and*

$$F(v) = \int_{\Sigma_v^\psi} f \, \mathrm{d}\sigma_{\Sigma_v^\psi,g} \tag{2.33}$$

where $\mathrm{d}\sigma_{\Sigma_v^\psi,g}$ *is the Riemannian area* $N-1$*-form induced over* Σ_v^ψ*. If* $C > 0$ *exists such that*

for any $M^{\psi}_{]t,t'[}$, $\|\mathbf{grad}_g\psi(x)\|_g \geq C$ *and the level sets* Σ^{ψ}_v *of* ψ *are without boundary, then for any* k *such that* $0 \leq k \leq p$, *for any* $v \in]t,t'[$, *one has*

$$\frac{\mathrm{d}^k F}{\mathrm{d}v^k}(v) = \int_{\Sigma^{\psi}_v} A^k_{\psi,g} f \, \mathrm{d}\sigma_{\Sigma^{\psi}_v,g} \tag{2.34}$$

with

$$A_{\psi,g} f = \mathrm{div}_g\,(\boldsymbol{\nu} f)\,\frac{1}{\|\mathbf{grad}_g\psi(x)\|_g} \qquad \boldsymbol{\nu} = \frac{\mathbf{grad}_g\psi(x)}{\|\mathbf{grad}_g\psi(x)\|_g} \tag{2.35}$$

proof.

We prove the formula at the first order of derivation, namely for $k = 1$

$$\frac{\mathrm{d}F}{\mathrm{d}v}(v) = \frac{\mathrm{d}}{\mathrm{d}v}\int_{\Sigma^{\psi}_v} A_{\psi,g} f \, \mathrm{d}\sigma_{\Sigma^{\psi}_v,g} \tag{2.36}$$

as the case for $k > 1$ can be obtained by recursion.
The absence of critical points of ψ implies that the level sets Σ^{ψ}_v of ψ determine a foliation of the open manifold $M^N_{]t,t'[}$. Moreover all the level sets are diffeomorphic by after Theorem 2.2.1 and a vector field $\boldsymbol{\xi}$ generating a family of one-parameter group of diffeomorphisms Fl_t parametrized by differences of values of ψ can be found, i.e.

$$\boldsymbol{\xi} = \frac{\mathbf{grad}_g\psi(x)}{\|\mathbf{grad}_g\psi(x)\|^2_g} = \chi\boldsymbol{\nu} \qquad \chi = \frac{1}{\|\mathbf{grad}_g\psi(x)\|_g}. \tag{2.37}$$

In order to pass the derivative into the integral in eq.(2.36) we use the transport property of integral under the action of the one-parameter group of diffeomorphisms:

$$\begin{aligned}\frac{\mathrm{d}F}{\mathrm{d}v}(v) &= \lim_{s\to+\infty}\frac{\int_{\mathrm{Fl}_s(\Sigma^{\psi}_v)} f\,\mathrm{d}\sigma_{\Sigma^{\psi}_v,g} - \int_{\Sigma^{\psi}_v} f\,\mathrm{d}\sigma_{\Sigma^{f}_v,g}}{s} = \lim_{s\to+\infty}\int_{\Sigma^{\psi}_v}\frac{\mathrm{Fl}^*_s(f\,\mathrm{d}\sigma_{\Sigma^{\psi}_v,g}) - (f\,\mathrm{d}\sigma_{\Sigma^{\psi}_v,g})}{s} = \\ &= \int_{\Sigma^{\psi}_v}\mathcal{L}_{\boldsymbol{\xi}}(f\,\mathrm{d}\sigma_{\Sigma^{\psi}_v,g}) = \int_{\Sigma^{\psi}_v}\chi\mathcal{L}_{\boldsymbol{\nu}}(f\,\mathrm{d}\sigma_{\Sigma^{\psi}_v,g}) = \int_{\Sigma^{\psi}_v}\chi\left[\mathcal{L}_{\boldsymbol{\nu}}(f)\mathrm{d}\sigma_{\Sigma^{\psi}_v,g} + f\mathcal{L}_{\boldsymbol{\nu}}(\mathrm{d}\sigma_{\Sigma^{\psi}_v,g}))\right]\end{aligned} \tag{2.38}$$

where we have used the definition of the Lie derivative $\mathcal{L}_{\boldsymbol{\xi}}$ of forms with respect to the vector field $\boldsymbol{\xi}$, and we used its linearity with respect to reparametrization of the one-parameter group of diffeomorphisms. As

$$\mathcal{L}_{\boldsymbol{\nu}}(\mathrm{d}\sigma_{\Sigma^{\psi}_v,g}) = \mathrm{Tr}^g(\mathrm{II})\mathrm{d}\sigma_{\Sigma^{\psi}_v,g} = \tau_{1,g}\mathrm{d}\sigma_{\Sigma^{\psi}_v,g}\ , \tag{2.39}$$

where II_g is the second fundamental form of the hypersurface Σ^{ψ}_v and $\tau_{1,g}$ is the sum of principal curvatures (see Appendix A), the last expression in eq.(2.38) can be rewritten as

$$\frac{\mathrm{d}F}{\mathrm{d}v}(v) = \int_{\Sigma^{\psi}_v}\chi\left[\mathcal{L}_{\boldsymbol{\nu}}(f) + f\tau_{1,g}\right]\mathrm{d}\sigma_{\Sigma^N_v,g}\,. \tag{2.40}$$

In order to complete the proof it is sufficient to show that $\mathrm{div}_g(f\boldsymbol{\nu})$ is equal to the expression in square brackets in eq.(2.40). Let us choos an adapted orthonormal frame $(\boldsymbol{\nu}, \boldsymbol{e}_1, ..., \boldsymbol{e}_{N-1})$ to

the regular set Σ_v^ψ, we have

$$\begin{aligned}\mathrm{div}_g(f\boldsymbol{\nu}) &= \sum_{i=1}^{N-1} g(\nabla_{\boldsymbol{e}_i}(f\boldsymbol{\nu}), \boldsymbol{e}_i) + g(\nabla_{\boldsymbol{\nu}}(f\boldsymbol{\nu}), \boldsymbol{\nu}) = \\ &= \sum_{i=1}^{N-1} fg(\nabla_{\boldsymbol{e}_i}\boldsymbol{\nu}, \boldsymbol{e}_i) + \sum_{i=1}^{N-1} (\nabla_{\boldsymbol{e}_i} f)\, g(\boldsymbol{\nu}, \boldsymbol{e}_i) + fg(\nabla_{\boldsymbol{\nu}}\boldsymbol{\nu}, \boldsymbol{\nu}) + (\nabla_{\boldsymbol{\nu}} f) g(\boldsymbol{\nu}, \boldsymbol{\nu})\,.\end{aligned} \tag{2.41}$$

Using the definition of the second fundamental form $\mathrm{II}_g(\mathbf{X}, \mathbf{Y}) = g(\nabla_{\mathbf{X}}\boldsymbol{\nu}, \mathbf{Y})$ and the orthormality of the adapted frame we obtain:

$$\mathrm{div}_g(f\boldsymbol{\nu}) = f \sum_{i=1}^{N-1} g(\nabla_{\boldsymbol{e}_i}\boldsymbol{\nu}, \boldsymbol{e}_i) + (\nabla_{\boldsymbol{\nu}} f) = f\mathrm{Tr}^g(\mathrm{II}_g) + \mathcal{L}_{\boldsymbol{\nu}} f = \mathcal{L}_{\boldsymbol{\nu}} f + f\tau_{1,g} \tag{2.42}$$

as the actions of the covariant derivative and of the Lie derivative coincide on functions.

Remark 4. *This results is implicitly contained in the geometrical microcanonical formalism developed by Rugh in [Rug97, Rug98, Rug01] and Franzosi [Fra11]. Nevertheless we present this proof as we are interested to stress the connection among the thermodynamics of a (configurational) microcanonical system and the* ***geometrical properties*** *related with the* ***Riemannian structure*** *of configuration space.*

As a corollary of the theorem above we obtain the following results for Euclidean spaces:

Corollary 2.2.4 (Federer,Laurence ([Fed14][Lau89])). *Let $O \subset \mathbb{R}^p$ be a bounded open set. Let $\psi \in \mathcal{C}^{n+1}(\overline{O})$ be constant on each connected component of the boundary ∂O and $f \in \mathcal{C}^n(O)$. Define $O_{t,t'} = \{x \in O \mid t < \psi(x) < t'\}$ and*

$$F(v) = \int_{\{\psi=v\}} f \ \mathrm{d}\sigma^{p-1} \tag{2.43}$$

where $d\sigma^{p-1}$ represents the Lebesgue measure of dimension $p-1$. If $C > 0$ exists such that for any $x \in O_{t,t'}$, $\|\mathbf{grad}_{\mathbb{R}^p}\psi(x)\|_{\mathbb{R}^p} \geq C$, then for any k such that $0 \leq k \leq n$, for any $v \in]t, t'[$, one has

$$\frac{\mathrm{d}^k F}{\mathrm{d}v^k}(v) = \int_{\{\psi=v\}} A^k_{\psi,\mathbb{R}^p} f \ \mathrm{d}\sigma^{p-1}\ . \tag{2.44}$$

with

$$A_{\psi,\mathbb{R}^p} f = \mathrm{div}_{\mathbb{R}^p}\left(\frac{\mathbf{grad}_{\mathbb{R}^p}\psi}{\|\mathbf{grad}_{\mathbb{R}^p}\psi\|_{\mathbb{R}^p}} f\right) \frac{1}{\|\mathbf{grad}_{\mathbb{R}^p}\psi\|_{\mathbb{R}^p}} \tag{2.45}$$

Remark 5. *The operator $A_{\psi,g}$ acting on the set of C^∞ functions defined over the manifold $\mathcal{B}_N$* ***is not*** *a derivation. Although $A_{\psi,g}$ is $\mathbb{R}$-linear (as it is the sum of $\mathbb{R}$-linear operators),* ***it does***

***not verify the Leibniz rule**, i.e.:*

$$
\begin{aligned}
A_{\psi,g}(fh) &= f_1 f_2 \chi \tau_{1,g} + f_2 \mathcal{L}_{\boldsymbol{\xi}_N}(f_1) + f_1 \mathcal{L}_{\boldsymbol{\xi}_N}(f_2)\chi\tau_{1,g} = f_1(f_2\chi\tau_{1,g} + \mathcal{L}_{\overline{\boldsymbol{\xi}}_N} f_2) + \\
&+ f_2(f_1\chi\tau_{1,g} + \mathcal{L}_{\overline{\boldsymbol{\xi}}_N} f_1) - (f_1 f_2)\chi\tau_{1,g} = \\
&= f_1 A_{\psi,g}(f_2) + f_2 A_{\psi,g}(f_1) - (f_1 f_2)\chi\tau_{1,g} \neq \\
&\neq f_1 A_{\psi,g}(f_2) + f_2 A_{\psi,g}(f_1)\,.
\end{aligned}
\tag{2.46}
$$

for two arbitrary C^∞ functions f_1, f_2 over $\mathcal{B}_N$

Theorem 2.2.3 allows also to calculate higher order derivatives of the microcanonical partition function $\Omega_n(\bar{v})$ at any order.

Corollary 2.2.5 (Higher order derivatives of the microcanonical partition function)**.** *Let O be an open bounded set of a N-dimensional Riemannian manifold Λ_q, g and let ∇ be a Levi-Civita connection. Let $\overline{V}_N \in \mathcal{C}^{p+1}(\overline{O})$ be a generalized potential constant on each connected component of the boundary $\partial\overline{O}$ and $f \in \mathcal{C}^p(O)$. Define $M^N_{]\bar{v}_0,\bar{v}_1[} = \left\{x \in O | \bar{v}_0 < \overline{V}_N(x) < \bar{v}_1\right\}$ and*

$$
\Omega_N(\bar{v}) = \int_{\Sigma^N_{\bar{v}}} \mathrm{d}\mu^{N-1}_{\bar{v}} \tag{2.47}
$$

where $\mathrm{d}\mu^{N-1}_{\bar{v}}$ is the microcanonical $(N-1)$-area-form of eq.(2.32) induced over $\int_{\Sigma^N_{\bar{v}}}$. If there exists $C > 0$ such that for any $M^N_{]\bar{v}_0,\bar{v}_1[}$, $\|\mathbf{grad}_g \overline{V}_N(x)\|_g \geq C$, and if the level sets $\Sigma^N_{\bar{v}}$ of $\overline{V}_N$ are without boundary, then for any k such that $0 \leq k \leq p$, for any $\bar{v} \in]\bar{v}_0, \bar{v}_1[$, one has

$$
\frac{\mathrm{d}^k \Omega_N}{\mathrm{d}\overline{v}^k}(\bar{v}) = \int_{\Sigma^f_{\bar{v}}} A^k_\mu(1)\, \mathrm{d}\mu^{N-1}_{\bar{v}} \tag{2.48}
$$

with

$$
A_\mu(f) = f \mathrm{div}_g\left(\overline{\boldsymbol{\xi}}_N\right) + \overline{\chi}_N \mathcal{L}_{\boldsymbol{\nu}_N}(f) = f\overline{\zeta}_N + \mathcal{L}_{\overline{\boldsymbol{\xi}}_N}(f) \tag{2.49}
$$

Remark 6 (Derivatives of $\Omega_N(\bar{v})$ and properties of diffeomorphisms of level sets)**.** *Equations (2.48) and (2.49) relate the thermodynamic behaviour of the system considered (higher derivatives of microcanonical partition function) with the diffeomorphic properties of equipotential level sets through the scalar quantities related to the vector field $\overline{\boldsymbol{\xi}}_N$: its divergence $\overline{\zeta}_N$ and its module $\overline{\chi}_N$. This would lead to the conclusion that some suitable analytical constraint on the behaviour of $\overline{\zeta}_N$ and $\overline{\chi}_N$ can determine the absence of phase transitions in certain given family of level sets.*

Resorting to the above given formulas, we can readily express the derivatives of the microcanonical entropy as integrals of quantities over hypersurfaces only related to vector field $\overline{\boldsymbol{\xi}}_N$. This is an important point because it constitutes the key point to understand the origin of the difficulty of the present formulation of the Necessity Theorem.
Equations(2.48) and eqs.(2.49) allow to derive the links between microcanonical thermodynamics on one side and the geometrical properties of the vector field $\overline{\boldsymbol{\xi}}_N$ on the other side. The core

of the proof of Necessity Theorem (Theorem 1.4.2) consists in constructing uniform bounds in N for the derivatives of configurational microcanonical entropy $\overline{S}_N(\bar{v})$ up to the fourth order: so we begin by calculating the derivatives of configurational microcanonical partition function $\Omega_N(\bar{v})$ up to the fourth order with respect to $\bar{v}$

$$
\begin{aligned}
\frac{\mathrm{d}\Omega_N}{\mathrm{d}\bar{v}}(\bar{v}) &= \int_{\Sigma_{\bar{v}}^{\overline{V}_N}} \overline{\zeta}_N \, \mathrm{d}\mu_{\bar{v}}^{N-1} \\
\frac{\mathrm{d}^2\Omega_N}{\mathrm{d}\bar{v}^2}(\bar{v}) &= \int_{\Sigma_{\bar{v}}^{\overline{V}_N}} \left[\overline{\zeta}_N^2 + \mathcal{L}_{\overline{\boldsymbol{\xi}}_N}(\overline{\zeta}_N)\right] \mathrm{d}\mu_{N\bar{v}}^{N-1} \\
\frac{\mathrm{d}^3\Omega_N}{\mathrm{d}\bar{v}^3}(\bar{v}) &= \int_{\Sigma_{\bar{v}}^{\overline{V}_N}} \left[\overline{\zeta}_N^3 + 3\overline{\zeta}_N \mathcal{L}_{\overline{\boldsymbol{\xi}}_N}\left(\overline{\zeta}_N\right) + \mathcal{L}_{\overline{\boldsymbol{\xi}}_N}^{(ii)}(\overline{\zeta}_N)\right] \mathrm{d}\mu_{\bar{v}}^{N-1} \\
\frac{\mathrm{d}^4\Omega_N}{\mathrm{d}\bar{v}^4}(\bar{v}) &= \int_{\Sigma_{\bar{v}}^{\overline{V}_N}} \left[\overline{\zeta}_N^4 + 6\overline{\zeta}_N^2 \mathcal{L}_{\overline{\boldsymbol{\xi}}_N}(\overline{\zeta}_N) + 4\overline{\zeta}_N \mathcal{L}_{\overline{\xi}_N}^{(ii)}(\overline{\zeta}_N) + 3\left(\mathcal{L}_{\overline{\boldsymbol{\xi}}_N}(\overline{\zeta}_N)\right)^2 + \mathcal{L}_{\overline{\boldsymbol{\xi}}_N}^{(iii)}(\overline{\zeta}_N)\right] \mathrm{d}\mu_{\bar{v}}^{N-1}
\end{aligned}
\tag{2.50}
$$

We recall that the configurational microcanonical entropy density is given by

$$
\overline{S}_N(\overline{v}) = \frac{1}{N} \ln \Omega_N(\overline{v}) = \frac{1}{N} \ln \int_{\Sigma_{\bar{v}}^{\overline{V}_N}} \mathrm{d}\mu_{\overline{v}}^{N-1} \tag{2.51}
$$

so its derivatives are given by:

$$
\begin{aligned}
\frac{\mathrm{d}\overline{S}_N}{\mathrm{d}\overline{v}}(\overline{v}) &= \frac{1}{N}\frac{\Omega_N'(\overline{v})}{\Omega_N(\overline{v})} \\
\frac{\mathrm{d}^2\overline{S}_N}{\mathrm{d}\overline{v}^2}(\overline{v}) &= \frac{1}{N}\left[\frac{\Omega_N''(\overline{v})}{\Omega_N(\overline{v})} - \left(\frac{\Omega_N'(\overline{v})}{\Omega_N(\overline{v})}\right)^2\right] \\
\frac{\mathrm{d}^3\overline{S}_N}{\mathrm{d}\overline{v}^3}(\overline{v}) &= \frac{1}{N}\left[\frac{\Omega_N'''(\overline{v})}{\Omega_N(\overline{v})} - 3\frac{\Omega_N''(\overline{v})}{\Omega_N(\overline{v})}\frac{\Omega_N'(\overline{v})}{\Omega_N(\overline{v})} + 2\left(\frac{\Omega_N'(\overline{v})}{\Omega_N(\overline{v})}\right)^3\right] \\
\frac{\mathrm{d}^4\overline{S}_N}{\mathrm{d}\overline{v}^4}(\overline{v}) &= \frac{1}{N}\left[\frac{\Omega_N^{(iv)}(\overline{v})}{\Omega_N(\overline{v})} - 4\frac{\Omega_N'''(\overline{v})\Omega_N'(\overline{v})}{\Omega_N^2(\overline{v})} + 12\frac{\Omega_N'^2(\overline{v})\Omega_N''(\overline{v})}{\Omega_N^3(\overline{v})} - 3\left(\frac{\Omega_N''(\overline{v})}{\Omega_N(\overline{v})}\right)^2 - 6\left(\frac{\Omega_N'(\overline{v})}{\Omega_N(\overline{v})}\right)^4\right].
\end{aligned}
\tag{2.52}
$$

To express also the derivatives of the microcanonical entropy density in terms of the scalar functions $\overline{\chi}_N$ and $\overline{\zeta}_N$, and of their Lie derivatives with respect to the vector field $\overline{\boldsymbol{\xi}}_N$, it is convenient to introduce the following notation for the average of a generic measurable function $f : M^N \to \mathbb{R}$ over the hypersurface $\Sigma_{\bar{v}}^{\overline{V}_N}$ endowed with microcanonical measure $\mathrm{d}\mu_{\bar{v}}^{N-1}$.

$$
\langle f \rangle_{\overline{v},\mu} = \frac{\displaystyle\int_{\Sigma_{\bar{v}}^{\overline{V}_N}} f \mathrm{d}\mu_{\overline{v}}^{N-1}}{\displaystyle\int_{\Sigma_{\bar{v}}^{\overline{V}_N}} \mathrm{d}\mu_{\overline{v}}^{N-1}} = \frac{\displaystyle\int_{\Sigma_{\bar{v}}^{\overline{V}_N}} f \mathrm{d}\mu_{\overline{v}}^{N-1}}{\Omega_N(\overline{v})} . \tag{2.53}
$$

Consequently, we introduce the quantities

$$
\begin{aligned}
&\mathrm{Var}_{\overline{v},\mu}(f) = \mathrm{Cuml}^{(2)}_{\overline{v},\mu}(f) = \left\langle f^2 \right\rangle_{\overline{v},\mu} - \langle f \rangle^2_{\overline{v},\mu} \\
&\mathrm{Corr}_{\overline{v},\mu}(f;g) = \langle fg \rangle_{\overline{v},\mu} - \langle f \rangle_{\overline{v},\mu} \langle g \rangle_{\overline{v},\mu} \\
&\mathrm{Cuml}^{(3)}_{\overline{v},\mu}(f) = \left\langle f^3 \right\rangle_{\overline{v},\mu} - 3 \langle f \rangle_{\overline{v},\mu} \left\langle f^2 \right\rangle_{\overline{v},\mu} + 2 \langle f \rangle^3_{\overline{v},\mu} \\
&\mathrm{Cuml}^{(4)}_{\overline{v},\mu}(f) = \left\langle f^4 \right\rangle_{\overline{v},\mu} - 4 \left\langle f^3 \right\rangle_{\overline{v},\mu} \langle f \rangle_{\overline{v},\mu} + 12 \left\langle f^2 \right\rangle_{\overline{v},\mu} \langle f \rangle^2_{\overline{v},\mu} - 3 \left\langle f^2 \right\rangle^2_{\overline{v},\mu} - 6 \langle f \rangle^4_{\overline{v},\mu}
\end{aligned}
\tag{2.54}
$$

which represent the variance, the correlation function, and the 3rd and 4th order cumulants on the hypersurface $\Sigma^{\overline{V}_N}_{\overline{v}}$ with measure $\mathrm{d}\mu^{N-1}_{\overline{v}}$, respectively.

With this notation and substituting eqs.(2.50) in eqs.(2.52) it is possible to show that the derivatives of the microcanonical entropy at a non critical value $\overline{v}$, and at fixed N, can be tightly related to the vector field $\overline{\boldsymbol{\xi}}_N$ which generates the diffeomorphisms among the equipotential level sets:

$$
\begin{aligned}
&\frac{\mathrm{d}\overline{S}_N}{\mathrm{d}\overline{v}}(\overline{v}) = \frac{1}{N} \left\langle \overline{\zeta}_N \right\rangle_{\overline{v},\mu} \\
&\frac{\mathrm{d}^2\overline{S}_N}{\mathrm{d}\overline{v}^2}(\overline{v}) = \frac{1}{N} \left[\mathrm{Var}_{\overline{v},\mu}(\overline{\zeta}_N) + \left\langle \mathcal{L}_{\overline{\boldsymbol{\xi}}_N}(\overline{\zeta}_N) \right\rangle_{N\overline{v},\mu} \right] \\
&\frac{\mathrm{d}^3\overline{S}_N}{\mathrm{d}\overline{v}^3}(\overline{v}) = \frac{1}{N} \left[\mathrm{Cuml}^{(3)}_{\overline{v},\mu}(\overline{\zeta}_N) + 3\mathrm{Corr}_{\overline{v},\mu}\left(\overline{\zeta}_N; \mathcal{L}_{\overline{\boldsymbol{\xi}}_N}(\overline{\zeta}_N)\right) + \left\langle \mathcal{L}^{(ii)}_{\overline{\boldsymbol{\xi}}_N}\left(\overline{\zeta}_N\right) \right\rangle_{\overline{v},\mu} \right] \\
&\frac{\mathrm{d}^4\overline{S}_N}{\mathrm{d}\overline{v}^4}(\overline{v}) = \frac{1}{N} \Bigg[\mathrm{Cuml}^{(4)}_{\overline{v},\mu}(\overline{\zeta}_N) + 6\mathrm{Corr}_{\overline{v},\mu}\left(\overline{\zeta}^2_N; \mathcal{L}_{\overline{\boldsymbol{\xi}}_N}(\overline{\zeta}_N)\right) + 3\mathrm{Var}_{\overline{v},\mu}\left(\mathcal{L}_{\overline{\boldsymbol{\xi}}_N}(\overline{\zeta}_N)\right) + \\
&+ 4\mathrm{Corr}_{\overline{v},\mu}\left(\overline{\zeta}_N; \mathcal{L}^{(ii)}_{\overline{\boldsymbol{\xi}}_N}(\overline{\zeta}_N)\right) - 12 \left\langle \overline{\zeta}_N \right\rangle_{\overline{v},\mu} \mathrm{Corr}_{N\overline{v},\mu}\left(\overline{\zeta}_N; \mathcal{L}_{\overline{\boldsymbol{\xi}}_N}(\overline{\zeta}_N)\right) + \left\langle \mathcal{L}^{(iii)}_{\overline{\boldsymbol{\xi}}_N}\left(\overline{\zeta}_N\right) \right\rangle_{\overline{v},\mu} \Bigg] = \\
&= \frac{1}{N} \Bigg[\mathrm{Cuml}^{(4)}_{\overline{v},\mu}(\overline{\zeta}_N) + 4\mathrm{Corr}_{\overline{v},\mu}\left(\overline{\zeta}_N; \mathcal{L}^{(ii)}_{\overline{\boldsymbol{\xi}}_N}(\overline{\zeta}_N)\right) + 3\mathrm{Var}_{\overline{v},\mu}\left(\mathcal{L}_{\overline{\boldsymbol{\xi}}_N}(\overline{\zeta}_N)\right) + \\
&+ 6 \left\langle \overline{\zeta}_N \right\rangle_{\overline{v},\mu} \left(\mathrm{Corr}_{\overline{v},\mu}\left(\Delta\overline{\zeta}_N; \mathcal{L}_{\overline{\boldsymbol{\xi}}_N}(\overline{\zeta}_N)\right)\right) + \left\langle \mathcal{L}^{(iii)}_{\overline{\boldsymbol{\xi}}_N}\left(\overline{\zeta}_N\right) \right\rangle_{\overline{v},\mu} \Bigg]
\end{aligned}
\tag{2.55}
$$

where for sake of simplicity we have introduced the quantity

$$
\Delta\overline{\zeta}_N = \frac{\overline{\zeta}^2_N}{\left\langle \overline{\zeta}_N \right\rangle_{\overline{v},\mu}} - 2\overline{\zeta}_N \ . \tag{2.56}
$$

As mentioned above, the first important consequence that can be argued by eqs.(2.55) is that, in principle, it is possible to directly control the behaviour of microcanonical entropy and its derivatives at any finite N and in the thermodynamic limit. This is obtained by imposing some conditions on the behaviour of the components of the vector $\overline{\boldsymbol{\xi}}_N$.

This result opens the possibility to refine the Pettini-Franzosi Theorem. In fact, the requirement of diffeomorphicity among the equipotential level sets at *any finite* N - in a given interval of $\overline{v}$ values - is not sufficient to avoid the occurrence of a phase transition in the *thermodynamic limit*

in the same interval of specific potential energy values. Thanks to eqs.(2.55) it is possible to control *asymptotically* in N "how" and/or "how much" the level sets have to be diffeomorphic among themselves in order to prevent the occurrence of phase transitions. This is shown in what follows.

2.3 Results of simulation on φ^4-model on 2D-lattice

In this Section we present the results of Monte Carlo numerical simulations on equipotential level set of the φ^4-model on a 2d-lattice with periodic boundary conditions (PBC) to calculate the geometrical averages appearing in eqs.(2.55). This study has been performed in order to identify which terms composing the derivatives of the specific configurational microcanonical entropy with respect to the specific potential energy is not uniformly bounded in N, as is expected according to the proof of Theorem 1.4.2.
The simulations have been performed using the same codes used to obtain the results reported in subsection 2.1.4, for systems with a total number of degrees of freedom $N = 10 \times 10 = 100$, $N = 20 \times 20 = 400$, $N = 30 \times 30 = 900$, $N = 40 \times 40 = 1600$ and $N = 50 \times 50 = 2500$. The simulations were performed with vanishing magnetization as initial condition, for 2×10^7 steps, a number sufficient to guarantee the convergence of the reported quantities.

Numerical results on $\partial_{\bar{v}}\overline{S}_N$ and related quantities

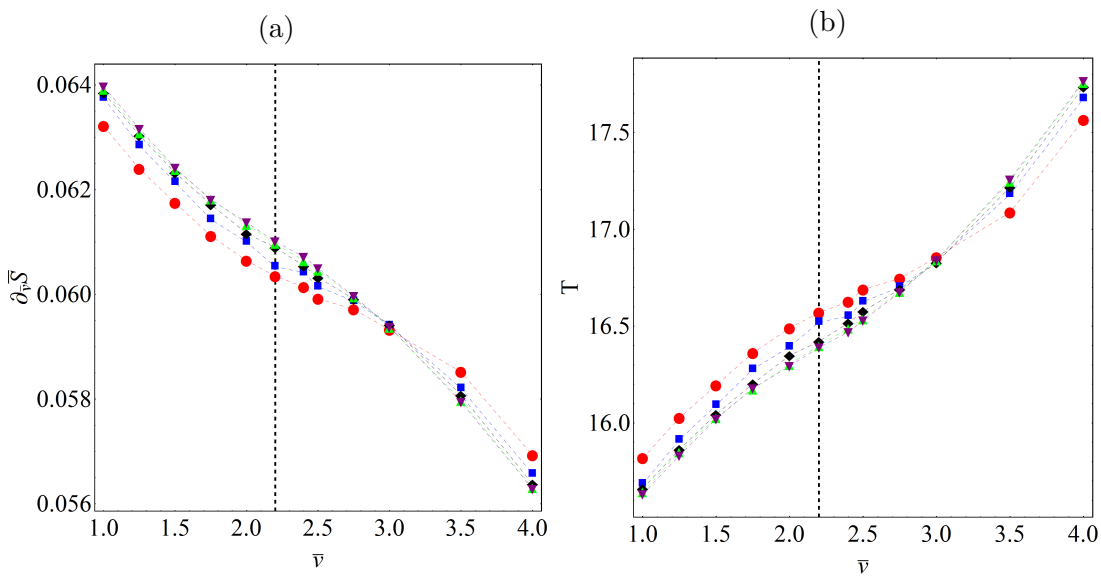

Figure 2.5: First order derivative of configurational microcanonical entropy with respect to specific energy $\bar{v}$ (a) and caloric curve (b) for lattices with different N; in particular, $N = 100$ (red dots), $N = 400$ (blue squares), $N = 900$ (black diamonds), $N = 1600$ (green triangles), $N = 2500$ (purple reversed triangles).

In what follows the results are reported for the first derivative of the specific microcanonical configuration entropy with respect to $\bar{v}$ as a function of $\bar{v}$ (Figure 2.5). An inflection point is

found around the transition value $\bar{v} \sim 2.2$; this result is compatible with what is expected from a statistical analysis in the microcanonical ensemble.
In analogy with microcanonical statistical mechanics, the *configurationl microcanonical temperature* T is defined as the inverse of the first derivative of specific configurational microcanonical entropy with respect to $\bar{v}$:

$$T(\bar{v}) = \left(\frac{\partial \overline{S}_N}{\partial \bar{v}} \right)^{-1} \tag{2.57}$$

and the plot of this function on the $\bar{v}$-T plane is the configurational *caloric curve*. The results in this case (see Figure 2.5) show a qualitative agreement with the caloric curve computed in the microcanonical ensemble (cfr.[CCP98]).

Numerical results on $\partial^2_{\bar{v}} \overline{S}_N$ and related quantities

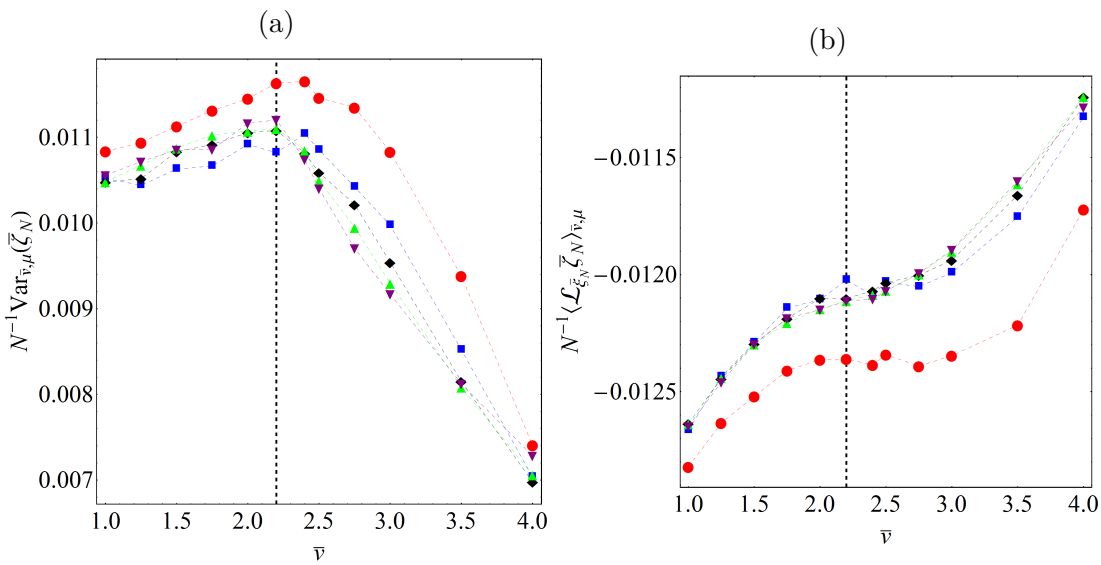

Figure 2.6: Variance of $\overline{\zeta}_N$ (a) and average of Lie derivative of $\overline{\zeta}_N$ with respect to the vector field $\overline{\boldsymbol{\xi}}_N$ generating the diffeomorphism among equipotential level sets vs. the specific energy $\bar{v}$ for lattices with different N. In particular, $N = 100$ (red dots), $N = 400$ (blue squares), $N = 900$ (black diamonds), $N = 1600$ (green triangles), $N = 2500$ (purple reversed triangles).

In this subsection the behaviour of the second derivative of the specific microcanonical configurational entropy and related quantities are studied. In Figure 2.6 we report the variance of $\overline{\zeta}_N$ and its Lie derivative along $\overline{\boldsymbol{\xi}}_N$ averaged on $\Sigma_{\bar{v}}^{\overline{V}_N}$ endowed with the configurational microcanonical measure. The sum of these two contributions gives rise to the second derivative of the configurational microcanonical entropy with respect to $\bar{v}$. These two terms have opposite signs: the variance of $\overline{\zeta}_N$ is positive by definition, while the average of its Lie derivative is negative. Hence, the behaviour of the second order derivative of the configurational microcanonical entropy is given by the competition between these two terms. In particular, we stress that a phase transition is signaled by a non strictly concave microcanonical entropy according to microcanonical statistical analysis: in the framework here proposed, a phase transition would be induced when the variance of $\overline{\zeta}_N$ its greater or equal to the average of its derivatives along

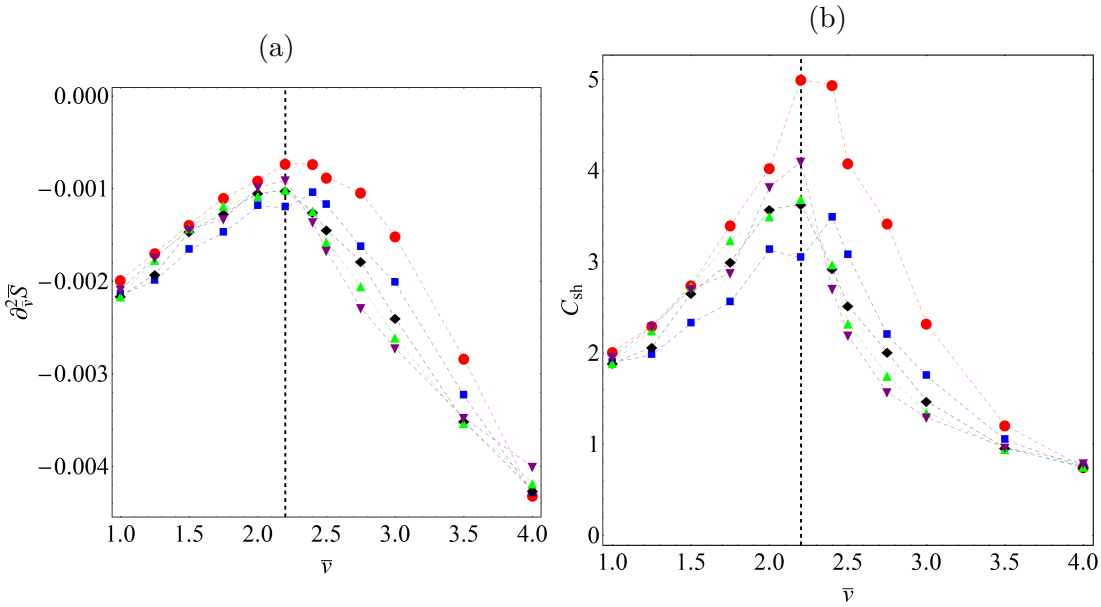

Figure 2.7: Second order derivative of configurational microcanonical specific entropy with respect to specific energy (a) and the configurationl specific heat vs. the specific energy $\bar{v}$ for lattices with different N. In particular, $N = 100$ (red dots), $N = 400$ (blue squares), $N = 900$ (black diamonds), $N = 1600$ (green triangles), $N = 2500$ (purple reversed triangles).

the flow generating the diffeomorphisms. This fact could suggest a stronger "inhomogeneity" of the equipotential level sets near the critical value of the specific potential energy.

The results reported in Figure 2.6 (b) evidenciate that a relative maximum of the variance $\overline{\zeta}_N$ on the equipotential level sets is present at the transition point. This affects the behaviour of the second derivative of the configurational microcanonical entropy (see Figure 2.7 (a)) with respect to $\bar{v}$: it shows a maximum around the transition point $\bar{v} \sim 2.2$ that does not seem to vanish with N as is expected for a second order phase transition. This counter intuitive phenomenology seems to be compatible with finite-size effects already reported in the literature for the φ^4-model on a 2d lattice studied in the microcanonical ensemble. In fact, in [BPH05] it is reported that the negative value of the minimum of the microcanonical entropy has a non monotonic N-dependence at the transition point: at increasing N it initially decreases and then it increases tending towards zero.

As for the temperature, it is possible to define a *configurational microcanonical specific heat* in analogy with the common definition in the microcanonical ensemble:

$$C_{sh}(\bar{v}) = \frac{\mathrm{d}\bar{v}}{\mathrm{d}T} = -\frac{\left(\frac{\partial \overline{S}_N}{\partial \bar{v}}\right)^2}{\frac{\partial^2 \overline{S}_N}{\partial \bar{v}^2}} \,. \tag{2.58}$$

As can be observed in Figure 2.7(b), this observable seems to show a slightly divergent behaviour only for very high N. This can be explained by the fact that the divergence of specific heat for this model is logarithmic: further (computationally heavy) investigations would be required to better evidence the transitional features.

Numerical results on $\partial^3_{\bar{v}}\overline{S}_N$ and related quantities

$f(\bar{v})$	$\mathrm{d}f/\mathrm{d}\bar{v}$
$\mathrm{Var}_{N\bar{v},\mu}(\overline{\zeta}_N)$	$\mathrm{Cumul}^{(3)}_{N\bar{v},\mu}\left(\overline{\zeta}_N\right) + 2\mathrm{Corr}_{N\bar{v},\mu}\left(\overline{\zeta}_N; \mathcal{L}_{\overline{\boldsymbol{\xi}}_N}\overline{\zeta}_N\right)$
$\left\langle \mathcal{L}_{\overline{\boldsymbol{\xi}}_N}\overline{\zeta}_N \right\rangle_{N\bar{v},\mu}$	$\left\langle \mathcal{L}^{(ii)}_{\overline{\boldsymbol{\xi}}_N}\overline{\zeta} \right\rangle_{N\bar{v},\mu} + \mathrm{Corr}_{N\bar{v},\mu}\left(\overline{\zeta}_N; \mathcal{L}_{\overline{\boldsymbol{\xi}}_N}\overline{\zeta}_N\right)$

Table 2.1: Components of third derivative of specific configurational microcanonical entropy with respect to $\bar{v}$.

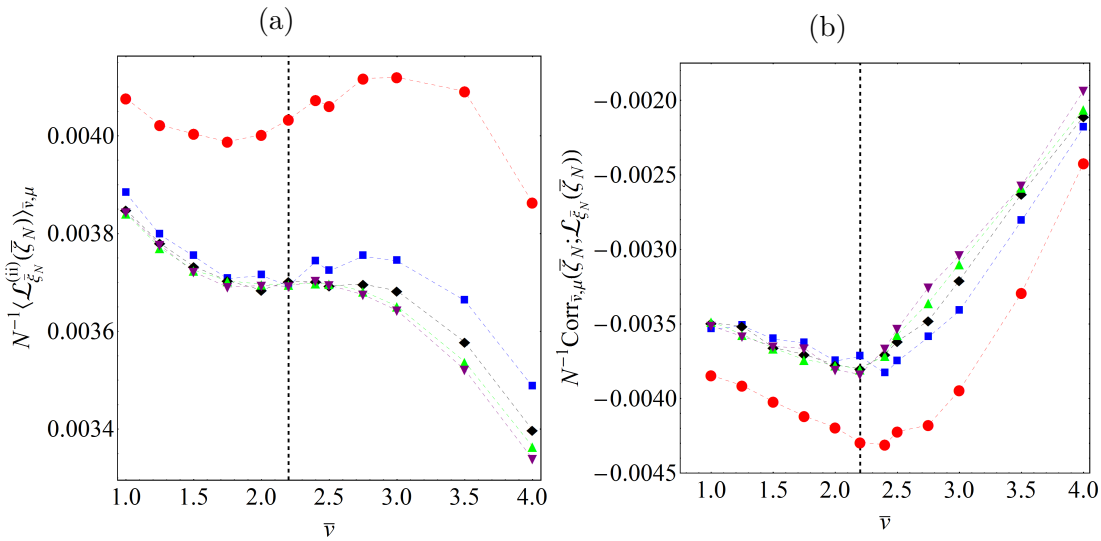

Figure 2.8: Average over the regular equipotential level sets of the second order Lie derivative of $\overline{\zeta}_N$ in direction $\overline{\boldsymbol{\xi}}_N$ (a) and correlation with respect to configurational microcanoinical measure μ between $\overline{\zeta}_N$ and its derivative in direction $\overline{\boldsymbol{\xi}}_N$ vs. the specific energy $\bar{v}$ for lattices with different N. In particular, $N = 100$ (red dots), $N = 400$ (blue squares), $N = 900$ (black diamonds), $N = 1600$ (green triangles), $N = 2500$ (purple reversed triangles).

In this Subsection we present the results of numerical simulations for the third derivative of the configurational microcanonical entropy with respect to $\bar{v}$, and for its related geometrical quantities. In the classical formulation of Franzosi-Pettini Theorems the loss of analyticity of the second order derivative of the Helmholtz free energy is expected to be associated with a loss of analyticity of the third order derivative of specific configurational microcanonical entropy with respect to $\bar{v}$. Hence the study of the single terms entering it is important because it allows to identify which terms can be responsible for its asymptotic loss of analyticity. In Table 2.1 are reported the derivatives of each term entering the second order derivative of the specific configurational microcanonical entropy according to eqs.(2.55).

The results show that the third order derivative of the specific configurational microcanonical entropy tends toward a step-like pattern - which gets steeper at increasing N - in coincidence of the critical value of the specific potential energy $\bar{v} \sim 2.2$ (see Figure 2.9(b)).

This means that *a priori* there would be at least one term entering the third order derivative of specific configurational microcanonical energy whose derivative diverges at the critical specific energy. The results reported in Figure 2.8 show that the second order Lie derivative of $\overline{\zeta}_N$ with

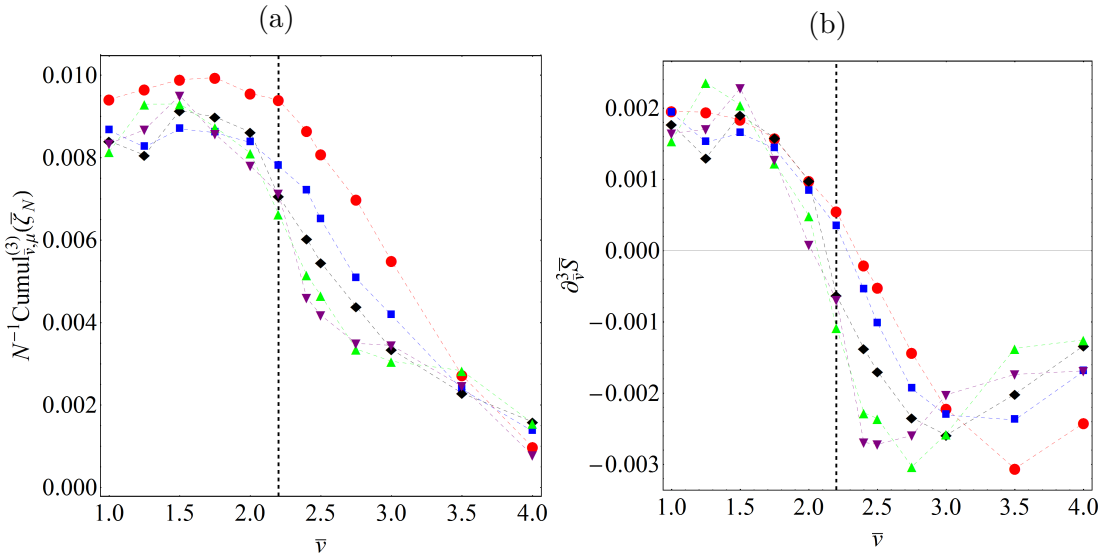

Figure 2.9: Third cumulant of $\overline{\zeta}_N$ with respect to configurational microcanonical measure (a) and specific microcanonical configurational entropy vs. the specific energy $\bar{v}$ for lattices with different N. In particular, $N = 100$ (red dots), $N = 400$ (blue squares), $N = 900$ (black diamonds), $N = 1600$ (green triangles), $N = 2500$ (purple reversed triangles).

$f(\bar{v})$	$\mathrm{d}f/\mathrm{d}\bar{v}$
$\mathrm{Cuml}^{(3)}_{N\bar{v},\mu}\overline{\zeta}_N$	$\mathrm{Cuml}^{(4)}_{N\bar{v},\mu}\overline{\zeta} + 3\left\langle\overline{\zeta}_N\right\rangle_{\bar{v},\mu}\left(\mathrm{Corr}_{\bar{v},\mu}\left(\Delta\overline{\zeta}_N;\mathcal{L}_{\overline{\boldsymbol{\xi}}_N}(\overline{\zeta}_N)\right)\right)$
$\mathrm{Corr}_{N\bar{v},\mu}\left(\overline{\zeta}_N;\mathcal{L}_{\overline{\boldsymbol{\xi}}_N}\overline{\zeta}_N\right)$	$\mathrm{Corr}_{N\bar{v},\mu}\left(\overline{\zeta}_N;\mathcal{L}^{(ii)}_{\overline{\boldsymbol{\xi}}_N}\overline{\zeta}_N\right) + \mathrm{Var}_{N\bar{v},\mu}\left(\mathcal{L}_{\overline{\boldsymbol{\xi}}_N}\overline{\zeta}_N\right) + $ $+\left\langle\overline{\zeta}_N\right\rangle_{N\bar{v},\mu}\mathrm{Corr}_{N\bar{v},\mu}\left(\Delta\overline{\zeta}_N;\mathcal{L}_{\overline{\boldsymbol{\xi}}_N}\overline{\zeta}_N\right)$
$\left\langle\mathcal{L}_{\overline{\boldsymbol{\xi}}_N}\overline{\zeta}_N\right\rangle$	$\mathrm{Corr}_{N\bar{v},\mu}\left(\overline{\zeta}_N;\mathcal{L}^{(ii)}_{\overline{\boldsymbol{\xi}}_N}\overline{\zeta}_N\right) + \left\langle\mathcal{L}^{(iii)}_{\overline{\boldsymbol{\xi}}_N}\overline{\zeta}_N\right\rangle$

Table 2.2: Components of third order derivative of specific configurational microcanonical entropy with respect to $\bar{v}$.

respect to $\overline{\boldsymbol{\xi}}_N$, and the correlation between $\overline{\zeta}_N$ and its first order Lie derivative along $\overline{\boldsymbol{\xi}}_N$, are not responsible for any divergence because at the critical potential energy they have an inflection point and a relative minimum, respectively.

The only term whose derivative seems to diverge at the critical potential energy value is the third order cumulant of $\overline{\zeta}_N$ (properly rescaled with N), that exhibits a step like behaviour analogous to the one of the third order derivative of the entropy. This means that at least one term appearing in the derivative with respect to $\bar{v}$ of the third order cumulant of $\overline{\zeta}_N$ diverges at increasing N.

Numerical results on $\partial^4_{\bar{v}}\overline{S}_N$ and related quantities

In this Subsection the results concerning the fourth order derivative of configurational microcanonical entropy with respect to specific potential energy $\bar{v}$ and the related terms are reported. As discussed in the previous Subsection, the step-like profile of the third order derivative of the entropy implies a (negative) divergence with N of the fourth order derivative of the specific

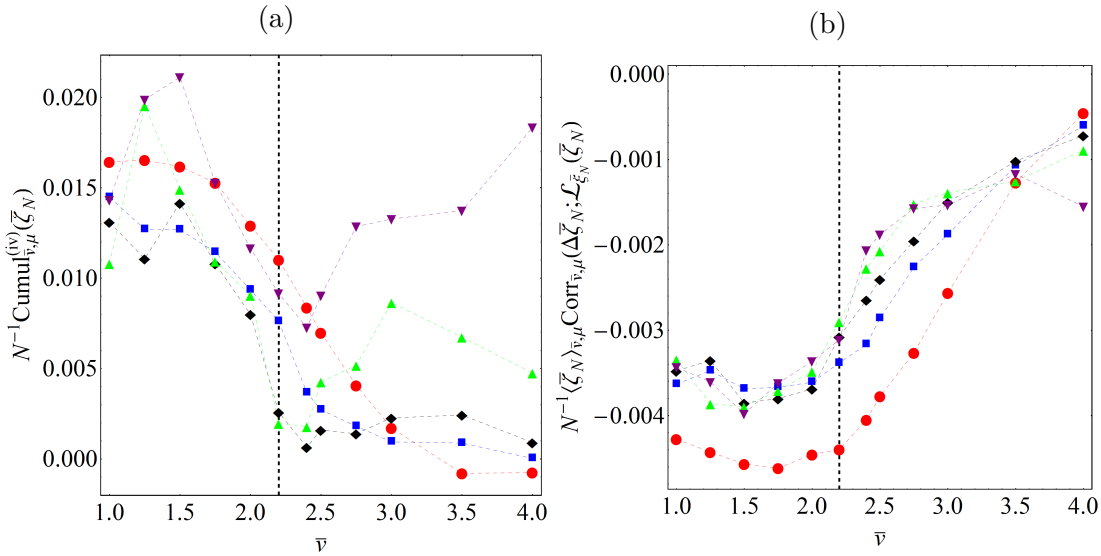

Figure 2.10: Components of the derivative of the third order cumulants of $\overline{\zeta}_N$ with respect $\bar{v}$: fourth order cumulant of $\overline{\zeta}_N$ (a) and correlation terms (b) vs. the specific energy $\bar{v}$ for lattices with different N. In particular, $N = 100$ (red dots), $N = 400$ (blue squares), $N = 900$ (black diamonds), $N = 1600$ (green triangles), $N = 2500$ (purple reversed triangles).

configurational microcanonical entropy: this is generated by some divergence in the derivative of third order cumulant of $\overline{\zeta}_N$ with respect to $\bar{v}$. In Table 2.2 it is remarked that only two terms contribute to the derivative of the third cumulant of $\overline{\zeta}_N$: the fourth order cumulant of $\overline{\zeta}_N$ and a very complex correlation term involving $\overline{\zeta}_N$ and its Lie derivatives with respect to $\overline{\boldsymbol{\xi}}_N$. The results from numerical simulations on these two terms are reported in Figure 2.10.

The correlation term (see Figure 2.10 (b)) does not present any divergent behaviour with N as the sequence of functions converges to a bounded function. It follows that the divergence of the fourth order derivative of the configurational microcanonical entropy can be only due to the fourth cumulant of $\overline{\zeta}_N$, rescaled by N^{-1}.

This idea is supported by the numerical results on the other terms that enter in the fourth order derivative of the entropy (see Figure 2.12 and Figure 2.12 (b)) converges uniformly in N to bounded functions in an interval of $\bar{v}$ containing the critical value. The results of numerical calculation of the fourth order cumulant of $\overline{\zeta}_N$ are reported in Figure 2.10 (a): a behaviour coherent with a negative increasing peak in correspondence of the critical value of potential energy is observed for $N \leq 1600$. The results obtained for $N = 2500$ are not reliable because the numerical computation of a fourth cumulant requires a huge computational effort as N increases because of the slowing down of convergence rate with respect to what happens for the averages, correlations and variances. Great quantitative and qualitative differences in the profile of this cumulant are found for different Monte Carlo simulations at a fixed large N value. Moreover, as the fourth cumulant dominates the behaviour of the fourth order derivative of the entropy with respect to $\bar{v}$ its asymptotic negative divergence cannot be observed for large values of N.

Nevertheless, the information that can be retrieved from the profile of the third order derivative of the microcanonical entropy allows to inductively conclude that *the term* $N^{-1}\mathrm{Cumul}^{(4)}_{N\bar{v},\mu}\overline{\zeta}_N$

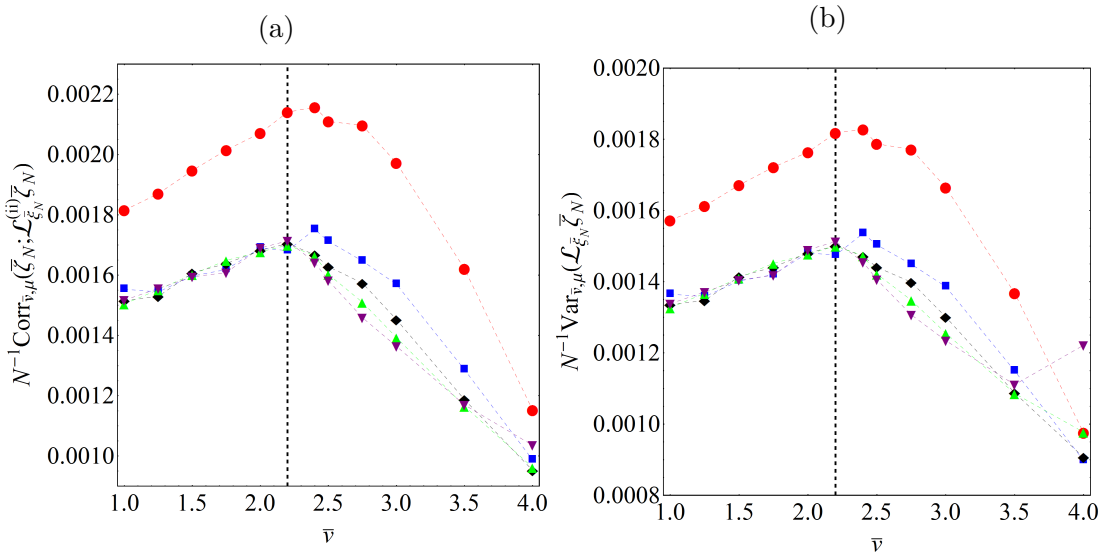

Figure 2.11: Correlation of the second order Lie derivative of $\overline{\zeta}_N$ and $\overline{\zeta}_N$ (a) and variance of Lie derivative of $\overline{\zeta}_N$ with respect to $\overline{\boldsymbol{\xi}}_N$ vs. the specific energy $\bar{v}$ for lattices with different N. In particular, $N = 100$ (red dots), $N = 400$ (blue squares), $N = 900$ (black diamonds), $N = 1600$ (green triangles), $N = 2500$ (purple reversed triangles).

is not uniformly bounded in N, and this contradicts an intermediated result in proof[6] *of Theorem 1.4.2 where the same term is predicted to vanish for $N \to +\infty$.*

2.3.1 From the numerical simulation to the revision of the Franzosi-Pettini necessity Theorem: outlooks and perspectives

The results presented above guide the theoretical search for conditions that have to be added to the hypotheses of the Necessity Theorem 1.4.2 both to exclude the ϕ^4-model on 2d lattice from the domain of validity of the same theorem and, consequently, to provide its generalization and a refinement of the whole Topological Theory of phase transitions.
The main way to provide such a refinement should seem to fulfil two main requirements:

[6] *In the original formulation of the theorem the bounds where derived for the average, variance and cumulants of $A(\chi_N)/\chi_N$ which corresponds, in our notation, to the divergence of $\boldsymbol{\xi}_N$*

$$\frac{A(\chi_N)}{\chi_N} = \zeta_N = \mathrm{div}_g \boldsymbol{\xi_N} = \mathrm{div}_g \frac{\mathbf{grad}_g V_N}{\|\mathbf{grad}_g V_N\|^2} = N \mathrm{div}_g \frac{\mathbf{grad}_g \overline{V}_N}{\|\mathbf{grad}_g \overline{V}_N\|^2} = N\overline{\zeta}_N \,. \tag{2.59}$$

For this terms, under the hypothesis of the theorem, the following uniform bounds are derived

$$\begin{aligned}
&\lim_{N\to+\infty} \langle \zeta_N \rangle_{N\bar{v},\mu} = \lim_{N\to+\infty} N^{-1} \langle \overline{\zeta}_N \rangle_{N\bar{v},\mu} \mathbb{R} \\
&\lim_{N\to+\infty} N\mathrm{Var}_{N\bar{v},\mu}\zeta_N = \lim_{N\to+\infty} N^{-1}\mathrm{Var}_{N\bar{v},\mu}\overline{\zeta}_N \in \mathbb{R}^+ \\
&\lim_{N\to+\infty} N^2\mathrm{Cumul}^{(3)}_{N\bar{v},\mu}\zeta_N = \lim_{N\to+\infty} N^{-1}\mathrm{Cumul}^{(3)}_{N\bar{v},\mu}\overline{\zeta}_N = 0 \\
&\lim_{N\to+\infty} N^3\mathrm{Cumul}^{(4)}_{N\bar{v},\mu}\zeta_N = \lim_{N\to+\infty} N^{-1}\mathrm{Cumul}^{(4)}_{N\bar{v},\mu}\overline{\zeta}_N = 0 \,.
\end{aligned} \tag{2.60}$$

This is equivalent to state that ζ_N has the same asymptotic limit of the distribution of the sum of N independent, identically distributed random variables.

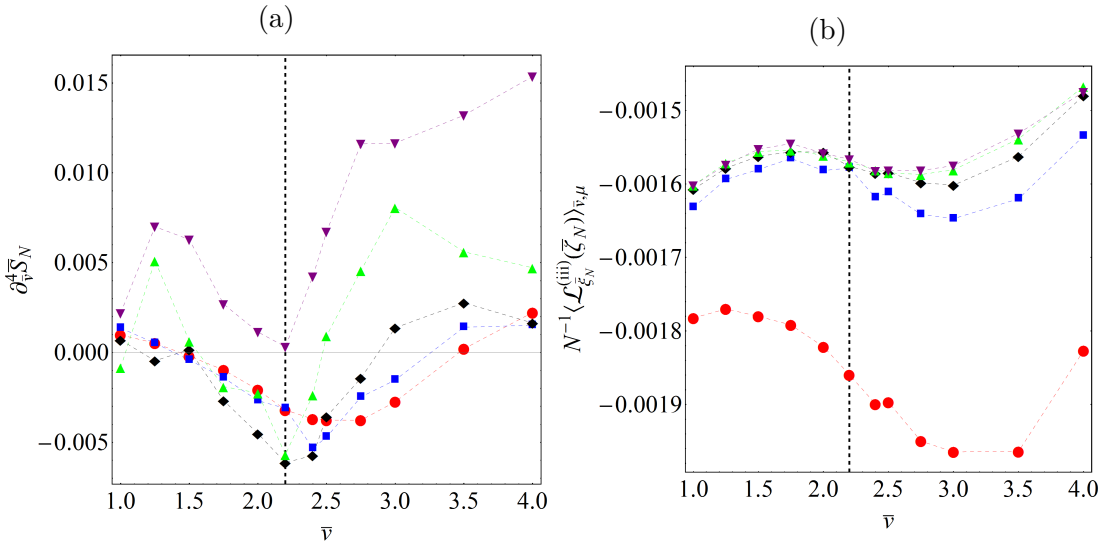

Figure 2.12: Fourth order derivative of specific configurational microcanonical entropy (a) and average of third order Lie derivative of $\overline{\zeta}_N$ with respect to $\overline{\xi}_N$ (b) vs. the specific energy $\bar{v}$ for lattices with different N. In particular, $N = 100$ (red dots), $N = 400$ (blue squares), $N = 900$ (black diamonds), $N = 1600$ (green triangles), $N = 2500$ (purple reversed triangles).

- it has to allow the derivation of uniform bounds in N for the (rescaled) fourth cumulants of $N^{-1}\overline{\zeta}_N$, namely the divergence of the vector field $\overline{\boldsymbol{\xi}}_N$ whose properties are widely discussed in section 2.2;
- such refinement should derive from a formalization of the concept of "asymptotic diffeomorphicity" heuristically introduced in section 2.1. introduced

A possible way to refine the Necessity Theorem would consist in adding an hypothesis of uniform boundedness in N of a *suitable* norm of class k for the vector field and its derivatives, i.e.

$$\|\overline{\boldsymbol{\xi}}_N\|_{k,M^{\overline{V}_N}_{[\bar{v}_0,\bar{v}_1]}} = N^{\alpha_0}\sup_{M^{\overline{V}_N}_{[\bar{v}_0,\bar{v}_1]}} \|\overline{\boldsymbol{\xi}_N}\|_g + \sum_{l=1}^{k} N^{\alpha_l} |\nabla^l \overline{\boldsymbol{\xi}}_N|_{M^{\overline{V}_N}_{[\bar{v}_0,\bar{v}_1]}} \leq B < +\infty \qquad \forall N \in \mathbb{N} \quad (2.61)$$

where

$$|\nabla^l \overline{\boldsymbol{\xi}}_N|_{M^{\overline{V}_N}_{[\bar{v}_0,\bar{v}_1]}} = \sup_{\substack{p \in M^{\overline{V}_N}_{[\bar{v}_0,\bar{v}_1]} \\ \mathbf{x}_1,\ldots,\mathbf{x}_l \in \mathfrak{X}\left(M^{\overline{V}_N}_{[\bar{v}_0,\bar{v}_1]}\right)}} \frac{\|\nabla_{\mathbf{x}_l}\left(\nabla_{\mathbf{x}_{l-1}}\left(\ldots\left(\nabla_{\mathbf{x}_1}\overline{\boldsymbol{\xi}}_N\right)\ldots\right)\right)\|_g}{\|\mathbf{X}_1\|_g, \ldots, \|\mathbf{X}_l\|_g} \quad (2.62)$$

and $(\alpha_0, \ldots, \alpha_l) \in \mathbb{Q}$ are the parameters that have to be fixed in order to construct uniform bounds in N for $N^{-1}\text{Cumul}^{(4)}\overline{\zeta}_N$. Through the eq.(2.61) the concept of asymptotic diffeomorphicity is introduced as uniform boundedness of the covariant derivative at any order of the vector field $\overline{\boldsymbol{\xi}}_N$.

2.4 Geometrization of thermodynamics through regular equipotential level sets

Eqs.(2.55) open to the possibility of directly associating the microcanonical entropy and its derivatives to geometrical features of regular equipotential level sets. In fact, using the notation introduced in this Section

$$\zeta_N(p) = \mathrm{div}_{\mathbb{R}^N}(\overline{\boldsymbol{\xi}}_N)(p) = \mathrm{div}_{\mathbb{R}^N}\left(\overline{\chi}_N \boldsymbol{\nu}_N\right)(p) = \overline{\chi}_N(p) h_{1,g_{\mathbb{R}^N}}(p) + (\mathcal{L}_{\boldsymbol{\nu}_N}\overline{\chi}_N)(p) \tag{2.63}$$

where $p \in \Sigma_{\overline{v}}^{\overline{V}_N} \subset \mathbb{R}^N$ and $h_{1,g_{\mathbb{R}^N}}$ is the sum of principal curvatures of $\Sigma_{\overline{v}}^{\overline{V}_N}$ immersed in $\mathbb{R}^N$ endowed with the metric induced by the ambient space (see Appendix A).
Substituting the above expression in the first of Eqs.(2.50)

$$\begin{aligned}\frac{\mathrm{d}\Omega_N}{\mathrm{d}\overline{v}}(\overline{v}) =& N \int_{\Sigma_{N\overline{v}}^N} \left[-\chi_N h_{1,g_{\mathbb{R}^N}} + (\mathcal{L}_{\nu_N}\chi_N)\right] \mathrm{d}\mu_{N\overline{v}}^{N-1} = \\ =& N \int_{\Sigma_{N\overline{v}}^N} \left[-\chi_N (h_{1,g_{\mathbb{R}^N}} + (\mathcal{L}_{\nu_N}(-\log\chi_N))\right] \exp\left[-\log\chi_N\right] \mathrm{d}\sigma_{N\overline{v}}^{N-1}\end{aligned} \tag{2.64}$$

where the last expression has been derived to compare this result with well known results in the theory of manifolds with density.

2.4.1 Regular equipotential surfaces as manifolds with density

The derivatives of configurational microcanonical partition function with respect to $\overline{v}$ are reported in eq.(2.50) *only* as functions of integral quantities of $\overline{\zeta}_N$ and its Lie derivatives with respect to the vector field $\overline{\boldsymbol{\xi}}_N$. This establishes a strong relation between configurational microcanonical thermodynamics and diffeomorphic properties of the level sets; this was motivated by the search for a proper framework to define the concept of "asymptotic change of topology". Another possible approach to this problem would consist to interpret the integral quantities that enter eqs.(2.50) in terms of "geometrical observables" (especially curvatures) of the equipotential level sets and of the (configuration) ambient space. Eq.(2.63) suggests a link between $\overline{\zeta}_N$ and the mean curvature of equipotential level sets. Nevertheless, at this level it is not clear how to give a pure geometrical interpretation of the integrals in eqs. (2.50). To attain this result, we consider quite recent results on the differential geometry of *manifolds with density*[7] [Mor05][CHH+06]. In this framework, usual geometric quantities (as curvatures) of a Riemannian manifold are redefined in order to encode in the geometry also the information carried by an arbitrary measure over a manifold.
Let M be a Riemannian manifold endowed with a metric g, and consider an immersed codimension one submanifold $\Sigma \subset M$; the Riemannian volume forms dVol_g and $\mathrm{d}\sigma_{\Sigma,g}$ are induced on the manifold M and Σ respectively.
To construct a manifold with density, a density function $\Psi : M \longrightarrow \mathbb{R}^+$ is defined on M so that

[7] This objects are widely studied in the context of isoperimetric problems and in optimal transportation theory.

the volume form and the area form on Σ are rescaled in order to give respectively

$$\begin{aligned} \mathrm{dVol}_\Psi &= \Psi \mathrm{dVol}_g = \exp[\psi]\mathrm{dVol}_g \\ \mathrm{d}\sigma_{\Sigma,\Psi} &= \Psi \mathrm{d}\sigma_{\Sigma,g} = \Psi \mathrm{dVol}_g\Big|_S = \exp[\psi]\mathrm{dVol}_g\Big|_\Sigma . \end{aligned} \tag{2.65}$$

where $\psi = \ln \Psi$.
The mean curvature $h_{1,g} = \tau_{1,g}/(N-1)$ of the hypersurface Σ is redefined with the introduction of the density such that the sum of principal curvatures $\tau_{1,g,\Psi}$ is directly proportional to the variation of area element $\mathrm{d}\sigma_{\Sigma,\Psi}$ at the first order in normal direction to the level set hypersurfaces, i.e.

$$\mathcal{L}_{\boldsymbol{\nu}} \mathrm{d}\sigma_{\Sigma,\Psi} = -\tau_{1,g,\Psi} \mathrm{d}\sigma_{\Sigma,\Psi} = -(N-1) h_{(1,g,\Psi)} \mathrm{d}\sigma_{\Sigma,\Psi} \tag{2.66}$$

which is immediately verified.
For a manifold with density (M, g, Ψ) a natural extension of the sum of principal curvatures $\tau_{1,g}$ is thus given by:

$$\tau_{(1,g,\Psi)} = \tau_{1,g} + \mathcal{L}_{\boldsymbol{\nu}} \psi \tag{2.67}$$

where $\boldsymbol{\nu}_N$ is the normal vector field to the hypersurface. Consistently the first and second variation formula for the area of the hypersurface S are

$$\mathcal{A}_S = \int_S \mathrm{d}\sigma_\Psi \tag{2.68}$$

under the action of a diffeomorphism parametrized by t and generated by a vector field $W = w\nu$, such that $\mathrm{d}t(W) = 1$, we have [Bay03]

$$\frac{\mathrm{d}\mathcal{A}_S}{\mathrm{d}t} = \int_S -w\, h_{(1,g,\Psi)} \mathrm{d}\sigma_\Psi = \int_S -w\, (h_{1,g} + \mathcal{L}_\nu \psi)\, \exp[\psi] \mathrm{d}\sigma_g \tag{2.69}$$

and

$$\frac{\mathrm{d}^2\mathcal{A}_S}{\mathrm{d}t^2} = \int_S \left[\|\mathbf{grad}_g w\|_g^2 - w^2 \left(h_{1,g}^2 + \mathcal{L}_{\nu_N}(\mathcal{L}_{\boldsymbol{\nu}} \psi) - \tau_{2,g} - \mathrm{Ric}_g(\boldsymbol{\nu_N}, \boldsymbol{\nu}_N) \right) \right] \exp[\psi] \mathrm{d}\sigma_g \tag{2.70}$$

where $\tau_{2,g} = \|\mathrm{II}_g\|^2$ is the squared norm of the shape operator, i.e. it is the the sum of the squares of principal curvatures, and Ric_g is the Ricci curvature of the ambient space with metric g.
We easily see that with the identification $w = \overline{\chi}_N$, $\psi = -\log(\overline{\chi}_N)$ and, consequently, $\Psi = \overline{\chi}_N^{-1}$) we exactly obtain the expression in eqs.(2.64).

2.4.2 Rescaled metric in configuration space

In subsection 2.4.1 we have discussed how it is possible to interpret equipotential level sets equipped with the microcanonical measure as manifolds with density, "geometrizing" some features strictly related with measure properties.
Nevertheless, in an ideal program of "geometrization" of classical microcanonical thermodynam-

ics", *all the terms* in the integrands of eqs.(2.50) should be retrieved only from the geometrical and topological properties of the equipotential level sets and of the ambient space. In particular, according to what has been reported in the previous Subsection, the function $\overline{\chi}_N$ (well defined in absence of critical points of potential energy) and its derivatives in the normal direction $\boldsymbol{\nu}_N$ carry two distinct information that have to be "geometrized": one concerns the density measure $\Psi = e^{\overline{\chi}_N}$, while the other concerns the "velocity" of the vector field that "moves" the level set $w = \overline{\chi}_N$. A possible way consists in the introduction of a rescaled metric $\tilde{g}$ where the microcanonical measure $\mathrm{d}\mu_{\Sigma_{\bar{v}}^{\overline{V}_N}}$ and the vector field $\overline{\boldsymbol{\xi}}_N$ are "natural" in the sense that they are naturally included in the differential geometrical structure of the space.
In the following section we introduce the function $\phi_N : \mathcal{B}_N \subseteq \mathcal{X}_N \longrightarrow \mathbb{R}_0^+$ such that:

$$\phi_N = \log \overline{\chi}_N \tag{2.71}$$

to simplify the notation.
Although not strictly necessary, for further computations it is convenient to introduce a coordinate system $\{u^0, u^1, ..., u^{N-1}\}$ over $M_{[\bar{v}_0,\bar{v}_1]} \subset \mathcal{B}_N$ such that one coordinate parametrizes the specific potential energy

$$\mathrm{d}u^0 = \mathrm{d}\overline{V}_N \quad \Longrightarrow \quad \mathrm{d}u^0(\overline{\boldsymbol{\xi}}_N) = 1 \tag{2.72}$$

$\{\boldsymbol{\partial}_0, \boldsymbol{\partial}_1, ..., \boldsymbol{\partial}_{(N-1)}\}$ is the coordinate frame and $\{\mathrm{d}u_0, \mathrm{d}u_1, \ldots \mathrm{d}u_{(N-1)}\}$ its dual. The greek indices[8] run in the interval $[0; N-1]$ while the latin indices refer to the coordinate system over the level set hypersurfaces and run in the interval $[1; N-1]$.
With this coordinate choice the g metric of the ambient space reads

$$g = \sum_{\alpha=0}^{N-1}\sum_{\beta=0}^{N-1} g_{\alpha\beta}\mathrm{d}u^\alpha \otimes \mathrm{d}u^\beta = e^{2\phi_N}\mathrm{d}u^0 \otimes \mathrm{d}u^0 + \sum_{i=1}^{N-1}\sum_{j=1}^{N-1} g_{ij}\mathrm{d}u^i \otimes \mathrm{d}u^j \tag{2.73}$$

and the normal vector field $\overline{\boldsymbol{\nu}}_N$ defining the foliation of $M_{[\bar{v}_0,\bar{v}_1]}$ is

$$\boldsymbol{\partial}_0 = \overline{\boldsymbol{\xi}}_N \quad \Longrightarrow \quad \boldsymbol{\nu}_N = e^{-\phi_N}\boldsymbol{\partial}_0 \tag{2.74}$$

With such a choice of coordinates, the Riemannian volume form of the ambient space and the area form induced over a fixed $\Sigma_{\bar{v}}^{\overline{V}_N} \in M_{[\bar{v}_0,\bar{v}_1]}$ are respectively

$$\mathrm{dVol}_g = |\det(g_{\alpha,\beta})|\mathrm{d}u^0 \wedge ...\mathrm{d}u^{N-1} = e^{\phi_N}\,|\det(g_{ij})|\,\mathrm{d}u^0 \wedge \wedge \mathrm{d}u^1 \wedge ....\mathrm{d}u^{N-1} \tag{2.75}$$

and

$$\mathrm{d}\sigma_{\Sigma_{\bar{v}}^{\overline{V}_N},g} = |\det(g_{ij})|\mathrm{d}u^1 \wedge ... \wedge \mathrm{d}u^{N-1}\,. \tag{2.76}$$

Christoffel symbols $\Gamma^\alpha_{\beta\gamma}$ of the Levi-Civita connection ∇ associated with g are supposed to be given.
As reported in section 2.2, all the informations concerning the statistical mechanics of the configurational microcananical ensemble are given by functional depending on $\overline{\zeta}_N = \mathrm{div}_g\left(\overline{\boldsymbol{\xi}}_N\right)$

[8] Einstein's convention is assumed for repeated indices.

and its Lie derivatives respect to the same vector field $\overline{\boldsymbol{\xi}_N}$. Eq.(2.63) clearly shows that the mean curvature of $\Sigma_{\bar{v}}^{\overline{V}_N}$ and its derivatives with respect to $\boldsymbol{\nu}_N$ are the geometrical quantities of the level sets directly related with the derivatives of configurational microcanonical entropy. For these reasons we provide an explicit expression of the mean curvature and its first order Lie derivatives respect to the normal vector field as a function of Christoffel of Levi-Civita connection of metric g. With the choice of coordinates introduced at the beginning of this section, the sum of principle curvatures $\tau_{1,g}$ of a regular level sets $\Sigma_{\bar{v}}^{\overline{V}_N}$ is given by:

$$\begin{aligned}\tau_{1,g} &\equiv \sum_{i,j=1}^{N-1} \lambda_{i,g} = \sum_{i,j=1}^{N-1} \mathrm{II}_{ij} g^{ij} = \sum_{i,j=1}^{N-1} g(\nabla_{\partial_i} \nu_N, \partial_j) g^{ij} = \\ &= \sum_{i,l=1}^{N-1} g(\nabla_{\partial_i} \left(e^{-\varphi_N} \partial_0\right), \partial_j) g^{ij} = e^{-\varphi_N} \sum_{i,l=1}^{N-1} \Gamma_{i0}^k g_{kj} g^{ij} = e^{-\varphi_N} \Gamma_{0i}^i \,.\end{aligned} \tag{2.77}$$

where II is the second fundamental form on the equipotential level sets (see Appendix A for a brief review on differential geometry.).
Moreover, as a consequence of the Riccati's Equation applied to Weingarten operator under the action of the vector field $\boldsymbol{\nu}_N$, we obtain:

$$\mathcal{L}_{\boldsymbol{\nu}_N}(\tau_{1,g}) = -\tau_{2,g} - \mathrm{Ric}(\boldsymbol{\nu}_N, \boldsymbol{\nu}_N) \tag{2.78}$$

where $\tau_{2,g} = \sum_{i=1}^{N-1} \lambda_{i,g}^2$ is the sum of the squares of principal curvatures and Ric is the Ricci tensor of the ambient space. Using the coordinate system introduced above we obtain using definitions:

$$\begin{aligned}\mathrm{Ric}(\partial_0, \partial_0) &= \sum_{\alpha=0}^{N-1} g(R(\partial_\alpha, \partial_0)\partial_0, \partial_\alpha) = \partial_\alpha \Gamma_{00}^\alpha - \partial_0 \Gamma_{0\alpha}^\alpha + \Gamma_{\alpha\beta}^\alpha \Gamma_{00}^\beta - \Gamma_{0\beta}^\alpha \Gamma_{\alpha 0}^\beta = \\ &= \partial_i \Gamma_{00}^i - \partial_0 \Gamma_{i0}^i + \Gamma_{i0}^i \Gamma_{00}^0 - \Gamma_{0i}^0 \Gamma_{00}^i - \Gamma_{0j}^i \Gamma_{i0}^j\end{aligned} \tag{2.79}$$

$$\begin{aligned}\mathrm{Ric}(\nu_N, \nu_N) &= \mathrm{Ric}(e^{-\varphi_N}\partial_0, e^{-\varphi_N}\partial_0) = e^{-2\varphi_N} R_{00} = \\ &= e^{-2\varphi_N} \left(\partial_i \Gamma_{00}^i - \partial_0 \Gamma_{i0}^i + \Gamma_{i0}^i \Gamma_{00}^0 - \Gamma_{0i}^0 \Gamma_{00}^i - \Gamma_{0j}^i \Gamma_{i0}^j\right)\end{aligned} \tag{2.80}$$

while for the sum of the squares of principle curvatures is given by

$$\begin{aligned}\tau_{2,g} &= \mathrm{Tr}^g \left(W^2\right) = \mathrm{II}_{ij} \mathrm{II}_{kl} g^{jk} g^{il} = g\left(\nabla_{\partial_i}(e^{-\varphi_N}\partial_0), \partial_j\right) g\left(e^{-\varphi_N}\partial_0), \partial_l\right) g^{jk} g^{il} = \\ &= e^{-2\varphi_N} g_{mj} g_{nl} \Gamma_{i0}^m \Gamma_{k0}^n g^{jk} g^{il} = e^{-2\varphi_N} \Gamma_{i0}^k \Gamma_{k0}^i\end{aligned} \tag{2.81}$$

As anticipated, we endow the manifold $M_{[\bar{v}_0,\bar{v}_1]}^N$ in configuration space with a new metric $\tilde{g}$ satisfying the following properties:

1. the Riemannian area form $\mathrm{d}\sigma_{\tilde{g}}$ induced over the equipotential level sets $\Sigma_{\bar{v}}^N \in M_{[\bar{v}_0,\bar{v}_1]}^N$

from ambient space *would exactly correspond with the microcanonical density form*

$$\mathrm{d}\mu_{\bar{v}}^{N-1} = \mathrm{d}\tilde{\sigma}_{\Sigma_{\bar{v}}^{\overline{V}_N},\tilde{g}} = |\det(\tilde{g}_{ij})|\mathrm{d}u^0 \wedge \mathrm{d}u^1 \wedge ... \wedge \mathrm{d}u^{N-1}\,; \tag{2.82}$$

2. the vector field $\overline{\boldsymbol{\xi}}_N \in \mathfrak{X}(M^N_{[\bar{v}_0,\bar{v}_1]})$ coincides with the *normal vector to the equipotential hypersurfaces*

$$\tilde{g}(\overline{\boldsymbol{\xi}}_N, \overline{\boldsymbol{\xi}}_N) = 1 \quad \Longrightarrow \quad \tilde{\boldsymbol{\nu}}_N = \overline{\boldsymbol{\xi}}_N\,. \tag{2.83}$$

   in this way the derivation with respect to the parameter $\bar{v}$ (along the flow generated by $\overline{\boldsymbol{\xi}}_N$) coincides with the Lie derivative along the vector field $\tilde{\boldsymbol{\nu}}_N$.

We notice that the first condition concerns the properties of the metric restricted to the *tangent space of hypersurfaces* $\Sigma_{\bar{v}}^{\overline{V}_N}$ while the second condition concerns a rescaling in *normal direction*. This suggests that a possible choice for $\tilde{g}$ can be done by performing two different conformal rescalings for the components of the metric g, i.e. the tangent and normal ones to the equipotential level sets, as follows:

$$\begin{cases} \tilde{g}(\boldsymbol{\nu}_N, \boldsymbol{\nu}_N) = e^{-2\phi_N} g(\boldsymbol{\nu}_N, \boldsymbol{\nu}_N) \\ \tilde{g}(\boldsymbol{X}, \boldsymbol{Y}) = e^{2\Xi\phi_N} g(\boldsymbol{X}, \boldsymbol{Y}) \qquad \text{with} \qquad \Xi = \dfrac{1}{N-1} \\ \tilde{g}(\boldsymbol{X}, \boldsymbol{\nu}_N) = g(\boldsymbol{X}, \boldsymbol{\nu}_N) = 0 \end{cases} \tag{2.84}$$

where $\boldsymbol{\nu}_N$ is the normal vector field to the equipotential level sets $\Sigma_{\bar{v}}^{\overline{V}_N}$ with respect to the metric g, and $\boldsymbol{X}, \boldsymbol{Y} \in T_p\Sigma_{\bar{v}}^{\overline{V}_N}$ are vector fields belonging to the tangent bundle of a leaf $\Sigma_{\bar{v}}^{\overline{V}_N} \in M^{\overline{V}_N}_{[\bar{v}_0,\bar{v}_1]}$.

Remark 7 (Restrictions to the definition of the rescaled metric $\tilde{g}$)**.** *It has to be stressed that the suggested rescaling change of metric on $M^{\overline{V}_N}_{[\bar{v}_0,\bar{v}_1]}$ is possible only in the case of absence of critical points of the specific potential energy $\overline{V}_N$, i.e. when the function $\overline{\chi}_N = \|\mathbf{grad}_g \overline{V}_N\|_g^{-1} > 0$ is non singular. In this case the rescaled metric $\tilde{g}$ defined in(2.84) is well defined and it is positive definite so that $(M^{\overline{V}_N}_{[\bar{v}_0,\bar{v}_1]}, \tilde{g})$ is a Riemannian manifold. As the specific potential energy is in the closure of the Morse function set in $M^{\overline{V}_N}_{[\bar{v}_0,\bar{v}_1]}$ for a large class of potentials. This implies that* ***the proposed rescaling of the metric g for the geometrization of microcanonical thermodynamics is possible only under the hypothesis of diffeomorphicity of equipotential level sets $\Sigma_{\bar{v}}^{\overline{V}_N} \in M^{\overline{V}_N}_{[\bar{v}_0,\bar{v}_1]}$ at any finite N***

Using the local coordinate system $\{u_\alpha\}_{\alpha=0,\dots,(N-1)}$ introduced at the beginning of this section, the rescaled metric $\tilde{g}$ reads

$$\begin{aligned} \tilde{g} &= \sum_{\alpha=0}^{N-1}\sum_{\beta=0}^{N-1} \tilde{g}_{\alpha\beta}\mathrm{d}u^\alpha \mathrm{d}u^\beta = e^{-2\varphi_N} g_{00}\mathrm{d}u^0 \otimes \mathrm{d}u^0 + \sum_{i=1}^{N-1}\sum_{j=1}^{N-1} e^{2\Xi\phi_N} g_{ij}\mathrm{d}u^i \otimes \mathrm{d}u^j = \\ &= \tilde{g}_{00}\ \mathrm{d}u^0 \otimes \mathrm{d}u^0 + \sum_{i=1}^{N-1}\sum_{j=1}^{N-1} \tilde{g}_{ij}\ \mathrm{d}u^i \otimes \mathrm{d}u^j\,. \end{aligned} \tag{2.85}$$

With this rescaling of the metric it is quite simple to verify both condition (item 1)

$$\begin{aligned} \mathrm{d}\tilde{\sigma}_{\Sigma_{\overline{v}}^{\overline{V}_N},\tilde{g}} &= |\det(\tilde{g}_{ij})|\mathrm{d}u^1 \wedge ... \wedge \mathrm{d}u^{N-1} = \left(\prod_i^{N-1} \overline{e}^{2\Xi\phi_N}\right)^{1/2} |\det(g_{ij})|\mathrm{d}u^1 \wedge ... \wedge \mathrm{d}u^{N-1} = \\ &= e^{\phi_N}\ |\det(g_{ij})|\mathrm{d}u^1 \wedge ... \wedge \mathrm{d}u^{N-1} = \overline{\chi}_N \mathrm{d}\sigma_{\Sigma_{\overline{v}}^{\overline{V}_N},g} = \mathrm{d}\mu_{\Sigma_{\overline{v}}^{\overline{V}_N}} \end{aligned} \tag{2.86}$$

and condition (item 2)

$$\tilde{g}(\overline{\boldsymbol{\xi}}_N, \overline{\boldsymbol{\xi}}_N) = \mathrm{d}u^0(\overline{\boldsymbol{\xi}}_N) \otimes \mathrm{d}u^0(\overline{\boldsymbol{\xi}}_N) = 1 \quad \Longrightarrow \quad \tilde{\boldsymbol{\nu}}_N = \overline{\boldsymbol{\xi}}_N (= \boldsymbol{\partial}_0) \tag{2.87}$$

in last equation we have used (2.26).

Remark 8 (Preservation of ambient space volume)**.** *The new metric introduced in eqs.*(2.84) *preserves the Riemannian volume form* dVol_g*, in fact*

$$\begin{aligned} \mathrm{dVol}_{\tilde{g}} &= |\tilde{g}(\alpha,\beta)|\mathrm{d}u^0 \wedge \mathrm{d}u^1 \wedge ... \wedge \mathrm{d}u^{N-1} = \left(\prod_i^{N-1} e^{2\Xi\varphi_N}\right)^{1/2} |\det(g_{ij})|\mathrm{d}u^0 \wedge ... \wedge \mathrm{d}u^{N-1} = \\ &= e^{\varphi_N}\det(g_{ij})|\mathrm{d}u^0 \wedge ... \wedge \mathrm{d}u^{N-1} = \overline{\chi}_N|\det(g_{ij})|\mathrm{d}u^0 \wedge ... \wedge \mathrm{d}u^{N-1} = \mathrm{dVol}_g \end{aligned} \tag{2.88}$$

From the point of view of thermodynamic properties of the system, this means that the Gibbs' microcanonical volume $\Omega_{\mathrm{Gibbs},N}$ *and the Gibbs' microcanonical entropy* $\overline{S}_{Gibbs,N} = N^{-1}\ln\Omega_{\mathrm{Gibbs},N}$ *are invariant for the transformation of the metric in eq.*(2.84)*.*

The introduction of the rescaled metric $\tilde{g}$ allows to express the derivatives of configurational microcanonical entropy in terms of geometric properties of $\Sigma_{\overline{v}}^{\overline{V}_N}$.
The microcanonical partition function $\Omega_N(\overline{v})$ becomes simply the Riemannian area of the hypersurfaces $\Sigma_{\overline{v}}^{\overline{V}_N}$

$$\Omega_N(\overline{v}) = \int_{\Sigma_{\overline{v}}^{\overline{V}_N}} \mathrm{d}\tilde{\sigma}_{\Sigma_{\overline{v}}^{\overline{V}_N},\tilde{g}}\,. \tag{2.89}$$

Moreover, as required, the vector field that generates the one-parameter group of diffeomorfisms $\mathrm{Fl}_{\overline{v}}$ among equipotential level sets coincides with the normal vector field $\tilde{\boldsymbol{\nu}}_N$.
According to eq.(2.90), the Lie derivative along the vector field that generate the diffeomorphism $\tilde{\boldsymbol{\nu}}_N$ of the area form reads in rescaled metric $\tilde{g}$

$$\mathcal{L}_{\overline{\boldsymbol{\nu}}_N}(\mathrm{d}\tilde{\sigma}_{\Sigma_{\overline{v}}^{\overline{V}_N},\tilde{g}}) = \mathrm{Tr}^{\tilde{g}}(\mathrm{II}_{\tilde{g}})\mathrm{d}\tilde{\sigma}_{\Sigma_{\overline{v}}^{\overline{V}_N},g} = \tau_{1,\tilde{g}}\mathrm{d}\tilde{\sigma}_{\Sigma_{\overline{v}}^{\overline{V}_N},\tilde{g}}\ , \tag{2.90}$$

our rescaling is consistent with our purposes of "geometrizating" the configurational microcanonical thermodynamics if $\tau_{1,\tilde{g}} = \mathrm{div}_g\overline{\boldsymbol{\xi}}_N$.
In the next Subsection a characterization of some geometrical properties of the Riemannian manifolds $(M_{\overline{v}_0,\overline{v}_1}^{\overline{V}_N}, \tilde{g})$ and of the equipotential level sets $\Sigma_{\overline{v}}^{\overline{V}_N} \subset M_{\overline{v}_0,\overline{v}_1}^{\overline{V}_N}$ is given in order to establish a link between the geometry with rescaled metric $\tilde{g}$, the geometry induced by the metric g, and configurational microcanonical thermodynamics.

2.4.3 Geometry of Riemannian Manifolds $(M^{\overline{V}_N}_{[\bar{v}_0,\bar{v}_1]},\tilde{g})$ and $(\Sigma^{\overline{V}_N}_{\bar{v}},\tilde{g}\big|_{\Sigma^{\overline{V}_N}_{\bar{v}}})$

By the use of local coordinate system in $\{u_\alpha\}_{\alpha=0,\dots,(N-1)}$ we can compute the geometrical properties of the manifold $(M^{\overline{V}_N}_{[\bar{v}_0,\bar{v}_1]},\tilde{g})$ of diffeomorphic level sets $\Sigma^{\overline{V}_N}_{\bar{v}}$ endowed with the rescaled metric $\tilde{g}$ defined in (2.84).

This leads to the fact that the mean curvature of the equipotential level sets in configuration space with the rescaled metric $\tilde{g}$ coincides with the divergence of $\overline{\xi}_N$ in configuration space *with the non rescaled metric* g. Moreover, the curvature of the ambient manifold is related to the possibility to use some important results in differential topology (i.e. as the Chern-Lashof Theorem) which relate the global curvature integral of submanifolds immersed in space with constant scalar curvature and their topological invariants.
The geometric quantities calculated in the configuration space with the rescaled metric $(M^{\overline{V}_N}_{[\bar{v}_0,\bar{v}_1]},\tilde{g})$ are tilded and expressed in terms of the geometrical quantities calculated in $(M^{\overline{V}_N}_{[\bar{v}_0,\bar{v}_1]},g)$ and the rescaling function ϕ_N.

Christoffel symbols (Levi-Civita connection associated to $\tilde{g}$)

The starting point to characterize the geometry of the configuration space, and of the regular equipotential level sets foliating it, consists in computing the Christoffel symbols associated withthe Levi-Civita connection $\tilde{\nabla}$ of the metric $\tilde{g}$.
Using the definition of Christoffel symbols, we obtain:

$$\widetilde{\Gamma}^0_{00}=\frac{1}{2}\tilde{g}^{0\alpha}\left(2\partial_0\tilde{g}_{0\alpha}-\partial_\alpha\tilde{g}_{00}\right)=\frac{1}{2}\tilde{g}^{00}\partial_0\tilde{g}_{00}=\frac{1}{2}g^{00}\partial_0 g_{00}+g^{00}g_{00}\partial_0\phi_N=\Gamma^0_{00}-\delta^0_0\partial_0\phi_N=0 \tag{2.91}$$

$$\begin{aligned}\widetilde{\Gamma}^0_{ij}&=\frac{1}{2}\tilde{g}^{0\alpha}\left(\partial_i\tilde{g}_{\alpha j}+\partial_j\tilde{g}_{\alpha i}-\partial_\alpha\tilde{g}_{ij}\right)=-\frac{1}{2}\tilde{g}^{00}\partial_0\left(\tilde{g}_{ij}\right)=-\frac{1}{2}e^{2\phi_N}g^{00}\partial_0\left[e^{2\Xi\phi_N}g_{ij}\right]=\\&=e^{2(\Xi+1)\phi_N}\left(\Gamma^0_{ij}-\Xi g_{ij}\partial^0\phi_N\right)\end{aligned} \tag{2.92}$$

$$\begin{aligned}\widetilde{\Gamma}^0_{j0}&=\frac{1}{2}\tilde{g}^{0\alpha}\left(\partial_j\tilde{g}_{\alpha 0}+\partial_0\tilde{g}_{\alpha j}-\partial_0\tilde{g}_{0j}\right)=\frac{1}{2}\tilde{g}^{00}\partial_j\left(\tilde{g}_{00}\right)=\frac{1}{2}e^{2\phi_N}g^{00}\partial_j\left(e^{-2\phi_N}g_{00}\right)=\\&=\Gamma^0_{j0}-\delta^0_0\partial_j\phi_N=0\end{aligned} \tag{2.93}$$

$$\begin{aligned}\widetilde{\Gamma}^i_{00}&=\frac{1}{2}\tilde{g}^{i\alpha}\left(\partial_0\tilde{g}_{\alpha 0}+\partial_0\tilde{g}_{\alpha 0}-\partial_\alpha\tilde{g}_{00}\right)=\frac{1}{2}e^{-2\Xi\phi_N}g^{ij}\partial_j\left(e^{-2\phi_N}g_{00}\right)=e^{-2(\Xi+1)\phi_N}\left[\Gamma^i_{00}+g_{00}\partial^j\phi_N\right]=\\&=0\end{aligned} \tag{2.94}$$

$$\widetilde{\Gamma}^k_{0i} = \frac{1}{2}\tilde{g}^{k\alpha}\left(\partial_i\tilde{g}_{\alpha 0} + \partial_0\tilde{g}_{i\alpha} - \partial_\alpha\tilde{g}_i 0\right) = \frac{1}{2}e^{-2\Xi\phi_N}g^{kl}\partial_0\left(e^{2\Xi\phi_N}g_{il}\right) = \frac{1}{2}g^{kl}\partial_0 g_{li} + \Xi g^{kl}g_{li}\partial_0\phi_N =$$
$$= \Gamma^k_{0i} + \Xi\delta^k_i\partial_0\phi_N \tag{2.95}$$

$$\widetilde{\Gamma}^i_{jk} = \frac{1}{2}\tilde{g}^{i\alpha}\left(\partial_j\tilde{g}_{\alpha k} + \partial_k\tilde{g}_{\alpha j} - \partial_\alpha g_{jk}\right) = \frac{1}{2}e^{-2\Xi\phi_N}g^{il}\left[\partial_j(e^{2\Xi\phi_N}g_{li}) + \partial_k(e^{2\Xi\phi_N}g_{lj}) - \partial_l(e^{2\Xi\phi_N}g_{ij})\right] =$$
$$= \Gamma^i_{jk} + \Xi\left(\delta^i_k\partial_j\phi_N + \delta^i_j\partial_k\phi_N - g_{jk}\partial^i\phi_N\right) \tag{2.96}$$

Principal curvatures, Ricci curvatures, Scalar curvature

The expression of the sum of principal curvatures $\tilde{\tau}_{1,\tilde{g}}$ of equipotential level sets $\Sigma^N_{\bar{v}}$ in the Riemannian manifolds $(M^{\overline{V}_N}_{\bar{v}_0,\bar{v}_1}, \tilde{g})$ is given according to the definition by

$$\tilde{\tau}_{(1,\tilde{g})} = \widetilde{\mathrm{II}}_{ij}\tilde{g}^{ij} = \tilde{g}(\tilde{\nabla}_{\boldsymbol{\partial}_i}\tilde{\boldsymbol{\nu}}_N, \boldsymbol{\partial}_j)\tilde{g}^{ij} = \tilde{g}(\nabla_{\boldsymbol{\partial}_i}\boldsymbol{\partial}_0, \boldsymbol{\partial}_j)e^{-2\Xi\varphi_N}g^{ij} = \widetilde{\Gamma}^k_{0i}e^{2\Xi\phi_N}g_{kj}e^{2\Xi\phi_N}g^{ij} = \widetilde{\Gamma}^k_{0i}g_{kj}g^{ij}$$
$$= \left(\Gamma^k_{0i} + \frac{\delta^i_k}{N-1}\partial_0\phi_N\right)\delta^k_i = \Gamma^i_{0i} + \frac{\delta^i_i}{N-1}\partial_0\log\left(\overline{\chi}_N\right) = \overline{\chi}_N\tau_{(1,g)} + \mathcal{L}_{\boldsymbol{\nu}_N}(\overline{\chi}_N) = \mathrm{div}_g\overline{\boldsymbol{\xi}}_N \tag{2.97}$$

This gives the expected results that *the sum of curvatures of equipotential level sets embedded in configuration space with the rescaled metric $\tilde{g}$ coincides with the divergence of the vector field $\overline{\boldsymbol{\xi}}_N$ in the non rescaled configuration space.*

Lie derivatives of sums of principal curvatures are involved in the calculation of the higher order derivatives of the configurational microcanonical partition function and entropy. The formula for the first order Lie derivative of the sum of principal curvatures along the normal field is given by

$$\mathcal{L}_{\tilde{\boldsymbol{\nu}}_N}(\tilde{\tau}_{1,\bar{g}}) = \partial_0\tilde{\tau}_{1,\bar{g}} = -\tilde{\tau}_{2,\tilde{g}} - \widetilde{\mathrm{Ric}}(\tilde{\boldsymbol{\nu}}_N, \tilde{\boldsymbol{\nu}}_N) = -\tilde{\tau}_{2,\tilde{g}} - \widetilde{\mathrm{Ric}}_{00} \tag{2.98}$$

(its derivation is reported in Appendix A) where and $\widetilde{\mathrm{Ric}}$ is the Ricci tensor of ambient space with the rescaled metric $\tilde{g}$.

The sums of square of principal curvatures (the called "second order mean curvature") is given by:

$$\tilde{\tau}_{2,\tilde{g}} = \widetilde{\mathrm{II}}_{ij}\widetilde{\mathrm{II}}_{kl}\tilde{g}^{jk}\tilde{g}^{il} = \tilde{g}\left(\tilde{\nabla}_{\boldsymbol{\partial}_i}\boldsymbol{\partial}_0, \boldsymbol{\partial}_j\right)\tilde{g}\left(\tilde{\nabla}_{\boldsymbol{\partial}_k}\boldsymbol{\partial}_0, \boldsymbol{\partial}_l\right)\tilde{g}^{jk}\tilde{g}^{il} = \widetilde{\Gamma}^k_{i0}\widetilde{\Gamma}^i_{k0} =$$
$$= \left(\Gamma^k_{i0} + \frac{\delta^i_k}{(N-1)}\partial_0\phi_N\right)\left(\Gamma^i_{k0} + \frac{\delta^k_i}{(N-1)}\partial_0\phi_N\right) = e^{2\phi_N}\tau_{2,g} + 2\frac{e^{\phi_N}\tau_{1,g}}{(N-1)}\partial_0\phi_N + \frac{(\partial_0\phi_N)^2}{(N-1)}. \tag{2.99}$$

The relevant curvature properties of the configuration space for our problem are contained in the Ricci tensor; its contraction with the metric tensor gives the scalar Riemannian curvature of the total space that appears in many theorems and results concerning total curvature integral

over immersed submanifolds.
From eqs.(2.98) and (2.97) it is possible to derive the expression of the component $\widetilde{\mathrm{Ric}}_{00}$ in space with rescaled metric as a function of the same component for the Ricci tensor in space with metric g:

$$\widetilde{\mathrm{Ric}}_{00} = \widetilde{\mathrm{Ric}}(\widetilde{\boldsymbol{\nu}}_N, \widetilde{\boldsymbol{\nu}}_N) = -\partial_0\left(\tilde{\tau}_{1,g}\right) - \tilde{\tau}_{2,g} = \mathrm{Ric}_{00} - \frac{N+1}{N-1}\Gamma^i_{i0}\partial_0\phi_N - \Xi\partial_0\phi_N\partial_0\phi_N - \partial_0^2\phi_N \tag{2.100}$$

The Ricci tensor $\widetilde{(\mathrm{Ric}_\Sigma)}_{ij}$ restricted over the potential level sets which transforms under conformal changes as follows (see [Bes07])

$$\begin{aligned}\widetilde{(\mathrm{Ric}_\Sigma)}_{ij} &= \partial_k\widetilde{\Gamma}^k_{ij} - \partial_j\widetilde{\Gamma}^k_{ki} + \widetilde{\Gamma}^k_{kl}\widetilde{\Gamma}^l_{ij} - \widetilde{\Gamma}^k_{jl}\widetilde{\Gamma}^l_{ki} = (\mathrm{Ric}_\Sigma)_{ij} - \frac{N-3}{N-1}\left[\nabla_{\boldsymbol{\partial}_i}\partial_j\phi_N - \frac{(\partial_i\phi_N)(\partial_j\phi_N)}{N-1}\right] + \\ &+ \frac{(N-1)\Delta_\Sigma\phi_N - (N-2)\|\mathbf{grad}_{g_\Sigma}\phi_N\|^2_{g_\Sigma}}{(N-1)^2}g_{ij} = (\mathrm{Ric}_\Sigma)_{ij} - F^{(1)}_{ij} + F^{(2)}g_{ij}\end{aligned} \tag{2.101}$$

being Δ_Σ the Laplace-Beltrami operator restricted on the regular potential level set

$$\Delta_\Sigma f = g^{ij}\Gamma^k_{ij}\partial_k f - \partial_i\partial^i f\,. \tag{2.102}$$

The components of the Ricci tensor along tangent direction to level sets $\Sigma^{\overline{V}_N}_{\bar{v}}$ are given by

$$\begin{aligned}\widetilde{\mathrm{Ric}}_{ij} &= \partial_0\widetilde{\Gamma}^0_{ji} - \partial_j\widetilde{\Gamma}^0_{0i} + \widetilde{\Gamma}^0_{00}\widetilde{\Gamma}^0_{ij} + \widetilde{\Gamma}^0_{0k}\widetilde{\Gamma}^k_{ij} + \widetilde{\Gamma}^k_{k0}\widetilde{\Gamma}^0_{ji} - \widetilde{\Gamma}^0_{j0}\widetilde{\Gamma}^0_{i0} - \widetilde{\Gamma}^0_{jk}\widetilde{\Gamma}^k_{0i} - \widetilde{\Gamma}^k_{j0}\widetilde{\Gamma}^0_{ki} + \widetilde{(\mathrm{Ric}_\Sigma)}_{ij} = \\ &= \mathrm{Ric}_{ij} + \left(e^{2(\Xi+1)\phi_N} - 1\right)\left[\partial_0\Gamma^0_{ij} + \Gamma^0_{00}\Gamma^0_{ij} + \Gamma^0_{ij}\Gamma^k_{0k} - \left(\Gamma^0_{jk}\Gamma^k_{0i} + \Gamma^k_{j0}\Gamma^0_{ik}\right)\right] + \\ &+ 2e^{2(\Xi+1)\phi_N}\partial_0\phi_N\Gamma^0_{ij} + \partial_j\partial_i\phi_N - \Gamma^k_{ij}\partial_k\phi_N + \partial_j\phi_N\partial_i\phi_N + \\ &- g_{ij}e^{2(\Xi+1)\phi_N}\Xi\left(3\partial^0\phi_N\partial_0\phi_N + \partial_0\partial^0\phi_N + \Gamma^k_{0k}\partial^0\phi_N\right) - F^{(1)}_{ij} + F^{(2)}g_{ij}\end{aligned} \tag{2.103}$$

The other components of Ricci tensor in rescaled metric read:

$$\begin{aligned}\widetilde{\mathrm{Ric}}_{0i} &= \partial_\alpha\widetilde{\Gamma}^\alpha_{i0} - \partial_i\Gamma^\alpha_{\alpha 0} + \Gamma^\alpha_{\alpha\beta}\Gamma^\beta_{ij} - \Gamma^\alpha_{\beta 0}\Gamma^\beta_{\alpha 0} = \mathrm{Ric}_{i0} - \frac{N-2}{N-1}\partial_0\partial_i\phi_N - \Gamma^0_{00}\partial_i\phi_N + \\ &- \frac{N}{N-1}\Gamma^j_{j0}\partial_i\phi_N + \frac{N-2}{N-1}\Gamma^k_{i0}\partial_k\phi_N + \Gamma^0_{i0}\partial_0\phi_N - g_{00}\Gamma^0_{ij}\partial^j\phi_N + g_{ik}\partial^j\Gamma^k_{j0}\end{aligned} \tag{2.104}$$

It follows that the scalar curvature of the equipotential level sets is given by

$$\mathcal{R}_\Sigma = \tilde{g}^{ij}\widetilde{(\mathrm{Ric}_\Sigma)}_{ij} = e^{-2\Xi\phi_N}\left(\mathcal{R}_\Sigma + 2\frac{(N-2)}{(N-1)}\Delta\phi_N - \frac{(N-3)(N-2)}{(N-1)^2}\|\mathbf{grad}_g\phi_N\|^2_g\right) \tag{2.105}$$

while the scalar curvature of the ambient space $\tilde{\mathcal{R}}$ in rescaled metric reads

$$\begin{aligned}
&\widetilde{\mathcal{R}} = \widetilde{g}^{\alpha\beta}\widetilde{\mathrm{Ric}}_{\alpha\beta} = \widetilde{g}^{00}\widetilde{\mathrm{Ric}}_{00} + \widetilde{g}^{ij}\widetilde{\mathrm{Ric}}_{ij} = e^{2\phi_N} g^{00}\mathrm{Ric}_{00} + \\
&+ e^{-2\Xi\phi_N} g^{ij}\mathrm{Ric}_{ij} - e^{2\phi_N}\left[\frac{2N}{N-1}\Gamma^i_{i0}\phi_N + \frac{3N}{N-1}\partial^0\phi_N\partial_0\phi_N - 2\partial_0\partial^0\phi_N\right] + \\
&+ \left(e^{2\phi_N} - e^{2\Xi\phi_N}\right) g^{ij}\left[\partial_0\Gamma^0_{ij} + \Gamma^0_{00}\Gamma^0_{ij} + \Gamma^0_{ij}\Gamma^k_{0k} - \left(\Gamma^0_{jk}\Gamma^k_{0i} + \Gamma^k_{j0}\Gamma^0_{ik}\right)\right] + 2e^{2\phi_N}\partial_0\Gamma^0_{ij}g^{ij} + \\
&+ \frac{3N-5}{N-1}e^{-2\phi_N\Xi}\left(\Delta_\Sigma\phi_N + \|\mathbf{grad}_\Sigma\phi_N\|^2_{g_\Sigma}\right)
\end{aligned} \tag{2.106}$$

2.4.4 Geometrical interpretation of the configurational microcanonical statistical mechanics

The metric rescaling introduced above allows to give a *pure geometrical interpretation of configurational microcanonical entropy and its derivatives.* If we apply the rule proved in eq.(2.40) to pass the derivatives of the control parameter $\bar{v}$ into the integral of(2.89) we obtain:

$$\begin{aligned}
\frac{\mathrm{d}\Omega_N}{\mathrm{d}\bar{v}} &= \int_{\Sigma^{\overline{V}_N}_{\bar{v}}} \mathcal{L}_{\bar{v}}(\mathrm{d}\sigma_{\Sigma^{\overline{V}_N}_{\bar{v}},\tilde{g}}) = \int_{\Sigma^{\overline{V}_N}_{\bar{v}}} \tau_{1,\tilde{g}}\ \mathrm{d}\sigma_{\Sigma^{\overline{V}_N}_{\bar{v}},\tilde{g}} \\
\frac{\mathrm{d}^2\Omega_N}{\mathrm{d}\bar{v}^2} &= \int_{\Sigma^{\overline{V}_N}_{\bar{v}}} \mathcal{L}_{\bar{v}}(\tau_{1,\tilde{g}}\,\mathrm{d}\sigma_{\Sigma^{\overline{V}_N}_{\bar{v}},\tilde{g}}) = \int_{\Sigma^{\overline{V}_N}_{\bar{v}}} \left[\tau^2_{1,\tilde{g}} + \mathcal{L}_{\boldsymbol{\nu}_N}(\tau_{1,\tilde{g}})\right]\ \mathrm{d}\sigma_{\Sigma^{\overline{V}_N}_{\bar{v}},\tilde{g}} \\
\frac{\mathrm{d}^3\Omega_N}{\mathrm{d}\bar{v}^3} &= \int_{\Sigma^{\overline{V}_N}_{\bar{v}}} \left[\tau^3_{1,\tilde{g}} + 3\tau_{1,\tilde{g}}\mathcal{L}_{\boldsymbol{\nu}_N}(\tau_{1,\tilde{g}}) + \mathcal{L}_{\boldsymbol{\nu}_N}\left(\mathcal{L}_{\boldsymbol{\nu}_N}(\tau_{1,\tilde{g}})\right)\right]\ \mathrm{d}\sigma_{\Sigma^{\overline{V}_N}_{\bar{v}},\tilde{g}} \\
\frac{\mathrm{d}^4\Omega_N}{\mathrm{d}\bar{v}^4} &= \int_{\Sigma^{\overline{V}_N}_{\bar{v}}} \Big[\tau^4_{1,\tilde{g}} + 6\tau^2_{1,\tilde{g}}\mathcal{L}_{\boldsymbol{\nu}_N}(\tau_{1,\tilde{g}}) + 4\tau_{1,\tilde{g}}\mathcal{L}_{\boldsymbol{\nu}_N}(\mathcal{L}_{\boldsymbol{\nu}_N}(\tau_{1,\tilde{g}})) + \\
&\quad + 3\tau_{1,\tilde{g}}\left(\mathcal{L}_{\boldsymbol{\nu}}(\tau_{1,\tilde{g}})\right)^2 + \mathcal{L}_{\boldsymbol{\nu}_N}(\mathcal{L}_{\boldsymbol{\nu}_N}(\mathcal{L}_{\boldsymbol{\nu}_N}(\tau_{1,\tilde{g}})))\Big]\mathrm{d}\sigma_{\Sigma^{\overline{V}_N}_{\bar{v}},\tilde{g}}
\end{aligned} \tag{2.107}$$

and consequently, using eqs.(2.55),(**??**) and the definition of mean curvature in (**??**) we obtain for the derivatives of specific configurational microcanonical entropy:

$$\frac{\mathrm{d}\overline{S}_N}{\mathrm{d}\bar{v}}(\bar{v}) = \frac{1}{N}\langle\tau_{1,\tilde{g}}\rangle_{\bar{v},\tilde{\sigma}} = \frac{(N-1)}{N}\langle h_{\tilde{g}}\rangle_{\bar{v},\tilde{\sigma}} \tag{2.108}$$

$$\begin{aligned}
\frac{\mathrm{d}^2\overline{S}_N}{\mathrm{d}\bar{v}^2}(\bar{v}) &= \frac{1}{N}\left[\langle\tau^2_{1,\tilde{g}}\rangle_{\bar{v},\tilde{\sigma}} + \langle\mathcal{L}_{\nu_N}(\tau_{1,\tilde{g}})\rangle^2_{\bar{v},\tilde{\sigma}} - \langle\tau_{1,\tilde{g}}\rangle^2_{N\bar{v},\tilde{\sigma}}\right] = \\
&= \frac{(N-1)}{N}\left[(N-1)\mathrm{Var}_{N\bar{v},\tilde{\sigma}}(h_{\tilde{g}}) + \langle\mathcal{L}_{\nu_N}(h_{\tilde{g}})\rangle_{N\bar{v},\tilde{\sigma}}\right]
\end{aligned} \tag{2.109}$$

$$\frac{\mathrm{d}^3\overline{S}_N}{\mathrm{d}\overline{v}^3} = \frac{1}{N}\Big[\left\langle\tau^3_{1,\tilde{g}}\right\rangle_{\bar{v},\tilde{\sigma}} + 3\left\langle\tau_{1,\tilde{g}}\mathcal{L}_{\nu_N}(\tau_{1,\tilde{g}})\right\rangle_{\bar{v},\tilde{\sigma}} + \left\langle\mathcal{L}^{(ii)}_{\nu_N}(\tau_{1,\tilde{g}})\right\rangle_{\bar{v},\tilde{\sigma}} +$$
$$+ 3\left\langle\tau_{1,\tilde{g}}\right\rangle_{\bar{v},\tilde{\sigma}}\left\langle\mathcal{L}_{\nu_N}(\tau_{1,\tilde{g}})\right\rangle_{\bar{v},\tilde{\sigma}} - 3\left\langle\tau_{1,\tilde{g}}\right\rangle^2_{\bar{v},\tilde{\sigma}}\left\langle\tau_{1,\tilde{g}}\right\rangle_{\bar{v},\tilde{\sigma}} + 2\left\langle\tau_{1,\tilde{g}}\right\rangle^3_{\bar{v},\tilde{\sigma}}\Big] =$$
$$= \frac{(N-1)}{N}\left[(N-1)^2\mathrm{Cumul}^{(3)}_{\bar{v},\sigma}(h_{1,\tilde{g}}) + (N-1)\mathrm{Cov}_{\bar{v},\sigma}(h_{1,\tilde{g}};\mathcal{L}_{\nu_N}(h_{1,\tilde{g}})) + \left\langle\mathcal{L}^{(ii)}_{\nu_N}(h_{1,\tilde{g}})\right\rangle_{\bar{v},\tilde{\sigma}}\right] \tag{2.110}$$

$$\frac{\mathrm{d}^4\overline{S}_N}{\mathrm{d}\overline{v}^4}(\bar{v}) = \frac{1}{N}\Bigg[\mathrm{Cuml}^{(4)}_{\bar{v},\mu}(\tau_{1,\tilde{g}}) + 6\mathrm{Cov}_{\bar{v},\mu}\left(\tau_{1,\tilde{g}};\tau_{1,\tilde{g}}\mathcal{L}_{\nu_N}(\tau_{1,\tilde{g}})\right) + 3\mathrm{Var}_{\bar{v},\mu}\left(\mathcal{L}_{\nu_N}(\tau_{1,\tilde{g}})\right) +$$
$$+ 4\mathrm{Cov}_{\bar{v},\mu}\left(\tau_{1,\tilde{g}};\mathcal{L}^{(ii)}_{\nu_N}(\tau_{1,\tilde{g}})\right) + 12\mathrm{Cov}_{\bar{v},\mu}\left(\tau^2_{1,\tilde{g}};\mathcal{L}_{\nu_N}(\tau_{1,\tilde{g}})\right) + \left\langle\mathcal{L}^{(iii)}_{\nu_N}(\tau_{1,\tilde{g}})\right\rangle_{\bar{v},\mu}\Bigg] =$$
$$= \frac{(N-1)}{N}\Bigg[(N-1)^3\mathrm{Cuml}^{(4)}_{\bar{v},\mu}(h_{1,\tilde{g}}) + 6(N-1)^2\mathrm{Cov}_{\bar{v},\mu}\left(h_{1,\tilde{g}};h_{1,\tilde{g}}\mathcal{L}_{\nu_N}(h_{1,\tilde{g}})\right) + \tag{2.111}$$
$$+ 12(N-1)^2\mathrm{Cov}_{\bar{v},\mu}\left(h^2_{1,\tilde{g}};\mathcal{L}_{\nu_N}(h_{1,\tilde{g}})\right) + 3(N-1)\mathrm{Var}_{\bar{v},\mu}\left(\mathcal{L}_{\nu_N}(h_{1,\tilde{g}})\right) +$$
$$+ 4(N-1)\mathrm{Cov}_{\bar{v},\mu}\left(h_{1,\tilde{g}};\mathcal{L}^{(ii)}_{\nu_N}(h_{1,\tilde{g}})\right) + \left\langle\mathcal{L}^{(iii)}_{\nu_N}(h_{1,\tilde{g}})\right\rangle_{\bar{v},\mu}\Bigg]$$

where the statistical quantities are calculated over the level sets $\Sigma^{\overline{V}_N}_{\bar{v}}$ using the induced Riemannian area form $\mathrm{d}\sigma_{\Sigma^{\overline{V}_N}_{\bar{v}},\tilde{g}}$ that coincides with the microcanonical area measure.
It has to be stressed that in the Riemannian formulation proposed for the configurational microcanonical ensemble **the inverse of microcanonical temperature** $\beta(\bar{v}) = T^{-1}(\bar{v}) = (\partial\overline{S}_N/\partial\bar{v})$ **coincides for large** N **with the average of the mean curvature of the associated equipotential level set** $\Sigma^{\overline{V}_N}_{\bar{v}}$ **giving a quite simple geometrical interpretation of this basic statistical mechanics observable**.
More in general, the geometrical interpretation of statistical mechanics in configurational microcanonical ensemble can help the research of other signatures at finite N, with respect to topological changes, that signal the presence of phase transitions. In i particular we remark that an interesting possible starting point for further investigations consists in the formalization in geometrical terms of a condition that can allow to prevent the second order derivative of entropy to be non-negative. In fact, according to the theory of microcanonical statistical analysis (briefly reviewed insection 1.3) a signature of phase transition in the microcanonical ensemble is the non-concavity of the entropy, i.e. $\partial^2_{\bar{E}}\overline{S}_N \geq 0$ or $\lim_{N\to+\infty}\partial^2_{\bar{E}}\overline{S}_N(\bar{E}_c) = 0$.
Assuming that the same signature of phase transitions is observed also in configuration space, the condition that has to be imposed to prevent phase transitions in thermodynamic limit is given by

$$\mathrm{Var}_{\bar{v},\bar{\sigma}}\tilde{h}_{1,\tilde{g}} \leq B < \left\langle\mathcal{L}_{\tilde{\boldsymbol{\nu}}_N}\tilde{h}_{1,\tilde{g}}\right\rangle \qquad \forall N \in \mathbb{N}\ . \tag{2.112}$$

In this framework, the problem of phase transitions could be formulated in terms of suitable condition that has to be imposed to the mean curvature field $\tilde{h}_{1,\tilde{g}}$ in order to satisfy the condition

in eq.(2.112) and that can be possibly read as a geometrical characterization of a topological asymptotic change.
The most difficult issue to overcome in this scheme of refinement of the Necessity Theorem is constituted by the derivation of an upper bound of the variance of the mean curvature over a level set. This aspect is still an open problem; nevertheless some possible strategies to derive upper bounds of the variance have been investigated. A promising starting point to attain this aim would be the Poincar Inequality [Led05]

$$\lambda_1 \mathrm{Var}_{\bar{v},\bar{\sigma}} f \leq \left\langle \|\mathbf{grad}_g f\|^2 \right\rangle_{\bar{v},\bar{\sigma}} \tag{2.113}$$

where λ_1 is the first non trivial eigenvalues of the Laplace-Beltrami operator. Lower bounds on λ_1 for compact riemannian manifolds (M, g) with non-negative Ricci curvature have been obtained by Li-Yau and Zhong-Yang (see [Li93] and reference therein)

$$\lambda_{1,g}(M) \geq \frac{\pi^2}{\mathrm{diam}_g^2(M)} \tag{2.114}$$

where $\mathrm{diam}_g(M)$ is the diameter of the manifold. Another important results is the Lichnerowicz theorem:

Theorem 2.4.1 (Lichnerowicz theorem)**.** *et M be an N-dimensional compact manifold without boundary. Suppose that the Ricci curvature of M is bounded from below by*

$$\mathrm{Ric}_{ij} \geq (N-1)K \tag{2.115}$$

for some constant $K > 0$, then the first nonzero eigenvalue of the Laplacian on M must satisfy

$$\lambda_{1,g}(M) \geq NK \tag{2.116}$$

Moreover, equality holds if and only if M is isometric to a standard sphere of radius $K^{-1/2}$.

Despite of the fact that these results would seem to suggest the possibility to easily construct non tautological geometrical conditions on the mean curvature $\tilde{h}_{1,\tilde{g}}$, the condition of non-negative Ricci curvature $\widetilde{(\mathrm{Ric})}_{ij}$ seems to not be easily verifiable *a priori* from eq.(2.101) nor *a posteriori* from the results of numerical simulations on equipotential level sets as it is a pointwise condition.

2.5 Persistent homology: a method to "compute" topology

In the previous chapter it has been stressed that the Topological Theory has the great advantage, with respect to other approaches on phase transitions, to provide at the same time a minimalist and powerful mathematical framework for the understanding of the deep origin of phase transitions: the topological properties of the equipotential level sets. Despite this, the topological approach suffers from computational difficulties, and analytic topological information can be obtained only for a very few models.

Also the direct numerical measurement of topological properties of the configuration space of physical systems faces serious computational issues because of the high dimensionality of the associated manifolds. The idea that some of the mentioned computational obstacles could be overcome comes from the observation of the existence of new computational tools in the fields of discrete geometry and topology. These new methods have already been developed for analysing data in high-dimensional spaces[NSW08]. Hence, we expect that they could be useful to investigate topological changes also in physical configuration spaces by identifying their homology from random samples.

In what follows we resort to *persistent homology* analysis. Persistent homology [Ghr08, CZ05, Car09], a particular sampling-based technique from algebraic topology, was originally introduced in 2002 [ELA02] by Edelsbrunner *et al* with the aim of extracting coarse topological information from high-dimensional datasets [NSW08]. In a nutshell, while *homology* detects the connected components, tunnels, voids of a given topological space, persistent homology computes multi-scale homological features obtained from a discrete sample of a topological space X by foliating it appropriately. Hitherto, the study of persistent homology has already proved useful in various fields like biological and medical data analysis, neuroscience [PET+14], sensor network coverage problems [DSG07], to quote just a few of them.

Here persistent homology is applied to the study of equilibrium phase transitions. Two models are considered for which we rigorously know what to expect: the so-called Mean-Field XY model (MFXY) and the classical lattice φ^4 model already introduced before. For the MFXY model both the thermodynamics and the configuration space topology are exactly known, whence the topological origin of phase transition is rigorously ascertained; while for the φ^4 model it is analytically known that the phase transition does not correspond to any topology change in configuration space at any *finite* N.

The benchmarking so performed gives sharp and unambiguous results in the good direction. This could open new interesting perspectives for practical applications of the topological theory of phase transitions.

2.5.1 The Mean-Field XY Model.

The mean-field XY model is defined by the Hamiltonian [AR95, CDR09]

$$\begin{aligned} \mathcal{H}(p,\varphi) &= \sum_{i=1}^{N} \frac{p_i^2}{2} + \frac{J}{2N} \sum_{i,j=1}^{N} [1-\cos(\varphi_i-\varphi_j)] \\ &- h \sum_{i=1}^{N} \cos\varphi_i \ . \end{aligned} \tag{2.117}$$

Here $\varphi_i \in [0, 2\pi]$ is the rotation angle of the ith rotator and h is an external field. Defining at each site i a classical spin vector $\mathbf{m}_i = (\cos\varphi_i, \sin\varphi_i)$, the model describes a planar (XY) Heisenberg system with interactions of equal strength among all the spins. We consider the ferromagnetic case $J = 1$. The equilibrium statistical mechanics of this system is exactly described, in the thermodynamic limit, by mean-field theory. In the limit $h \to 0$, the system

has a continuous phase transition, with classical critical exponents, at the critical temperature $T_c = 1/2$, or at the critical energy density $E_c/N = 3/4$ [AR95].

The entire configuration space M of the model is an N-dimensional torus, parametrized by N angles. The submanifolds $M_v \subset M$ are defined by

$$\begin{aligned} M_v &= \mathcal{V}^{-1}(-\infty, v] \\ &= \{(\varphi_1, \ldots, \varphi_N) \in M : \mathcal{V}(\varphi_1, \ldots, \varphi_N) \leq v\} \ , \end{aligned} \tag{2.118}$$

i.e., defined by the constraint that the potential energy per particle $\mathcal{V} = V/N$ does not exceed a given value v.

Morse theory states that topology changes of the M_v occur in correspondence with critical points of $\mathcal{V}$, i.e., those points where $\nabla\mathcal{V} = 0$. This implies that there are no topological changes for $\mathcal{V} > 1/2 + h^2/2$, i.e., all the M_v with $\mathcal{V} > 1/2 + h^2/2$ are diffeomorphic to the whole M.

The Euler characteristic, a topological invariant of the manifolds M_v which is *exactly* computed in Ref.[CPC00, CPC03], is defined by

$$\chi(M_v) = \sum_{k=0}^{N} (-1)^k \mu_k(M_v) \ , \tag{2.119}$$

where the Morse number μ_k is the number of critical points of $\mathcal{V}$ that have index k [Mil63].

After a monotonic growth with v, a sharp, discontinuous jump to zero of $\chi(M_v)$ is found at the phase transition point, that is, at $v_c = 1/2 + 0^+$. However, as already shown in [CPC00, CPC03], it is just this major topological change occurring at v_c that is related to the thermodynamic phase transition of the Mean Field XY model.

2.5.2 Topological analysis

Some basic fact are here reported concerning the topological analysis which begins by sampling the configuration space of each system at different energies. Then persistent homology analysis is applied

2.5.3 Samples of the configuration space

We begin by constructing samples of the configuration spaces to be studied. For the MF XY model, this is done by numerically integrating the equations of motion derived from Hamiltonian ((2.117)) with the external field set to $h = 0$ for a system of N spins, with N up to 6000. The numerical integration is performed by means of a fifth-order optimal symplectic algorithm [MA92]. We sampled the configuration space for the following values of the energy density $\varepsilon = E/N = 0.6, 0.75, 0.88$, that is, below, at, and above the critical energy, respectively. The system is initialized with a Gaussian distribution for both conjugated variables $\{\varphi_i, p_i\}$. The total angular momentum ($P = \sum_i p_i = 0$) is imposed to vanish. Given the initial conditions for the aforementioned energies, the system dynamics is evolved for a $T = 1.26 \cdot 10^7$ time steps, with an integration step of $\Delta t = 0.05$. With these integration step and the use of a fifth order

symplectic algorithm the relative energy fluctuations were kept at $\Delta E/E \simeq 10^{-9}$. Then 6000 snapshots are uniformly sampled in time after a transient dynamics to equilibrate kinetic and potential energies to their equipartition values.
For the ϕ^4 model we set $J = 1, m^2 = 2, d = 3$ and $\lambda = 0.1$ in the Hamiltonian ((**??**)). We consider a 3D cubic lattice with 8^3 sites, periodic boundary conditions, and an integration time step $\Delta t = 0.05$. With these parameters, the use of a third order symplectic algorithm [Cas95a] kept the relative energy fluctuations at $\Delta E/E \simeq 10^{-9}$ (a lower order algorithm was required in this case with respect to the MFXY model because trigonometric functions are replaced by the polynomial form of the ϕ^4 potential). Then the Hamiltonian dynamics is numerically simulated at two different values of the energy density, that is, $\varepsilon = 25$ well below the transition energy density $\varepsilon_c \simeq 31$ [CCC+98a], and $\varepsilon = 35$ well above ε_c.

2.5.4 Persistent Homology

The main idea of persistent homology is to build an increasing sequence of simplicial complexes, called a *filtration* (see [CZ05]), from a *point cloud*, i.e. a set of points embedded in a metric space. We report a detailed mathematical description of persistent homology in Appendix C refer the interested reader to [CZ05]. Here we streamline the topological analysis. The standard way to obtain a simplicial complex from a set of points S is to construct its ρ-Rips-Vietoris complex [CZ05], an abstract simplicial complex that can be defined on any set of points in a given metric space $\mathcal{M}$. The n simplices of the ρ-Rips-Vietoris complex are determined by subsets of $n+1$ points $\{p_0, \ldots, p_n\}$ such that $D(p_i, \rho) \cap D(p_j, \rho) \neq \emptyset$ for all $i \neq j \in \{0, \ldots, n\}$, where $D(p, \rho)$ is ball of radius ρ centered at p. Persistent homology is a powerful instrument in that it does not select just an ρ value, but rather studies how the homology of the space, and in particular of the ρ-Rips-Vietoris complexes, changes as ρ varies. As ρ is increased, simplexes are added in the ρ-Rips-Vietoris simplicial complex. A new simplicial complex is added to the filtration only when a new simplex is born along the (continuous) parameter ρ. i.e., the ρ-Rips-Vietoris complex has changed. Thus the filtration is discrete: it can be indexed by integers, useful to characterize the topological features of the space.

2.5.5 Simplicial Complexes in configuration space

In most applications of persistent homology, the parameter ρ is taken to represent the Euclidean distance between points in S. In the case of physical configuration spaces we replace it by a Riemannian one. In fact, the configuration space M of a standard Hamiltonian systems (that is with quadratic kinetic energy) equipped with the Jacobi metric [Pet07a], is a *complete Riemannian manifold*, which means that given any two points there exists a length-minimizing geodesic connecting them (Hopf-Rinow theorem [**?**]). Of course this is also the case of the mean-field XY and ϕ^4 models, thus the distance among two points P_1 and P_2 in M is:

$$d(P_1, P_2) = \int_{P_1}^{P_2} \left([E - V(\varphi_1, \ldots, \varphi_N)] \sum_{k=1}^{N} (d\varphi^k)^2 \right)^{\frac{1}{2}} \tag{2.120}$$

In other words, computing this distance requires solving the equations of motion with assigned initial and final conditions. In practice this is computationally very heavy. We therefore take advantage of the robustness of topological information with respect to metrical deformations and observe that the integral contains a non constant factor multiplying the Euclidean arc length. We then choose to approximate $d(P_1, P_2)$ by replacing the factor by its mean among the initial and final values:

$$d(p_1, p_2) = \frac{1}{2}(\sqrt{E - V(p_1)} + \sqrt{E - V(p_2)})d_{eucl}(p_1, p_2) \tag{2.121}$$

$$d_{eucl}(p_1, p_2) = \sqrt{\sum_{k=1}^{N}(\varphi^k(p_2) - \varphi^k(p_1))^2} \tag{2.122}$$

An important computational issue lies in the size of the produced simplicial complexes. Indeed, already for a sample of the configuration space S with cardinality $N = 6000$ points, the set of complexes will contain a huge number of simplices hindering efficient computation, since the number of all simplices for all dimensions up to $N - 1$ scales as number of subsets of N, that is 2^N. So, we first restrict ourselves to the study of the first two homology groups, H_0 and H_1, which allows us to consider only simplices up to dimension 2 and then adopt a sub-sampling strategy which allows to reduce the dimension of the problem by choosing a representative subset of points $L \subset S$ without losing important topological features of the configuration space. The sub-sampling is based on a suitable selection of landmark points called *sequential maxmin* [SML05, GH10]. In sequential maxmin, the first landmark is picked randomly from S. Inductively, if L_{i-1} is the set of the first $i - 1$ landmarks, then let the i-th landmark be the point of S which maximizes the distance ((2.121)) from all the points of L_{i-1}. Since the starting node is chosen at random, the resulting L subsets will change if the algorithm is iterated. In our case, this allows us to perform a bootstrap-like procedure, by repeatedly subsampling the full point clouds and then aggregating the homological signatures detected. The results we present are obtained from 20 different sub-samples, each containing 300 points.

2.5.6 Results

Persistent homology computes the generators of topological features (homology groups) persisting across different scales and assigns them birth and death values related to their points of appearance and disappearance along the filtration. That is, when the radius ρ of the balls varies, for any persistent generator g we have the value of the parameter ρ of the filtration where g first appears (birth index indicated by β_g) and the value where it disappears (death index indicated by δ_g). In this way, connected components, one-dimensional cycles, three-dimensional voids and similar higher order structures of the topological space $\mathcal{M}$ acquire a weight proportional to the length of their persistence interval, $\pi_g = \delta_g - \beta_g$. Note that for H_0, $\pi_g = \delta_g$, because all (dis)connected components are already present at the beginning. For higher order homology groups H_k the generators can instead appear and disappear freely along the filtration.

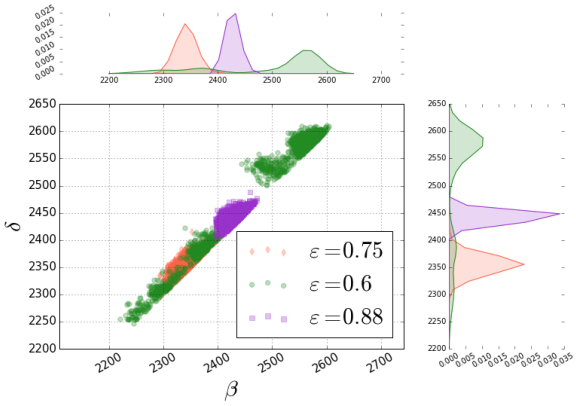

Figure 2.13: (Color online) Persistence diagram for the $MFXY$ model. H_1 persistence distributions below ($\varepsilon = 0.6$), at ($\varepsilon_c = 0.75$), and above ($\varepsilon = 0.88$) the phase transition.

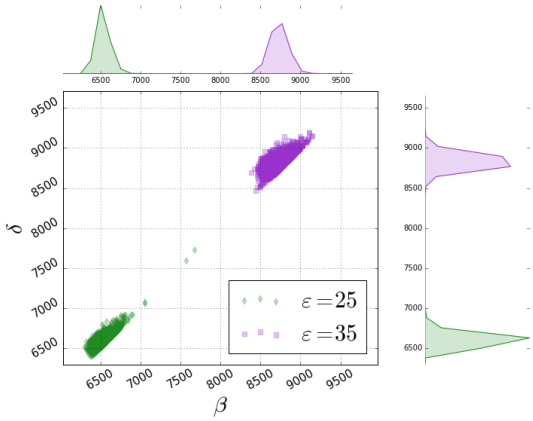

Figure 2.14: (Color online) Persistence diagram for the ϕ^4 model. H_1 persistence distributions below ($\varepsilon = 25$) and above ($\varepsilon = 35$) the phase transition, occurring at the critical energy density $\varepsilon_c \simeq 31$.

In Figures Figure 2.13 and Figure 2.14 the basic descriptors of persistent homology, that is, persistence diagrams, are displayed for the H_1 generators of the $MFXY$ model and of the ϕ^4 model, respectively.

Usually one considers important topological features to be those associated with generators of H_n such that their π_g is large with respect to some meaningful length.
In our case we do not have a given reference scale. We can however compare the results obtained at energies below and above the transition energy in order to look for topological signatures of a phase transition. We show the distributions of δ_g for the H_0 generators of the $MFXY$ model (Fig. Figure 2.15) and of the ϕ^4 model (Fig. Figure 2.16). In the former case, as the energy is increased, the peak of the distribution δ_g of H_0 becomes progressively narrower and centred at larger ρ-values. To the contrary, in the latter case the peak of the distribution shifts to larger ρ values at higher energies, but it does not broaden.

In order to show that this behaviour is genuinely due to topological features and not due to the different geometrical sizes of the point clouds, we take the point cloud at the lowest energy

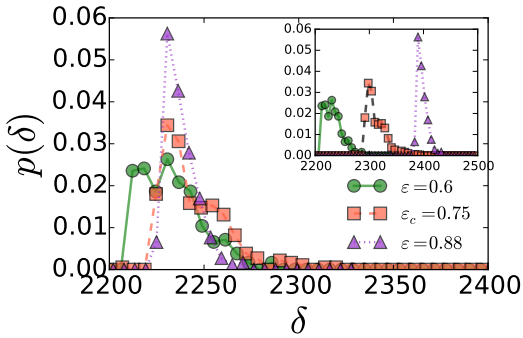

Figure 2.15: Homological features of the $MFXY$ model. Raw (inset) and rescaled (main plot) distributions of deaths for the generators of the first homology group H_0. Note that the width and shape of the distributions change across the transition, becoming more and more narrow as the energy is increased

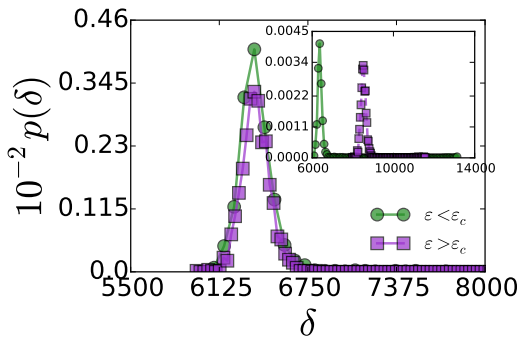

Figure 2.16: Homological features of the ϕ^4 model. Raw (inset) and rescaled (main plot) distributions of deaths for the generators of the first homology group H_0. At variance with the $MFXY$ model, here there is no appreciable change in the width and shape of the distributions across the transition. The green points refer to $\varepsilon = 25 < \varepsilon_c$. The velvet points refer to $\varepsilon = 35 > \varepsilon_c$.

and affinely rescale the point clouds at higher energies as to make them comparable i.e.

$$d_{ij}(\varepsilon) \to \frac{\langle d(\varepsilon_0\rangle}{\langle d(\varepsilon)\rangle} d_{ij}(\varepsilon) \tag{2.123}$$

where $d_{ij}(\varepsilon)$ is the distance between points i and j for the pointcloud at energy density ε. In this way, we can meaningfully compare the persistences of generators belonging to clouds of different size. Below the transition of the MFXY model, the distribution of the H_0 persistences of configuration space covers more scales than it does at and above the transition energy, respectively. This broader distribution means that the corresponding point cloud is heterogeneously distributed in the embedding space $\mathcal{M}$ compared to the distributions, definitely more homogeneous, in the other two cases. No variation of the peak widths of the H_0 persistence distributions is observed in the case of the ϕ^4 model.

Figures Figure 2.15 and Figure 2.16 display the raw (inset) and rescaled (main plot) distributions of deaths for the generators of the first homology group H_0. The rescaling is necessary to make the point clouds, sampled at different energies, comparable. In fact, the death and

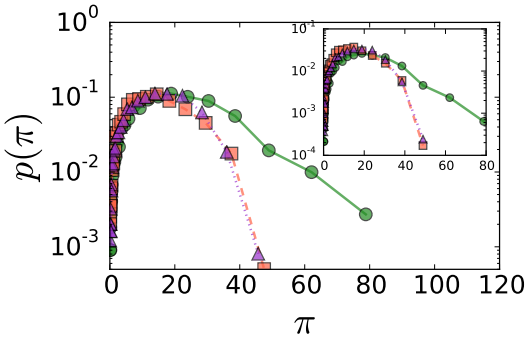

Figure 2.17: Distributions of persistences for the generators of the homology group H_1 in the case of the $MFXY$ model. In this case the difference in functional forms for the H_1 persistence distribution below and above the transition is even clearer.

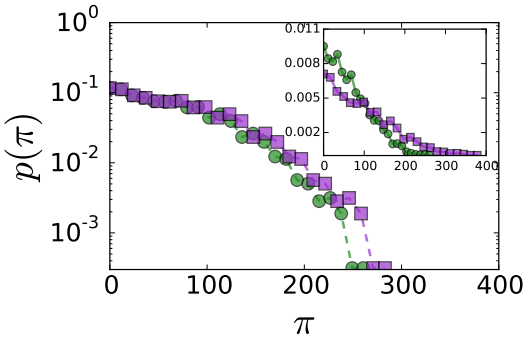

Figure 2.18: Distributions of persistences for the generators of the homology group H_1 in the case of the ϕ^4 model. In this case no difference is found in functional form for the H_1 persistence distributions below and above the transition.

birth indexes are the values of the radius of the balls where the generators appear and disappear. Thus, without the rescaling, β_g and π_g would reflect the size of the underlying manifold. Note that for the $MFXY$ model the width and shape of the distributions change across the transition, becoming more and more narrow as the energy is increased, while there is no appreciable change in the ϕ^4 case. The different topological signatures highlight the presence of a topological change in the case of the MFXY model, that is absent in the ϕ^4 model. In Figures Figure 2.17 and Figure 2.18 the distributions of persistences for the generators of the homology group H_1 confirm what is found for H_0. In this case the difference in functional forms for the H_1 persistence distribution below and above the $MFXY$ transition is even clearer, while, again, we find no differences for the ϕ^4 model.

Now let us comment about the hollowness detected by the H_1 homology group. For what concerns the MFXY model, below the phase transition energy, the H_1 persistence distribution displays a long tail which disappears at and above the transition (Fig. Figure 2.17). We observe that the three sets of points superpose for values of π less then approximately 25. This range of π values, in the present context, can be attributed to what is commonly referred to as noise, whereas larger π-values are usually considered as bringing about meaningful topological information. Thus, the stronger persistence of meaningful cycles, which corresponds to the long tail observed below the phase transition point of the MFXY model, certainly probes a change of "shape" of configuration space. And this change of shape can be interpreted as the signature of a change of the dimension of high order homology groups.
Let us remark that the performed samplings of configuration space submanifolds are definitely sparse and they could not be other then sparse had we taken billions of points. Not to speak of the huge total number of simplexes, growing as 2^N with N the number of sample points. This notwithstanding, the results shown in Fig. Figure 2.17 clearly tell us that the MFXY phase transition corresponds to a change of the topology of the configuration space submanifolds, in perfect agreement with the available theoretical knowledge. The same concordance is found in the case of the ϕ^4 model where we see that the difference in H_1 persistences disappears, in perfect agreement with a-priori known absence of topological changes of the underlying configuration space in correspondence with the phase transition.

Finally, in Figures Figure 2.19 and Figure 2.20 we show the outcomes of a different method of getting insight to the "shape" of data obtained by sampling the configuration space of the $MFXY$ and ϕ^4 models, respectively. This is the so called *persistence landscape* which combines the main tool of persistent homology method, that is, persistence diagram, with statistics [**?**]. With respect to the barcode or persistence diagram this descriptor has the technical advantage of being a function, thus allowing the use of the vector space structure of its underlying function space to apply the theory of random variables with values in this space. Theory and details of this method can be found in Refs. [**?**] and [**?**]. In practice, one proceeds by computing the H_1 homology for a subsample of the original dataset, then one associates to each generator a symmetric tent-shaped function peaking in the middle of the persistence interval of the corresponding generators and finally one considers the envelope of the functions defined in this way over all the generators. Informally, one can think of the persistence landscape as the envelope

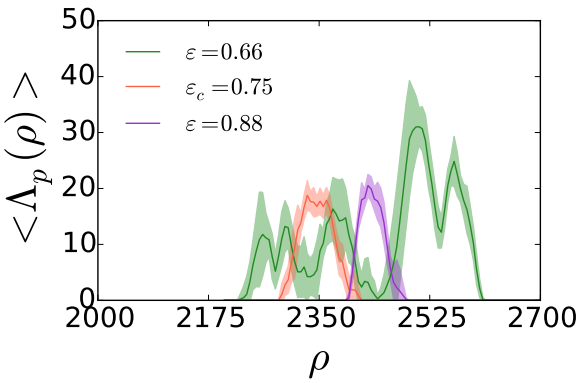

Figure 2.19: (Color online) Average persistence landscape of the H_1 homology for the $MFXY$ model. Λ_p is the average function (see text) reported as a function of the radius ρ of the balls used to construct the Rips-Vietoris simplicial complex. The "shadows" around solid lines are 95% confidence band.

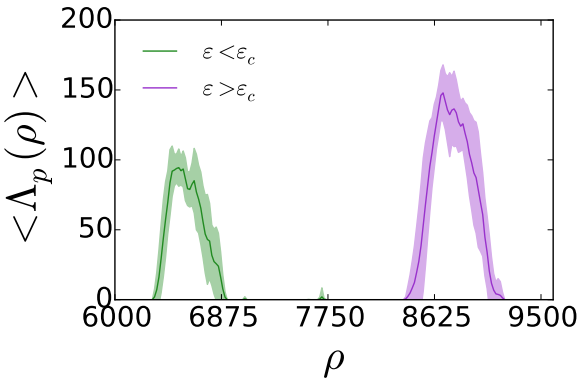

Figure 2.20: (Color online) Average persistence landscape of the H_1 homology for the ϕ^4 model. Λ_p is the average function (see text) reported as a function of the radius ρ of the balls used to construct the Rips-Vietoris simplicial complex. The "shadows" around solid lines are 95% confidence band.

of the $\pi/4$-clockwise rotated persistence diagram (operation that can be given a proper mathematical definition) thus associating a curve $\Lambda_p(\rho)$ to each persistence diagram. In our case, we iterated this procedure for the different subsamples, in our case 20 subsamples, obtaining the curve $\langle\Lambda_p(\rho)\rangle$ averaged over the samples. Each curve reported in Figure Figure 2.19 reports the results for different energy values: below, at, and above the phase transition point. A marked difference is again obtained above and below the phase transition in the case of the $MFXY$ model, and no relevant difference between the patterns below and above the phase transition in the case of the ϕ^4 model, apart from a meaningless translation.

2.5.7 Some remarks on the application of persistent homology to Topological Theory

The results reported for each model in the Figures shown in the preceding Section, and especially the comparison with those reported in Figures Figure 2.17, Figure 2.18, Figure 2.19

and Figure 2.20 are strongly supportive of the validity of the application of persistent homology to probe major topological changes in the configuration spaces of physical systems undergoing phase transitions.

The results reported in the present work show that persistent homology, by providing handy computational tools (which are presently available as open access software packages), can lend new credit to the prospective practical interest of the topological theory of phase transitions. And, especially, since improvements of the numerical algorithms are continuously underway. Moreover, this opens many fascinating and challenging questions related with the mentioned necessarily sparse sampling of high dimensional manifolds. It is not out of place to mention that this situation is reminiscent of Montecarlo methods which typically allow efficient estimates of multiple integrals in high dimensional spaces with very sparse samplings. Monte Carlo methods owe their efficacy to the so called *importance sampling* technique, suggesting that further developments in the proposed application of the persistent homology could be found in a somewhat similar direction.

PART II

Self organization and out-of-thermal equilibrium PTs in biological systems

CHAPTER 3 Basics facts on the theory of long range interactions among biomolecules

A review on the state of art of search of selective long range electrodynamic interactions among biomolecules is presented in this chapter. Main theoretical background of ongoing researches are presented; in particular some main aspect of the so called *Fröhlich condensation* (the analogous of Bose-Einstein condensation for out-of-thermal-equilibrium systems) are recalled in relation to the possibility to activate such long range interactions among biomolecules.

3.1 Motivations

The maintenance of cell functions is based on a precise orchestration of functional interactions among different biomolecules such as DNA, RNA and proteins. Although these basic mechanisms generally do not exhibit strict spatial organization, they seem forced into a very accurate temporal -or dynamic- pattern. This raises the question of what types of physical forces can, in the cellular environment (or environments), bring the various actors of complex biochemical processes both in the right place, at the right time and in the right order so as to ensure the essential cellular functions. Random encounters between cognate partners involved in biochemical reactions cannot explain such a level of *dynamical* organization in cellular environments; if only random forces acted on biomolecules they would undertake brownian diffusion and, for the typical conditions in cells environments, the average encounter time for cognate partner of biochemical reactions would result to be much greater then one observed experimentally in real systems. Some mechanisms have been proposed to (partially) explain such an efficiency for biomolecules to find their targets: one of the most celebrated examples in this sense is the facilitated diffusion (such example will be briefly discussed later). Although such a mechanism successfully allows to explain how some molecules find their targets in the right time, such a theory requires the presence of structures on which the molecules "slide": it remains an unsolved problem to understand how singular components can find each other within in the "mess" of cellular environment to self-assembly in such complex structures.
In this framework it seems quite reasonable to formulate the hypothesis of the existence of mutual interactions among biomolecules of non negligible effects on the distance range of $0.1-1\mu$m (corresponding to the typical cellular length scale), in order to create the dynamical organization discussed before by facilitating the encounters of cognate partners of biochemical reactions. In order to be compatible with what observed in real biological systems, such interactions should be *selective*, in the sense that they should be established only among the "right" molecules, and should require a mechanism of *activation* (i.e. an external energy supply) in order to act only at the "right" moment.
As discussed later in detail in the following Sections, biological systems are characterized by

conditions that seem to screen every possible long range interaction (specifically electrostatic interactions) while other interactions (chemical bonds, hydrogen bonds, dispersive and Van der Waals interactions) are short range acting at a distance of the order of few Angstroms. Nevertheless, a more detailed analysis, inspired by the the theories formulated by H. Fröhlich in '60s and '70s, reveals that *electrodynamic long range interactions* are possible. Moreover, it has been recently shown from first principles that, in the context of classical electrodynamics, these interactions can act at a long distance only among resonant oscillators and out-of-thermal-equilibrium. In this chapter some of these aspects are reviewed.

3.2 Intermolecular interactions

Intermolecular interactions are responsible of mutual interactions exerted among molecules in every state of matter. In order to clarify what we mean with long-range or short-range interactions (as some improper use of these terms has been done in the literature) we recall that an interaction potential $V(\boldsymbol{r})$ is *short-range* in a d-dimensional space if

$$\lim_{|\boldsymbol{r}|\to+\infty} V(\boldsymbol{r})r^d < +\infty \tag{3.1}$$

while, if the limit in eq.(3.1) diverges, the potential is *long-range*. The intermolecular interactions in biological systems are of electromagnetic nature due to to energy and length scales typical of such systems.

In the following sections relevant potential among biomolecules are reviewed.

3.2.1 Electrostatic interactions

In general biomolecules (DNA,RNA,proteins) have a non negligible net charge and a large dipole moment; it is thus reasonable to wonder which is the role played by electrostatic interactions in biological systems at the molecular scale. Electrostatic interactions are established among electric charges, ions, permanent dipoles, and non vanishing multipolar moments of molecular charge distributions. Electrostatic interactions include the polarization induced in atoms and molecules by electrostatic fields generated by surrounding free electric charges and permanent electric dipoles. Such interactions organise and stabilize the structure of biomolecules contributing to determine their shape and their biological functions. The electrostatic field generated by a given biomolecule is determined by many factors ad the superficial charge distribution, the presence of a solvent (water) and the ionic population of the surrounding environment. The electrostatic interactions among biomolecules are reviewed with emphasis on the effects of the surrounding environment and on the Debye shielding phenomena.

3.2.1.1 Electrostatic interactions in vacuum

Let us consider the electrostatic potential ϕ at a point $\boldsymbol{r}$ of physical space generated by a charge distribution $\{q_i, \boldsymbol{r}_i\}$,

$$\phi(\boldsymbol{r}) = \sum_i \frac{q_i}{|\boldsymbol{r} - \boldsymbol{r}_i|}, \tag{3.2}$$

It is possible to rewrite $|\boldsymbol{r} - \boldsymbol{r}_i|$ as

$$|\boldsymbol{r} - \boldsymbol{r}_i| = \sqrt{(\boldsymbol{r} - \boldsymbol{r}_i)^2} = r\sqrt{1 - \frac{2\boldsymbol{r}.\boldsymbol{r}_i}{r^2} + \left(\frac{\boldsymbol{r}_i}{r}\right)^2}, \tag{3.3}$$

with $r = |\boldsymbol{r}|$. As we are interested to the effects of electrostatic forces on length scales much larger than the characteristic molecular dimensions, we can consider $r \gg r_i \equiv |\boldsymbol{r}_i|$, $\forall i$. In such a case the electrostatic potential ϕ can be expanded in Taylor series

$$\begin{aligned}
\phi(\boldsymbol{r}) &= \frac{1}{r}\sum_i q_i \left\{1 - \frac{2\boldsymbol{r_i}.\boldsymbol{r}}{r^2} + \left(\frac{\boldsymbol{r_i}}{r}\right)^2\right\}^{-1/2} \\
&= \frac{1}{r}\sum_i q_i \left\{1 + \frac{\boldsymbol{r_i}.\boldsymbol{r}}{r^2} - \frac{1}{2}\left(\frac{\boldsymbol{r_i}}{r}\right)^2 + \frac{3}{2}\left(\frac{\boldsymbol{r_i}.\boldsymbol{r}}{r^2}\right)^2 + \cdots\right\} \\
&= \frac{1}{r}\sum_i q_i \left\{1 + \frac{\boldsymbol{r_i}.\boldsymbol{r}}{r^2} + \frac{1}{2}\left(3\left(\frac{\boldsymbol{r_i}.\boldsymbol{r}}{r^2}\right)^2 - \left(\frac{\boldsymbol{r_i}}{r}\right)^2\right) + \cdots\right\}.
\end{aligned} \tag{3.4}$$

So the previous formula can be rewritten as:

$$\phi(\boldsymbol{r}) = \frac{Q}{r} - \sum_{\alpha=1}^{3} \mu_\alpha \frac{\partial}{\partial x_\alpha}\left(\frac{1}{r}\right) - \frac{1}{2}\sum_{\alpha=1}^{3}\sum_{\beta=1}^{3} M_{\alpha\beta}\frac{\partial}{\partial x_\alpha}\frac{\partial}{\partial x_\beta}\left(\frac{1}{r}\right) + \cdots. \tag{3.5}$$

with

$$Q = \sum_i q_i \ , \quad \mu_\alpha = \sum_i q_i x_{i,\alpha} \text{ and } \ M_{\alpha\beta} = \sum_i q_i x_{i,\alpha} x_{i,\beta} \ ;$$

where $x_{i,\alpha}$ are the components of the vector $\boldsymbol{r}_i$, $\alpha = 1, 2, 3$. Q is the total charge, $\boldsymbol{\mu}$ is the dipole momentum vector and $\boldsymbol{M}$ is the quadrupole momentum tensor. It follows that the eq.(3.5) naturally leads to a multipole expansion. Generally electric dipoles generate a field which decreases with distance as $1/r^2$, for quadrupole moments $1/r^3$,for octoupole moments $1/r^4$, etc. etc. In the case of a neutral distribution the first term of the eq.(3.5) is zero, and the electrostatic field is of course a long-range dipolar one.

The multipolar expansion can be applied also in the case of the interaction among an external electrostatic field ϕ and a set of charges $\{q_i, \boldsymbol{r}_i\}$

$$U(\boldsymbol{r}_i) = \sum_i q_i \phi(\boldsymbol{r}_i). \tag{3.6}$$

so substituting $\boldsymbol{r}_i$ for $\boldsymbol{r}+\boldsymbol{r}_i$ with $r \gg r_i$ (*i.e.* the charge distribution is spread around $\boldsymbol{r}$), we obtain:

$$\begin{aligned} U &= \sum_i q_i \left\{ \phi(\boldsymbol{r}) + \sum_\alpha x_{i,\alpha} \frac{\partial}{\partial x_\alpha}\phi(\boldsymbol{r}) + \frac{1}{2}\sum_\alpha \sum_\beta x_{i,\alpha} x_{i,\beta} \frac{\partial}{\partial x_\alpha}\frac{\partial}{\partial x_\beta}\phi(\boldsymbol{r}) \right\} \\ &= \left\{ Q + \sum_\alpha \mu_\alpha \frac{\partial}{\partial x_\alpha} + \frac{1}{2}\sum_\alpha \sum_\beta M_{\alpha\beta} \frac{\partial}{\partial x_\alpha}\frac{\partial}{\partial x_\beta} + \cdots \right\} \phi(\boldsymbol{r}), \end{aligned} \tag{3.7}$$

where Q, $\boldsymbol{\mu}$, $\boldsymbol{M}$,...are the multipole moments of the charge set previously introduced. The dipole contribution to the interaction is determined by the electric field ϵ given by $\boldsymbol{\epsilon} = -\boldsymbol{\nabla}\phi$. So it is possible to calculate the electrostatic interaction potential among biomolecules in the "far field" limit; this is obtained by considering a system composed by a molecule A, characterized by a set of charges $\{q_{A,i}, \boldsymbol{r}_{A,i}\}$, and the electrostatic potential generated by the charge distribution $\{q_{B,j}, \boldsymbol{r}_{B,j}\}$ of a molecule B (with $\boldsymbol{r}_{A,i}$ and $\boldsymbol{r}_{B,j}$ we have indicated the position of the charges $q_{A,i}$ e $q_{B,j}$ with respect to the center of mass of the molecules A e B, respectively). For distances much greater than the characteristic dimensions of the molecules A and B, the interaction potential can be calculated from the eqs.(3.7) and (3.5):

$$\begin{aligned} U(\boldsymbol{r}) &= \left\{ Q_A + \mu_{A,\alpha}\,\partial^\alpha + \frac{1}{2} M_{A,\alpha\beta}\,\partial^\alpha\partial^\beta + \cdots \right\} \phi^B(\boldsymbol{r}) \\ &= \left\{ Q_A + \mu_{A,\alpha}\,\partial^\alpha + \frac{1}{2} M_{A,\alpha\beta}\,\partial^\alpha\partial^\beta + \cdots \right\} \left\{ \frac{Q_B}{r} - \mu_{B,\lambda}\,\partial^\lambda \left(\frac{1}{r}\right) \right. \\ &\qquad \left. + \frac{1}{2} M_{B,\lambda\rho}\,\partial^\lambda\partial^\rho \left(\frac{1}{r}\right) + \cdots \right\}, \end{aligned} \tag{3.8}$$

where $\boldsymbol{r}$ is the vector joining the mass centres of both molecules, where $\alpha, \beta, \gamma, \rho = 1, 2, 3$, and x^1, x^2 and x^3 are the components of the vector $\boldsymbol{r}$ [1]. Hence *in the vacuum* long range interactions are possible. In particular this are:

- the *coulombic electrostatic potential* which depends on the total electric charge

$$U_{coulombian}(r) \simeq \frac{Q_A Q_B}{r}. \tag{3.9}$$

- the *dipole-dipole* interaction potential, given by

$$U_{dd}(r) = -\mu_{A,\alpha}\mu_{B,\lambda}\partial^\alpha\partial^\lambda \left(\frac{1}{r}\right) = \mu_{A,\alpha}\mu_{B,\lambda}\left(\frac{\delta^{\alpha\lambda}}{r^3} - 3\frac{x^\alpha x^\lambda}{r^5}\right). \tag{3.10}$$

  the latter is the only contribution if one of the two biomolecules is electrically neutral.

Higher moments decay with distance as r^{-n}, with $n > d$, resulting in short-range interactions.

[1] The Einstein convention is assumed for repeated indices

3.2.1.2 Dielectric medium and Debye Shielding

In the previous discussion, the effects of the surrounding environment on the intermolecular interactions have been neglected. In biological systems the environment is substantially constituted of a water solution of freely moving ions.
Water is a dielectric medium [2] and in the limit for which it can be considered as a continuous medium, we can adopt the classic theory of polarizable media applies. The polarization field $\boldsymbol{P}$ for isotropic media is given by

$$\boldsymbol{P} = \chi_e \boldsymbol{E}, \tag{3.11}$$

where χ_e is the electric susceptibility [3], in the limit of an arbitrarily small electric field $\boldsymbol{E}$. Such a condition is typically satisfied by biological systems; in the cellular membranes the double layer electric field is of the order of 10^9volts/cm so that the polarization induced in the medium by any external electric field that is negligible. For electric fields generated by a charge distribution $\rho(\boldsymbol{r})$ the relations holds

$$\begin{cases} \boldsymbol{D}(\boldsymbol{r}) = \boldsymbol{E}(\boldsymbol{r}) + 4\pi \boldsymbol{P}(\boldsymbol{r}) \\ \\ \nabla \cdot \boldsymbol{D}(\boldsymbol{r}) = 4\pi\rho(\boldsymbol{r})\,. \end{cases} \tag{3.12}$$

Substituting the relation eqs. (3.11) in (3.12) we obtain an equation for the electric field $\boldsymbol{E}$:

$$\boldsymbol{\nabla} \cdot \boldsymbol{E} = \frac{4\pi\rho}{\varepsilon}. \tag{3.13}$$

where $\varepsilon = 1 + 4\pi\chi_e$ is the electrostatic dielectric constant, thus the effect of the polarizability of the medium is that the electrostatic interactions are screened by a factor $1/\varepsilon$; for the pure water at $300K$ the electrostatic dielectric constant is $\varepsilon \sim 80$.
For media with a high concentration of freely moving ions (as in the case of biological systems) the value of the electric field is strongly affected because these freely moving ions tend to screen any electrostatic field so that $\lim_{r\to+\infty} r\phi(r) = 0$, where $\phi(\boldsymbol{r})$ is the electrostatic potential.
A first theoretical derivation of this screening effect has been obtained by Debye and Hückel in the framework of the electrolytes theory [DH23]: the electrostatic potential $\phi(\boldsymbol{r})$ originated by a single electric charge q in presence of N_{ion} ionic species, each of them with a ionic valence Z_j and a numerical concentration n_j, at temperature T is given by:

$$\Phi(\boldsymbol{r}) = \frac{q}{\varepsilon r} e^{-r/\lambda_D}, \tag{3.14}$$

where λ_D is the Debye-Hückel length

$$\lambda_D^{-1} = \left(\frac{e^2 \mathrm{N}_A}{\varepsilon k_B T} \sum_j Z_j n_j \right)^{-1/2} \tag{3.15}$$

[2] We remember that a dielectric is an insulator that can be macroscopically polarized by the presence of an electric field

[3] We recall that for isotropic media eq.(3.11) is a matricial equation where $\boldsymbol{\chi}_e$ is a rank-two tensor. In what follows we will consider only the case of isotropic medium.

being k_B is the Boltzmann constant, T the temperature of the system and N_A the Avogadro's number.
Therefore, while electrostatic potentials diverge for short distances, at a distance greater than λ_D electrostatic forces are small according to the ionic strength $\sum_j n_j$of the electolyte solution.
We can estimate the value of the Debye length λ_D, for instance, in conditions comparable with physiological ones for a solution with a NaCl concentration of the order $C = 0.1\text{mol.L}^{-1}$.
In such a case, this is equivalent to set $\sum_j Z_j^2 e^2 n_j \simeq 2e^2 C$, where e is the elementary charge and the electrostatic dielectric constant[4] $\varepsilon = 80$ and $T = 300\text{K}$, yielding to:

$$\lambda_D = \left(\frac{8\pi e^2 C}{\varepsilon k T}\right)^{-1/2} \simeq 9.75 \text{ Å}\,.$$

This value is two orders of magnitude smaller than the range of the potentials should be responsible of dynamically organizing the biomolecular machinery in cells. Moreover, the Debye length is even smaller than the characteristic linear dimensions of the proteins (of the order $30 - 60$ Å).
So the electrostatic interactions between any pair of biomolecules *can hardly play any role, in biological conditions, for the dynamical organization inside the cell* except for short distance interactions. For instance, short distance forces play a central role for the so called *facilitated diffusion*[vHB89]. At the best of our knowledge, such a mechanism has been initially proposed by Adam and Delbrück [AD68] who pointed out how many structures are topologically well-suited to act as tracks for diffusion in one or two dimensions (for instance in the case of cellular membranes, or 1-dimensional structures as the DNA, microfilaments, microtubules and soon). In such conditions, the molecules can find their targets by sliding along these structures thus considerably reducing the characteristic encounter time. This is the effect of the reduction of the dimensionality of the space domain where the diffusion takes place. This mechanism has been invoked to explain the characteristic encounter time for the LAC operon of *E. coli* whose target is situated on a long DNA chain: such an encounter time is some orders of magnitude smaller than the one predicted by assuming brownian diffusion of the Lac operon in a 3-dimensional space [Bar81]. This process is substantially diffusive and electrostatic and Van der Waals (see the following section) forces keep the sliding molecule close to the DNA chain on which it moves.

3.2.2 Dispersive interactions

The previously described physical interactions are all *electrostatic* ones. As is well known, there is another type of interatomic and intermolecular interactions acting electrically neutral object; there interactions are the *dispersive forces*[Isr15, Par73] and their action range is typically of the order of a few Angstroms.
This class of interactions includes London and Van Der Walls forces. The existence of this

[4]The dielectric constant of water solutions with freely moving ions is quite close to the pure water dielectric water constant, so with an extimed value of the order of 80, as reported in [Glu64].

forces is explained by quantum mechanics and QED[5]. Qualitative, by two neutral non polar atoms in their fundamental state have finite fluctuations of the dipole moments around zero. The energy of two isolated neutral atoms is corrected by a dipole-dipole interaction potential at the first-order perturbation expansion which is proportional to the product of the averages of the two dipole moments. This contribution vanishes when the two atoms are both in the fundamental state. The second order corrections to the interaction potential are due to the coupling among instantaneous fluctuations of dipole moments and is proportional to $1/r^6$.
More in general, three main different kind of interactions is due to similar mechanism involving instantaneous coupling among fluctuating electric dipole moments or induced polarization effects:

- *Keesom's interactions*, also called *orientation effects*, are established among two permanent dipoles whose orientations fluctuates due to thermal noise; electrostatic interactions tend to correlate the orientation of the molecules giving rise to the *Keesom potential*:

$$U(\boldsymbol{r})_{orient} = -\frac{\mu_1^2\mu_2^2}{3k_BT\,(\varepsilon)^2}\frac{1}{r^6}\ ; \tag{3.16}$$

- *Debye's interactions*, or inductive effects, among permanent dipoles and the dipolar moment induced by them in a non polar molecule. The Debye potential is given by [Deb21]:

$$U(\boldsymbol{r})_{ind} = -\frac{\mu_1^2\alpha_2 + \mu_2^2\alpha_1}{\varepsilon_r^2}\frac{1}{r^6} \tag{3.17}$$

  where $\alpha_{1,2}$ are the polarizabilities of the molecules;

- *London's interactions*, or dispersive interactions among two non polar molecules with polarizabilities α_i and first ionization energies corresponding to $h\nu_i$, whose expression is given by [EL30, Lon37]:

$$U(\boldsymbol{r})_{disp} = -\frac{1}{(4\pi\varepsilon_0)^2}\frac{3h\nu_1\nu_2\alpha_1\alpha_2}{2\,(\nu_1+\nu_2)\,r^6} \tag{3.18}$$

  where h is the Planck constant.

The first two interactions are described in terms of classical electrodynamics, as they involve a polar molecules. To the contrary, the dispersive interactions among non polar molecules (although polarizable) can only be described quantum mechanics. In the general case, two polar or polarizable molecules interact through the superposition of the previously mentioned interactions, them all decrease with a power law r^{-6}, where r is the intermolecular distance:

$$\begin{aligned} U(\boldsymbol{r})_\nu &= U(\boldsymbol{r})_{orient} + U(\boldsymbol{r})_{ind} + U(\boldsymbol{r})_{disp} = \\ &= -\frac{1}{r^6}\left[\frac{\mu_1^2\mu_2^2}{3\,(4\pi\varepsilon_0\varepsilon_r)^2\,\kappa_BT} + \frac{\mu_1^2\alpha_2+\mu_2^2\alpha_1}{(4\pi\varepsilon_0\varepsilon_r)^2} + \frac{3}{4}\frac{h\nu\alpha_1\alpha_2}{(4\pi\varepsilon_0)^2}\right] \end{aligned} \tag{3.19}$$

[5]In the contest of QED such interactions are due to the exchange of virtual photons among atoms.

which is known as *Wan der Waals* potential. As $U(\boldsymbol{r}) \propto 1/r^6$, the corresponding decays as $1/r^7$. The characteristic properties of these forces are non trivial:

- anisotropy of the interaction, as consequence of the dependence of the polarizability on the mutual orientation of the biomolecules;
- non-additivity, due to reflection many body effects for the fields generated by biomolecules;
- retardation effects, concerning only the dispersive component as it is an electrodynamic potential; these effects are due to the finite propagation time of the electromagnetic waves between two dipoles when this is comparable with the characteristic time scale of dipole fluctuations. Casimir e Polder have shown how these effects are appreciable on a length scale approximatively of $30nm$ and that for distances greater then $100nm$ London potential decreases as r^{-7} [CP48].

3.2.2.1 Hamacker Theory for extended spheres in vacuum

In 1937 Hamaker derived the Van der Waals interaction potential for two extended spheres of radii R_1 and R_2 in the vacuum [Ham37], under two approximations: the retardation effects were neglected at any distance, and neglecting many body effects (in particular neglecting the effects due to the presence of surrounding molecules), whence:

$$\begin{aligned} U(z; R_1, R_2) = &- \frac{A}{6}\left[\frac{2R_1R_2}{z^2-(R_1+R_2)^2}+\right. \\ &\left.+\frac{2R_1R_2}{z^2-(R_1-R_2)^2}+\ln\left(\frac{z^2-(R_1+R_2)^2}{z^2-(R_1-R_2)^2}\right)\right]. \end{aligned} \tag{3.20}$$

where A is the so called *Hamacker coefficient*, whose value strongly depends on the properties of the medium surrounding the spheres (which can even change the sign of A), $z = R_1 + R_2 + r$ is the distance between the centres, i.e. the sum of the radii R_1,R_2 and r is the distance between the spheres surfaces.
Recent studies have pointed out that Van der Waals interactions among proteins have a range of the order $\sim 3-5\mathring{A}$ and can be considered as contact interactions, therefore inaugurate to drive the dynamical organization in cells if this requires to go beyond random encounters between reaction partners.

3.3 Electrodynamic long range interactions among biomolecules

3.3.1 Why electrodynamic interactions can be long range in biological systems

As shown in previous sections, the main interactions which take place among biomolecules in physiological conditions are short-range, with a typical range of a few Angstroms. It follows

that such interactions cannot explain the dynamical organization observed on scales of the order of $1 \div 2.5 \cdot 10^3 \mathring{A}$. We have seen that the range of electrostatic forces is drastically shortened by the screening effects due to generated by freely moving ions and by the dielectric properties of water.
Nevertheless, some experimental observations suggest the possibility that in the same conditions *electrodynamic long-range interactions* can be possible. In fact:

- it has been experimentally shown that electrolytic solutions behave like pure dielectrics with no screening effects on the electrodynamic field for frequencies higher a $\gtrsim$ 250MHz;
- it has been measured that for frequencies higher then ~ 1 THz the dielectric constant of water has a value around ~ 4, a much smaller value respect to the electrostatic case.
- absorption Raman spectra and far-infrared spectra of biomolecules have peaks for frequencies in the THz domain, generally attributed to collective vibrational modes of the whole molecule or of a large part of it.

We will examine in detail each of these aspects.

3.3.1.1 Behaviour of electrolyte solutions for high frequency electric field

In order to deepen the understanding of the role of electrodynamic interactions among biomolecules it is interesting to mention some relevant experimental results due to Xammar Oro et al. [JRdXOG92].
The setup of these experiments consists in preparing a cell containing an electrolytic solution and applying to it an alternate sinusoidal tension using electrodes: in this way the impedance Z of the electrolytic solution is measured as a function of the frequency of the applied tension(see Figure 3.1 (a)). An electrolyte solution is equivalent to a parallel RC circuit (see Figure 3.1 (b)): the capacity C represents the dispersion of the dielectric, while the resistance R accounts for the dissipations.
For such a circuit the value of the impedance is given by:

$$Z = \left(\frac{1}{R^2} + \omega^2 C^2 \right)^{-1/2}, \tag{3.21}$$

where ω is the frequency of the applied tension and the following relations hold

$$R = 1/g\sigma \quad \text{and} \quad C = g\varepsilon, \tag{3.22}$$

where σ is the conductivity and ε is the dielectric constant both depending by ω, while g is a geometric factor. As it can be deduced from eq.(3.21), when ω tends to zero the value of the impedance is dominated by the effects of the resistor; in this regime the solution behaves as a pure conductor. For high values of ω, the impedance becomes capacitative and tends to zero for $\omega \to +\infty$.

The transition between these two regimes takes place for a frequency ω_M, known as *Maxwell's frequency*[6], satisfying the equation:

$$Z(\omega_M) = Z(\omega = 0)/\sqrt{2}, \quad i.e., \quad \omega_M = 1/RC = \sigma/\varepsilon. \tag{3.23}$$

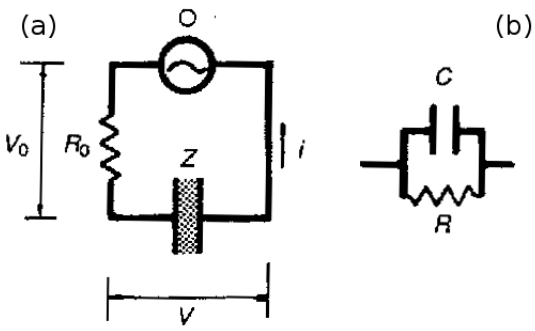

Figure 3.1: Measure circuit used by Xammar Oro et al.[JRdXOG92]. O oscillator, R_0 resistor, Z measure cell;(b) Equivalent circuit for cells filled with an electrolyte.(Figure adapted by [JRdXOG92])

The main results obtained by Xammar Oro et al. are reported in fig. 3.2; where the impedance of the electrolytic solution is plotted as a function of the frequency ω of the applied tension. The different curves represent different distances h among the electrodes (a null distance corresponds to the case of an ideal solution so that the condition eq.(3.21) is exactly verified). As it can be argued from fig.3.2, the impedance reduces considerably for $\omega > \omega_M$ and attains zero for very high frequencies[7]. In other words, as predicted by eq.(3.21), the electrolyte looses its conductive properties for sufficiently high frequencies and behaves like a dielectric medium. For an electrolyte of ionic strength close to physiological conditions, the Maxwell's frequency has been estimated around 255 MHz.

The results found by Xammar Oro et al. represent the dynamical analogue of the Debye screening effect. In particular it can be observed that in the limit of high frequencies freely moving ions do not screen the electric field generated by an oscillating distribution of charges. In the static case, the electrostatic potential generated by a fixed charge q is described by the Poisson equation:

$$\nabla^2\Phi(\boldsymbol{r}) = -\frac{4\pi}{\varepsilon}\rho(\boldsymbol{r}), \quad \text{with} \quad \rho(\boldsymbol{r}) = q\delta(\boldsymbol{r} - \boldsymbol{r}_0) + \rho_{others}(\boldsymbol{r}). \tag{3.24}$$

where $\boldsymbol{r}_0$ is the position of the fixed charge and $\rho_{others}(\boldsymbol{r})$ is the charge density at $\boldsymbol{r}$ due to the presence of freely moving ions in the stationary limit;[8] the last terms in eq.(3.24) is entirely

[6] In facts, such frequency has been originally predicted by Maxwell [Max54].

[7] It has to be stressed that the Maxwell's frequency as defined in the eq.(3.23) is obtained extrapolating $h = 0$ as explained [JRdXOG08]

[8] In such a case we have considered a continuous charge distribution modelling the ions in the electrolytic solution

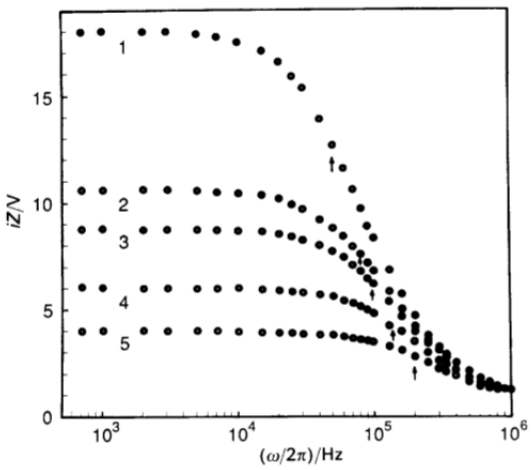

Figure 3.2: Product of the impedance Z and of the current i in the cell containing the elctrolyte solution[JRdXOG08]. The current is maintained constant. Different curves correspond to different values of the space among electrodes (spaces increases from 1 to 5); the arrows indicate the frequency such that $Z(\omega_M) = Z(\omega = 0)/\sqrt{2}$.(Figure adapted by [JRdXOG08])

responsible of the screening effect.

In the context of classical electrodynamics, a similar equation can be derived considering the Coulomb gauge ($\boldsymbol{\nabla} \cdot \boldsymbol{A} = 0$) and writing the Fourier transform (in frequency) of the electrodynamic version of the Poisson equation for a field generated by an oscillating charge q in presence of an ion density distribution $\rho_{others}(\boldsymbol{r}, \omega)$. One gets

$$\nabla^2 \Phi(\boldsymbol{r}, \omega) = -\frac{4\pi}{\varepsilon} \rho(\boldsymbol{r}, \omega), \tag{3.25}$$

with $\rho(\boldsymbol{r}, \omega) = q(\omega)\delta(\boldsymbol{r} - \boldsymbol{r}_0) + \rho_{others}(\boldsymbol{r}, \omega)$ being $\boldsymbol{r}_0$ the position of the oscillating charge q and $\rho_{others}(\boldsymbol{r}, \omega)$ the Fourier Transform of density charge of freely moving ions in $\boldsymbol{r}$. In the cell cytoplasm the majority of charges can be considered static so that $\rho_{others}(\boldsymbol{r}, \omega) = \rho_{others}(\boldsymbol{r})\delta(\omega)$. The latter equation holds for a purely dielectric material. Whereas, for a purely conductive medium as is the intracellular one, the contribution of the induced charges fluctuations has to be considered, so that $\rho_{others}(\boldsymbol{r}, \omega)$ can be different from zero when $\omega > 0$: in this context the induced current is given by Ohm's Law: $\boldsymbol{j}(\boldsymbol{r}, \omega) = \sigma(\omega)\boldsymbol{E}(\boldsymbol{r}, \omega)$. Using the continuity equation, when $\boldsymbol{r} \neq \boldsymbol{r}_0$, or in other terms $i\omega\rho_{others}(\boldsymbol{r}, \omega) = \boldsymbol{\nabla} \cdot \boldsymbol{j}(\boldsymbol{r}, \omega)$, the total charge density is given by

$$\begin{aligned} \rho(\boldsymbol{r}, \omega) &= q(\omega)\delta(\boldsymbol{r} - \boldsymbol{r}_0) + \rho_{others}(\boldsymbol{r}, \omega) \\ &= q(\omega)\delta(\boldsymbol{r} - \boldsymbol{r}_0) - \frac{i\sigma(\omega)}{\omega} \boldsymbol{\nabla} \cdot \boldsymbol{E}(\boldsymbol{r}, \omega), \end{aligned} \tag{3.26}$$

when $\omega > 0$. Here the second term on the right-hand side corresponds to the Fourier Transform of the induced charge density and describes the *dynamical* effects of the Debye screening. On the other side, it can be noticed that the same term becomes zero when $\omega \to +\infty$.

In fact for sufficiently high frequencies, the medium looses its conductive properties and the Debye screening effect is absent.

3.3.1.2 Electrodynamic dielectric constant of water

From classical electrodynamics it is known that the relative permittivity is an adimensional complex number, i.e.

$$\varepsilon_r(\omega) = \frac{\varepsilon(\omega)}{\varepsilon_0}, \tag{3.27}$$

where $\varepsilon(\omega)$ is a complex number, called *absolute permittivity* of the medium, which is generally a function of the frequency of the applied external electromagnetic field and ε_0 is the vacuum permittivity. Using the polar representation of complex numbers, the phase of permittivity corresponds to the phase difference among the polarization field $\boldsymbol{P}$ and the applied electric field $\boldsymbol{E}$.
The relative permittivity can be decomposed in a real and an imaginary part, i.e. [Jac07]:

$$\varepsilon_r(\omega) = \varepsilon_r^{'}(\omega) - \imath\varepsilon_r^{''}(\omega) \tag{3.28}$$

where $\imath$ is the imaginary unit. The real part is related to the energy stored in the medium while the imaginary part is related with dissipations;
In such a context, theory and experiments on water permittivity [Ell07] show a drop of both imaginary and real parts of the permittivity for frequencies in the range $\sim 0.1 - 1$ THz (3.3).

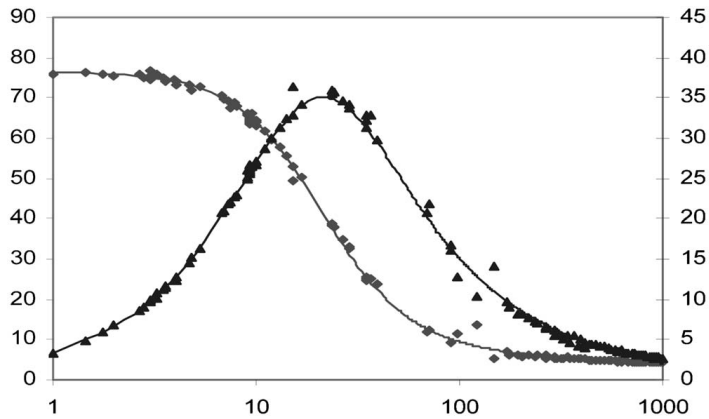

Figure 3.3: (Adapted by [Ell07])Theoretical (line) and experimentally measured (dots) water permittivity at the temperature of 300 K as a function of frequency expressed (in GHz). The real part of permittivity ε' is reported in black diamond (referred to left axes) and the imaginary part ε'' with black triangles (referred to right axes).

3.3.1.3 Collective vibrational modes of biomolecules at thermal equilibrium

Biomolecules are not rigid bodies: they have a number of vibrational modes proportional to the number of atomic groups which constitute them. Such modes, which are generally coupled among themselves, can be decoupled in the elastic approximation and treated as normal modes,

in the context of quantum mechanics[9]. It is possible to study and observe the equilibrium vibrational spectrum of a molecule by means of Raman or far-infrared spectroscopy ($\sim 0.1 - 10$ THz). In this spectral region many absorption peaks have been observed for many proteins; such peaks have been commonly attributed to collective oscillation modes of the protein (vedi Figs. (??) e (??)).

When these oscillation modes are activated also conformational changes are produced, and if, for instance, they have a no vanishing dipole moment, these behave like oscillating dipoles coupled by an electromagnetic field oscillating at the same frequencies. As previously observed, the water dielectric properties change dramatically in this range of frequencies; it is then reasonable to investigate the possibility that *long range electrodynamic* interactions establish among biomolecules set in.

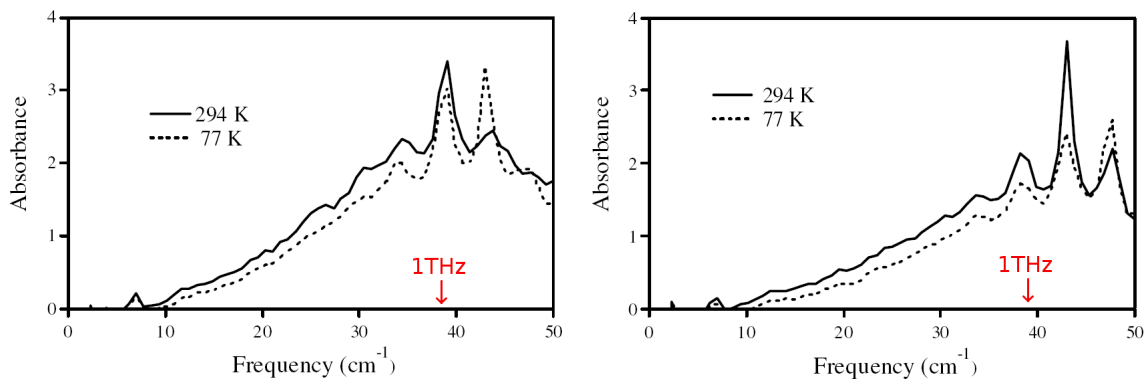

Figure 3.4: (Adapted by [MWHB02]) Absorption spectra in far infrared domain for lysozime (left) and myoglobine (right).

3.3.2 Electrodynamic interactions among by biomolecules

As said in previous sections, biomolecules have in general a non vanishing net charge and dipole moment. It is then reasonable to wonder what kind of electrodynamic interactions can be possibly activated among biomolecules when collective vibrational modes are set in some mechanism (for example, energy injection by ATP hydrolysis).

This hypothesis has been put forward and theoretically explored by H. Fröhlich in the late 60's and 70's. In a series of articles [Frö68, Frö72, Frö77, Fro78, Frö80] he depicted a very interesting theoretical framework where the activation of giant dipole oscillations in biomolecules (thus of low frequency modes) external energy supply would result in the activation of two-body long-range interactions between biomolecules. Moreover these interactions would be *selective* only when oscillating dipoles are resonant.

This theoretical framework it the "reference frame" and the starting point of the research project

[9]For an extended dissertation on collective modes (phonons) which involve the coherent motion of all the atoms or a large part, of them, see[Kit04]

(including experimental, numerical and theoretical studies) where this PhD thesis is partially rooted. As mentioned above the milestones of the theory are:

- the activation of giant dipole oscillations in biomolecules, through a mechanism analogous to Bose-Einstein condensation but applied to phonons in an open system (a bio-molecule) that is known as *Fröhlich condensation*;
- the activation of resonant (selective) long-range electrodynamic interactions. In the original Fröhlich theory these interactions are derived in the context of quantum electrodynamics and are predicted to be active at thermodynamic equilibrium. Recent developments [PPT15] have pointed out that these interactions can be derived from *classical electrodynamics* and can be active *only out-of-thermodynamic equilibrium.*

In the next subsections, both aspects are revisited in the light of more recent results.

3.3.3 Fröhlich condensation

In order to explain the activation of giant dipole oscillations in biological macro-molecules, prerequisite for the activation of long-range electrodynamic interactions, H. Fröhlich proposed a phase transitional mechanism analogous to the Bose-Einstein condensation for a set of quantum oscillators, coupled with a thermal bath, with a source supplying energy and interacting among themselves through a coupling with thermal bath (representing anharmonicity of the system). In its original approach Fröhlich [Frö68, Frö77] considered the extraordinary dielectric and polarization properties that can be found in living matter at a microscopic level; for instance, he noticed that the electric fields intensity in cell membranes can be of the order of 10^5V/cm; a remarkably high value that can be also higher near proteins, nucleic acids, etc. In this case oscillations in polar systems are accompanied by polarization waves associated with an electric field that can mediate long range interactions; the quanta of polarization field are subject to thermal fluctuations and non linear interactions among normal modes take place due to the strong polarization field. The same conceptual scheme has been applied to phonons describing the quanta of vibrational normal modes of a biomolecule, in contact with a thermal bath and an external source of energy (for instance energy supplied by esothermal processes as ATP hydrolization); also in this case the coupling among normal modes is mediated by a thermal bath and take into account for anahrmonicity.
In the more detail, the model system considered by Fröhlich is composed of three subsystems:

- a set of N harmonic oscillators with frequencies $\{\omega_i\}_{i=1,\dots,N}$ representing the *normal modes of a principal system* (transverse modes of the polarization field or, equivalently, vibrational modes of a biomolecule). Each mode is characterized by an occupation number n_{ω_i} and the energy in each mode is obviously given by $E_{\omega_i} = n_{\omega_i}\hbar\omega_i$;
- an *external source* providing energy to the harmonic oscillators of the considered system. If s_{ω_i} is the average number of quanta that excite the i-th mode, the total supplied energy

rate is given by

$$W_s = \sum_{\omega_i}^{N} s_{\omega_i} \hbar \omega_i \tag{3.29}$$

- a *thermal bath* characterized by a temperature T, ($\beta = (k_{\text{Bol}} T_B)^{-1}$) coupled in different ways to the normal modes of the considered system. The one-boson exchange process among the principal system and the thermal bath is described by a term of the form:

$$\frac{\mathrm{d}n_{\omega_i,\phi}}{\mathrm{d}t} = -\phi_{\omega_i} \left(n_{\omega_i} \exp\left[\beta\hbar\omega_i\right] - (n_{\omega_i} + 1) \right) \tag{3.30}$$

while the process describing the energy exchanges between normal modes of the principal system, mediated by the thermal bath, takes the form[10]

$$\dot{n}_{\omega_i,\chi} = \chi_{\omega_i} \sum_{\omega_j} \chi_{\omega_i\omega_j} \left[n_{\omega_i}(n_{\omega_j} + 1) - n_{\omega_j}(\langle n_{\omega_i} + 1) e^{\beta\hbar(\omega_j - \omega_i)} \right] . \tag{3.31}$$

This last contribution to the rate equation has the relevant property that it conserves the total number of bosons, i.e. $\sum_{\omega_i} \dot{n}_{\omega_i,\chi} = 0$ so that

$$S = \sum_{\omega_i} s_{\omega_i} = \sum_{\omega_i} \phi_{\omega_i} \left(n_{\omega_i} \exp\left[\beta\hbar\omega_i\right] - (n_{\omega_i} + 1) \right) . \tag{3.32}$$

For a system of this kind, Fröhlich's theory postulated a set of N-coupled rate equations that describe the temporal evolution of the occupation numbers n_{ω_i} of each normal mode for the principal system:

$$\begin{aligned} \frac{\mathrm{d}n_{\omega_i}}{\mathrm{d}t} =& \langle s_{\omega_i} \rangle - \varphi_{\omega_i} [\langle n_{\omega_i} \rangle e^{\beta\hbar\omega_i} - (n_{\omega_i} + 1)] \\ & - \sum_{j=1}^{N} \chi_{\omega_i\omega_j} \left[n_{\omega_i}(n_{\omega_j} + 1) - n_{\omega_j}(n_{\omega_i} + 1) e^{\beta\hbar(\omega_j - \omega_i)} \right], \qquad i = 1, ..N \end{aligned} \tag{3.33}$$

where $\varphi_{\omega_i} \equiv \varphi(\beta, \omega_i)$ is the coefficient associated with the term describing the linear coupling of the i-th mode of the principal system with the thermal bath and $\Lambda_{\omega_i\omega_j} \equiv \Lambda(\beta, \omega_i, \omega_j)$ is the coefficient associated with the non linear coupling between the i-th and the j-th normal mode of the system mediated by the thermal bath. A large number of free parameters have been thus introduced;then, in order to simplify the rate eqs.(3.33), the coupling constants are generally assumed to be independent on the frequencies, i.e. $\varphi_{\omega_i} = \varphi$ and $\chi_{\omega_i} = \chi$.
The form of the terms appearing in the rate equations for occupation numbers has been derived by Fröhlich in the original articles from heuristic considerations. A more refined derivation based on stochastic mechanics and Markov-chain representation of the boson exchange among the principal system, the thermal bath and the external source has been recently suggested [Pre12]. Moreover a microscopic quantum Hamiltonian model has been suggested in the '80s

[10] It has to be noticed that the term $\omega_j = \omega_i$ gives a zero contribution so that it can be formally included in the sum in this case

by Wu and Austin [WA77, WA78a, WA78b, WA81] in order to derive Fröhlich rate equations; this will be discussed in more details, and generalized to semi-classical systems, in the following sections of this manuscript.

In order to characterize the main qualitative aspects of the system described by the set of eqs.(3.33), the stationary solutions, i.e. $\dot{n}_{\omega_i}$ are studied.

When there is no energy injection, $S = \sum_i^N s_i = 0$ the system admits as stationary solutions the Planck distribution

$$n_{\omega_i} = \frac{1}{e^{\beta\hbar\omega_i} - 1}. \tag{3.34}$$

On the other side, if $s_{\omega_i} \neq 0$ but the coefficient describing non linear interactions is zero, i.e. $\chi = 0$, the stationary solution is given by

$$n_{\omega_i} = \frac{s_{\omega_i} + \varphi}{\varphi\left(e^{\beta\hbar\omega_i} - 1\right)} = \frac{s_{\omega_i}}{\varphi} + \frac{1}{\left(e^{\beta\hbar\omega_i} - 1\right)} \tag{3.35}$$

so that the presence of an external energy supply has the only effect to increase the total number of bosons present into the system for sufficiently high values of S. When both the external injection of energy and the non linear interactions among normal modes are present, the stationary solutions of Fröhlich rate equations are formally given by

$$n_{\omega_i} = \frac{A_{\omega_i}}{\exp\left[\beta\left(\hbar\omega_i - \mu\right)\right]} \tag{3.36}$$

where

$$A_{\omega_i} = \frac{s_{\omega_i}}{\varphi + \sum_{\omega_j} \chi\, n_{\omega_j}} \qquad \exp\left[-\beta\mu\right] = \frac{\varphi + \sum_{\omega_j} \chi(1 + n_{\omega_j})}{\varphi + \sum_{\omega_j} \chi n_{\omega_j} \exp\left[\beta\hbar\omega_j\right]}. \tag{3.37}$$

It has to be noticed that the stationary solution eq.(3.36) has the same form of the Bose-Einstein distribution in the grancanonical bosons ensemble with an effective chemical potential μ s.t.

$$\hbar\omega_1 > \mu \geq 0 \tag{3.38}$$

where $\omega_1 = \min_{\{\omega_i\}_{i=1,\ldots,N}} \omega_i$. In this case it is in principle possible to find an upper bound to the total number of bosons in the principal system:

$$n_{Tot} = \sum_{\omega_i} n_{\omega_i} < \left(1 + \frac{s_{\omega_i}\left(1 - \exp\left[-\beta\hbar\omega_1\right]\right)\varphi}{\chi S}\right) \sum_{\omega_i} \frac{1}{\exp\left[\beta\left(\hbar\omega_i - \mu\right)\right] - 1} \tag{3.39}$$

according to the original argument given by Fröhlich's , if the sum is replaced by an integral it is possible to construct an upperbound on N which is independent of S. This conclusion contradicts the result that the number of bosons increases linearly with S, so that replacing the sum with an integral in eq.(3.39) is incorrect as μ tends to $\hbar\omega_1$ and n_{ω_1} tends to become very large compared with any n_{ω_k}. This leads to the so called *Fröhlich condensation*: when *the supply of energy is sufficiently high*, the lowest frequency mode is strongly excited. It has to be remarked that finally, Fröhlich condensation can be regarded as a *phase transitional phenomenon* in sys-

tem out-of-thermodynamic equilibrium, where the fraction of the energy contained in the lowest frequency mode is a sort of order parameter and the injected energy is the control parameter. This mechanism can explain the activation of low frequency vibrational modes ($\sim 10^{11}$Hz) in proteins that consequently behave as microscopic oscillating antennas. Hence arising question is if and in which conditions long range interactions can take place if such collective oscillations in biomolecules (considered as oscillating electric dipoles) are activated.

3.3.4 Classical electrodynamic long range interactions two oscillating dipole

Following the approach of [Pre13] and [PPT15], we shall consider a simple system composed by two biomolecules A and B, with a dipole moments $\boldsymbol{\mu}_A$ and $\boldsymbol{\mu}_B$ oscillating at frequencies ω_A and ω_B respectively. In such a case, the equations of motions are given by:

$$\begin{cases} \ddot{\boldsymbol{\mu}}_A + \gamma_A \dot{\boldsymbol{\mu}}_A + \omega_A^2 \boldsymbol{\mu}_A = \zeta_A \boldsymbol{E}_B(\boldsymbol{r}_A, t) + \boldsymbol{f}_A(\boldsymbol{\mu}_A, t) \\ \ddot{\boldsymbol{\mu}}_B + \gamma_B \dot{\boldsymbol{\mu}}_B + \omega_B^2 \boldsymbol{\mu}_B = \zeta_B \boldsymbol{E}_A(\boldsymbol{r}_B, t) + \boldsymbol{f}_B(\boldsymbol{\mu}_B, t). \end{cases} \tag{3.40}$$

As the dipole approximation has been considered, the interaction between the molecules placed at $\boldsymbol{r} = \boldsymbol{r}_{B,A}$ is mediated by the electric field $\boldsymbol{E}_{A,B}(\boldsymbol{r}, t)$ created by the oscillations of the dipole moments of each molecule.
The associated coupling constants are $\zeta_A = Q_A^2/m_A$, with Q_A and m_A being respectively the effective charge and effective mass for the dipole A; analogous expressions hold for B-labelled coupling constants. Dissipative effects are represented by terms where damping coefficients $\gamma_{A,B}$ appear, and the functions $\boldsymbol{f}_{A,B}$ stand for possible anharmonic contributes for each dipole, and possible external forcing.
An estimation of the mean interaction energy between the oscillators described by eq.(3.40) can be obtained writing the time-Fourier transform of these equations. The starting point is the harmonic and conservative sub-system

$$\begin{cases} \ddot{\boldsymbol{\mu}}_A + \omega_A^2 \boldsymbol{\mu}_A = \zeta_A \boldsymbol{E}_B(\boldsymbol{r}_A, t) \\ \ddot{\boldsymbol{\mu}}_B + \omega_B^2 \boldsymbol{\mu}_B = \zeta_B \boldsymbol{E}_A(\boldsymbol{r}_B, t), \end{cases} \tag{3.41}$$

where the normal modes are defined as the frequencies ω_N such that $\boldsymbol{\mu}_{A,B}(t) = \boldsymbol{\mu}_{A,B} e^{i\omega_N t}$ are solutions for the system in eq.(3.41). In order to calculate ω_i the expression for $\boldsymbol{E}_{A,B}(r, t)$ is required. Passing then to the Fourier transform in the frequency domain

$$\boldsymbol{E}(\boldsymbol{r}, \omega) = \frac{1}{(2\pi)} \int_{-\infty}^{+\infty} \boldsymbol{E}(\boldsymbol{r}, t) e^{i\omega t} \mathrm{d}t \tag{3.42}$$

and using classical electrodynamics theory, it can be derived, the dipolar approximation, the electric field at $\boldsymbol{r}$ generated by an oscillating dipole at the origin in a reference frame is given

by:

$$\boldsymbol{E}(\boldsymbol{r},\omega) = \boldsymbol{\chi}^E(r,\omega)\boldsymbol{\mu}(\omega), \tag{3.43}$$

where $\boldsymbol{\mu}(\omega)$ is the Fourier transform of the dipole moment, that in our case has been assumed to oscillate harmonically, $\boldsymbol{\mu}(\omega) = \boldsymbol{\mu}_{A,B}\delta(\omega - \omega_N)$, and $\boldsymbol{\chi}^E(r,\omega)$ is the electric susceptibility of the electric field, a tensor of rank 2 that in the case of a dipole oriented along the z axes takes the form:

$$\begin{aligned}
\chi^E_{xx}(\boldsymbol{r},\omega) = \chi^E_{yy}(\boldsymbol{r},\omega) &= -\frac{e^{\pm i\omega\sqrt{\varepsilon(\omega)}r/c}}{\varepsilon(\omega)r^3}\left(1 \mp \frac{i\omega\sqrt{\varepsilon(\omega)}r}{c} - \frac{\omega^2\varepsilon(\omega)r^2}{c^2}\right), \\
\chi^E_{zz}(\boldsymbol{r},\omega) &= \frac{2e^{\pm i\omega\sqrt{\varepsilon(\omega)}r/c}}{\varepsilon(\omega)r^3}\left(1 \mp \frac{i\omega\sqrt{\varepsilon(\omega)}r}{c}\right), \text{ e} \qquad \text{and} \\
\chi^E_{ij}(\boldsymbol{r},\omega) &= 0 \quad \text{per} \quad i \neq j,
\end{aligned} \tag{3.44}$$

the sign $\pm$ is attributed to the positive or negative sign of $\mathrm{Im}(\omega\sqrt{\varepsilon(\omega)})$, respectively. For real values of ω_N, each element $\chi_{ii}(r,\omega_N)$ of $\boldsymbol{\chi}(r,\omega_N)$ is a complex number whose imaginary part represents the dissipative effects due to the propagation of the field[**?**].
Since in computing the normal modes dissipative effects are neglected, we will consider in the follow only the real part of each element of $\boldsymbol{\chi}$, denoted by χ'_{ii}.
Substituting these results in eq.(3.41), the following system is derived:

$$\begin{cases} (\omega_A^2 - \omega_N^2)\mu_{A,i} = \zeta_A\chi'_{ii}(r,\omega_N)\mu_{B,i} \\ (\omega_B^2 - \omega_N^2)\mu_{B,i} = \zeta_B\chi'_{ii}(r,\omega_N)\mu_{A,i} \end{cases} . \tag{3.45}$$

The existence of non-trivial solutions for (3.45) is assured by the hypothesis that the determinant is vanishing, in particular:

$$(\omega_A^2 - \omega_N^2)(\omega_B^2 - \omega_N^2) - \zeta_A\zeta_B(\chi'_{ii}(r,\omega_N))^2 = 0. \tag{3.46}$$

After some calculation, two possible solutions for ω_N^2 are derived for each direction i; these solutions will be denoted by $\omega^2_{i,+}$ and $\omega^2_{i,-}$ satisfying the equation

$$\omega^2_{i,\pm} - \frac{1}{2}\left\{\left(\omega_A^2 + \omega_B^2\right) \pm \sqrt{\left(\omega_A^2 - \omega_B^2\right)^2 + 4\zeta_A\zeta_B(\chi'_{ii}(r,\omega_{i,\pm}))^2}\right\} = 0. \tag{3.47}$$

Notice that for to compute the normal frequencies $\omega_{i,\pm}$, the system eq.(3.41) is rewritten as a system of six decoupled harmonic oscillators with frequencies $\omega_{i,\pm}$, $i = 1,2,3$ and energies $E_{i,\pm} = \omega_{i,\pm}J_{i,\pm}$, where $J_{i,\pm}$ are the associated action constants, fixed by the initial conditions of the system. In eq. (3.47), the frequencies $\omega_{i,\pm}$ are whereas implicitly expressed while an explicit, even if approximated, expression is required for $\omega_{i,\pm}$ in order to calculate the total energy and the interaction energy of the dipoles system. Two fundamental cases are distinguished:

- the **non resonant** case with $\omega_A \gg \omega_B$ (or analogously $\omega_A \ll \omega_B$), yielding at the leading

order:

$$\omega_{i,\pm}^2 - \frac{1}{2}\left\{\left(\omega_A^2+\omega_B^2\right) \pm \left(\omega_A^2-\omega_B^2\right)\left(1+\frac{2\zeta_A\zeta_B(\chi'_{ii}(r,\omega_{i,\pm}))^2}{\left(\omega_A^2-\omega_B^2\right)^2}\right)\right\} \simeq 0,$$

from which:

$$\omega_{i,\pm}^2 - \omega_{A,B}^2 \mp \frac{\zeta_A\zeta_B(\chi'_{ii}(r,\omega_{i,\pm}))^2}{\omega_A^2-\omega_B^2} = 0\ , \quad \text{where} \quad \omega_{A,B} \quad \begin{cases} \omega_A & \text{for} \quad \omega_{i,+}, \\ \omega_B & \text{for} \quad \omega_{i,-}. \end{cases} \tag{3.48}$$

Applying the Laplace Inversion Theorem of the complex analysis , after some steps, the explicit expression for $\omega_{i,\pm}(r)$ can been obtained:

$$\omega_{i,\pm}(r) \simeq \omega_{A,B} \pm \underbrace{\frac{\zeta_A\zeta_B(\chi'_{ii}(r,\omega_{A,B})))^2}{2\omega_{A,B}\left(\omega_A^2-\omega_B^2\right)}}_{\Delta(\omega_{A,B})_i}. \tag{3.49}$$

Using the expression for the energy for angle-action variables, the total energy of the system is given by:

$$\begin{aligned} E_{tot} &= \sum_i E_{i,+} + E_{i,-} = \sum_i \omega_{i,+}J_{i,+} + \omega_{i,-}J_{i,-} \\ &= \underbrace{\sum_i \omega_A J_{i,+} + \omega_B J_{i,-}}_{\substack{\text{Energy of} \\ \text{the decoupled system}}} + \underbrace{\sum_i \Delta(\omega_A)_i J_{i,+} - \Delta(\omega_B)_i J_{i,-}}_{\text{Interaction energy } U}. \end{aligned} \tag{3.50}$$

The first term of the sum represents the energy of the decoupled system, while the second term corresponds to the interaction energy $U(r)$ of the system that, according to the equation eq.(3.49), scales proportionally to $\left(\chi'_{ii}(r,\omega_{A,B})\right)^2$.
From eq.(3.44), in the limit $r \ll c/\omega_{A,B}$ (near field limit), the interaction is found to be short-range one, as $\left(\chi'_{ii}(r,\omega_{A,B})\right)^2$ is of order $1/r^6$ (in fact, the term proportional to $1/r^3$ in eq.(3.44) is dominant). For large distances $r \gg c/\omega_{A,B}$ (far field limit), retardation effects make the interaction energy spatially oscillate with an envelope proportional to $1/r^2$.

- the **resonant case** with, $\omega_A \simeq \omega_B = \omega_0$, for which eq.(3.47) simplifies to:

$$\omega_{i,\pm}^2 - \omega_0^2 \mp \sqrt{\zeta_A\zeta_B}\chi'_{ii}(r,\omega_{i,\pm}) = 0. \tag{3.51}$$

As seen before, the following expression is obtained for $\omega_{i,\pm}(r)$:

$$\omega_{i,\pm}(r) = \omega_0 + \sum_{n=1}^{\infty} \frac{(\pm 1)^n}{n!}\frac{d^{n-1}}{d\omega^{n-1}}\left[\left\{\frac{\sqrt{\zeta_A\zeta_B}\chi'_{ii}(r,\omega)}{\omega+\omega_0}\right\}^n\right]_{\omega=\omega_0}. \tag{3.52}$$

which at first order takes the form:

$$\omega_{i,\pm}(r) \simeq \omega_0 \pm \underbrace{\sqrt{\zeta_A \zeta_B}\frac{\chi'_{ii}(r,\omega_0)}{2\omega_0}}_{\Delta(\omega_0)_i}. \tag{3.53}$$

where now the first contribution for the correction to the frequency is proportional χ'_{ii}. In this case the total energy is given by:

$$E_{tot} = \underbrace{\sum_i \omega_0 J_{i,+} + \omega_0 J_{i,-}}_{\substack{\text{Energy of} \\ \text{the decoupled system}}} + \underbrace{\sum_i \Delta(\omega_0)_i \left(J_{i,+} - J_{i,-}\right)}_{\text{Interaction energy } U} \tag{3.54}$$

So according to eqs.(3.53) and (3.44), $U(r)$ will be a polynomial in $1/r^\alpha$ with $\alpha \leq 3$ (the dimensionality of physical space): hence the potential is so a *long-range* one at any distance. In particular, from eq. (3.44) in the near field limit $r \ll c/\omega_0$, the interaction is proportional to $1/r^3$, while oscillates for larger distances with an envelope proportional to $1/r$.

In conclusion it can be observed that:

- in the context of classical electrodynamics *long range resonant interactions can be activated* for a pair of oscillating dipoles;
- Considering eq.(3.54) it can be observed that the interaction energy is attractive, i.e. $\Delta U(r) < 0$, when the system is *out-of-thermal equilibrium*: in fact, under the hypothesis that the energy is equally distributed among all oscillation modes (or in other words $J_{i,\pm} = \text{cost}$) the interaction energy vanishes. In order to activate long-range *attractive* forces it is necessary, for instance, that $J_{z,+} > J_{z,-}$, where $J_{z,\pm}$ represents the action associated to longitudinal modes. In order words, an out-of-equilibrium condition is necessary. This is sound in view of application to real biological systems because many biochemical reactions need to be activated by an energy input given, typically, by ATP or GTP hydrolysis.

3.4 Developments in research of long range interactions among biomolecules

In this chapter, the theoretical framework of the research aiming to find long-range electrodynamic interactions among biomolecules in physiological conditions has been depicted. This fascinating hypothesis, if experimentally verified, would entail a major leap forward in our comprehension of the processes -in the long term- that drive the dynamics of biomolecules in living matter with even possible implications for medical applications [KDT+07]. Even if Fröhlich propositions have stimulated a very active theoretical research between the 70's and the 90's the persistent lack of experimental confirmations have marginalized this research field. The reason is that the experimental techniques were not sufficiently developed to provide a clear evidence of the Fröhlich condensation and/or the activation of long range electrodynamic interactions among biomolecules in aqueous solution at least *in vitro*. This is mostly due to the fact the THz frequency range, which corresponds to the expected range of frequency of collective biomolecular oscillations, is very difficult to investigate with classical spectroscopic techniques. In fact because of thermal noise it is very difficult to realize sufficiently precise THz sources and detectors, moreover it is a hard task to extract protein absorption in aqueous solution because the vibrational modes of water belong to the same frequency range.
A partial renewed interest in Fröhlich's theories comes from the fact that it has been evoked in Penrose-Hameroff's theory of consciousness as a possible underlying mechanism for the set in of coherent quantum states in neuronal microtubles, that is in "wet and warm" biological conditions [HP96, HP14].
Only recently, technical developments in THz spectroscopy and in experimental methods for the study of molecular dynamics has given new impetus to the research on Fröhlich condensation and long-range electrodynamics interactions.
In the very last years the development and refinement of spectroscopic techniques in THz domain and of techniques the dynamics of biomolecules dynamic with great precision re-open the way for research of Fröhlich condensation and long range interactions.
Some indirect evidence of Fröhlich-like condensation in dry protein has been recently obtained [LRW+15] observing structural deformation of crystallized protein subjected to THz radiation using X-Ray crystallography. In the following chapters we report about new theoretical and numerical outcomes-worked out during this thesis work. They are aimed to a further refinement of the presented theoretical framework picture and to the interpretation of new experimental results obtained with proteins in water solution investigating both the possibility to induce Fröhlich condensation in real biomolecules and, consequently, the activation of electrodynamic long range interactions. In particular

- Fröhlich condensation phenomena has been theoretically derived in quantum mechanics framework, nevertheless it seems an ambitious statement to claim for quantum behaviour of vibrational collective modes of biomolecules as this objects are very "heavy". In chapter 4 it is discussed how it is possible to derive analogous rate equations analogous to Fröhlich ones in semi-classical approximation considering a classical Hamiltonian system describing

the dynamics of the a system coupled with a thermal bath and an external source of energy;

- in chapter 5 it is discussed the theoretical interpretation of very recent out-of-thermal equilibrium THz spectroscopy experiment on biomolecules in water solution; the outcomes would be a first evidence of Fröhlich-like condensation in biomolecules in water solution;

- in chapter 7 the some results of some numerical feasibility studies is reported for the detection of long range interactions among biomolecules in water solutions; the main idea is that mutual long range interactions would affect the dynamics of biomolecules also when they are very far apart respect to their characteristic dimensions. Such results have been used to provide a validation of a partially new experimental technique using Fluorecence Correlation Spectroscopy to study diffusion behaviour of biomolecules in a wide range of concentration to retrieve information on the presence of long range interactions.

CHAPTER 4 From theory to experiment and return: Fröhlich condensation in classical systems

In this chapter an *original* derivation of Fröhlich-like rate equations is derived for a system of classical harmonic oscillators representing the vibrational (normal) modes of a generic macro-biomolecule. The Time Dependent Variational Principle is used to associate a *classical* Hamiltonian model to a microscopic quantum model originally introduced by Wu and Austin. Then, the Koopman-Von Neumann formalism is applied to the associated classical Liouville equation to derive Fröhlich-like rate equations for the action variables of the normal modes.

4.1 Looking for Fröhlich condensation in classical open systems: motivations

As mentioned in the previous chapter, Fröhlich rate equations (3.33) for the occupation numbers, in the Fock's representation of the normal modes amplitudes, of a generic biomolecule were originally put froward heuristically. Therefore, the original formulation of Fröhlich condensation was lacking a microscopic model.
In the '80s Wu and Austin derived the Fröhlich rate equations from a *quantum Hamiltonian system* describing - in a second quantization formalism - the normal modes dynamics associated to the mechanical deformation of a protein, to the coupling with a thermal bath, and to the coupling with an external energy source. For a long time this model has been the only "microscopic" description of the dynamics underlying Fröhlich condensation.

A semiclassical approach based on a suitably defined Markov process among the energy levels of the system has been recently considered in order to derive the Fröhlich rate equations. In this model the transition probabilities among the energy levels of the system are estimated in an heuristic way. Also in this case the spectrum of the energy levels is assumed to be discrete, so that neither this model can be interpreted in terms of classical dynamics [Pre12]. The construction of a quantum or of a markovian dynamics among discrete states to derive Fröhlich condensation seems quite questionable when applied to the internal vibrational modes of a protein. In fact, thermal noise allows for transitions of frequencies of the order $\nu_T \sim k_B T/h$ which, at room temperature ($T = 300\,\mathrm{K}$), gives $\nu_T \sim 6.6\,\mathrm{THz}$ which is larger than the expected frequencies of protein collective vibrations. Moreover, let us consider the average energy of each molecule considered as an harmonic oscillator at the lowest frequency

$$H_{est} = \frac{p^2}{2m_{red}} + \frac{1}{2} m_{red} \omega_{low}^2 \Delta x^2 \tag{4.1}$$

where m_{red} is the effective reduced mass associated to the lowest frequency vibrational mode

of a protein. From the Equipartition Theorem it follows that

$$\left\langle p\frac{\partial H_{est}}{\partial p}\right\rangle = \frac{\langle p^2\rangle}{m_{est}} = k_B T \quad \Rightarrow \quad \sigma_p = \sqrt{\langle p^2\rangle} = \sqrt{m_{red}k_B T} \tag{4.2}$$

and an estimation of the De Broglie wavelength associated with the oscillator is given by

$$\lambda_{\text{DeBroglie}} = \frac{h}{\sigma_p} = \frac{h}{\sqrt{m_{red}k_B T}} \tag{4.3}$$

where h is the Planck constant; for a protein we can consider $m_{red} \simeq 10KDa \approx 1.66 \times 10^{-23}Kg$ and a temperature of $T = 37 \simeq 310K$, eq.(4.3) yields $\lambda_{\text{DeBroglie}} \approx 2.5 \times 10^{-12}$m. As the typical hydrodynamic radius of a protein is of the order of magnitude of $\approx$ 1nm it follows that the De Broglie wavelength is about three orders of magnitude smaller then typical molecular linear dimensions.

For this reason, Fröhlich rate equations should be derived from a model of *classical harmonic oscillators* representing the vibrational modes of a protein, a thermal bath and an external source of energy. Therefore we proceed to derive a classical Hamiltonian model from the Wu-Austin original quantum Hamiltonian by resorting to a "dequantization" technique called Time Dependent Variational Principal (TDVP). A Liouville equation is then associated with the classical Hamiltonian so obtained. Finally, the rate equations for the classical actions are worked out using the Koopman-Von Neumann (KvN) description of classical mechanics. This allows to treat Liouville equation in the Hilbert space of square integrable functions on phase space, in analogy with the standard quantum mechanical formalism.

4.2 Quantum Hamiltonian to describe Fröhlich condensation: Wu and Austin model

As mentioned above, Fröhlich condensation is a phase transition phenomenon predicted by considering the stationary solutions of the rate equations (3.33), these describe the time evolution of the occupation numbers of the normal mode states. In the Fröhlich original formulation the rate equations have been written quite directly in an heuristic way: this method reveals all its power in opening a new research pathway. Nevertheless it leaves open the problem of a microscopic dynamical model from which these rate equations can be derived; this is necessary both to deepen the comprehension of this phenomenon and possibly to allow an *a priori* estimation of the coupling parameters ϕ_{ω_i} and $\chi_{\omega_i\omega_j}$ from the knowledge of the microscopic details of the system.

Since Fröhlich put forward a quantum model, the first microscopic model proposed to derive Fröhlich rate equations was a *Hamiltonian quantum model* [WA77, WA78a], by Wu and Austin, formulated in second quantization formalism. LEt us sketch the main aspects of this model, as it constitutes the starting point to derive a classical microscopic model for Fröhlich condensation.

In what follows we indicate with $\widehat{a}_{\omega_i}, \widehat{a}^\dagger_{\omega_i}$ the quantum creation/annihilation operator for the

vibrational normal modes of the main system (i.e. a biomolecule) with frequency $\omega_i \in \mathcal{I}_{sys}$. Such a system is put in contact with a thermal bath which represents the degrees of freedom of the environment surrounding the protein and, possibly, other normal modes of the protein which can be considered at thermal equilibrium with the surrounding environment. The thermal bath is characterized by a temperature T_B and it is represented by a collection of harmonic oscillators with characteristic frequencies $\Omega_j \in \mathcal{I}_{bth}$ whose annihilation/creation operators are $\widehat{b}_{\Omega_j}$ and $\widehat{b}^\dagger_{\Omega_j}$, respectively.
In order to put the system representing normal modes of the protein out of thermal equilibrium, an external source of energy is necessary: such an external source is represented as another thermal bath at temperature $T_S \gg T_B$. Also in this case the thermal bath is described by a collection of harmonic oscillators with frequencies $\Omega'_k \in \mathcal{I}_{src}$, the quantum annihilation/creation operators of which are $\widehat{c}_{\Omega'_k}$ and $\widehat{c}^\dagger_{\Omega'_k}$. These three sets of harmonic oscillators can be regarded as three subsystems of a larger isolated system $\mathcal{S}$ (we coherently indicate with $\mathcal{I}_{\mathcal{S}}$ the set of all the normal modes of the system) whose quantum dynamics is described by the Hamiltonian

$$\widehat{H}_{Tot} = \widehat{H}_0 + \widehat{H}_{Int} = \tag{4.4}$$

where $\widehat{H}_0$ is the free Hamiltonian of the three sets of harmonic oscillators representing normal modes:

$$\widehat{H}_0 = \sum_{\omega_i \in \mathcal{I}_{sys}} \hbar\omega_i \; \widehat{a}^\dagger_{\omega_i}\widehat{a}_{\omega_i} + \sum_{\Omega_j \in \mathcal{I}_{bath}} \hbar\Omega_j \; \widehat{b}^\dagger_{\Omega_j}\widehat{b}_{\Omega_j} + \sum_{\Omega'_k \in \mathcal{I}_{src}} \hbar\Omega'_k \; \widehat{c}^\dagger_{\Omega'_k}\widehat{c}_{\Omega'_k} \,. \tag{4.5}$$

The interactions among normal modes are described by $\hat{H}_{Int}$; in the original formulation by Wu and Austin such interaction term has the form:

$$\begin{aligned}\widehat{H}_{IntWA} =& \widehat{H}_{sys-bth} + \widehat{H}_{src-sys} + \widehat{H}_{sys-bath-sys} = \sum_{\omega_i \in \mathcal{I}_{sys}, \Omega_j \in \mathcal{I}_{bth}} \eta_{\omega_i\Omega_j} \; \widehat{a}^\dagger_{\omega_i}\widehat{b}_{\Omega_B} + \\ &+ \sum_{\omega_i \in \mathcal{I}_{sys}, \Omega'_k \in \mathcal{I}_{src}} \xi_{\omega_i\Omega'_k} \; \widehat{a}^\dagger_{\omega_i}\widehat{c}_{\Omega'_k} + \sum_{\omega_{A_i}, \omega_{A_j} \in \mathcal{I}_{sys}, \Omega_k \in \mathcal{I}_{bth}} \chi_{\omega_i\omega_j\Omega_k} \; \widehat{a}^\dagger_{\omega_i}\widehat{a}_{\omega_j}\widehat{b}^\dagger_{\Omega_k} + \text{h.c.}\end{aligned} \tag{4.6}$$

where $\eta_{\omega_i\Omega_j}, \xi_{\omega_i\Omega'_k}, \chi_{\omega_i\omega_j\Omega_k} \in \mathbb{C}$ are the coupling constants describing the linear interactions among the thermal bath modes and the protein modes, the linear interactions between the external source and the protein, and the mode-mode interactions among the protein normal modes mediated by the thermal bath, respectively.
From these terms it is possible to derive the Fröhlich rate equations, by resorting to time dependent perturbation theory; details are given in the literature of Refs. [WA77][WA78a] and in the reference work by J. Pokorny [PW13].
However, the mode coupling term corresponds to a potential energy unbounded from below and, consequently, this would give rise to dynamical instability of the system and, in the quantum context, to the *absence of a finite energy ground state*. This problem led to a strong criticism against the Wu and Austin Hamiltonian and also against the ensemble of Fröhlich condensation theory [Bol99] [RMM+09]. Let us put $\xi_{\omega_i\Omega'_k} = 0$ so that only the interactions among the normal modes of the main system and the thermal bath are considered. An upper bound for the ground

state energy can be derived considering a normalized trial state $|\psi\rangle$; a possible choice for such a state has the form:

$$|\psi\rangle = \prod_{\omega_i \in \mathcal{I}_{sys}} \prod_{\Omega_j \in \mathcal{I}_{bth}} |n_{\omega_i}\rangle \otimes \left|z_{\Omega_j}\right\rangle \tag{4.7}$$

where $|N_{\omega_i}\rangle$ is a normalized bosonic state where the occupation number N_{ω_i} is fixed, i.e.

$$|N_{\omega_i}\rangle = \frac{\widehat{a}^\dagger_{\omega_i}}{\sqrt{N_{\omega_i}!}} |0\rangle \tag{4.8}$$

while $\left|z_{\Omega_j}\right\rangle$ is a Glauber quasi-classical or coherent state [Gla63][ZG+90] satisfying in general

$$\widehat{b}_{\Omega_j} \left|z_{\Omega_j}\right\rangle = z_{\Omega_j} \left|z_{\Omega_j}\right\rangle \qquad \text{and} \qquad \left\langle z_{\Omega_j}\right| \widehat{b}^\dagger_{\Omega_j} = \left\langle z_{\Omega_j}\right| z^*_{\Omega_j} \,. \tag{4.9}$$

As coherent states are eigenstates of the annihilation operator they can be interpreted as "quasi-classical" states, meaning that the annihilation of a single boson does not alter the state.
The values of $\{n_{\omega_i}\}_{\omega_i \in \mathcal{I}_{sys}}$ and $\left\{z_{\Omega_j}\right\}_{\Omega_j \in \mathcal{I}_{bth}}$ and the upper bound on the minimum of the bath-system interaction energy (ignoring linear interactions) results to be in this case

$$\begin{aligned} E_{sb,0} \leq \langle\psi| \widehat{H}_{sb} |\psi\rangle = \sum_{\omega_i \in \mathcal{I}_{sys}} \hbar\omega_i N_{\omega_i} + \sum_{\Omega_j \in \mathcal{I}_{bth}} \hbar\Omega_j \left|z_{\Omega_j}\right|^2 + \\ + \sum_{\omega_i \in \mathcal{I}_{sys}, \Omega_j \in \mathcal{I}_{bth}} N_{\omega_i} \left(\chi_{\omega_i\omega_i\Omega_j} z^*_{\Omega_j} + \chi_{\omega_i\omega_i\Omega_j} z_{\Omega_j}\right) . \end{aligned} \tag{4.10}$$

if $z_{\Omega_j} \in \mathbb{R}$ and such that $2\mathrm{Re}\left(\chi_{\omega_i\omega_i\Omega_j}\right) z_{\Omega_j} < 0$ then it possible for z_{Ω_j} to satisfy also the condition

$$\hbar\omega_i + 2\mathrm{Re}\left(\chi_{\omega_i\omega_i\Omega_j}\right) \sum_{\Omega_j} z_{\Omega_j} < 0 \tag{4.11}$$

and it follows that for large N_{ω_i} the expectation value of the interaction Hamiltonian between the thermal bath and the system is not bounded from below.
Such a problem can be easily fixed by adding a term with a quartic dependence on the creation/annihilation operators of the form

$$\begin{aligned} \widehat{H}_{intQ} = \sum_{\omega_i,\omega_j,\omega_k,\omega_l \in \mathcal{I}_{sys}} \Big[\kappa_{(1)\omega_i\omega_j\omega_k\omega_l} \, \widehat{a}^\dagger_{\omega_i} \widehat{a}^\dagger_{\omega_j} \widehat{a}_{\omega_k} \widehat{a}_{\omega_l} + \\ + \kappa_{(2)\omega_i\omega_j\omega_k\omega_l} \, \widehat{a}^\dagger_{\omega_i} \widehat{a}^\dagger_{\omega_j} \widehat{a}^\dagger_{\omega_k} \widehat{a}_{\omega_l} + \kappa_{(3)\omega_i\omega_j\omega_k\omega_l} \widehat{a}^\dagger_{\omega_i} \widehat{a}^\dagger_{\omega_j} \widehat{a}^\dagger_{\omega_k} \widehat{a}^\dagger_{\omega_l} \Big] + \text{h.c.} \end{aligned} \tag{4.12}$$

as using the same trial function $|\psi\rangle$ the expectation value of the Hamiltonian operator is now given by

$$\langle\psi| \widehat{H}_{intQ} |\psi\rangle = \sum_{\omega_{A_i} \in \mathcal{I}_{sys}} \kappa_{(1)\omega_i\omega_j\omega_i\omega_j} N_{\omega_i} \left[\sum_{\omega_j \in \mathcal{I}_{sys}/\omega_i} N_{\omega_j} + N_{\omega_i} \right] . \tag{4.13}$$

so that the previously calculated upper bound to the ground level energy does not go to $-\infty$ for large values of N_{ω_i}.
Such a quartic interaction stands for a anharmonic interaction among the normal modes of the

protein, a broadly studied topic of relevance to energy transport in proteins.

4.3 Dequantization of Wu and Austin Hamiltonian by Time Dependent Variational Principle (TDVP)

In this section, a classical Hamiltonian system with its canonical equations is associated to the quantum system described by the quantum Hamiltonian of eqs. (4.4), (4.6) and (4.12). This result is obtained by applying the Time Dependent Variational Principle (TDVP) technique[1] [KS80][Kra08] This consists in the evaluation of the time-dependent operator action on coherent states of quantum harmonic oscillators. The scalar parameters describing the coherent states become generalized coordinates of a classical dynamical system whose equations of motion can be derived from a variational principle.
In more details, we make the ansatz that the wavefunction is parametrized by N parameters $\{x_i\}_{i=1,...,N}$

$$|\psi\rangle = |\psi(x_1, ..., x_N)\rangle \ . \tag{4.14}$$

where the parameters $x_i = x_i(t)$ are in general functions of time. For a quantum system with Hamiltonian $\widehat{H}_{Tot}$ the equations of motion of the x_i can be derived using the following variational principle (equivalent to the Least Action principle)

$$\delta S = 0 \qquad \text{with} \qquad S = \int_0^t L(\psi, \bar{\psi}) \ \mathrm{d}t' \tag{4.15}$$

where $L(\psi,)$ is the Lagrangian associated to the system

$$L(\psi, \bar{\psi}) = \frac{\imath\hbar}{2} \frac{\left\langle \psi | \dot{\psi} \right\rangle - \left\langle \dot{\psi} | \psi \right\rangle}{\langle \psi | \psi \rangle} - \frac{\langle \psi | \, \widehat{H}_{Tot} \, | \psi \rangle}{\langle \psi | \psi \rangle} \ . \tag{4.16}$$

The equations of motions derived from eq.(4.15) can be worked out in the framework of classical Hamiltonian dynamics.
The classical Hamiltonian is associated with the quantum one by simply taking the expectation value of the Hamiltonian operator $\widehat{H}_{tot}$ over the state $|\psi(x_1, ..., x_N)\rangle$, that is

$$H_{Tot} = \langle \psi(x_1, ..., x_N) | \, \widehat{H}_{Tot} \, | \psi(x_1, ..., x_N) \rangle \ . \tag{4.17}$$

The Poisson brackets $\{\cdot, \cdot\}$ depend only on the chosen parametrization for the wavefunction. Starting from the variables

$$w_i = \imath\hbar \left\langle \psi | \frac{\partial \psi}{\partial x_i} \right\rangle = -\imath\hbar \left\langle \frac{\partial \psi}{\partial x_i} | \psi \right\rangle \tag{4.18}$$

[1] the same technique, much more deepened from mathematical and conceptual point of view, has been proposed as a "dequantization" technique by [JS10] as a sort inverse procedure respect to the geometrical quantization.

it is possible to the define the antisymmetric tensor

$$W_{ij} = \frac{\partial w_j}{\partial x_i} - \frac{\partial w_i}{\partial x_j} \tag{4.19}$$

such that the equation of motion is implicitly given by

$$\sum_{j=1}^{N} W_{ij}\dot{x}_j = \frac{\partial H_{Tot}}{\partial x_i}\,. \tag{4.20}$$

If the condition $\mathrm{Det}W_{ij} \neq 0$ holds then the matrix $\mathcal{W}_{ij} = \left(W^{-1}\right)_{ij}$ defines the Poisson brackets for the classical Hamiltonian system

$$\{f, g\} = \sum_{i,j}^{N} \frac{\partial f}{\partial x_i}\mathcal{W}_{ij}\frac{\partial g}{\partial x_j}\,. \tag{4.21}$$

This formalism can be applied to the quantum system described by the quantum Hamiltonian of eq.(4.4) to construct a classical Hamiltonian system associated to it.
The choice of the parametrization for the wavefunction is quite arbitrary and the TDVP, as any other variational principle, restricts the dynamics to a certain region of the Hilbert space.
The Hamiltonian is expressed in terms of creation/annihilation operators of the quantum harmonic oscillators which describe the system; for this reason, the wavefunction has been chosen as a product of the coherent states introduced before. In particular in this case

$$|\Psi(t)\rangle = \prod_{\omega_i\in\mathcal{I}_{sys},\Omega_j\in\mathcal{I}_{bth},\Omega'_k\in\mathcal{I}_{src}} |z_{\omega_i}(t)\rangle_{sys} \otimes \left|z_{\Omega_j}(t)\right\rangle_{bth} \otimes \left|z_{\Omega'_k}(t)\right\rangle_{src} \tag{4.22}$$

where $|z_{A_i}(t)\rangle_{sys}\,, |z_{B_k}(t)\rangle_{bth}\,, \left|z_{C_p}(t)\right\rangle_{src}$ are *normalized* coherent states for the normal modes of the main system, of the thermal bath and of the external source, respectively: their general form is given by

$$|z\rangle = \exp\left[-\frac{|z|^2}{2}\right]\sum_{k=0}^{+\infty}\frac{z^k}{\sqrt{k!}}\,|k\rangle = \exp\left[-\frac{|z|^2}{2}\right]\sum_{k=0}^{+\infty}\frac{\left(z\hat{a}^\dagger\right)^k}{k!}\,|0\rangle \qquad \text{where} \quad z = z(t) \in \mathbb{C}\,. \tag{4.23}$$

From the definition of coherent states eq.(4.9) it follows that the expectation value for the occupation number is given by the squared norm of z

$$\langle n_i(t)\rangle = \langle z(t)|\,\widehat{a}^\dagger\widehat{a}\,|(t)\rangle = |z(t)|^2 \tag{4.24}$$

so, as we are interested in writing rate equations for these quantities, we parametrize the wavefunction $\psi(t)$ with the set of real parameters $\{(n_i, \theta_i)\}_{i\in\mathcal{I}_\mathcal{S}}$ such that

$$z_i = n_i^{1/2}\exp\left[-\imath\theta_i\right] \quad\Longrightarrow\quad z_i^* = n_i^{1/2}\exp\left[\imath\theta_i\right] \qquad n_i = |z_i|^2 \qquad i \in \mathcal{I}_\mathcal{S}. \tag{4.25}$$

Using eq.(4.18) it is possible to derive the Poisson brackets associated with the variables $\{(n_i,\theta_i)\}_{i\in\mathcal{I}_\mathcal{S}}$:

$$
\begin{aligned}
w_{n_i} &= \imath\hbar\left\langle \{(n_j,\theta_j\}_{j\in\mathcal{I}_\mathcal{S}} \,|\frac{\partial}{\partial n_i}\{(n_j,\theta_j\}_{j\in\mathcal{I}_\mathcal{S}}\right\rangle = \\
&= \frac{\imath\hbar}{\partial n_i/\partial|z_i|}\left\langle \{(n_j,\theta_j\}_{j\in\mathcal{I}_\mathcal{S}}\right| \frac{\partial}{\partial|z_i|}\otimes_{j\in\mathcal{I}_\mathcal{S}}\left(\exp\left[-\frac{|z_j|^2}{2}\right]\sum_{k=0}^{+\infty}\frac{|z_j|^k\exp\left[-\imath k\theta_j\right]\left(\widehat{a}_j^\dagger\right)^k}{k!}|0\rangle\right) = \\
&= \frac{\imath\hbar}{2|z_i|}\Big(-|z_i|\left\langle \{(n_j,\theta_j\}_{j\in\mathcal{I}_\mathcal{S}}\,|\,\{(n_j,\theta_j\}_{j\in\mathcal{I}_\mathcal{S}}\right\rangle + \exp[-\imath\theta_i]\left\langle \{(n_j,\theta_j\}_{j\in\mathcal{I}_\mathcal{S}}\right|\widehat{a}_j^\dagger\left|\{(n_j,\theta_j\}_{j\in\mathcal{I}_\mathcal{S}}\right\rangle\Big) = \\
&= \frac{\imath\hbar}{2|z_i|}(-|z_i| + |z_i|\exp[\imath\theta_i]\exp[-\imath\theta_i]) = 0
\end{aligned}
\tag{4.26}
$$

$$
\begin{aligned}
w_{\theta_i} &= \imath\hbar\left\langle \{(n_j,\theta_j\}_{j\in\mathcal{I}_\mathcal{S}}\right|\frac{\partial}{\partial\theta_i}\left|\{(n_j,\theta_j\}_{j\in\mathcal{I}_\mathcal{S}}\right\rangle = \\
&= \imath\hbar\left\langle \{(n_j,\theta_j\}_{j\in\mathcal{I}_\mathcal{S}}\right|\frac{\partial}{\partial\theta_i}\otimes_{j\in\mathcal{I}_\mathcal{S}}\left(\exp\left[-\frac{|z_j|^2}{2}\right]\sum_{k=0}^{+\infty}\frac{|z_j|^k\exp\left[-\imath k\theta_j\right]\left(\widehat{a}_j^\dagger\right)^k}{k!}|0\rangle\right) = \\
&= \imath(-\imath)\hbar|z_i|\exp[-\imath\theta_i]\left\langle \{(n_j,\theta_j\}_{j\in\mathcal{I}_\mathcal{S}}\right|\widehat{a}_i^\dagger\left|\{(n_j,\theta_j\}_{j\in\mathcal{I}_\mathcal{S}}\right\rangle = \hbar|z_i|^2 = \hbar n_i\,.
\end{aligned}
\tag{4.27}
$$

and, consequently, using the definition (4.19) the entries of the matrix W are

$$
W_{\theta_i\theta_k} = W_{n_in_k} = 0 \tag{4.28}
$$

$$
W_{n_i\theta_k} = -W_{\theta_kn_i} = \frac{\partial w_{\theta_k}}{\partial n_i} - \frac{\partial w_{n_i}}{\partial\theta_k} = \hbar\delta_{i,k}\,. \tag{4.29}
$$

and its inverse has the form

$$
\mathcal{W}_{\theta_i\theta_k} = \mathcal{W}_{n_in_k} = 0 \tag{4.30}
$$

$$
\mathcal{W}_{\theta_in_k} = -\mathcal{W}_{n_k\theta_i} = \frac{\delta_{i,k}}{\hbar}\,. \tag{4.31}
$$

Consequently it follows that the variables $J_\omega = \hbar n_\omega$ and θ_ω are canonically conjugated variables. The classical Hamiltonian $H = H_0 + H_{IntWA} + H_{IntQuad}$ for the variables $\{(\theta_\omega, J_\omega)\}_{\omega\in\mathcal{I}_\mathcal{S}}$ is given by a free classical part

$$
\begin{aligned}
H_0 = \langle\Psi(\theta_\omega,J_\omega)|\,\hat{H}_0\,|\Psi(\theta_\omega,J_\omega)\rangle &= \sum_{\omega_i\in\mathcal{I}_{sys}}\omega_iJ_{\omega_i} + \sum_{\Omega_k\in\mathcal{I}_{bth}}\Omega_kJ_{\Omega_k} + \\
&+ \sum_{\Omega'_p\in\in\mathcal{I}_{src}}\Omega'_pJ_{\Omega'_p}
\end{aligned}
\tag{4.32}
$$

by a semi-classical Wu and Austin interaction part

$$
\begin{aligned}
H_{IntWA} &= \langle \Psi(\theta_\omega, J_\omega) | \, \hat{H}_{IntWA} \, | \Psi(\theta_\omega, J_\omega) \rangle = \\
&= \sum_{\omega_i \in \mathcal{I}_{sys}} \sum_{\Omega_k \in \mathcal{I}_{bth}} \frac{|\eta_{\omega_i \Omega_k}|}{\hbar} J_{\omega_i}^{1/2} J_{\Omega_k}^{1/2} \cos\left(\theta_{\omega_i} - \theta_{\Omega_k} + \theta_{\eta_{\omega_i \Omega_k}}\right) + \\
&+ \sum_{\omega_i \in \mathcal{I}_{sys}} \sum_{\Omega'_p \in \mathcal{I}_{src}} \frac{|\xi_{\omega_i \Omega'_p}|}{\hbar} J_{\omega_i}^{1/2} J_{\Omega'_k}^{1/2} \cos\left(\theta_{\omega_i} - \theta_{\Omega'_p} + \theta_{\xi_{\omega_i \Omega'_p}}\right) + \\
&+ \sum_{\omega_i, \omega_j \in \mathcal{I}_{sys}} \sum_{\Omega_k \in \mathcal{I}_{bth}} \frac{|\chi_{\omega_i \omega_j \Omega_k}|}{\hbar^{3/2}} J_{\omega_i}^{1/2} J_{\omega_j}^{1/2} J_{\Omega_k}^{1/2} \cos\left(\theta_{\omega_i} - \theta_{\omega_j} + \theta_{\Omega_k} + \theta_{\chi_{\omega_i \omega_j \Omega_k}}\right)
\end{aligned}
\tag{4.33}
$$

and by the quadratic term

$$
\begin{aligned}
H_{IntQ} = \langle \Psi(\theta_\omega, J_\omega) | \, \hat{H}_{IntQ} \, | \Psi(\theta_\omega, J_\omega) \rangle = & \sum_{\omega_i, \omega_j, \omega_k, \omega_l \in \mathcal{I}_{sys}} J_{\omega_i}^{1/2} J_{\omega_j}^{1/2} J_{\omega_k}^{1/2} J_{\omega_l}^{1/2} \\
& \left[\frac{|\kappa_{(1)\omega_i \omega_j \omega_k \omega_l}|}{\hbar^2} \cos\left(\theta_{\omega_i} + \theta_{\omega_j} - \theta_{\omega_k} - \theta_{\omega_l} + \theta_{\kappa_{(1)\omega_i \omega_j \omega_k \omega_l}}\right) + \right. \\
& \frac{|\kappa_{(2)\omega_i \omega_j \omega_k \omega_l}|}{\hbar^2} \cos\left(\theta_{\omega_i} + \theta_{\omega_j} + \theta_{\omega_k} - \theta_{\omega_l} + \theta_{\kappa_{(2)\omega_i \omega_j \omega_k \omega_l}}\right) + \\
& \left. + \frac{|\kappa_{(3)\omega_i \omega_j \omega_k \omega_l}|}{\hbar^2} \cos\left(\theta_{\omega_i} + \theta_{\omega_j} + \theta_{\omega_k} + \theta_{\omega_l} + \theta_{\kappa_{(3)\omega_i \omega_j \omega_k \omega_l}}\right) \right]
\end{aligned}
\tag{4.34}
$$

where each complex coupling constant is given in polar representation. In what follows, the coupling constants are considered real and rescaled s.t.

$$
\begin{aligned}
& \theta_{\eta_{\omega_i \Omega_k}} = \theta_{\xi_{\omega_i \Omega'_p}} = \theta_{\chi_{\omega_i \omega_j \Omega_k}} = \theta_{\kappa_{(1,2,3)\omega_i \omega_j \omega_k \omega_k}} = 0 \\
& \tilde{\eta}_{\omega_i \Omega_K} = \frac{|\eta_{\omega_i \Omega_k}|}{\hbar} \quad \tilde{\xi}_{\omega_i \Omega'_p} = \frac{|\xi_{\omega_i \Omega'_p}|}{\hbar} \quad \tilde{\chi}_{\omega_i \omega_j \Omega_k} = \frac{|\chi_{\omega_i \omega_j \Omega_k}|}{\hbar^{3/2}} \quad \tilde{\kappa}_{(1,2,3)\omega_i \omega_j \omega_k \omega_l} = \frac{|\kappa_{(1,2,3)\omega_i \omega_j \omega_k \omega_l}|}{\hbar^2}
\end{aligned}
\tag{4.35}
$$

with these choices, the total Hamiltonian of the system reads

$$H_{Tot}(\{(J_{\omega_i},\theta_{\omega_i}\}_{\omega_i\in\mathcal{I}_{\mathcal{S}}}) = \sum_{\omega_i\in\mathcal{I}_{sys}} \omega_i J_i + \sum_{\Omega_j\in\mathcal{I}_{bth}} \Omega_j J_{\Omega_j} + \sum_{\Omega_k'\in\mathcal{I}_{src}} \Omega_k' J_{\Omega_k{}'} +$$
$$+ \sum_{\omega_i\in\mathcal{I}_{sys}} \sum_{\Omega_j\in\mathcal{I}_{bth}} \eta_{\omega_i\Omega_j} J_{\omega_i}^{1/2} J_{\Omega_j}^{1/2} \cos\left(\theta_{\omega_i}-\theta_{\Omega_j}\right) + \sum_{\omega_i\in\mathcal{I}_{sys}} \sum_{\Omega_k'\in\mathcal{I}_{src}} \xi_{\omega_i\Omega_k'} J_{\omega_i}^{1/2} J_{\Omega_k'}^{1/2} \cos\left(\theta_{\omega_i}-\theta_{\Omega_k'}\right) +$$
$$\sum_{\omega_i,\omega_j\in\mathcal{I}_{sys}} \sum_{\Omega_k\in\mathcal{I}_{bth}} \chi_{\omega_i\omega_j\Omega_k}\ J_{\omega_i}^{1/2} J_{\omega_j}^{1/2} J_{\Omega_k}^{1/2} \cos\left(\theta_{\omega_i}-\theta_{\omega_j}+\theta_{\Omega_k}\right) +$$
$$+ \sum_{\omega_i,\omega_j,\omega_k,\omega_l\in\mathcal{I}_{sys}} J_{\omega_i}^{1/2} J_{\omega_j}^{1/2} J_{\omega_k}^{1/2} J_{\omega_l}^{1/2} \Bigg[\kappa_{(1)\omega_i\omega_j\omega_k\omega_l} \cos\left(\theta_{\omega_i}+\theta_{\omega_j}-\theta_{\omega_k}-\theta_{\omega_l}\right) +$$
$$\kappa_{(2)\omega_i\omega_j\omega_k\omega_l} \cos\left(\theta_{\omega_i}+\theta_{\omega_j}+\theta_{\omega_k}-\theta_{\omega_l}\right) + \kappa_{(3)\omega_i\omega_j\omega_k\omega_l} \cos\left(\theta_{\omega_i}+\theta_{\omega_j}+\theta_{\omega_k}+\theta_{\omega_l}\right) \Bigg] . \tag{4.36}$$

In order to derive Fröhlich-like rate equations, the dynamics of the action variables J_{ω_i} of the system has to be studied. We could choose to investigate the dynamics of the system by letting observable quantities evolve in time (according to Hamilton's equations of motion) and then performing time averaging and an averaging on different initial conditions compatible with the assumption that the two subsystems $\mathcal{I}_{bth}$ and $\mathcal{I}_{src}$ are two thermal baths with different temperatures. However, this method has some disadvantages: the integration should be done numerically for the presence of non-linear interactions terms in the Hamiltonian and for the large number of degrees of freedom that would be necessary to simulate the dynamics of the thermal baths. Moreover, long integration times would be necessary to attain the convergence of time averages, and, finally, this would be a computational effort providing a redundant information on the phase dynamics.
Another way to derive rate equations for the J_{ω_i} consists in a more "statistical" approach: the dynamical variable to consider is the phase space distribution function $\rho(\{(J_\omega,\theta_\omega)\}_{\omega\in\mathcal{I}_{\mathcal{S}}},t)$ so that the rate equations are written for the *statistical averages of actions variables*

$$\langle J_{\omega_i}(t)\rangle = \int J_{\omega_i}\rho(\{(J_\omega,\theta_\omega)\}_{\omega\in\mathcal{I}_{\mathcal{S}}},t) \prod_{\omega\in\mathcal{I}_{\mathcal{S}}} \mathrm{d}J_{\omega_i}\mathrm{d}\theta_{\omega_i} \ . \tag{4.37}$$

The following Section is dedicated to the problem of deriving classical Fröhlich-like rate equations from the Liouville equation for the distribution function ρ.

4.4 Derivation of Fröhlich-like rate equations using Koopman-Von Neumann (KvN) formalism

4.4.1 General considerations concerning KvN formalism

Let $\rho(\{(J_\omega,\theta_\omega)\}_{\omega\in\mathcal{I}_{\mathcal{S}}};t)$ be a probability density function for the whole system described by the Hamiltonian in eq. (4.36); according to the Liouville Theorem the evolution of ρ associated

with this Hamiltonian is given by

$$\frac{\partial \rho}{\partial t} = \{H, \rho\} = -\imath \mathcal{L}_H(\rho) \tag{4.38}$$

where $\{\cdot,\cdot\}$ are the canonical Poisson brackets

$$\begin{aligned}\{f,g\} = &\sum_{\omega_i}\left(\frac{\partial f}{\partial J_{\omega_i}}\frac{\partial g}{\partial \theta_{\omega_i}} - \frac{\partial g}{\partial J_{\omega_i}}\frac{\partial f}{\partial \theta_{\omega_i}}\right) + \sum_{\Omega_j}\left(\frac{\partial f}{\partial J_{\Omega_j}}\frac{\partial g}{\partial \theta_{\Omega_j}} - \frac{\partial g}{\partial J_{\Omega_j}}\frac{\partial f}{\partial \theta_{\Omega_j}}\right) + \\ &+ \sum_{\Omega'_k}\left(\frac{\partial f}{\partial J_{\Omega'_k}}\frac{\partial g}{\partial \theta_{\Omega'_k}} - \frac{\partial g}{\partial J_{\Omega'_k}}\frac{\partial f}{\partial \theta_{\Omega'_k}}\right) .\end{aligned} \tag{4.39}$$

and $\mathcal{L}_H(\cdot) = \imath\{H,\cdot\}$ is the *Liouville operator* acting on functions defined on the phase space of the system. An interesting method to study and solve Liouville equations relies on the Koopman-Von Neumann (KvN) formalism developed in the 30's: a formal analogy among Liouville and Schrödinger equation is established such that also classical mechanics can be formulated in the framework of a Hilbert space of square integrable functions.
In our case the Hilbert space of complex square integrable functions in phase space is $L^2(\Lambda_{\{(J_\omega,\theta_\omega)\}_{\omega\in\mathcal{I}_\mathcal{S}}})$ with the inner product defined by

$$\langle f|g\rangle = \int_{\lambda_{\{(J,\alpha)\}_{\omega\in\mathcal{I}_\mathcal{S}}}} f^* g \prod_{\omega\in\mathcal{I}_\mathcal{S}} \mathrm{d}J_\omega\, \mathrm{d}\theta_\omega = \prod_{\omega\in\mathcal{I}_\mathcal{S}} \int_0^{2\pi} \mathrm{d}\theta_\omega \int_0^{+\infty} \mathrm{d}J_\omega\ f^* g \tag{4.40}$$

with $f, g \in L^2(\Lambda_{\{(J_\omega,\theta_\omega)\}_{\omega\in\mathcal{I}_\mathcal{S}}})$. On this space we can define the action of the Liouville operator

$$\hat{\mathcal{L}}_H\,|f\rangle = \mathcal{L}_H(f)\ . \tag{4.41}$$

and consider the domain $\mathcal{D}_{\hat{\mathcal{L}}_H} \subseteq L^2(\Lambda_{\{(J_\omega,\theta_\omega)\}_{\omega\in\mathcal{I}_\mathcal{S}}})$ where the Liouville operator is self-adjoint, namely, $\widehat{\mathcal{L}}_H^\dagger = \widehat{\mathcal{L}_H}$ and $\mathcal{D}_{\hat{\mathcal{L}}_H} = \mathcal{D}_{\widehat{\mathcal{L}}_H^\dagger}$.
Let $\psi(\{(J,\theta)\}_{\mathcal{I}_\mathcal{S}};t) \in \mathcal{D}_{\hat{\mathcal{L}}_H}$ be a normalized time-dependent function [2] such that

$$\imath\frac{\partial \psi}{\partial t}(\mathbf{J},\boldsymbol{\theta};t) = \hat{\mathcal{L}}_H \psi(\mathbf{J},\boldsymbol{\theta};t) \tag{4.42}$$

then it is possible to demonstrate that $\rho = \|\psi\|_{L^2(\Lambda_{(J,\theta)})} = \psi^*\psi$ is a normalized function for which (4.38) holds. Moreover as $\hat{\mathcal{L}}_H$ is a self-adjoint operator it represents the unitary time evolution of the wave function as

$$\psi(\{(J,\theta)\}_{\mathcal{I}_\mathcal{S}};t) = \exp\left[-\imath t\hat{\mathcal{L}}_H\right]\psi(\{(J,\theta)\}_{\mathcal{I}_\mathcal{S}};0) \tag{4.43}$$

in analogy with quantum mechanics. With this formalism the problem of deriving rate equations (3.33) for the average values of the actions (which are the analogous of quantum occupation

[2] This formulation is equivalent to Schrödinger representation in classical quantum mechanics.

numbers) for the main system normal modes ω_i can be expressed in this formal way:

$$\frac{\mathrm{d}}{\mathrm{d}t}\langle J_{\omega_i}\rangle_t = \frac{\mathrm{d}}{\mathrm{d}t}\langle\psi(t)|\,\hat{\mathcal{M}}_{J_{\omega_i}}\,|\psi(t)\rangle = \imath\,\langle\psi(t)|\left[\hat{\mathcal{L}}_H, \hat{\mathcal{M}}_{J_{\omega_i}}\right]|\psi(t)\rangle \tag{4.44}$$

where $\hat{\mathcal{M}}_{J_{\omega_i}}$ is a multiplicative operator acting on $L^2(\Lambda_{\{(J_\omega,\theta_\omega)\}_{\omega\in\mathcal{I}_\mathcal{S}}})$ such that

$$\hat{\mathcal{M}}_{J_{\omega_i}}\,|\psi\rangle = |J_{\omega_i}\psi\rangle\ . \tag{4.45}$$

Now let us suppose that the Liouville operator can be decomposed as

$$\hat{\mathcal{L}_H} = \hat{\mathcal{L}}_{H_0} + \hat{\mathcal{L}}_{H_{Int}}(t) \tag{4.46}$$

where the eigenfunctions of $\hat{\mathcal{L}}_{H_0}$ operator are known and the operator $\hat{\mathcal{L}}_{H_{Int}}$ can be treated as a time dependent perturbation, which is adiabatically turned on and off from $t=-\infty$ to $t=+\infty$. Then the analogous of the Interaction representation is adopted as a suitable formalism to study this class of systems. In particular, if $|\psi(t)\rangle_S$ is the wave function in the Schrödinger representation, its expression in Interaction representation $|\psi(t)\rangle_I$ reads

$$|\psi(t)\rangle_I = \exp\left[\imath t\hat{\mathcal{L}}_{H_0}\right]|\psi(t)\rangle_S \tag{4.47}$$

and given a generic operator $\hat{A}_S$ in Schrödinger picture its expression in Interaction picture $\hat{A}_I$ reads

$$\hat{A}_I(t) = \exp\left[\imath t\hat{\mathcal{L}}_{H_0}\right]\hat{A}_S\exp\left[-\imath t\hat{\mathcal{L}}_{H_0}\right]\ . \tag{4.48}$$

With this formalism the time evolution of $|\psi(t)\rangle_I$ can be written through the unitary evolution operator $\hat{U}(t;t_0)$ satisfying

$$|\psi(t)\rangle_I = \hat{U}(t;t_0)\,|\psi(t_0)\rangle_I \tag{4.49}$$

$$\imath\frac{\partial U(t;t_0)}{\partial t} = \hat{\mathcal{L}}_{H_{int}}(t)\hat{U}(t;t_0) \tag{4.50}$$

and the formal solution of (4.50) is given by

$$U(t;t_0) = \mathbb{I} - \imath\int_{t_0}^{t}\hat{\mathcal{L}}_{H_{int}}(t')\hat{U}(t';t_0)\,\mathrm{d}t'\,. \tag{4.51}$$

At first order in $\hat{\mathcal{L}}_{H_{int}}(t')$, the unitary evolution operator $\hat{U}(t;t_0)$ in the right hand side of eq. is substituted by the identity operator meaning that the state $|\psi(t_0)\rangle_I$, if the perturbation is turned on at t_0, can be approximated at zeroth order by $|\psi(t_0)\rangle_I \simeq |\psi(t_0)\rangle_S$ and assumed to be coincident with Schrödinger picture (i.e. $|\psi(0)\rangle = |\psi_0\rangle$), then

$$|\psi(t)\rangle_I \approx \left(\hat{\mathbb{I}} - \imath\int_{-\infty}^{t}\hat{\mathcal{L}}_{H_{int}}(t')\right)|\psi_0\rangle_I \tag{4.52}$$

and, as $\hat{\mathcal{L}}_{H_{int}}(t')$ is a self-adjoint operator, the time evolution for the "bra" has the form

$$\langle\psi(t)|_I \approx \langle\psi_0|_I \left(\hat{\mathbb{I}} + \imath \int_{-\infty}^{t} \hat{\mathcal{L}}_{H_{int}}(t')\right) . \tag{4.53}$$

The time derivative of the multiplicative operator $\hat{\mathcal{M}}_{J_{\omega_i}}$ in interaction picture is derived according to eq.(4.48)

$$\left(\dot{\hat{\mathcal{M}}}_{J_{\omega_i}}\right)_I = \imath \left(\left[\hat{\mathcal{L}}_H, \hat{\mathcal{M}}_{J_{\omega_i}}\right]\right)_I = \imath \exp\left[\imath t \hat{\mathcal{L}}_{H_0}\right] \left[\hat{\mathcal{L}}_H, \hat{\mathcal{M}}_{J_{\omega_i}}\right] \exp\left[-\imath t \hat{\mathcal{L}}_{H_0}\right] . \tag{4.54}$$

This means that the average (4.44) can be entirely rewritten using the interaction picture as

$$\begin{aligned}
&\frac{\mathrm{d}}{\mathrm{d}t} \langle J_{\omega_i}\rangle_t =_I \langle\psi(t)| \left(\dot{\hat{\mathcal{M}}}_{J_{\omega_i}}\right)_I |\psi(t)\rangle_I = \imath_I \langle\psi(t)| \left(\left[\hat{\mathcal{L}}_H, \hat{\mathcal{M}}_{J_{\omega_i}}\right](t)\right)_I |\psi(t)\rangle_I = \\
&\approx \imath \langle\psi_0| \left(\hat{\mathbb{I}} + \imath \int_{-\infty}^{t} \hat{\mathcal{L}}_{H_{int}}(t')\,\mathrm{d}t'\right) \left(\left[\widehat{\mathcal{L}}_H, \hat{\mathcal{M}}_{J_{\omega_i}}\right](t)\right)_I \left(\hat{\mathbb{I}} - \imath \int_0^t \hat{\mathcal{L}}_{H_{int}}(t')\,\mathrm{d}t'\right) |\psi_0\rangle = \\
&= \imath \langle\psi_0| \left(\left[\hat{\mathcal{L}}_H, \hat{\mathcal{M}}_{J_{\omega_i}}\right](t)\right)_I |\psi_0\rangle + \int_0^t \langle\psi_0| \left[\left(\left[\widehat{\mathcal{L}}_{H_{int}}, \widehat{\mathcal{M}}_{J_{\omega_i}}\right](t)\right)_I, \left(\widehat{\mathcal{L}}_{H_{int}}(t')\right)_I\right] |\psi_0\rangle\,\mathrm{d}t'
\end{aligned} \tag{4.55}$$

4.4.2 Liouvillian operator properties of Wu-Austin-like model

In order to derive the equivalent of Fröhlich rate equations in a classical context, we now apply the method described in the previous Section to the model described by the Hamiltonian in eq.(4.36). Let us introduce the *multiplicative* operator for scalar functions $\widehat{\mathcal{M}}_{f(\{(J_\omega,\theta_\omega)\}_{\omega\in\mathcal{I}_\mathcal{S}})}$ with

$$\widehat{\mathcal{M}}_{f(\{(J_\omega,\theta_\omega)\}_{\omega\in\mathcal{I}_\mathcal{S}})} |\psi\rangle = f(\{(J_\omega,\theta_\omega)\}_{\omega\in\mathcal{I}_\mathcal{S}})\psi = |f(\{(J_\omega,\theta_\omega)\}_{\omega\in\mathcal{I}_\mathcal{S}})\psi\rangle \tag{4.56}$$

and the *derivative* operators respect to angular variables $\widehat{D}_{\theta_\omega}$ and respect to action variables $\widehat{D}_{J_\omega}$ whose actions are given by

$$\widehat{D}_{J_\omega} |\psi\rangle = -\imath\partial_{J_\omega} f \qquad \widehat{D}_{\theta_\omega} |\psi\rangle = -\imath\partial_{\theta_\omega} f . \tag{4.57}$$

The commutation rules for such operators are obviously given by

$$\begin{aligned}
&\left[\widehat{\mathcal{M}}_{f(\{(J_\omega,\theta_\omega)\}_{\omega\in\mathcal{I}_\mathcal{S}})}, \widehat{\mathcal{M}}_{g(\{(J_\omega,\theta_\omega)\}_{\omega\in\mathcal{I}_\mathcal{S}})}\right] = 0 && \text{(commutativity of functions product)} \\
&\left[\widehat{D}_{J_{\omega_i}}, \widehat{D}_{\theta_{\omega_j}}\right] = \left[\widehat{D}_{J_{\omega_i}}, \widehat{D}_{J_{\omega_j}}\right] = \left[\widehat{D}_{\theta_{\omega_i}}, \widehat{D}_{\theta_{\omega_j}}\right] = 0 && \text{(Schwarz Theorem for } C^2 \text{ functions)} \\
&\left[\widehat{D}_{J_{\omega_i}}, \widehat{\mathcal{M}}_{f(\{(J_\omega,\theta_\omega)\}_{\omega\in\mathcal{I}_\mathcal{S}})}\right] = -\imath\widehat{\mathcal{M}}_{\partial_{J_{\omega_i}} f(\{(J_\omega,\theta_\omega)\}_{\omega\in\mathcal{I}_\mathcal{S}})} && \text{(Leibniz' Rule of derivation)} \\
&\left[\widehat{D}_{\theta_{\omega_i}}, \widehat{\mathcal{M}}_{f(\{(J_\omega,\theta_\omega)\}_{\omega\in\mathcal{I}_\mathcal{S}})}\right] = -\imath\widehat{\mathcal{M}}_{\partial_{\theta_{\omega_i}} f(\{(J_\omega,\theta_\omega)\}_{\omega\in\mathcal{I}_\mathcal{S}})} .
\end{aligned} \tag{4.58}$$

in particular the following case, of particular for our problem, can be derived by the general formulas (4.58)

$$\begin{aligned}
&\left[\widehat{D}_{J_{\omega_i}}, \widehat{\mathcal{M}}_{J^q_{\omega_j}}\right] = -\imath q \widehat{\mathcal{M}}_{J^{q-1}_{\omega_i}} \delta_{ij} \qquad \omega_i, \omega_j \in \mathcal{I}_{\mathcal{S}} \quad q \in \mathbb{Z} \\
&\left[\widehat{D}_{\boldsymbol{\alpha}\cdot\boldsymbol{\theta}}, \widehat{\mathcal{M}}_{\exp[\imath\boldsymbol{\beta}\cdot\boldsymbol{\theta}]}\right] = (\boldsymbol{\alpha}\cdot\boldsymbol{\beta})\ \widehat{\mathcal{M}}_{\exp[\imath\boldsymbol{\beta}\cdot\boldsymbol{\theta}]} \qquad \boldsymbol{\alpha}\cdot\boldsymbol{\beta} = \sum_{\omega_i\in\mathcal{I}_{\mathcal{S}}} \alpha_{\omega_i}\beta_{\omega_i} \\
&\left[\widehat{D}_{\boldsymbol{\alpha}\cdot\boldsymbol{\theta}}, \widehat{\mathcal{M}}_{\cos[\boldsymbol{\beta}\cdot\boldsymbol{\theta}]}\right] = \imath(\boldsymbol{\alpha}\cdot\boldsymbol{\beta})\ \widehat{\mathcal{M}}_{\sin[\boldsymbol{\beta}\cdot\boldsymbol{\theta}]} \qquad \left[\widehat{D}_{\boldsymbol{\alpha}\cdot\boldsymbol{\theta}}, \widehat{\mathcal{M}}_{\sin[\boldsymbol{\beta}\cdot\boldsymbol{\theta}]}\right] = -\imath(\boldsymbol{\alpha}\cdot\boldsymbol{\beta})\ \widehat{\mathcal{M}}_{\cos[\boldsymbol{\beta}\cdot\boldsymbol{\theta}]}
\end{aligned} \tag{4.59}$$

where

$$\widehat{D}_{\boldsymbol{\alpha}\cdot\boldsymbol{\theta}} = -\imath \sum_{\omega\in\mathcal{I}_{\mathcal{S}}} \alpha_\omega \widehat{\partial}_{\theta_\omega} \qquad \alpha_\omega \in \mathbb{R}, . \tag{4.60}$$

With this definition it follows that the free Liouville operator $\widehat{\mathcal{L}}_{H_0}$ for the system we considered can be rewritten as:

$$\widehat{\mathcal{L}}_{H_0} = -\imath \sum_{\omega\in\mathcal{I}_{\mathcal{S}}} \omega \widehat{\partial}_{\theta_\omega} = \widehat{D}_{\boldsymbol{\omega}\cdot\boldsymbol{\theta}}\ . \tag{4.61}$$

The interaction Liouville operator is can be seen as the sum of four contributions

$$\widehat{\mathcal{L}}_{H_{int}}(t) = \widehat{\mathcal{L}}_{H_{sys-bth}}(t) + \widehat{\mathcal{L}}_{H_{sys-src}}(t) + \widehat{\mathcal{L}}_{H_{sys-bth-src}}(t) + \widehat{\mathcal{L}}_{H_{IntQ}}(t) \tag{4.62}$$

where the explicit time dependence takes into account the adiabatic switching off of the interaction at $t = +\infty$; this can be obtained by the introduction of a term of the form $\exp[-\lambda t]$ where $\lambda > 0$ is the inverse time scale on which the interaction is supposed to be active.
The term $\widehat{\mathcal{L}}_{H_{sys-bth}}(t)$ and $\widehat{\mathcal{L}}_{H_{sys-src}}(t)$ describes the linear interactions among the normal modes of the protein, of the thermal bath, and of the external source of energy; they are respectively given by

$$\begin{aligned}
\widehat{\mathcal{L}}_{H_{sys-bth}}(t) = \sum_{\omega\in\mathcal{I}_{sys}} \sum_{\Omega\in\mathcal{I}_{bth}} &\exp(-\lambda t)\, \eta_{\omega\Omega} \Big[\widehat{\mathcal{M}}_{J^{1/2}_\omega} \widehat{\mathcal{M}}_{J^{1/2}_\Omega} \widehat{\mathcal{M}}_{\sin(\theta_\omega-\theta_\Omega)} \left(\widehat{D}_{J_\omega} - \widehat{D}_{J_\Omega}\right) + \\
&+ \frac{1}{2}\widehat{\mathcal{M}}_{\cos(\theta_\omega-\theta_\Omega)} \left(\widehat{\mathcal{M}}_{J^{-1/2}_\omega} \widehat{\mathcal{M}}_{J^{1/2}_\Omega} \widehat{D}_{\theta_\omega} + \widehat{\mathcal{M}}_{J^{1/2}_\omega} \widehat{\mathcal{M}}_{J^{-1/2}_\Omega} \widehat{D}_{\theta_\Omega}\right)\Big]
\end{aligned} \tag{4.63}$$

and

$$\begin{aligned}
\widehat{\mathcal{L}}_{H_{sys-src}}(t) = \sum_{\omega\in\mathcal{I}_{sys}} \sum_{\Omega'\in\mathcal{I}_{src}} &\exp(-\lambda t)\, \eta_{\omega\Omega'} \Big[\widehat{\mathcal{M}}_{J^{1/2}_\omega} \widehat{\mathcal{M}}_{J^{1/2}_{\Omega'}} \widehat{\mathcal{M}}_{\sin(\theta_\omega-\theta_{\Omega'})} \left(\widehat{D}_{J_\omega} - \widehat{D}_{J_{\Omega'}}\right) + \\
&+ \frac{1}{2}\widehat{\mathcal{M}}_{\cos(\theta_\omega-\theta_{\Omega'})} \left(\widehat{\mathcal{M}}_{J^{-1/2}_\omega} \widehat{\mathcal{M}}_{J^{1/2}_{\Omega'}} \widehat{D}_{\theta_\omega} + \widehat{\mathcal{M}}_{J^{1/2}_\omega} \widehat{\mathcal{M}}_{J^{-1/2}_{\Omega'}} \widehat{D}_{\theta_{\Omega'}}\right)\Big]\ .
\end{aligned} \tag{4.64}$$

The Liouvillian operator representing non linear interaction term among normal modes of the main system with the thermal bath is given by

$$\begin{aligned}
&\widehat{\mathcal{L}}_{H_{sys-bth-sys}}(t) = \\
&= \sum_{\omega,\omega_i\in\mathcal{I}_{sys}} \sum_{\Omega_{bth}\in\mathcal{I}_{bth}} \exp(-\lambda t)\Big\{\widehat{\mathcal{M}}_{J_\omega^{1/2}}\widehat{\mathcal{M}}_{J_{\omega_i}^{1/2}}\widehat{\mathcal{M}}_{J_\Omega^{1/2}}\Big[\chi_{\omega\omega_i\Omega}\widehat{\mathcal{M}}_{\sin(\theta_\omega+\theta_\Omega-\theta_{\omega_i})}\left(\widehat{D}_{J_\omega}+\widehat{D}_{J_\Omega}\right)+ \\
&+\chi_{\omega_i\omega\Omega}\widehat{\mathcal{M}}_{\sin(\theta_{\theta_\omega-\omega_i}-\theta_\Omega)}\widehat{D}_{J_\omega}\Big]+\frac{1}{2}\widehat{\mathcal{M}}_{J_\omega^{-1/2}}\widehat{\mathcal{M}}_{J_{\omega_i}^{1/2}}\widehat{\mathcal{M}}_{J_\Omega^{1/2}}\Big[\chi_{\omega\omega_i\Omega}\widehat{\mathcal{M}}_{\cos(\theta_\omega+\theta_\Omega-\theta_{\omega_i})}+ \\
&\chi_{\omega_i\omega\Omega}\widehat{\mathcal{M}}_{\cos(\theta_{\omega_i}+\theta_\Omega-\theta_\omega)}\Big]\widehat{D}_{\theta_\omega}+\frac{1}{2}\widehat{\mathcal{M}}_{J_\omega^{1/2}}\widehat{\mathcal{M}}_{J_{\omega_i}^{1/2}}\widehat{\mathcal{M}}_{J_\Omega^{-1/2}}\widehat{\mathcal{M}}_{\cos(\theta_\omega+\theta_\Omega-\theta_{\omega_i})}\widehat{D}_{\theta_\Omega}\Big\}
\end{aligned} \tag{4.65}$$

Under the simplifying hypothesis that the coefficients $\kappa_{(n)\omega_i\omega_j\omega_k\omega_l}$ are symmetric with respect to the exchange of symbols then the terms representing quadratic anharmonic interactions among normal modes are given by

$$\begin{aligned}
&\widehat{\mathcal{L}}_{H_{intQ}}(t) = \sum_{\omega,\omega_i,\omega_j,\omega_k\in\mathcal{I}_{sys}} \exp(-\lambda t)\Big\{\widehat{\mathcal{M}}_{J_\omega^{1/2}}\widehat{\mathcal{M}}_{J_{\omega_i}^{1/2}}\widehat{\mathcal{M}}_{J_{\omega_j}^{1/2}}\widehat{\mathcal{M}}_{J_{\omega_k}^{1/2}}\Big[4\kappa_{(1)\omega\omega_i\omega_j\omega_k}\widehat{\mathcal{M}}_{\sin(\omega+\omega_i-\omega_j-\omega_k)}+ \\
&+\kappa_{(2)\omega\omega_i\omega_j\omega_k}\left(3\widehat{\mathcal{M}}_{\sin(\theta_\omega+\theta_{\omega_i}+\theta_{\omega_j}+\theta_{\omega_k})}+\widehat{\mathcal{M}}_{\sin(\theta_\omega-\theta_{\omega_i}-\theta_{\omega_j}-\theta_{\omega_k})}\right)+ \\
&+4\kappa_{(3)\omega\omega_i\omega_j\omega_k}\widehat{\mathcal{M}}_{\sin(\theta_\omega+\theta_{\omega_i}+\theta_{\omega_j}+\theta_{\omega_k})}\Big]\widehat{D}_{J_\omega}+\frac{1}{2}\widehat{\mathcal{M}}_{J_\omega^{1/2}}\widehat{\mathcal{M}}_{J_{\omega_i}^{1/2}}\widehat{\mathcal{M}}_{J_{\omega_j}^{1/2}}\widehat{\mathcal{M}}_{J_{\omega_k}^{1/2}}\Big[\\
&4\kappa_{(1)\omega\omega_i\omega_j\omega_k}\widehat{\mathcal{M}}_{\cos(\theta_\omega+\theta_{\omega_i}-\theta_{\omega_j}-\theta_{\omega_k})}+\kappa_{(2)\omega\omega_i\omega_j\omega_k}\left(3\widehat{\mathcal{M}}_{\cos(\theta_\omega+\theta_{\omega_i}+\theta_{\omega_j}-\theta_{\omega_k})}+\widehat{\mathcal{M}}_{\sin(\theta_\omega-\theta_{\omega_i}-\theta\omega_j-\theta\omega_k)}\right)+ \\
&+4k_{(3)\omega\omega_i\omega_j\omega_k}\widehat{\mathcal{M}}_{\sin(\theta_\omega+\theta_{\omega_i}+\theta_{\omega_j}+\theta_{\omega_k})}\Big]\widehat{D}_{\theta_\omega} \quad .
\end{aligned} \tag{4.66}$$

The particular form of the Liouville operator imposes some restriction on the domain of the L^2 functions on phase space that we have to consider. The Liouvillian operator for the model that has been introduced is invariant under angle translation by multiples of 2π

$$\exp[\imath 2\pi\widehat{D}_{\mathbf{k}\cdot\boldsymbol{\theta}}]\mathcal{L}_H(\boldsymbol{\theta},t)\exp[-\imath 2\pi\widehat{D}_{\mathbf{k}\cdot\boldsymbol{\theta}}] = \mathcal{L}_H(\boldsymbol{\theta}+2\pi\mathbf{k},t) = \mathcal{L}_H(\boldsymbol{\theta},t) \qquad \mathbf{k}\in\mathbb{Z}^{N_{tot}} \tag{4.67}$$

where N_{tot} is the total number of normal modes of the main system, of the thermal bath and of the external source. The property (4.67) implies that we can restraint the domain of the operator on the space of 2π-periodic functions with respect to the angle variables: this means that any function in the domain of the operator can be written in terms of Fourier series, i.e.

$$\psi(\{(J_\omega,\theta_\omega)\}_{\omega\in\mathcal{I}_\mathcal{S}},t) = \sum_{\mathbf{k}\in\mathbb{Z}^{N_{tot}}} \frac{1}{(2\pi)^{N_{tot}}/2}\phi_{\mathbf{k}}\left(\{(J_\omega\}_{\omega\in\mathcal{I}_\mathcal{S}},t\right)\exp[-\imath\mathbf{k}\cdot\boldsymbol{\theta}] \tag{4.68}$$

S with the normalization condition

$$\sum_{\mathbf{k}\in\mathbb{Z}^{N_{tot}}} \|\phi_{\mathbf{k}}\left(\{(J_\omega\}_{\omega\in\mathcal{I}_{\mathcal{S}}}, t\right)\|^2 = 1\,. \tag{4.69}$$

In order to verify that the Liouville operator considered is hermitian, it is sufficient to prove that the following operator, depending only on a pair of action-angle variables, is hermitian

$$\widehat{\mathcal{L}}_{test} = \widehat{\mathcal{M}}_{J_\omega^{k/2}}\widehat{\mathcal{M}}_{\sin(\theta_\omega+\delta)}\widehat{D}_{J_\omega} + \left(\mathbb{I} + \frac{1}{2}\widehat{\mathcal{M}}_{J_\omega^{k/2-1}}\widehat{\mathcal{M}}_{\cos(\theta_\omega+\delta)}\right)\widehat{D}_{\theta_\omega} \qquad \text{with} \quad k \geq 1 \tag{4.70}$$

so that

$$\begin{aligned}
&\left\langle g|\widehat{\mathcal{L}}_{test}f\right\rangle = \\
&= -\imath\int_0^{2\pi}\mathrm{d}\theta_\omega\int_0^{+\infty}\mathrm{d}J_\omega\; g^*\left[J_\omega^{k/2}\sin(\theta+\delta)\frac{\partial f}{\partial J} + \left(\frac{k}{2}J_\omega^{k/2-1}\cos(\theta_\omega+\delta)+1\right)\frac{\partial f}{\partial\theta_\omega}\right] = \\
&= -\imath\int_0^{2\pi}\mathrm{d}\theta_\omega J_\omega^{k/2}\sin(\theta_\omega+\delta)\,g^*f\Big|_{J=0}^{J=+\infty} + \imath\int_0^{2\pi}\mathrm{d}\theta_\omega\int_0^{+\infty}\mathrm{d}J_\omega\;\sin(\theta_\omega+\delta)\,J_\omega^{k/2}\frac{\partial g^*}{\partial_{J_\omega}} + \\
&+\imath\frac{k}{2}\int_0^{2\pi}\mathrm{d}\theta_\omega\int_0^{+\infty}\mathrm{d}J_\omega\sin(\theta_\omega+\delta)\,g^*f - \imath\frac{k}{2}\int_0^{+\infty}\mathrm{d}J_\omega\;\left(\cos(\theta_\omega+\delta)\,J_\omega^{k/2-1}+1\right)g^*f\Big|_{\theta=0}^{\theta=2\pi} + \\
&+\imath\frac{k}{2}\int_0^{2\pi}\mathrm{d}\theta_\omega\int_0^{+\infty}\mathrm{d}J_\omega\;\left(\cos(\theta_\omega+\delta)\,J_\omega^{k/2-1}+1\right)\frac{\partial g^*}{\partial\theta_\omega}f + \\
&-\imath\frac{k}{2}\int_0^{2\pi}\mathrm{d}\theta_\omega\int_0^{+\infty}\mathrm{d}J_\omega\;\sin(\theta_\omega+\delta)\,J_\omega^{k/2-1}g^*f = \\
&= \left\langle\widehat{\mathcal{L}}_{test}g|f\right\rangle - \imath\frac{k}{2}\int_0^{+\infty}\mathrm{d}J_\omega\;\left(\cos(\theta_\omega+\delta)\,J_\omega^{k/2-1}+1\right)g^*f\Big|_{\theta=0}^{\theta=2\pi} + \\
&-\imath\int_0^{2\pi}\mathrm{d}\theta_\omega J_\omega^{k/2}\sin(\theta_\omega+\delta)\,g^*f\Big|_{J=0}^{J=+\infty}\,.
\end{aligned} \tag{4.71}$$

So, if we consider a domain of functions in $L^2([0,2\pi]\times[0,+\infty))$ such that they are periodic in the angle variables and such that for both f, g

$$\lim_{J_\omega\longrightarrow 0} J_\omega^{1/4}\phi(\{J_\omega\}_{\omega\in\mathcal{I}_{\mathcal{S}}}) = 0 \tag{4.72}$$

holds then the operator $\widehat{\mathcal{L}}_{test}$ is hermitian and consequently the Liouville operator we considered to study Fröhlich condensation in classical systems is hermitian.

We notice that if we consider the Fourier representation of amplitude functions ψ as suggested in eq.(4.68) and we make the hypothesis that the only non zero component is $\phi_{\mathbf{0}}(\{J_\omega\}_{\omega\in\mathcal{I}_{\mathcal{S}}}, t)$ we can verify that the square root of the normalized Boltzmann distribution for equilibrium

independent harmonic oscillators

$$\phi_{\mathrm{Bol}}(J_\omega, t) = \sqrt{\frac{k_B T}{\omega}} \exp\left[-\frac{\omega J_\omega}{2k_B T}\right] \tag{4.73}$$

satisfies the condition in eq.(4.72).
In what follows we assume that the amplitude test function $|\psi(t)\rangle_S$ in Schrödinger representation has the form

$$|\psi(t)\rangle_S = \phi_{\mathbf{0}}(\{J_\omega\}_{\omega\in\mathcal{I}_\mathcal{S}}) = \prod_{\omega\in\mathcal{I}_{sys}} \phi(J_\omega, t) \prod_{\Omega\in\mathcal{I}_{bth}} \phi_{\mathrm{Bol}}(J_\Omega) \prod_{\Omega'\in\mathcal{I}_{src}} \phi_{\mathrm{Bol}}(J_{\Omega'})\,. \tag{4.74}$$

This assumption on the form of the states we are interested in takes into account for many physical approximation. The independence by angular variables (as $\phi_{\mathbf{k}}(\{J_\omega\}_{J_\omega\in\mathcal{I}_\mathcal{S}}, t) = 0$ for $\mathbf{k} \neq \mathbf{0}$) can be interpreted as the angular variable are not decorrelated among them. Moreover the factorization of the function depending by the actions in Boltzmann time-independent distribution functions for the single harmonic oscillator of the thermal bath and the external source of energy is a possible formalization of the behaviour of a thermal bath: the degrees of freedom has a given statistic andit is not influenced by the dynamics. Finally the factorization of the distribution function for the normal modes of the system translate the quite *strong approximation* that the *action variables of the main system are independent*, i.e.

$$\left\langle \prod_{\omega\in\mathcal{I}_\mathcal{S}} J_\omega^{k_\omega} \right\rangle \approx \prod_{\omega\in\mathcal{I}_\mathcal{S}} \left\langle J_\omega^{k_\omega} \right\rangle \tag{4.75}$$

4.4.3 Derivation of rate equations for actions expectation values J_{ω_i}

In order to derive the analogous of Fröhlich rate equation according to eq.(4.55) we had to derive the form of the Liouville operator and of the commutator of the Liouville opeartor with multiplicative operator by J_{ω_i} in Interaction picture.
We first notice that for an operator $\widehat{\mathcal{A}}_I(t)$ in Interaction picture

$$\frac{\mathrm{d}\widehat{\mathcal{A}}_I(t)}{\mathrm{d}t} = \exp\left(\imath t\widehat{\mathcal{L}}_{H_0}\right)\left[\widehat{\mathcal{A}}_S(t), \widehat{\mathcal{L}}_{H_0}\right]\exp\left(-\imath t\widehat{\mathcal{L}}_{H_0}\right) \tag{4.76}$$

so that the time dependence of the operator in the interaction is acquired only by multiplicative operators for functions which depends by angular variables $\widehat{\mathcal{M}}_{f(\{\theta_\omega\}_{\omega\in\mathcal{I}_\mathcal{S}})}$; in the Liouville operator associated to the Hamiltonian eq.(4.36) such functions have the general form

$$\begin{aligned} \widehat{\mathcal{M}}_{\cos(\mathbf{k}\cdot\boldsymbol{\theta})} &= \frac{\widehat{\mathcal{M}}_{\exp(\imath\mathbf{k}\cdot\boldsymbol{\theta})} + \widehat{\mathcal{M}}_{\exp(-\imath\mathbf{k}\cdot\boldsymbol{\theta})}}{2} \\ \widehat{\mathcal{M}}_{\sin(\mathbf{k}\cdot\boldsymbol{\theta})} &= \frac{\widehat{\mathcal{M}}_{\exp(\imath\mathbf{k}\cdot\boldsymbol{\theta})} - \widehat{\mathcal{M}}_{\exp(-\imath\mathbf{k}\cdot\boldsymbol{\theta})}}{2\imath}\,. \end{aligned} \tag{4.77}$$

with $\mathbf{k} \in \mathbb{R}^{N_{Tot}}$. As the following differential equation holds

$$\begin{aligned}\frac{\mathrm{d}\left(\widehat{\mathcal{M}}_{\pm\imath\exp(\pm\imath\mathbf{k}\cdot\boldsymbol{\theta})}\right)_I}{\mathrm{d}t} &= \frac{\mathrm{d}}{\mathrm{d}t}\left[\exp\left(\imath t\widehat{\mathcal{L}}_{H_0}\right)\left(\widehat{\mathcal{M}}_{\pm\imath\exp(\pm\imath\mathbf{k}\cdot\boldsymbol{\theta})}\right)_S\exp\left(\imath t\widehat{\mathcal{L}}_{H_0}\right)\right] = \\ &= \pm\imath\left(\mathbf{k}\cdot\boldsymbol{\omega}t\right)\left(\widehat{\mathcal{M}}_{\pm\imath\exp(\pm\imath\mathbf{k}\cdot\boldsymbol{\theta})}\right)_I(t)\end{aligned} \tag{4.78}$$

it follows that

$$\left(\widehat{\mathcal{M}}_{\pm\imath\exp(\pm\imath\mathbf{k}\cdot\boldsymbol{\theta})}\right)_I(t) = \exp\left(\pm\imath\mathbf{k}\cdot\boldsymbol{\omega}\right)\left(\widehat{\mathcal{M}}_{\pm\exp(\pm\imath\mathbf{k}\cdot\boldsymbol{\theta})}\right) \tag{4.79}$$

and consequently

$$\begin{aligned}\left(\widehat{\mathcal{M}}_{\cos(\mathbf{k}\cdot\boldsymbol{\theta})}\right)_I(t) &= \widehat{\mathcal{M}}_{\cos(\mathbf{k}\cdot(\boldsymbol{\theta}+\boldsymbol{\omega}t))} \\ \left(\widehat{\mathcal{M}}_{\sin(\mathbf{k}\cdot\boldsymbol{\theta})}\right)_I(t) &= \widehat{\mathcal{M}}_{\sin(\mathbf{k}\cdot(\boldsymbol{\theta}+\boldsymbol{\omega}t))}\,.\end{aligned} \tag{4.80}$$

Now we have all the elements to derive a Fröhlich like rate equations from eq.(4.55).

4.4.3.1 Linear term respect to $\widehat{\mathcal{L}}_{H_{Int}}$ in eq.(4.55)

We start considering the contribution of first order term in $\widehat{\mathcal{L}}_{H_{Int}}$ to the right hand side of rate equations (4.55). Such a term is given by the expectation value on the initial unperturbed state $|\psi_0(-\infty)\rangle$ of the commutator of the interaction Liouville $\widehat{\mathcal{L}}_{H_{Int}}$ operator with the multiplication operator for the action variables J_{ω_i} in Interaction picture.
Using commutation rules in eq.(4.59) and eqs.(4.80) the commutator in Interaction picture reads

$$\begin{aligned}&\left(\left[\hat{\mathcal{L}}_H, \hat{\mathcal{M}}_{J_{\omega_i}}\right]\right)_I(t) = (-\imath)\exp\left(-\lambda t\right)\Bigg(\sum_{\Omega\in\mathcal{I}_{sys}}\eta_{\omega_i\Omega}\widehat{\mathcal{M}}_{J^{1/2}_{\omega_i}}\widehat{\mathcal{M}}_{J^{1/2}_{\Omega}}\widehat{\mathcal{M}}_{\sin\left[\theta_{\omega_i}-\theta_\Omega+(\omega_i+\Omega)t\right]}+ \\ &+\sum_{\Omega'\in\mathcal{I}_{src}}\xi_{\omega_i\Omega'}\widehat{\mathcal{M}}_{J^{1/2}_{\omega_i}}\widehat{\mathcal{M}}_{J^{1/2}_{\Omega'}}\widehat{\mathcal{M}}_{\sin\left[\theta_{\omega_i}-\theta_{\Omega'}+(\omega_i-\Omega')t\right]}+ \\ &+\sum_{\omega_j\in\mathcal{I}_{sys}}\sum_{\Omega\in\mathcal{I}_{bth}}\widehat{\mathcal{M}}_{J^{1/2}_{\omega_i}}\widehat{\mathcal{M}}_{J^{1/2}_{\omega_j}}\widehat{\mathcal{M}}_{J^{1/2}_{\Omega}}\Big(\chi_{\omega_i\omega_j\Omega}\widehat{\mathcal{M}}_{\sin\left[\theta_{\omega_i}+\theta_\Omega-\theta_{\omega_j}+(\omega_i+\Omega-\omega_j)t\right]}+ \\ &-\chi_{\omega_j\omega_i\Omega}\widehat{\mathcal{M}}_{\sin\left[\theta_{\omega_i}-\theta_{\omega_j}-\theta_\Omega+(\omega_i-\omega_j-\Omega)t\right]}\Big)+ \\ &+\sum_{\omega_j,\omega_k,\omega_l\in\mathcal{I}_{sys}}\widehat{\mathcal{M}}_{J^{1/2}_{\omega_i}}\widehat{\mathcal{M}}_{J^{1/2}_{\omega_j}}\widehat{\mathcal{M}}_{J^{1/2}_{\omega_k}}\widehat{\mathcal{M}}_{J^{1/2}_{\omega_l}}\Bigg[4\kappa_{(1)\omega_i\omega_j\omega_k\omega_l}\widehat{\mathcal{M}}_{\sin\left[\theta_{\omega_i}+\theta_{\omega_j}-\theta_{\omega_k}-\theta_{\omega_l}+(\omega_i+\omega_j-\omega_k-\omega_l)t\right]}+ \\ &+\kappa^{(2)}_{\omega_i\omega_j\omega_k\omega_l}\left(\widehat{\mathcal{M}}_{\sin\left[\theta_{\omega_i}-\theta_{\omega_j}-\theta_{\omega_k}-\theta_{\omega_l}+(\omega_i-\omega_j-\omega_k-\omega_l)t\right]}+3\widehat{\mathcal{M}}_{\sin\left[\theta_{\omega_i}-\theta_{\omega_j}-\theta_{\omega_k}-\theta_{\omega_l}+(\omega_i-\omega_j-\omega_k-\omega_l)t\right]}\right)+ \\ &+\kappa^{(3)}_{A_iA_jA_kA_l}\widehat{\mathcal{M}}_{\sin\left[\theta_{\omega_i}+\theta_{\omega_j}+\theta_{\omega_k}+\theta_{\omega_l}+(\omega_i-\omega_j-\omega_k-\omega_l)t\right]}\Bigg]\end{aligned} \tag{4.81}$$

It has to be noticed that all terms contain a linear dependence by the sinus function of angular variables. When the expectation value of this terms is calculated on the state $|\psi_0\rangle$ of the form assumed in the eq.(4.74), it gives a null contribution as averages of linear trigonometric functions

of each variables are taken on the interval $[0; 2\pi]$. That means that the lowest order contributions to rate equations for expectation values of action variables J_{ω_i} come from quadratic term in $\widehat{\mathcal{L}}_{H_{Int}}$.

4.4.3.2 Second order term in $\widehat{\mathcal{L}}_{H_{Int}}$ in eq.(4.55)

The second order term respect to $\widehat{\mathcal{L}}_{H_{Int}}$ in right hand side of eq. (4.55) gives in general a not null contributions when the expectation value is calculated on the state $|\psi_0\rangle$ of eq.(4.74) as quadratic terms in trigonometric functions of angular variables appear.
The general form for this terms would given by

$$\left\langle \widehat{\mathcal{M}}_{J_\omega} \right\rangle = \sum_{(i),(ii)\in IdxSet} \langle\psi_0| \int_0^t \mathrm{d}t' \left[\left(\left[\widehat{\mathcal{L}}_{H_{(i)}}, \widehat{\mathcal{M}}_{J_\omega} \right] \right)_I (t), \left(\widehat{\mathcal{L}}_{H_{(ii)}} \right)_I (t') \right] |\psi_0\rangle \tag{4.82}$$

where $IdxSet = \{sys-bth,\, sys-src,\, sys-src-sys,\, intQ(1),\, intQ(2),\, intQ(3)\}$ is the set of indices labelling the different terms in interaction Liouville operator; this means that *a priori* there are 36 contributions to calculate. Nevertheless, some equivalent of selection rules can be applied due to the particular form of the state $|\psi_0(t)\rangle$ we have chosen. As argued in the previous paragraph, the terms in between the bra and ket has to be depend by pair power low of trigonometric function of each variable in order to give a not null contribution; this is possible only if with the same indices in *IdxSet* are considered.
Let us consider the detailed derivation of the contribution to the rate equations due to the term describing linear interactions among the bath and the main system as an example of the general procedure we used also in the other cases.
Let us start considering the operator at right hand side of (4.82) where $(i) = (ii) = sys - bth$ at a certain time $t > 0$ in Interaction picture

$$\begin{aligned}
&\int_0^t \left[\left(\left[\widehat{\mathcal{L}}_{H_{sys-bth}}, \widehat{\mathcal{M}}_{J_{\omega_i}} \right] \right)_I (t), \left(\widehat{\mathcal{L}}_{sys-bth} \right)_I (t') \right] \mathrm{d}t' = \\
&= \frac{1}{2} \sum_{\omega\in\tilde{\mathcal{I}}_{sys}} \sum_{\Omega,\tilde{\Omega}\in\mathcal{I}_{bth}} \int_0^t \exp(-\lambda t) \exp(-\lambda t')\, \eta_{\omega_i\tilde{\Omega}} \eta_{\omega\Omega} \widehat{\mathcal{M}}_{J_\omega^{1/2}} \widehat{\mathcal{M}}_{J_\Omega^{1/2}} \Bigg[\Bigg(\widehat{\mathcal{M}}_{J_{\omega_i}^{-1/2}} \widehat{\mathcal{M}}_{J_{\tilde{\Omega}}^{1/2}} \delta_{\omega,\omega_i} + \\
&- \widehat{\mathcal{M}}_{J_{\omega_i}^{1/2}} \widehat{\mathcal{M}}_{J_{\tilde{\Omega}}^{-1/2}} \delta_{\Omega,\tilde{\Omega}} \Bigg) \widehat{\mathcal{M}}_{\sin\left[\theta_{\omega_i} - \theta_{\tilde{\Omega}} + (\omega_i - \tilde{\Omega})t\right]} \widehat{\mathcal{M}}_{\sin[\theta_\omega - \theta_\Omega + (\omega-\Omega)t']} + \Bigg(\widehat{\mathcal{M}}_{J_{\omega_i}^{-1/2}} \widehat{\mathcal{M}}_{J_{\tilde{\Omega}}^{1/2}} \delta_{\omega,\omega_i} + \\
&- \widehat{\mathcal{M}}_{J_{\omega_i}^{1/2}} \widehat{\mathcal{M}}_{J_{\tilde{\Omega}}^{-1/2}} \delta_{\Omega,\tilde{\Omega}} \Bigg) \widehat{\mathcal{M}}_{\cos\left[\theta_{\omega_i} - \theta_{\tilde{\Omega}} + (\omega_i - \tilde{\Omega})t\right]} \widehat{\mathcal{M}}_{\cos[\theta_\omega - \theta_\Omega + (\omega-\Omega)t']} \Bigg) \Bigg] \mathrm{d}t'
\end{aligned} \tag{4.83}$$

and performing the integration over the time variable t' and considering the limit $\lambda \longrightarrow 0$ we obtain

$$\begin{aligned}
&\int_0^t \left[\left(\left[\widehat{\mathcal{L}}_{H_{sys-bth}}, \widehat{\mathcal{M}}_{J_{\omega_i}}\right]\right)_I(t), \left(\widehat{\mathcal{L}}_{sys-bth}\right)_I(t')\right] \mathrm{d}t' = \\
&= \frac{1}{2} \sum_{\omega \in \tilde{\mathcal{I}}_{sys}} \sum_{\Omega, \tilde{\Omega} \in \mathcal{I}_{bth}} \eta_{\omega_i \tilde{\Omega}} \eta_{\omega\Omega}\, \widehat{\mathcal{M}}_{J_\omega^{1/2}} \widehat{\mathcal{M}}_{J_\Omega^{1/2}} \frac{\sin\left(\frac{(\omega-\Omega)t}{2}\right)}{(\omega-\Omega)} \Bigg[\Bigg(\widehat{\mathcal{M}}_{J_{\omega_i}^{-1/2}} \widehat{\mathcal{M}}_{J_{\tilde{\Omega}}^{1/2}} \delta_{\omega,\omega_i} + \\
&- \widehat{\mathcal{M}}_{J_{\omega_i}^{1/2}} \widehat{\mathcal{M}}_{J_{\tilde{\Omega}}^{-1/2}} \delta_{\Omega,\tilde{\Omega}}\Bigg) \Bigg(\widehat{\mathcal{M}}_{\cos\left[\theta_\omega - \theta_\Omega - \theta_{\omega_i} + \theta_{\tilde{\Omega}} + \left(\omega - \Omega - \frac{\omega_i - \tilde{\Omega}}{2}\right)t\right]} + \\
&- \widehat{\mathcal{M}}_{\cos\left[\theta_\omega - \theta_\Omega + \theta_{\omega_i} - \theta_{\tilde{\Omega}} + \left(\omega - \Omega + \frac{\omega_i - \tilde{\Omega}}{2}\right)t\right]}\Bigg) + \Bigg(\widehat{\mathcal{M}}_{J_{\omega_i}^{-1/2}} \widehat{\mathcal{M}}_{J_{\tilde{\Omega}}^{1/2}} \delta_{\omega,\omega_i} - \widehat{\mathcal{M}}_{J_{\omega_i}^{1/2}} \widehat{\mathcal{M}}_{J_{\tilde{\Omega}}^{-1/2}} \delta_{\Omega,\tilde{\Omega}}\Bigg) \\
&\Bigg(\widehat{\mathcal{M}}_{\cos\left[\theta_\omega - \theta_\Omega - \theta_{\omega_i} + \theta_{\tilde{\Omega}} + \left(\omega - \Omega - \frac{\omega_i - \tilde{\Omega}}{2}\right)t\right]} + \widehat{\mathcal{M}}_{\cos\left[\theta_\omega - \theta_\Omega + \theta_{\omega_i} - \theta_{\tilde{\Omega}} + \left(\omega - \Omega + \frac{\omega_i - \tilde{\Omega}}{2}\right)t\right]}\Bigg)
\end{aligned} \tag{4.84}$$

When the expectation values is calculated over the states $|\psi_0\rangle$ the only terms that give a contributions are the ones for which $\exists \omega \in \mathcal{I}_{sys}$ and $\exists \Omega \in \mathcal{I}_{bth}$ such that the trigonometric functions in (4.84) do not depends any more by angular variables, i.e. $\omega = \omega_i$ and $\Omega = \tilde{\Omega}$. In this way the averages over angular variables give not null contributions; after this passages are performed the expression (4.84)

$$\begin{aligned}
&\langle\psi_0| \int_0^t \left[\left(\left[\widehat{\mathcal{L}}_{H_{sys-bth}}, \widehat{\mathcal{M}}_{J_{\omega_i}}\right]\right)_I(t), \left(\widehat{\mathcal{L}}_{sys-bth}\right)_I(t')\right] \mathrm{d}t' \,|\psi_0\rangle = \\
&= \sum_{\tilde{\Omega} \in \mathcal{I}_{bth}} \left(\frac{\pi}{2} \eta^2_{\omega_i \tilde{\Omega}}\right) \frac{\sin\left[\left(\omega - \tilde{\Omega}\right) t\right]}{\pi\left(\omega - \tilde{\Omega}\right)} \left(\left\langle \widehat{\mathcal{M}}_{J_{\tilde{\Omega}}} \right\rangle - \left\langle \widehat{\mathcal{M}}_{J_{\omega_i}} \right\rangle\right)
\end{aligned} \tag{4.85}$$

where the bracket in the previous expression refers to the averages over actions variables. According to the form for the $|\psi_0\rangle$ function assumed in eq.(4.74), we have for the expectation value of action variables of heath bath that

$$\left\langle \widehat{\mathcal{M}}_{J_{\tilde{\Omega}}} \right\rangle = \frac{k_B T_B}{\tilde{\Omega}} \,. \tag{4.86}$$

In the limit for which the thermal bath can be considered constituted by a continuum of normal modes the coefficient $\eta^2_{\omega\tilde{\Omega}}$ becomes a distribution function respect to the frequencies of thermal bath modes, i.e. $\eta^2_\omega(\tilde{\Omega})$ and obviously the sum becomes an integral over frequencies $\sum_{\tilde{\Omega} \in \mathcal{I}_{bth}} \rightarrow \int_0^{+\infty} \mathrm{d}\tilde{\Omega}$. As we are interested in the behaviour of the system for long times $t \gg \max_{\omega \in \mathcal{I}_{sys}, \tilde{\Omega} \in \mathcal{I}_{bth}} |\tilde{\Omega} - \omega|^{-1}$, the following approximation is assumed

$$\frac{\sin\left[\left(\omega - \tilde{\Omega}\right) t\right]}{\pi\left(\omega - \tilde{\Omega}\right)} \longrightarrow \delta(\omega - \tilde{\Omega}) \tag{4.87}$$

when the continuum limit for thermal bath modes is considered, being $\delta(x)$ the Dirac δ-distribution. Finally, the averages over the action variables are considered evaluated at t and not at $t_0 = 0$ in order to write a set of rate equations for J_{ω_i}, as in the spirit of perturbation theory, $|\psi_0(t)\rangle \approx |\psi_0(t)\rangle$; it follows that[3]

$$\left\langle \widehat{\mathcal{M}}_{J_{\omega_i}} \right\rangle = \int_0^{+\infty} J_{\omega_i} \|\phi_0(J_{\omega_i};0)\|^2 \approx \int_0^{+\infty} J_{\omega_i} \|\phi_0(J_{\omega_i};t)\|^2 = \left\langle \widehat{\mathcal{M}}_{J_{\omega_i}} \right\rangle (t) \ . \tag{4.88}$$

The final for the contribution due to the linear system-bath interaction is

$$\begin{aligned}
&\langle\psi_0| \int_0^t \left[\left(\left[\widehat{\mathcal{L}}_{H_{sys-bth}}, \widehat{\mathcal{M}}_{J_{\omega_i}} \right] \right)_I (t), \left(\widehat{\mathcal{L}}_{sys-bth} \right)_I (t') \right] \mathrm{d}t' \, |\psi_0\rangle = \left(\frac{\pi}{2} \eta^2_{\omega_i}(\omega_i) \right) \left[\frac{k_B T_B}{\omega_i} - \langle J_{\omega_i} \rangle \right] = \\
&= b_{\omega_i} \left[\frac{k_B T_B}{\omega_i} - \langle J_{\omega_i} \rangle \right]
\end{aligned} \tag{4.89}$$

where

$$b_{\omega_i} = \frac{\pi \eta^2_{\omega_i}(\omega_i)}{2\omega_i} \ . \tag{4.90}$$

An analogous is derived considering the terms due to the linear coupling among the principal system and the thermal bath:

$$\begin{aligned}
&\langle\psi_0| \int_0^t \left[\left(\left[\widehat{\mathcal{L}}_{H_{sys-src}}, \widehat{\mathcal{M}}_{J_{\omega_i}} \right] \right)_I (t), \left(\widehat{\mathcal{L}}_{sys-src} \right)_I (t') \right] |\psi_0\rangle \ \mathrm{d}t' = \frac{\pi \xi^2_{\omega_i(\omega_i)}}{2} \left(\frac{k_B T_P}{\omega_i} - \langle J_{\omega_i} \rangle \right) \simeq \\
&\simeq \frac{\pi \xi^2_{\omega_{A_i} \omega_{A_i}}}{2} \frac{k_B T_P}{\omega_{A_i}} = s_{\omega_i}
\end{aligned} \tag{4.91}$$

where in the last equation the approximation $\langle J_{\omega_i} \rangle (t) \ll \dfrac{k_B T_P}{\omega_i}$ has been made. This approximation correspond to the physical request of a continuous energy injection as s_{ω_i} is in general non-negative and time independent.

The contribution to rate equation given by the term in Liouvillian operator related to non linear interaction among the main system and the thermal bath is more complicate:

$$\begin{aligned}
&\langle\psi_0| \int_0^t \left[\left(\left[\widehat{\mathcal{L}}_{H_{sys-bth-sys}}, \widehat{\mathcal{M}}_{J_{\omega_i}} \right] \right)_I (t), \left(\widehat{\mathcal{L}}_{H_{sys-bth-sys}} \right)_I (t') \right] |\psi_0\rangle \ \mathrm{d}t' = \sum_{\omega \in \mathcal{I}_{sys}} \frac{\pi \chi^2_{\omega_i \omega}(|\omega - \omega_i|)}{2} \\
&\left[\frac{k_B T_B}{|\omega - \omega_i|} \left(\langle J_\omega \rangle - \langle J_{\omega_i} \rangle \right) + \mathrm{sgn}(\omega - \omega_i) \langle J_{\omega_i} J_\omega \rangle \right] \simeq \\
&\simeq \sum_{\omega_i \in \mathcal{I}_{sys}} \frac{\pi \chi^2_{\omega_i \omega}(|\omega - \omega_i|)}{2} \left[\frac{k_B T_B}{|\omega - \omega_i|} \left(\langle J_\omega \rangle - \langle J_{\omega_i} \rangle \right) + \mathrm{sgn}(\omega - \omega_i) \langle J_{\omega_i} \rangle \langle J_\omega \rangle \right]
\end{aligned} \tag{4.92}$$

[3] This passage is quite mathematically "ambiguous" ans reflects the hybrid character of the Interaction picture where both operators and states are considered to evolve with time. Nevertheless the approximation of eq.(4.88) is the same operated by Wu and Austin in original derivation of Fröhlich equations made the same approximation [WA78a].

where in the last approximated equality we have assumed that the correlation of actions of systems normal modes are negligible. Introducing the coefficients

$$c_{\omega\omega_i} = \frac{\pi k_B T_B \chi^2_{\omega_i\omega}(|\omega-\omega_i|)}{2|\omega-\omega_i|} \tag{4.93}$$

the eq.(4.92) simplifies

$$\begin{aligned}&\langle\psi_0|\int_0^t \left[\left(\left[\widehat{\mathcal{L}}_{H_{H_{sys-bth-sys}}}, \widehat{\mathcal{M}}_{J_{\omega_i}}\right]\right)_I(t), \left(\widehat{\mathcal{L}}_{H_{sys-bth-sys}}\right)_I(t')\right]|\psi_0\rangle\ \mathrm{d}t' = \\ &= \sum_{\omega_A\in\mathcal{I}_{sys}} c_{\omega\omega_i}\left[\left(\langle J_\omega\rangle - \langle J_{\omega_i}\rangle\right) + \frac{(\omega-\omega_i)}{k_B T_B}\langle J_{\omega_i}\rangle\langle J_\omega\rangle\right].\end{aligned} \tag{4.94}$$

There are further difficulties in the derivation of the contribution due to the terms in Liouvillian related to quadratic interactions among normal modes. In the previous cases the explicit time dependence which appears in rate equations through $\sin\left[(\omega_i-\Omega)t\right]/\left[\pi(\omega_i-\Omega)\right]$ has been managed considering a *continuum* for the thermal bath and replacing the sinc function by a δ-distribution. This would be incorrect for what concerns the *finite and countable* set of normal modes of the main system; for such a reason the sinc function is substituted

$$\frac{\sin\left[\Delta\omega_{(A)intQ}(\omega_i)t\right]}{\pi\Delta\omega_{(A)intQ}(\omega_i)} \approx \begin{cases} 0 & \text{when} \quad \Delta\omega_{(A)intQ}(\omega_i)\neq 0 \\ \dfrac{1}{\delta\omega_{sys}} & \text{when} \quad \Delta\omega_{(i)}=0 \end{cases} \tag{4.95}$$

where $\delta\omega_{sys} = \min\omega_j,\omega_k\in\mathcal{I}_{sys}(|\omega_j-\omega_k|)$ is the spectral resolution of the main system while and

$$\begin{aligned}\Delta\omega_{(1)intQ}(\omega_i) &= \omega_i+\omega_j-\omega_k-\omega_l \qquad & \Delta\omega_{(2,i)intQ}(\omega_i) &= \omega_i-\omega_j-\omega_k-\omega_l \\ \Delta\omega_{(2,ii)intQ} &= \omega_i+\omega_j+\omega_k-\omega_l \qquad & \Delta\omega_{(3)intQ} &= \omega_i+\omega_j+\omega_k+\omega_l\end{aligned} \tag{4.96}$$

are the resonance condition for the different quadratic terms. It can be noticed that with this approximation the contribution due to the terms $\widehat{\mathcal{L}}_{(3)intQ}$ are null as $\omega>0$. The other two quadratic terms give

$$\begin{aligned}&\langle\psi_0|\int_0^t \left[\left(\left[\widehat{\mathcal{L}}_{H_{(1)intQ}}, \widehat{\mathcal{M}}_{J_{\omega_i}}\right]\right)_I(t), \left(\widehat{\mathcal{L}}_{H_{(1)intQ}}\right)_I(t')\right]|\psi_0\rangle\ \mathrm{d}t' = \\ &= \sum_{\substack{\omega_j,\omega_k,\omega_l\in\mathcal{I}_{sys}\\ \omega_i+\omega_j-\omega_k-\omega_l=0}} \frac{16\pi\kappa^2_{(1)\omega_i\omega_j\omega_k\omega_l}}{\delta\omega_{sys}}\langle J_{\omega_l}\rangle\left(\langle J_{\omega_j}\rangle\langle J_{\omega_k}\rangle + \langle J_{\omega_i}\rangle\langle J_{\omega_k}\rangle - 2\langle J_{\omega_i}\rangle\langle J_{\omega_j}\rangle\right)\end{aligned} \tag{4.97}$$

and

$$\langle\psi_0|\int_0^t\left[\left(\left[\widehat{\mathcal{L}}_{H_{(2)intQ}},\widehat{\mathcal{M}}_{J_{\omega_i}}\right]\right)_I(t),\left(\widehat{\mathcal{L}}_{H_{(2)intQ}}\right)_I(t')\right]|\psi_0\rangle\ \mathrm{d}t' =$$
$$= \frac{3\pi}{\delta\omega_{sys}}\Bigg[\sum_{\substack{\omega_j\omega_k\omega_l\in\mathcal{I}_{sys}\\ \omega_i+\omega_j+\omega_k-\omega_l=0}} 3\kappa^2_{(2)\omega_i\omega_j\omega_k\omega_l}\langle J_{\omega_k}\rangle\Big(\langle J_{\omega_j}\rangle\langle J_{\omega_l}\rangle+2\langle J_{\omega_i}\rangle\langle J_{\omega_l}\rangle-\langle J_{\omega_i}\rangle\langle J_{\omega_j}\rangle\Big)+ \tag{4.98}$$
$$+\sum_{\substack{\omega_j\omega_k\omega_l\in\mathcal{I}_{sys}\\ \omega_i-\omega_j-\omega_k-\omega_l=0}}\kappa^2_{(2)\omega_i\omega_j\omega_k\omega_l}\langle J_{\omega_l}\rangle\langle J_{\omega_k}\rangle\Big(\langle J_{\omega_j}\rangle-3\langle J_{\omega_i}\rangle\Big)\Bigg].$$

Putting together all the contributions we have derived, a Fröhlich-like rate equations is obtained for expectation value of actions

$$\frac{\mathrm{d}\langle J_{\omega_i}\rangle}{\mathrm{d}t} = s_{\omega_i}+b_{\omega_i}\left[\frac{k_BT_B}{\omega_i}-\langle J_{\omega_i}\rangle\right]+\sum_{\substack{\omega_j\in\mathcal{I}_{sys}\\ \omega_j\neq\omega_i}}c_{\omega_i\omega_j}\left[\Big(\langle J_{\omega_j}\rangle-\langle J_{\omega_i}\rangle\Big)+\frac{\omega_j-\omega_i}{k_BT_B}\langle J_{\omega_i}\rangle\langle J_{\omega_j}\rangle\right]+$$
$$+\sum_{\substack{\omega_j,\omega_k,\omega_l\in\mathcal{I}_{sys}\\ \omega_i+\omega_j-\omega_k-\omega_l=0}}\frac{16\pi\kappa^2_{(1)\omega_i\omega_j\omega_k\omega_l}}{\delta\omega_{sys}}\langle J_{\omega_l}\rangle\Big(\langle J_{\omega_j}\rangle\langle J_{\omega_k}\rangle+\langle J_{\omega_i}\rangle\langle J_{\omega_k}\rangle-2\langle J_{\omega_i}\rangle\langle J_{\omega_j}\rangle\Big)$$
$$+\frac{3\pi}{\delta\omega_{sys}}\Bigg[\sum_{\substack{\omega_j\omega_k\omega_l\in\mathcal{I}_{sys}\\ \omega_i+\omega_j+\omega_k-\omega_l=0}}3\kappa^2_{(2)\omega_i\omega_j\omega_k\omega_l}\langle J_{\omega_k}\rangle\Big(\langle J_{\omega_j}\rangle\langle J_{\omega_l}\rangle+2\langle J_{\omega_i}\rangle\langle J_{\omega_l}\rangle-\langle J_{\omega_i}\rangle\langle J_{\omega_j}\rangle\Big)+$$
$$+\sum_{\substack{\omega_j\omega_k\omega_l\in\mathcal{I}_{sys}\\ \omega_i-\omega_j-\omega_k-\omega_l=0}}\kappa^2_{(2)\omega_i\omega_j\omega_k\omega_l}\langle J_{\omega_l}\rangle\langle J_{\omega_k}\rangle\Big(\langle J_{\omega_j}\rangle-3\langle J_{\omega_i}\rangle\Big)\Bigg]. \tag{4.99}$$

4.5 Discussion and properties of Fröhlich-like rate equations (4.99)

The set of rate (4.99) equations we have derived by solving Liouville equation associated to the Hamiltonian system (4.36) is quite close to the original set of Fröhlich equations (3.33). Moreover, neglecting the κ-terms, the eqs.(4.99) can be directly derived by eqs. (3.33) considering the limit $\omega_i\langle J_{\omega_i}\rangle \ll k_{\mathrm{Bol}}T_B$; this is related that in original Fröhlich set of rate equations the Planck distribution was assumed for normal modes of thermal bath and of energy source modes, while in the derivation we have proposed the Boltzmann distribution has been assumed. As in the original formulation of Fröhlich condensation theory, the main interest in writing rate equations is to find the stationary solutions. In order to make this study easier we provide a

nondimensionalization of eqs.(4.99): introducing the following set of variables

$$\tau = t\omega_0 \qquad \text{with} \qquad \omega_0 = \min_{\omega\in\mathcal{I}_{sys}} \omega \qquad y_{\omega_i} = \frac{\omega_i \langle J_{\omega_i}\rangle}{k_{\text{Bol}}T_B} \qquad \alpha_{\omega_i} = \frac{\omega_i}{\omega_0}$$
$$S_{\omega_i} = \alpha_{\omega_i}\frac{\tilde{s}_{\omega_i}}{k_{\text{Bol}}T_B} \qquad B_{\omega_i} = \frac{b_{\omega_i}}{\omega_0} \qquad C_{\omega_i\omega_j} = \frac{\tilde{c}_{\omega_i\omega_j}}{\omega_0} \qquad \Upsilon_{(1)\omega_i\omega_j\omega_k\omega_l} = \frac{16\pi\kappa_{(1)\omega_i\omega_j\omega_k\omega_l}(k_{\text{Bol}}T_B)^2}{\delta\omega_{sys}\omega_0^3}$$
$$\Upsilon_{(2)\omega_i\omega_j\omega_k\omega_l} = \frac{3\pi\kappa_{(2)\omega_i\omega_j\omega_k\omega_l}(k_{\text{Bol}}T_B)^2}{\delta\omega_{sys}\omega_0^3} \tag{4.100}$$

the eqs.(4.99) read

$$\begin{aligned}
\dot{y}_{\omega_i} = \frac{\mathrm{d}y_{\omega_i}}{\mathrm{d}\tau} &= S_{\omega_i} + B_{\omega_i}(1-y_{\omega_i}) + \sum_{\substack{\omega_j\in\mathcal{I}_{sys}\\ \omega_j\neq\omega_i}} C_{\omega_i\omega_j}\left[\left(\frac{\alpha_{\omega_i}}{\alpha_{\omega_j}}y_{\omega_j} - y_{\omega_i}\right) + \frac{(\alpha_{\omega_j}-\alpha_{\omega_i})}{\alpha_{\omega_j}}y_{\omega_i}y_{\omega_j}\right] + \\
&+ \sum_{\substack{\omega_j,\omega_k,\omega_l\in\mathcal{I}_{sys}\\ \omega_i+\omega_j-\omega_k-\omega_l=0}} \Upsilon_{(1)\omega_i\omega_j\omega_k\omega_l}\frac{y_{\omega_l}}{\alpha_{\omega_l}}\left(\frac{\alpha_{\omega_i}}{\alpha_{\omega_j}\alpha_{\omega_k}}y_{\omega_j}y_{\omega_k} + \frac{1}{\alpha_{\omega_k}}y_{\omega_i}y_{\omega_k} - 2\frac{1}{\alpha_{\omega_j}}y_{\omega_i}y_{\omega_j}\right) \\
&+ \Bigg[\sum_{\substack{\omega_j\omega_k\omega_l\in\mathcal{I}_{sys}\\ \omega_i+\omega_j+\omega_k-\omega_l=0}} 3\Upsilon_{(2)\omega_i\omega_j\omega_k\omega_l}\frac{y_{\omega_k}}{\alpha_{\omega_k}}\left(\frac{\alpha_{\omega_i}}{\alpha_{\omega_j}\alpha_{\omega_l}}y_{\omega_j}y_{\omega_l} + 2\frac{1}{\alpha_{\omega_l}}y_{\omega_i}y_{\omega_l} - \frac{1}{\alpha_{\omega_j}}y_{\omega_i}y_{\omega_j}\right) + \\
&+ \sum_{\substack{\omega_j\omega_k\omega_l\in\mathcal{I}_{sys}\\ \omega_i-\omega_j-\omega_k-\omega_l=0}} \Upsilon_{(2)\omega_i\omega_j\omega_k\omega_l}\frac{y_{\omega_k}y_{\omega_l}}{\alpha_{\omega_k}\alpha_{\omega_l}}\left(\frac{\alpha_{\omega_i}}{\alpha_{\omega_j}}y_{\omega_j} - 3y_{\omega_i}\right)\Bigg] \qquad \omega_i\in\mathcal{I}_{\omega_i}\,.
\end{aligned} \tag{4.101}$$

Some properties of eqs.(4.101) has to be noticed:

- if the system of normal modes thermalize at the temperature T_B, so that $\langle J_{\omega_i}\rangle = k_{\text{Bol}}T_B/\omega_i$, it follows that the variables $y_{\omega_i} = 1$;
- if we ignore the contribution due to the external source of energy, i.e. $S_{\omega_i} = 0$, we can easily observe that $y_{\omega_i} = 1$ is a stationary solution of the system, namely $\dot{y}_{\omega_i} = 0$. More strongly each sum give a null contribution; this is consistent with the physical interpretation that, if the system is not put in contact with the external source of energy the Boltzmann distribution is a stationary one for the system (thermodynamic equilibrium).

An analogous nondimensionalization procedure can be applied to eqs.(3.33) leading to

$$\begin{aligned}
\frac{\mathrm{d}y_{\omega_i}}{\mathrm{d}\tau} &= \tilde{S}_{\omega_i} + \tilde{B}_{\omega_i}\left(1 - \frac{y_{\omega_i}\exp\left[\rho\alpha_{\omega_i}\right]}{\rho\omega_i}\right) + \\
&+ \sum_{\substack{\omega_j\in\mathcal{I}_{sys}\\ \omega_j\neq\omega_i}} \tilde{C}_{\omega_i\omega_j}\left[\left(\frac{\alpha_{\omega_i}}{\alpha_j}\exp\left[\rho\left(\alpha_{\omega_j}-\alpha_{\omega_j}\right)\right]y_{\omega_j} - y_{\omega_i}\right) + y_{\omega_i}y_{\omega_j}\frac{\exp\left[\rho\left(\alpha_{\omega_j}-\alpha_{\omega_i}\right)\right]}{\rho\alpha_{\omega_j}}\right]
\end{aligned} \tag{4.102}$$

with $i = 1, ..., N_{sys}$ and, with reference to eqs.(3.33)

$$\rho = \frac{\hbar\omega_0}{k_{\text{Bol}}T_B} \qquad \tilde{S}_{\omega_i} = \frac{s_{\omega_i}}{\omega_0}\rho\alpha_{\omega_i} \qquad \tilde{B}_{\omega_i} = -\frac{\phi_{\omega_i}\rho\alpha_{\omega_i}}{\omega_0} \qquad \tilde{C}_{\omega_i\omega_j} = -\frac{\chi_{\omega_i\omega_j}}{\omega_0}\,. \tag{4.103}$$

We notice that $\rho \approx 1.3 \times 10^{-2}$ at typical temperature in biological systems $T_B \approx 310K$ and values of omega in the range of biomolecules vibrational modes, i.e. $\omega_0 \approx 0.5$THz. It follows that if the $\alpha_{\omega_i} \lesssim 10$ the exponentials in (4.102) can be approximated at the first order, i.e.$\exp(\rho x) \approx 1 + \rho x + o(\rho x)$. This naturally leads to eqs.(4.101).
In order to study Fröhlich condensation numerical integration of (4.101) for two systems of harmonic oscillators (representing vibrational normal modes of a biomolecule, i.e.) whose frequencies (in arbitrary units) are given by $\omega_n = 1 + n\delta\omega_{sys}$ where for the first set $n_1 = 0, 1, ..., 10$ and $\delta\omega_{sys1} = 1$ and for the second set $n_2 = 0, 1, ..., 20$ and $\delta\omega_{sys2} = 0.5$.
One of the main problem of this model (as in the case of quantum Wu-Austin one) is the extreme difficulty in providing an *a priori* estimation of the coupling constant for a real biosystem: the nondimensionalization of the equation partially solve the problem as only the ratios among the coefficients has to be known. As we are interested in a qualitative study of the behaviour of the system in order to asses that Fröhlich condensation is possible also in the classical mechanics framework, the coupling constants appearing in eqs.(4.101) are supposed to not be dependent by frequencies for sake of simplicity. In particular the condition $S_{\omega_i} = S$ can be physically interpreted as an energy injection rate which is independent by the frequency of the normal mode.
The Fröhlich condensation(-like) phenomena can be regarded as a **out-of-thermal-equilibrium phase transition**: slightly varying the energy injection rate (the *control parameter*) around a certain critical value the system attains a major changes in the energy distribution among normal modes resulting in a more "organized" phase (the energy is stocked mainly in the lowest frequency mode) . In order to characterize such major change in energy distribution among normal modes of the system, the equivalent of an *order parameter* for a finite set of normal modes is introduced:

$$\epsilon_{(cl),\omega_i}(t) = \frac{y_{\omega_i}(t)}{\sum\limits_{\omega_i \in \mathcal{I}_{sys}} y_{\omega_i}(t)} - \frac{1}{N_{sys}}\,. \tag{4.104}$$

As y_{ω_i} is the energy in the mode at frequency ω_i in $k_{\text{Bol}}T_B$ units, when the system is at thermal equilibrium it follows that $\epsilon_{\omega_i} = 0$; when the energy condensate in a mode $\epsilon_{\omega_i} > 0$. The range of each parameter ϵ_{ω_i} is $[-1/N_{sys}; 1 - 1/N_{sys}]$; the lower bound corresponds to a system at $T_{\omega_i} = 0$ *effective temperature* while the upper bound corresponds to the condition where all the energy is in the ω_i normal mode. In general the parameters $\epsilon_{\omega_i}(t)$ is a time dependent function; nevertheless, we are interested in stationary stationary solutions (namely such that $\dot{y}_{\omega_i} = 0$) that can eventually be attained if initial conditions are fixed such that $y_{\omega_i}(0) = 1$, so supposing that at the initial time the systems is at in equilibrium with the heat bath. In order to compare the qualitative behaviour of stationary solution of the classical and quantum derived rate equations, also the (4.102) has been numerically integrated for the set of frequencies $\mathcal{I}_{sys1}$ and with initial conditions $y_{\omega_i} = \rho\alpha_i/(\exp[\rho\alpha_{\omega_i}] - 1)$ coherently with the supposed Planck distribution at thermodynamic equilibrium. For the same reason a slightly different order

parameter is introduced in this case

$$\epsilon_{(qt),\omega_i}(t) = \frac{y_{\omega_i}(t)}{\sum\limits_{\omega_i \in \mathcal{I}_{sys}} y_{\omega_i}(t)} - \frac{\rho\alpha_{\omega_i}}{(\exp[\rho\alpha_{\omega_i}] - 1) \sum\limits_{\omega_j \in \mathcal{I}_{sys}} \frac{\alpha_{\omega_j}\rho}{\exp(\rho\alpha_{\omega_j})-1}} . \tag{4.105}$$

4.5.1 Results of numerical simulation

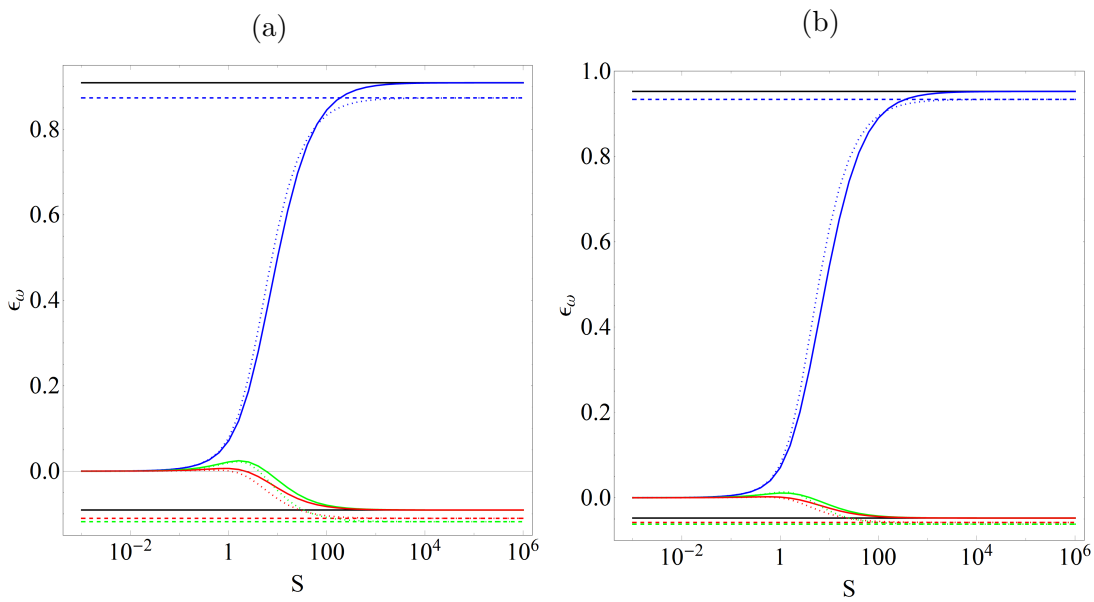

Figure 4.1: Comparison of numerical solution of Fröhlich rate equation in classical and quantum case. The ϵ_{ω_i} order parameter for both quantum (pointed lines)and classical (solid lines) case is reported vs. the injection energy rate $S_{\omega_i} = \tilde{S}_{\omega_i}$, for the three lowest frequencies of the system $\mathcal{I}_{sys1}$ (a) $\mathcal{I}_{sys2}$ (b) and , i.e. $\omega = 1$ (blue), $\omega_2 = 2$ (green), $\omega = 3$ (red). The other parameters of the system were set $B_{\omega_i} = \tilde{B}_{\omega_i} = 1$, $C_{\omega_i\omega_j} = \tilde{C}_{\omega_i\omega_j} = 0.1$ and $\Upsilon_{(1)} = \Upsilon(2) = 0$ (no quadratic contribution). The black solid lines correspond to the lower and upper bound of the order parameter in classical case, while dashed lines corresponds to the quantum upper bound of order parameter for $\omega = 1$ and to the quantum lower bound for $\omega = 2$ and $\omega = 3$.

In Fig.4.1 the results of numerical integration of the quantum rate equations (4.102) and of the classical rate equation(4.101) are reported for the set $\mathcal{I}_{sys1}$ and $\mathcal{I}_{sys2}$ with the initial conditions specified in the previous section. The other parameters in equations (4.102) and (4.101) were set $B_{\omega_i} = \tilde{B}_{\omega_i} = 1$, $C_{\omega_i\omega_j} = \tilde{C}_{\omega_i\omega_j} = 0.1$ and no quadratic interaction were considered in classical rate equations (namely $\Upsilon_{(1)} = \Upsilon(2) = 0$). This choice is justified by the fact that the results really depends by the ratios of coupling constants (i.e. S/B and C/B); the coefficient B has been chosen as reference parameteras it is directly related with characteristic thermalization time scale $\tau_{\text{therm}} \approx B^{-1}$. The choice $C/B = 0.1$ is coherent respect to what can be found in literature [PW13] for qualitative studies on Fröhlich condensation. The integration has been performed in each case for a time interval $\tau_{\text{Itg}} > 0$ sufficiently long such in order to guarantee that $|\epsilon_{\omega_i}(\tau) - \epsilon_{\omega_i}(\tau_{\text{stat}})| < 10^{-5}$ for $\tau_{\text{stat}}, t \in [0, t_{\text{Itg}}]$.

The results shows a qualitative and quantitative accord between classical and quantum case, as expected by the fact that the classical set of rate equations can be obtained by the quantum

one in the "hight temperature limit" as argued in previous section.
In particular, it can be observed that three qualitative different stationary state regimes are attained depending by the value of S (energy injection rate in adimensionalized units):

- *an equipartition regime* (example in blue in Fig.4.2) for $S \lesssim 0.5 \times 10^{-1}$ where the injected energy and not linear interactions among bath and normal modes are not sufficient to brake the equipartition energy, all the oscillator attain the thermodynamic equilibrium at a temperature $T_{\text{stat}} > T_B$;
- *a partial condensation regime* (example in green and purple in Fig.4.2) for $0.5 \times 10^{-1} \gtrsim S \gtrsim 100$ where the energy is not equally distribute among normal modes, and the lower normal modes has much more energy than the others;
- *a saturated condensation regime* (example in red in Fig.4.2) for $S \gtrsim 100$ the vibrational energy is condensed entirely in the lower normal modes and there is no energy in the higher normal modes.

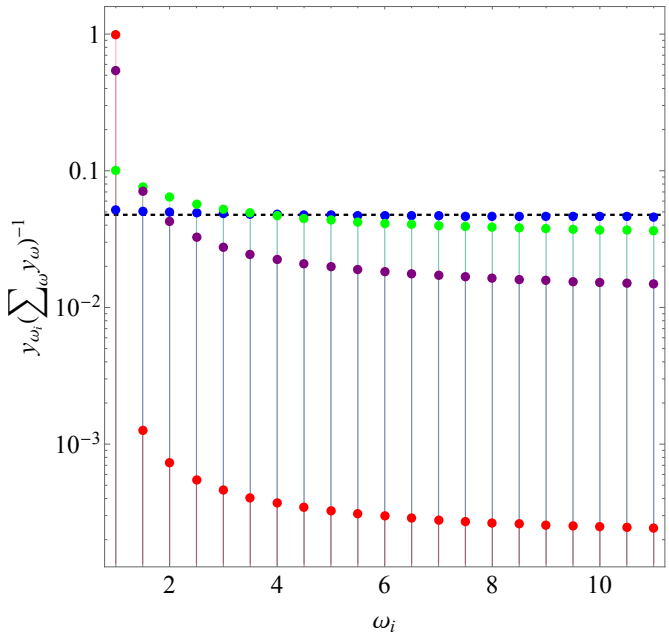

Figure 4.2: Fraction of energy in vibrational modes vs. frequencies of normal modes of the system $\mathcal{I}_{sys2}$. The coupling consant have been fixed $B = 1$, $C = 0.1$, $\tilde{\Upsilon}_{(1)} = 10^{-3}$ (this is sufficient to guarantee a finite bound from below for the classical Hamiltonian), $\tilde{\Upsilon}_{(2)} = 0$ and $S = 0.1$ (blue dots), $S = 1$ (green dots), $S = 10$ (purple dots), $S = 100$ (red dots). The equipartition state correspondsto dark dashe line. It has to be noticed the great difference among the energy fraction in lower normal mode is approximatlivy three order of magnitude higher in satured condensed phase.

This results (see Fig.4.3) have been tested for different values of C. It has observed that the Fröhlich-like condensation features are qualitatively stable and for lower values of C ($C = 0.01$ and $C = 0.001$) both in classical and quantum case. Moreover it can be conjectured that the

values of the threshold in energy injection rate to induce the condensation is inversely proportional to C. For the higher values of $C = 1$ the results does not seems to be also *quantitatively* different from what found for $C = 0.1$; this would suggest a saturation threshold for C. Nevertheless in this latter case the perturbative approach used to derive Fröhlich rate equations seems to be almost questionable.

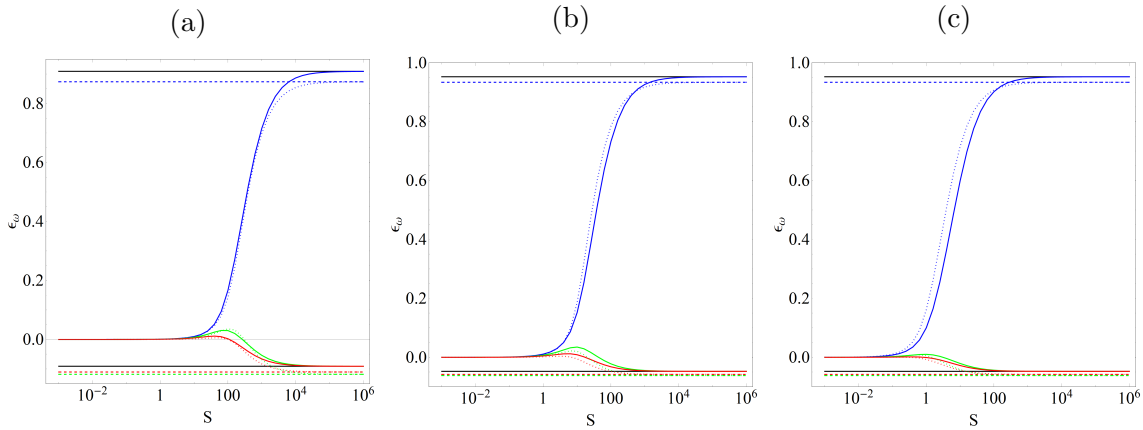

Figure 4.3: Comparison of numerical solution of Fröhlich rate equation in classical and quantum case. The ϵ_{ω_i} order parameter for both quantum (pointed lines)and classical (solid lines) case is reported vs. the injection energy rate $S_{\omega_i} = \tilde{S}_{\omega_i}$, for the three lowest frequencies of the system $\mathcal{I}_{sys2}$ with $C = 0.001$ (a),$C = 0.01$ (b) and $C = 1$(c). The frequencies are $\omega = 1$ (blue), $\omega_2 = 2$ (green), $\omega = 3$ (red). The other parameters of the system were set $B_{\omega_i} = \tilde{B}_{\omega_i} = 1$ and $\Upsilon_{(1)} = \Upsilon(2) = 0$ (no quadratic contribution). The black solid lines correspond to the lower and upper bound of the order parameter in classical case, while dashed lines corresponds to the quantum upper bound of order parameter for $\omega = 1$ and to the quantum lower bound for $\omega = 2$ and $\omega = 3$.

Fröhlich-like condensation phenomena observed by our numerical studies both in quantum and classical case shares some features with other transitional phenomena: the system undertakes a transition between a "more symmetric phase" (where the energy is equally distributed) and "less symmetric phase" (where the whole energy is condensed in first normal mode) when a certain critical point of the control parameter (the energy injection rate into the system) is traversed.

The effect of quartic direct interactions among normal modes on the order parameters ϵ_{ω_i} as functions of the energy injection rate S has been investigated in classical framework for the two frequency sets $\mathcal{I}_{sys1}$ and $\mathcal{I}_{sys2}$. Some different test have been done for $C = 0.1$ and and different values of $\Upsilon_{(1)}$ and $\Upsilon_{(2)}$.

To compare the results for the two systems $\mathcal{I}_{sys1}$ and $\mathcal{I}_{sys2}$, coefficients of terms derived by quadratic interactions have been chosen such that $\Upsilon_{(1)}\delta\omega_{sys} = \tilde{\Upsilon}_{(1)}$ and $\Upsilon_{(2)}\delta\omega_{sys} = \tilde{\Upsilon}_{(2)}$ where $\tilde{\Upsilon}_{(1)}$ and $\tilde{\Upsilon}_{(2)}$ are supposed to be constant.

The presence of terms in rate equations proportional to $\Upsilon_{(1)}$ has been verified to not affect in qualitative of quantitative way the Fröhlich condensation in classical systems for both the normal modes considered sets: the results are not reported in this case.

To the contrary the presence of the quartic term proportional to $\Upsilon_{(2)}$ seems to strongly affect the qualitative behaviour of the system for different values of S with a suppression of Fröhlich condensation. The effect is stronger for the system with more "dense" normal modes as showed in Fig.4.4, where the energy distribution is showed for $C = 0.1$, $\tilde{\Upsilon}_{(1)} = 10^{-3}$ and different values of $\tilde{\Upsilon}_2$. This suggest that quartic interactions responsible $\Upsilon_{(2)}$-term in Fröhlich rate equations allow the transfer of energy from lower frequency modes to higher frequency modes. This is consistent with the idea that a quartic oscillator exert a "confining" action: if too much energy tends to be condensed in lowest frequency normal mode, the quartic interactions limit the amplitude of its oscillations promoting the transfer of energy towards higher frequency normal modes. The analysis of the energy distribution among normal modes of the system $sys2$ shows clearly how the terms proportional to $\Upsilon_{(2)}$ populates higher frequency normal modes: especially $\omega = 3$ as the quadratic term proportional to $\kappa_{(2)}$ promotes the exchanges among this normal mode and the lowest frequency one.

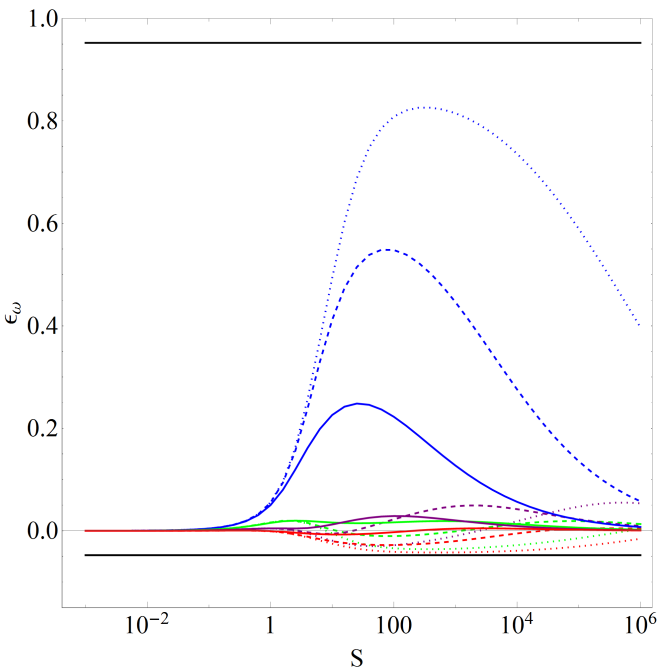

Figure 4.4: Order parameter ϵ_{ω_i} vs. adimensionalized injection rate S for frequencies $\omega = 1$(blue), $\omega = 2$(green), $\omega = 3$ (red), $\omega = 4$ (purple) of $\mathcal{I}_{sys2}$. The coupling consant have been fixed $B = 1$, $C = 0.1$, $\tilde{\Upsilon}_{(1)} = 10^{-3}$ (this is sufficient to guarantee a finite bound from below for the classical Hamiltonian), $\tilde{\Upsilon}_{(2)} = 10^{-6}$ (dotted line), $\tilde{\Upsilon}_{(2)} = 10^{-5}$ (dashed line) and $\tilde{\Upsilon}_{(2)} = 10^{-4}$ (solid line).

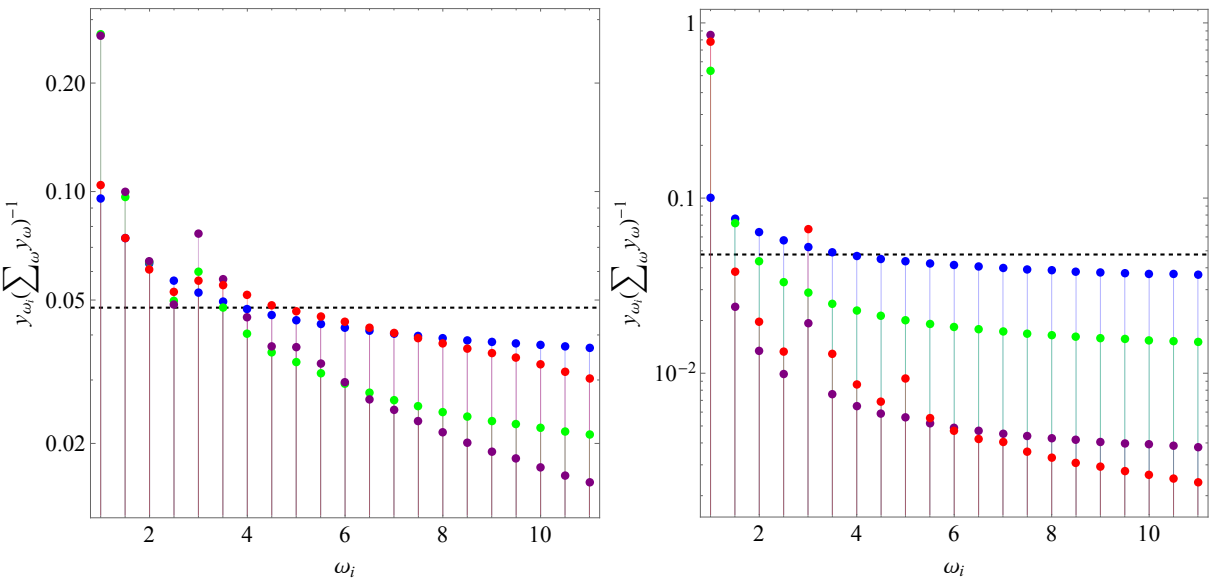

Figure 4.5: Fraction of energy in vibrational modes vs. frequencies of normal modes of the system $\mathcal{I}_{sys2}$. The coupling consant have been fixed $B = 1$, $C = 0.1$, $\tilde{\Upsilon}_{(1)} = 10^{-3}$ (this is sufficient to guarantee a finite bound from below for the classical Hamiltonian), $\tilde{\Upsilon}_{(2)} = 10^{-4}$ (a) and $\tilde{\Upsilon}_{(2)} = 10^{-6}$ (b) with $S = 1$ (blue dots), $S = 10$ (green dots), $S = 10^2$ (purple dots) and $S = 10^4$ (red dots). The equipartition state corresponds to dark dashe line. It can be noticed how at high values of S higher frequencies (especially $\omega = 3$ are excited).

4.6 Comments and conclusions

Fröhlich rate equations describe the dynamics of a system of harmonic oscillators in contact with an heat bath and an external source of energy. They have been heuristically derived and admit stationary solution where the energy is condensed in the lowest frequency mode when a certain supplied energy rate is over a certain threshold. This out-of-equilibrium transitional phenomenon represent a general paradigm for organization in biological systems and it could be responsible for long-range electrodynamic interactions among biomolecules in living matter. As such equations are very general and heuristically derived, they has been considered more as a metaphor than a model that can be adapted to describe realistic cases. This justifies the research of a microscopic model from which Fröhlich equations can be derived. Wu and Austin proposed a quantum Hamiltonian model that success in provide a microscopic underlying Fröhlich equations. Despite of this success this leaded to the idea that Fröhlich condensation is a phenomenon due to quantum effects and regarded as the equivalent of Bose condensation for out-of-equilibrium systems. Moreover, original Wu and Austin model have been strongly criticized as it was proved that their quantum Hamiltonian has not a finite energy ground state. The work presented in this chapter aimed to verify if Fröhlich condensation can take place also in classical systems and if it affected by the presence of interactions that can correct the absence of a finite lower bound for the Hamiltonian (so the total energy).

A classical Hamiltonian system is derived from Wu and Austin quantum Hamiltonian ("corrected" with added quartic interactions among normal modes of the main system to correct the lower bound behaviour) applying a "dequantization" technique (based on a semi-classical

approach): the Time Dependent Variational Principle (TDVP).
Fröhlich-like rate equations are derived from Liouville equation associated to classical Hamiltonian systems using the Koopman-Von Neumann formalism that allows to formulate classical mechanics in Hilbert space. This has the advantage that the derivation is *formally* very similar to the known one for quantum systems. The main difference relies to the fact that in classical case the equilibrium distribution for the heat bath is supposed to be the Boltzmann one while in quantum case is the Bose-Einstein one (with zero chemical potential).
The stationary solution where numerically derived by time integration of rate equations for initially conditions such that the system is at the thermodynamic equilibrium with the heat bath.
Results of numerical simulation allow to conclude that *Fröhlich-like condensation phenomena are possible also in classical systems derived by Wu and Austin quantum Hamiltonian through a "dequantization" procedure. In both the case, some features of phase transitions are found for this class of system as the existence of two different phases and a presence of a threshold in control parameter (the external energy injection rate).* The introduction of terms in rate equations derived from quartic direct interactions among normal modes *can affect the condensation of the energy* in the lowest frequency normal modes rate equation *weakening the phenomenon for very high values of injected energy.*
On one side this work opens the way for further research on Fröhlich-like condensation in classical mechanics framework especially for what concerns the analytical discussion of stationary solution. In particular it would be interesting to deepened the investigation of the analytical dependence of the order parameters ϵ_{ω_i} in the stationary state by the parameters in rate equations. On the other side Koopman-Von Neumann formalism has turned out to be a suitable mathematical tool to investigate the properties of out of thermal equilibrium systems. Rate equations for higher moment of J_{ω_i} variables (or equivalently for y_{ω_i}) can give more information on the form of stationary energy distribution for out-of-thermal equilibrium systems.
Finally it has to be stressed that it is already unsolved the major issue to derive or almost provide and *a priori* estimation of the coefficients in equation of (4.99) for a real protein in cellular environment. Such aim it seems very difficult to be attained due to the extreme complexity of the system constituted by protein, hydratation water and bulk water and molecular and atomic level. In particular the interactions among protein and surrounding environment (especial water molecules) is main object of current researches right now. Nevertheless, the work here presented is a little step in the direction to make the "Fröhlich condensation metaphor" a realistic model for biomolecules in living matter.

CHAPTER 5 Terahertz spectroscopy experiments for the observation of collective oscillations in biomolecules out-of-thermodynamic equilbrium

In this chapter the theoretical interpretation of experimental outcomes of THz spectroscopy experiment is discussed. Such experiments have been performed to research an evidence of *Fröhlich condensation* of vibrational energy in biomolecules in aqueous solution when they are put out-of-thermal-equilibrium. The theoretical interpretation of these very recent experimental results is here presented[1].

5.1 Terahertz spectroscopy on biomolecules: motivations and methods

Motivations of the experiments

In the previous chapter it has been argued that Fröhlich-like condensation phenomena can take place in classical system out-of-thermodynamic equilibrium and, consequently, also in quite "heavy" macromolecules (in the sense specified at the very beginning of the previous chapter) even in "wet and warm" biological environments.
Necessary conditions to obtain a stationary condensed state are the presence of non linear interactions among heath bath and normal vibrational modes of the considered system and that a sufficiently hight energy injection rate is provided.
Hence it seems natural to investigate if Fröhlich-like condensation is really exploited by biomolecules in living matter; as observed in chapter 3 the presence of collective oscillations in biomolecules would result in giant oscillations of electric dipole and, consequently, in the possibility to activate long-range electrodynamic resonant (selective) interactions.
A direct observation of collective oscillations in biomolecules in physiological conditions constitutes a real experimental challenge for many reasons. Terahertz domain spectroscopy requires to overcome technical difficulties; it represents a critical frequency range for electronic devices and the realization of sufficiently precise THz sources and detectors has been possible only in the last decade. Moreover other serious difficulties derived by the necessity of studying biomolecules in water solutions (being these very opaque media for Terahertz radiation) and in an out-of-equilibrium stationary state sustained by some external energy injection. It is in fact very well known that the absorption properties of water in THz domain is strongly affected by the presence of structured ensembles of water molecules [PSY+15]. Such properties

[1] Although the work of the author of this manuscript mainly concerns the theoretical interpretation of the experimental outcomes, he also directly participated to some experimental session giving his own advices on set-up definition and optimization.

have been very recently use [SDD15] to determine the thickness of hydratation water shall around protein. Experimental evidence of the existence of collective modes of vibration of proteins and of fragments of nucleic acids has been provided *at thermal equilibrium* by means of Raman and far-infrared (FIR) spectroscopy [Kei95]. Important results have been recently obtained in the characterization of collective vibrational motion at the *thermodynamic equilibrium* of biomolecules; such vibration and could be strongly affect their functional role *in vivo* systems[KCM06, CKY+07, KCHM07, HCK+11].
Despite of this it has been recently shown [PPT15] that at thermal equilibrium the energy exchange of a biomolecule with its environment through random thermal noise cannot activate long-range electrodynamic forces.
Evidence of deviation from the expected behaviour in relaxation to thermal equilibrium in *crystallized protein* has been found through X-ray crystallographic experiments on protein excited by THz-pulsed radiation [LRW+15].
Moreover, no experimental evidence was hitherto available of the possibility of exciting out-of-equilibrium collective oscillations of a biomolecule, that is, to generate the basic condition to activate intermolecular electrodynamic interactions in physiological conditions.
Very recent and innovative techniques in Terahertz spectroscopy developed by the team of Prof.Varani at the IES (Electronique institute) of Montpellier and by the team of prof.Ortolani at the University "La Sapienza"(Rome) allowed to perform for the first time Terahertz spectroscopy on out-of thermal equilibrium biomolecules in water solutions.

5.1.1 Set-up of the experiments

The experimental set-up is composed by three main parts that we shall discuss in detail:

- the test biomolecule used in the experiment (BSA) and the water solution properties;
- the mechanism of energy injection in collective vibrational mode of biomolecules, a necessary condition for the Fröhlich-like condensation;
- the Terahertz detection device used in the two experiments (Rome and Montpellier) based on "near-field" antennas[2]: a microwire-based THz spectroscopy in Montpellier and a rectenna-based THz spectroscopy in Rome.

Characteristic of the test biomolecule (BSA) and water solution

The possibility to activate collective oscillations in biomolecules has been experimentally investigated for an aqueous solution of Bovine Serum Albumine at the concentration of 1mg/ml. These conditions has been set in order to study the mechanical and dielectric properties of biomolecules in conditions more similar as possible to physiological ones. The salt (NaCl) has been added to the solution to screen electrostatic interactions. BSA (Bovine Serum Albumine)

[2]With "near-field" antennas we mean devices able to read the intensity of the electric field in a region very near (some micrometers) to the surface of the detection part of the antenna (a nano-wire in Montpellier device and a the gain of a nano-transistor in Rome device).

has been chosen as test protein: such biomolecule is mainly made out of α-helices (see Fig.5.1) and is a "model" since it is largely studied in the physico-chemical literature.

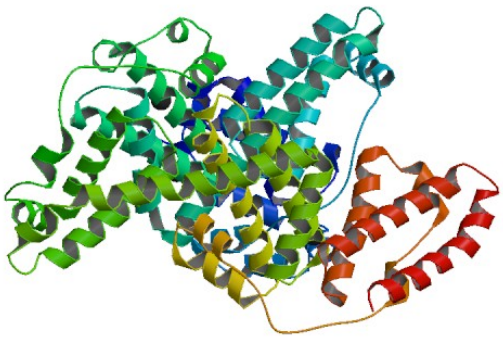

Figure 5.1: Crystal structure BSA

Mechanical properties of α-helices have been largely studied in the last thirty years as they could play a central role in energy trapping mechanisms in biomolecules. α-helices can be represented as a system of three one-dimensional chains of springs coupled among them (see 5.2): each chain is composed by two types of harmonic oscillators, alternated and representing hydrogen bonds and the backbone C=O group [Sco92].
Fröhlich-Holstein Hamiltonian is generally adopted to describe the dynamics of the harmonic oscillators into a single chain and their mutual couplings, it has been proved that the system admits stationary solitonic-like solutions (so without dispersion and dissipation). This means that the system energy can eventully store the injected energy in solitonic waves (the so called Davydov's soliton[Dav73, Dav77][Sco92][CHT97]) or in elliptic waves [TNC$^+$95][Sim09].
A fascinating hypothesisn propoesed by Del Giudice et al. in [DGDMV85] in the framework of Quantum Field Theory suggests an interplay among the excitation of Davydov's solitons in a biomolecule and the possibility to activate Fröhlich condensation both regarded as related to the creation of Goldstone's bosons in spontaneous-symmetry braking mechanism (SO(1) in the case of Davydov's soliton SO(3) for the Fröhlich condensation).
In particular the solitonic waves (or the elliptic ones) generated along an α-helix could be associated with local coherent polarization waves that can in principle contribute to align water dipolar molecules surrounding the chain: this would generate the spontaneous symmetry breaking in the orientation of water dipole and an enhancement of the total dipolar momentum of the whole system of biomolecule and surrounding water molecules.

Finally, many different estimation, based on theoretical models and experimental evidence [Cho83][Cho84], suggested that long α-helices have low-frequency accordion-like vibrational modes with $\nu \approx 0.65 \div 0.7$ THz, a range compatible with the possibility to activate long-range

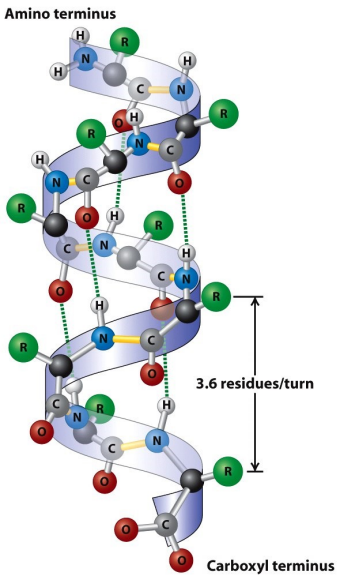

Figure 5.2: Molecular structure of α-helix. Hydrogen bonds are represented by dashed green lines. Figure adapted by [Lod08].

(not screened) electrodynamic interactions (as discussed in chapter 3).

Energy injection in vibrational normal modes

A key aspect of the experiments here discussed is the necessity to provide an energy injection rate that can exceed the threshold necessary to induce Fröhlich condensation (also in classical systems as observed in chapter 4).
An out-of-equilibrium state in BSA molecules is induced by means of optical pumping as follows. Each protein molecule is marked with a few Alexa488 fluorochrome molecules (covalently bonded at the lysine residues) excited by means of an Argon laser (wavelength 488 nm) and emits fluorescence around the wavelength 519 nm: it follows that about 0.15 eV per fluorochrome and per incident photon is available for an energy transfer to the protein and, partly, also to its environment. When the Argon laser operates at 500 μW the number of emitted photons per second is 1.2×10^{15}. The cross section of the fluorochrome Alexa488 is 3.2×10^{-16} cm^2, so that using 4×10^{-2} cm^2 for the laser beam section we find that each Alexa488 molecule receives about 10 photons per second. Each protein molecule has an average number of 5/6 fluorochromes attached to it so that, considering that some of them could be partly shadowed by the protein itself, we can assume that the average number of photons received by each protein per second belongs to the interval $25 \div 60$. Hence the upper bound for the energy rate injection W is estimated between 7.9×10^{-12} erg s^{-1} and 1.9×10^{-11} erg s^{-1}.

THz generators and detection devices

A typical experiment consists in measuring the dependence of the electromagnetic power detected by the near-field probes on the frequency of the THz radiation. All the measurements

have been performed at room temperature. Two THz-near-field absorption spectroscopy set-up of watery solutions of the protein operates into two distinct laboratories(Fig.5.3(a),(c)).

- The first set-up, developed in Montpellier, (Fig. 5.3 (a),(b)) used a micro-coaxial near-field probe put inside a metallic rectangular waveguide enabling a modal transition from TM01 Sommerfeld's to TE01 waveguide mode. The sub-wavelength diameter of the wire (12 μm) allows an extremely localized detection of the longitudinal component of the electric field at its end and on a volume of about 4 pl. A constitutive element of the experimental set-up is a tunable and continuous-wave primary source emitting in the $0.22 - 0.33 \approx$ THz frequency range with an average power of $1 \approx$ mW. The high spectral resolution (< 300 Hz) of the continuous-wave source allows an accurate detection of resonances.

  The emitted radiation beam is focused on the samples of protein solutions on which, at option, a 488 nm light beam – produced by an Argon laser – can also be focused. The blue light provides the proteins with the necessary energy to activate a collective vibrational state. The latter being an out-of-equilibrium state because it is kept by a non-thermal energy supply.

  A drop of the protein solution sample is placed under the near-field probe which is directly immersed inside the solution. A typical experiment consists in measuring the near-field electric field intensity through a reference medium (water) and the protein solution sample. A sweep through the frequency domain accessible to the THz source is performed alternatively when the blue light is switched-on and off to yield a difference spectrum showing the absorption features that are attributed to collective vibrations of each protein molecule.

  To optimize the coupling efficiency a particular attention must be paid to the position of the wire inside the guide, to the angular position of the bent portion of the wire and to the total length and diameter of the wire. The spectra were normalized to the spectrum of pure water in order to remove artefacts coming either from the water absorption or from the geometry of the experimental set-up.

- The second set-up, developed in Rome, (Fig. 5.3 (c),(d)) used a near-field probe rectenna composed of a planar metal bow-tie antenna with dimensions close to half-a-wavelength (at 0.3 THz) that enhanced the THz field in the feed gap region (volume of about 0.2 pl) and a plasma-wave field-effect transistor (FET) integrated in the feed gap of the antenna, that provides a DC-voltage – between Source and Drain contacts – proportional to the THz-field intensity[DS93, KKD+02, NMT+09]. An hemispherical silicon lens pressed on the back of the semiconductor substrate focused the THz radiation on the antenna simultaneously avoiding substrate interferences. After acquiring the empty-channel response spectrum of the device, a drop of protein solution was cast on the top (air) side of the device with a micropipette (a volume of 1 microliter was drop-casted). The drop extends over the entire antenna, but the radiation comes from below (i.e. from inside the substrate) and it is not attenuated by the whole drop. This set-up allows to minimize the optical depth of water, as the probe domain was reduced to a volume of 10×10 microns

in horizontal plane and to about 2 microns in vertical axis. Therefore, the number of molecules probed in this set-up is that present in a $10 \times 10 \times 2$ micron volume, 10^{-6} times less than the number of molecules present in a 1 mm^3 diffraction limited focus.

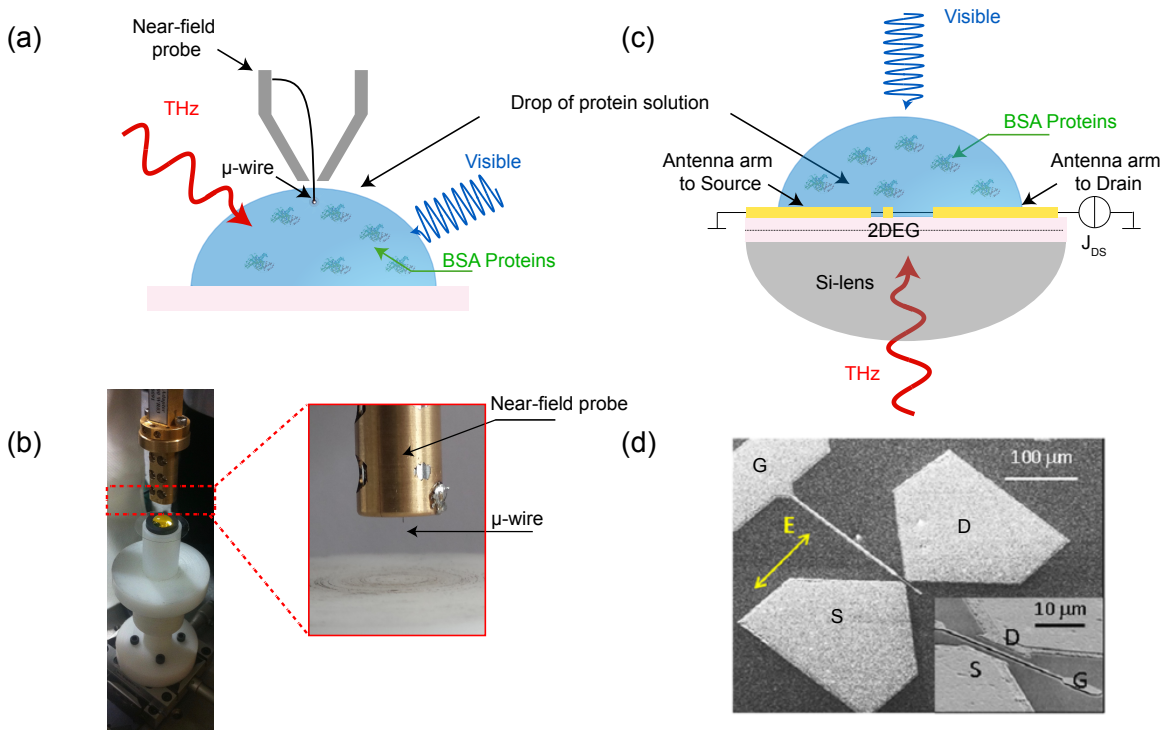

Figure 5.3: Experimental set-ups of THz absorption near-field spectroscopy. (a) A drop of the biological sample is placed under the near-field probe which is directly immersed inside the solution. (b) Picture of the near-field probe and its μ-wire. (c) A drop of the biological sample is placed above the near-field rectenna. (d) Electron-beam microscopy picture of the bow-tie antenna with its integrated FET.

It is really important to point out that these two very different set-ups give the same informations on absorption properties in THz domain of the watery solutions containing biomolecules; this allows a direct qualitative comparison between the experimental outcomes.
It has to be remarked that it is a major challenge to provide a theoretical model that describes quantitatively all the effects that characterize the response of the biomolecules in water solution to the THz radiation.

Moreover the complexity of the experimental set-up makes really hard to control some aspects as the exact volume and form of the drop used in each measure session[3].
Nevertheless Fröhlich-like condensation is a phenomenon that would be active only when energy is injected into protein, as pointed out before: this means that it would be possible to find a

[3]In order to give an idea of the difficulty in mounting a measure session, in Rome set-up, the drop of solution has to be put *by hand* into the gap of the microscopic transistor coupled with the planar antenna: the operator used a microscope to guide the tip of the pipette. A slight error in the positioning of the drop would irreversibly ruin the antenna. In Montpellier the nanowire antenna has to be directly put in the drop whose radius is less than a 1 mm

fingerprint of the phenomenon considering for each sample only the *difference spectra* of the received signal between laser on and laser off measures. Spectroscopic measures have been performed on solution with marked and non marked molecules and, in both the cases, with and without laser illumination.
The spectra of the protein solution without illumination was subtracted to the spectra with illumination (this correspond to consider the logarithm of absolute antenna response intensity ratio).
The hypothesis of activation of Fröhlich condensation-like phenomenon is not falsified only if a significant difference spectra when the laser is turned on is observed only with marked protein solution.

5.1.2 Experimental outcomes

All the reported measures refers to the case of fluorochrome-marked protein as the other considered cases (solution of pure water, pure water with salt, pure water salt and fluorochrome, pure water salt and not marked fluorochrome) exhibited almost null spectra between the cases where of laser illumination was turned on and off.
Figure 5.4 (a) presents the spectra obtained using the mic ro-coaxial probe in the absence of illumination (black circles) and in the presence of visible illuminations of different durations (from 3 to 9 min). In the former case (no illumination), there was no specific spectral feature in the studied frequency range while in the latter case (with illumination) we observed spectral resonances which become more evident for increasing duration of illumination. In particular, the strongest resonance appeared at 0.314 THz accompanied by three other minor resonances situated at 0.278, 0.285 and 0.322 THz; these values did not depend on the time of illumination and the strength of the resonances saturated after 9 min of illumination. Figure 5.4 (b) presents the spectra obtained using the rectenna probe for two durations of illumination. Also in this case we observed the appearance of evident resonances whose strength saturated at increasing durations of illumination. The spectra obtained using the two previously described methods and for the longer durations of illumination are shown in Figure 5.4 (c). The principal resonance at 0.314 THz is perfectly reproduced using two completely different and complementary set-ups.

Since THz extinction in water is huge (2000 dB/cm), the emergence of this spectral feature of the protein out of the water absorption background must be associated with the activation of a giant dipole moment. And this can happen only as a consequence of the activation of a coherent oscillation of the whole molecule. Moreover it appears only for marked protein; counterchecks performed on non marked protein and solution with the only fluorochrome Alexa488 does not manifest any significant change in absorption features when the laser illumination is turned on.

In Figure 5.7 the raw outcomes of the Rectenna-based absorption spectra obtained in Rome are reported. The spectra of the THz source without solution, of the THZ source with watery solution with and without LED blue illumination are reported, respectively. Whence the final result given in Figure 5.4 (b) is obtained as a difference spectrum. In Figure 5.4 (c) a comparison in given between the results of the two experiments. The agreement is strikingly good for what concerns the feature at 314 THz. The relevance of such excellent agreement relies on the facts

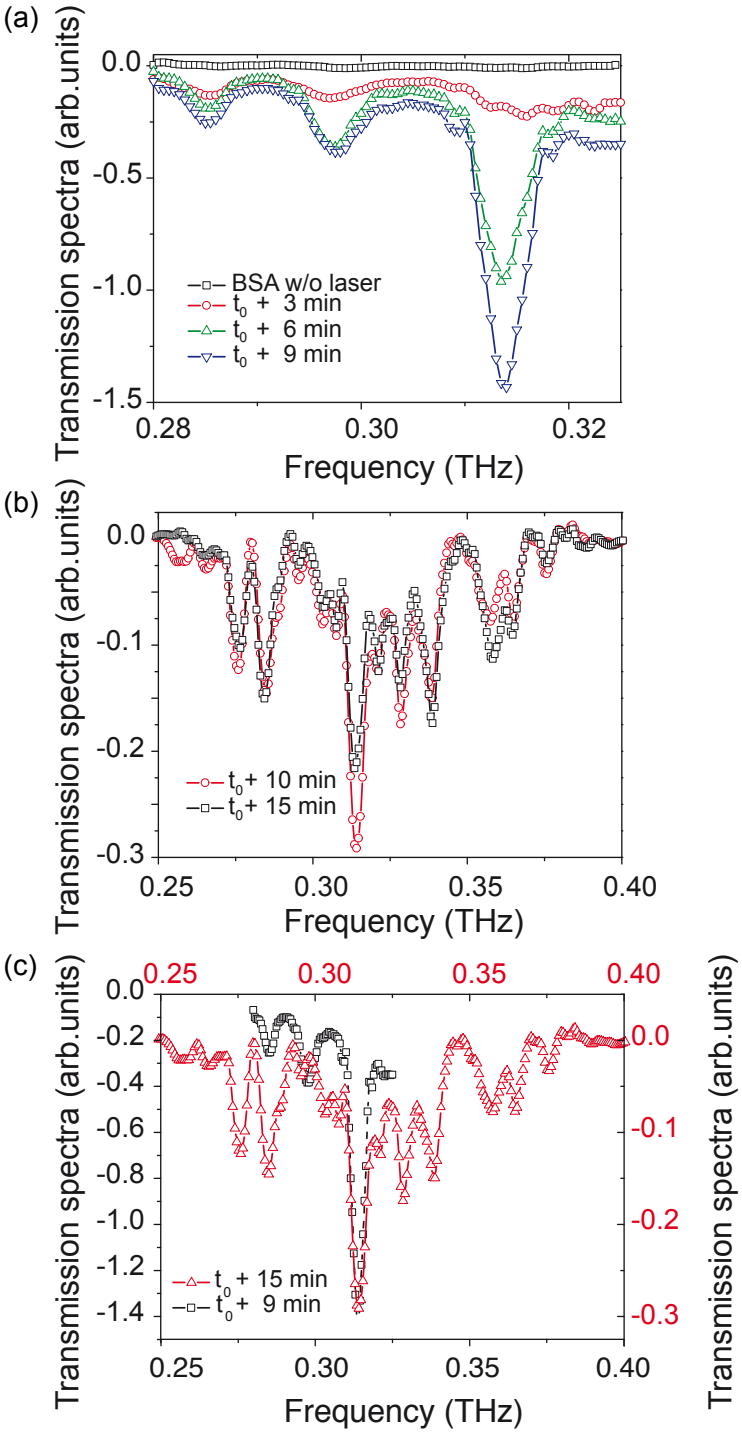

Figure 5.4: Normalized absorption spectra as functions of the frequency. (a) Spectra obtained using the micro-coaxial probe normalized to the water spectrum in the absence of illumination and in the presence of illuminations for the reported durations. (b) Spectra obtained using the rectenna, after subtraction of the protein solution without illumination, for the reported durations.(c) Comparison of the two normalized spectra for the longest illumination durations.

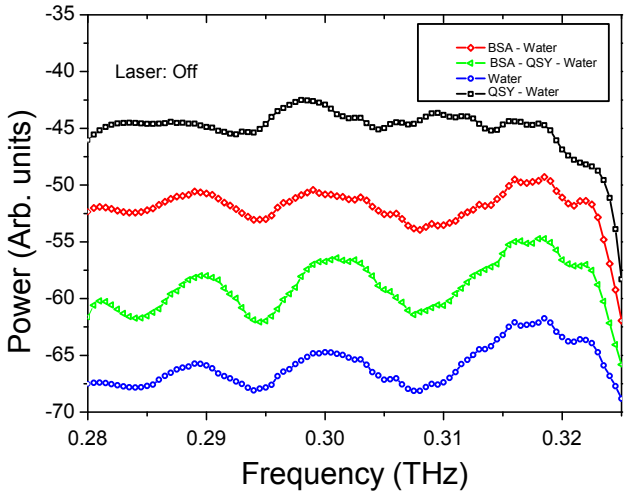

Figure 5.5: Microwire-based absorption spectra. No blue light illumination. Obtained with: water (blue circles); solvated AF488 in water (black squares); solvated non-labelled BSA in water (red rhombs); BSA labelled with AF488 solvated in water (green triangles).

that this results have been obtained by two different groups, into different labs with two different techniques.

5.2 Interpretation of experimental outcomes

5.2.1 A premise on methodology

Although the solution studied in these experiments is much simpler than real cell environment at molecular scale, it is really hard to derive a quantitative predictive model that describe the response of the solution to THz radiation. As mentioned in the introduction of this chapter, there are many aspects concerning water response to terahertz radiation and interaction among water molecule and proteins not already fully understood and object of ongoing researches. Facing to this situation, a "minimalistic" approach has been adopted: experimental outcomes has been explained using simplified models, each of them describing only some aspect or feature of the observations. Much more complex models aimed to a more detailed and precise interpretation and description of the experimental outcomes will be object of further investigations.

5.2.2 Interpretation of the absorption peak frequency

Since the BSA is a heart-shaped globular protein, a first rough estimate of a global oscillatory frequency is obtained considering a model of the molecule as composed of two masses m, equal to half the total protein mass, joined by a spring of elastic constant k given by $k = EA_0/l_0$, where E is the Young modulus of the protein, A_0 and l_0 are its transverse section and length at rest, respectively. Using $m = 33$ KDa, $A_0 \simeq 1.2 \times 10^{-13}\,\mathrm{cm}^2$, $l_0 \simeq 1.2 \times 10^{-7}$ cm, and $E = 6.75$ GPa, we find $\nu = (1/2\pi)\sqrt{k/m} \simeq 0.300$ THz which is close to the main resonance observed at 0.314 THz. A more refined approximation is obtained by modelling the protein with

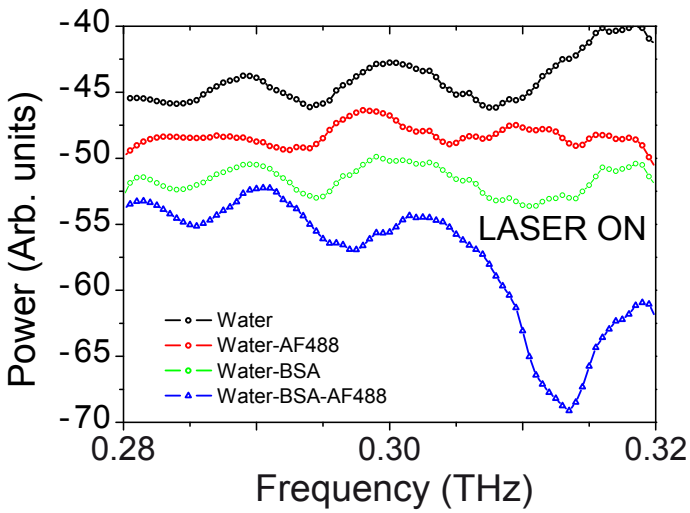

Figure 5.6: Microwire-based absorption spectra. With blue light illumination. Obtained with: solvated AF488 in water (black circles); solvated non-labelled BSA in water (red circles); BSA labelled with AF488 solvated in water (green triangles).

an elastic sphere and then considering its vibrational frequencies. The fundamental frequency of a spheroidal breathing mode of an elastic sphere is given by the formula [Bas94]

$$\nu_0 = (1/2\pi)[2(2l+1)(l-1)]^{1/2}\left(\frac{E}{\rho R_H^2}\right)^{1/2}$$

which holds for $l \geq 2$. Using the following data for the BSA protein: Young modulus $E = 6.75$ GPa obtained at room temperature using Brillouin light scattering of hydrated BSA proteins [PNE+13], hydrodynamic (Stokes) radius $R_H = 35$Å, and specific volume $1/\rho = 0.74$ derived from small-angle X-ray scattering (SAXS) experiments [MS07], we find for the lowest mode ($l = 2$) the frequency $\nu_0 = 308$ GHz which agrees within an error of about 2% with the observed peak value at $\nu = 314$ GHz.

Secondary resonances are also present in both spectra. A possible explanation could be tentatively given considering torsional modes. These could be activated at the frequencies given by the relation [Bas94]

$$\nu_t = \nu_0\left(\frac{(2l+3)}{2(2l+1)}\right)^{1/2}$$

whence, for $l = 2$ and $l = 3$, one finds $\nu = 257\ GHz$ and $\nu = 246\ GHz$ respectively. These could be associated with the two weaker absorption lines observed at $\nu = 278\ GHz$ and $\nu = 285\ GHz$. Here the larger discrepancy can be attributed to the non-spherical shape of the BSA, what entails the existence of different moments of inertia according to the rotation axis, whereas the breathing mode is insensitive to this fact.

5.2.3 Spectroscopic detection of the collective mode

In both experiments the collective oscillation of the BSA protein is seen as a spectroscopic absorption feature. At variance with standard absorption spectroscopy, where the radiation

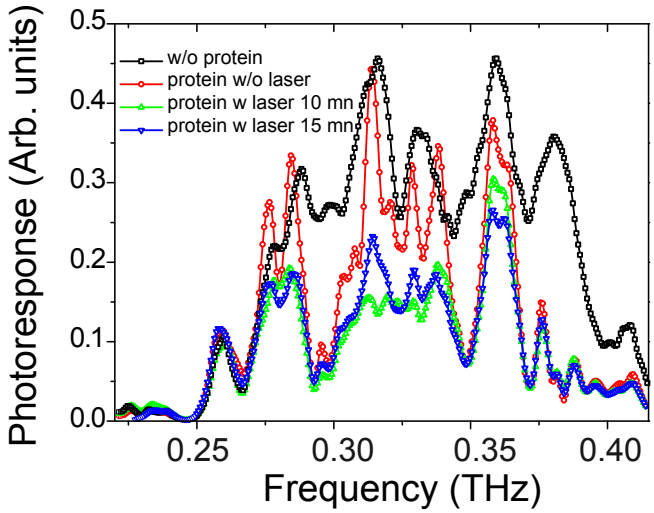

Figure 5.7: Rectenna-based absorption spectra. Response of water solution to THz radiation without blue illumination (black). Response of the systems water and protein when the blue illumination is on just after illumination(red series), after 10 minutes (green series) and after 15 minutes (blue).

entering the absorbing medium is responsible for the creation of atomic or molecular excited states, in the experiments reported here the THz radiation is used to detect an already excited state of the molecules. Actually, the collective oscillation of the proteins makes them behave as very small antennas (Hertzian dipoles) with the characteristic property of antennas of simultaneously absorbing and emitting electromagnetic radiation. However, the absorption along the THz optical path cannot be compensated by the radiation emitted by the oscillating dipoles because it spreads over all the directions in space. The net result is an absorption feature. If we denote with $\vec{\mu}(t)$ the dipole moment of a protein and with $\vec{E}(t) = \vec{E}_0 \cos(\omega t)$ the electric field of the THz radiation, the attenuation of the electric energy density within the drop of protein solution is proportional to the work done by the electric field, that is, $L = -\vec{\mu}(t) \cdot \vec{E}(t) = \mu E \cos\theta_E$ where θ_E is the angle among the electric dipole of the biomolecule and the electric field. The oscillation of the dipole moment is necessarily damped, due to the interaction with the surrounding molecules resulting in dissipations. Denoting by τ the lifetime of the activated collective oscillation and by ω_c its frequency, we can set $\vec{\mu}(t) = \vec{\mu}_0 e^{-t/\tau} \cos(\omega_c t)$. Thus, after averaging over all the relative orientations θ_E and all the phase differences ϕ between $\vec{\mu}(t)$ and $\vec{E}(t)$ such that the electric field does a positive work, we obtain

$$L(\omega) = 2 \int_0^{\pi} d\phi \int_0^{\infty} dt \mu_0 E_0 e^{-t/\tau} \omega_c \sin(\omega_c t) \cos(\omega t + \phi) \ . \tag{5.1}$$

This is the elementary attenuation process of the THz radiation. This process is repeated in time for each molecule at a rate proportional to the intensity of the drop illumination with the blue light. Moreover, the total attenuation is proportional to the concentration of absorbing molecules in the protein solution.

Equation (5.1) gives for $L(\omega)$ a Lorentzian shape centred at ω_c, the resonance frequency of the

collective oscillation of the BSA protein. Figure Figure 5.8 shows three different shapes of the function $L(\omega)$ obtained for different values of τ (in arbitrary units).

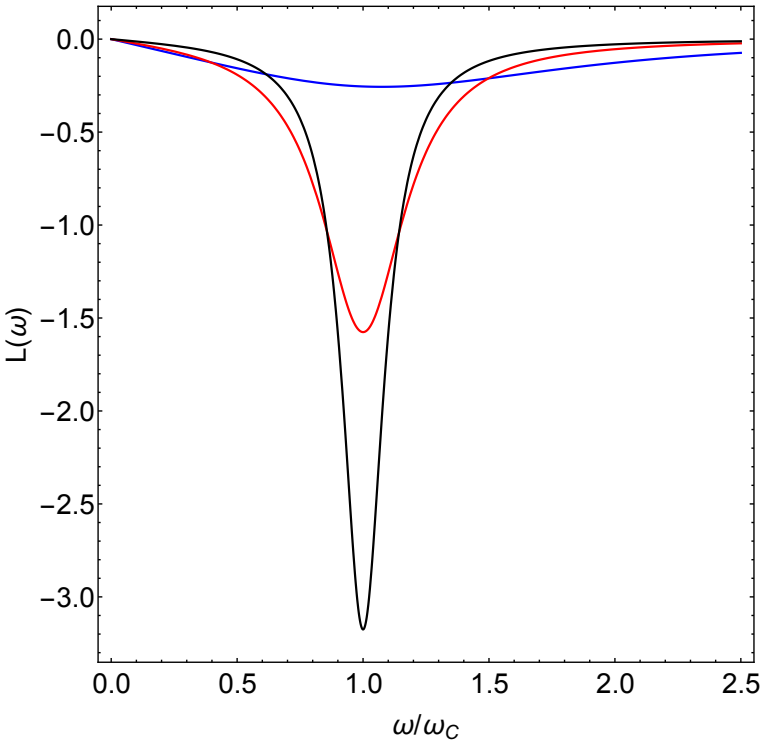

Figure 5.8: The function $L(\omega)$ of Eq.(5.1) is plotted in arbitrary units for three different values of τ. The blue line corresponds to $\tau = 1$, the red line to $\tau = 5$, the black line to $\tau = 10$, having set $\omega = 10$.

In Figures Figure 5.5 and Figure 5.6 several control spectra are reported which have been obtained with the microwire antenna. The two groups of spectra refer to the blue light emitting laser switched off and on, respectively. The observed absorption line at 314 GHz is clearly found only when the fluorochrome AF488 is attached to the BSA molecules and in presence of 4880Å laser light illumination of the protein solution. These spectra rule out any other origin of the observed absorption feature beside the proposed one in the main text of the present work.

5.3 Some remarks on THz spectroscopy measures

According the Fröhlich-like model it is also expected that the appearance of the resonance peak at 0.314 THz should exhibit a threshold-like behaviour when increasing the energy flowing through the protein. Figure 5.9 (a) presents a clear threshold in the intensity of the resonance peak when the optical input power exceeds 10 μW. By using the classical formalism for the analysis of the out-of-equilibrium phonon condensation (given in chapter 4) we have calculated the intensity of all the normal resonant modes of the BSA-protein (though in an idealised model) as a function of the source power injected through the protein. Figure 5.9 (b) highlights a threshold-like behaviour of the intensity of the fundamental mode that concentrate the input energy at the expenses of the excited modes. This theoretical threshold-like behaviour isin very good qualitative agreement with the experimentally observed threshold. By increasing the

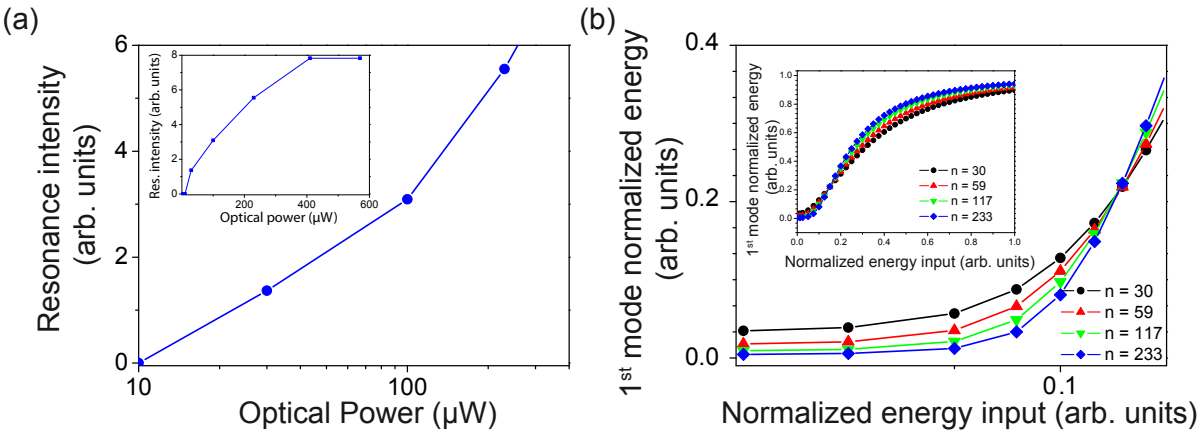

Figure 5.9: Threshold-like behaviour of giant dipolar oscillations. (a) Intensity of the resonant peak measured at 0.314 THz as a function of the optical laser power. (b) Normalized energy of the fundamental mode calculated as a function of the normalized source power. The different curves correspond to the reported numbers of normal modes of the BSA protein.

number of modes included in the calculation, this threshold becomes more and more evident. In addition to the already known existence of collective vibrational modes of biomolecules, observed in the past at thermal equilibrium by means of Far Infrared and Raman Spectroscopy, we show that strong out-of-equilibrium collective modes can be also activated and sustained by external energy pumping of a model protein.

We suggest that the observed phenomenology, notably the existence of a threshold in the energy supply rate, can be qualitatively understood as a non-equilibrium Bose-like condensation of the vibrational modes of the BSA protein, much in the spirit of a long-standing theoretical proposal put forward by H. Fröhlich, even though we have reformulated it in a classical context. Finally, the strikingly good agreement among the results obtained with two independent and different experiments, operating in two different laboratories, rules out the possibility of experimental artefacts.

Our study, through the strong absorption feature observed in a watery solution of the BSA protein, reveals that the protein vibrating in its collective spheroidal breathing mode has to be dressed by ordered layers of water molecules[4] in order to attain an effective dipole moment sufficiently large to overcome the strong absorption of bulk water. From basic facts of classical electrodynamics, two or more dipoles of large moment, oscillating out-of-equilibrium, can interact through long range electrodynamic forces [PPT15], thus our findings motivate suitable experimental attempts at detecting them [NSP+14].

[4]In [SDD15] it has been shown that BSA-molecules are dressed in aqueous solution by 8 layers of water molecules thus making an overall layer of 25 Åaround each molecule.

CHAPTER 6 Study of experimental strategies to detect long range interactions: Feasibility study

In this chapter, it is reported a numerical and theoretical investigation concerning the possibility to detect the presence of long-range interactions among biomolecules by studying their diffusion. In particular long- and short-range interactions would affect in a qualitative different way the dependence of self-diffusion coefficient as a function of the concentration of mutually diffusing particles. The work here reported has been published in [NSP+14].

6.1 Motivations

In previous chapter we have reported experimental outcomes whose theoretical interpretation suggest the that it is possible to activate collective oscillations in biomolecules when a sufficient energy injection rate is provided. Such collective oscillations in biomolecules would result in giant dipole oscillations due both to the deformation of biomolecule static dipole and of the hydratation water. From first principles of classical electromagnetism, this would imply that it is possible to activate in the same condition long-range electrodynamic classical interactions among oscillating dipoles *if they are resonant* (as in the case of identical molecules, i.e.). Nevertheless the observations of out-of-equilibrium giant dipole oscillations in biomolecules is not sufficient to answer to the following question: does Nature exploit these long-distance electrodynamic intermolecular forces in living matter? In other words, are these forces sufficiently strong to play the above surmised role? The complexity of such systems and the actual state of the theory make almost impossible to provide an a priori analytical answer to these fundamental questions.

The work presented in this chapter is the sequel of a paper [PFN+12] addressed the problem of estimating whether certain biomolecular interactions of electrodynamic origin could entail sizable effects in a parameter domain accessible to standard laboratory techniques. Though the answer was in principle affirmative for what concerns molecular concentrations, temperature and solvent properties, the physical observable chosen (the first encounter time between two interacting biomolecules) turns out hardly measurable in practice because it requires to follow the dynamics of single molecules. Thus the work presented in this chapter aims at filling this gap between theory and experimental feasibility. This is achieved by investigating some transport properties of long-range interactions acting among a set of particles freely moving in a fluid environment.

The novelty of the present work is that one dimensional analytic results in [PFN+12] are here replaced by 3D numerical results in a more realistic context. In fact, biomolecules, which are typically charged, move in three dimensional space where they are subjected to several interactions out of which there is at least one kind of long-range ones: electrostatic interactions. Thus

we begin by considering Coulomb interactions, both screened and unscreened, for which all the parameters can be precisely assigned. On this basis we get a reference scenario allowing an assessment of the sensitivity of diffusion to forces which are undoubtedly active among charged biomolecules. Then we make classical electrodynamic forces derived in Subsection 3.3.4 enter the game. By studying their possible competition with Coulomb forces we can find out how new characteristic features of the concentration dependence of diffusion can emerge making the difference with the previous case. Whence feasible experiments can be identified.
New experimental protocols have been developed to determine if in a system of diffusive particles (as biomolecules in cellular environments) are present mutual long-range interactions. This new experimental protocols demands both feasibility studies (numerical and theoretical) to asses the *possibility* to have a clear fingerprint of the presence of long-range interactions and numerical simulation to *validate* the theory on some benchmark case, where long-range interactions are "built-in" (as in the case of electrically charged diffusing particles subjected to electrostatic interactions in pure water, i.e.).
In what follows such work is presented: theoretical and numerical studies support a new experimental technique that allows to study the self-diffusion coefficient of these biomolecules in a very wide range of concentration (average intermolecular distance) when "activation condition" of collective giant dipole oscillations in BSA (see previous chapter) are realized. An important qualitative difference in the behaviour of self-diffusion as function of average intermolecular distance coefficient has been observed among long- and short-range forces both in *numerical simulation*. Numerical molecular dynamics simulations have been used to validate the use of a new experimental technique based on Fluorescence Correlation Spectroscopy for the detection of long range forces among diffusive particles (see next chapter).

6.2 Model and methods

In the following section a simple model of diffusing particles is considered, in order to study how long-range and short-range interactions affect their dynamics. The model equations, the molecular interaction potentials, the numerical algorithm and the relevant observables for the numerical study of an ensemble of mutually interacting particles in presence of an external random force shall be defined in what follows.

6.2.1 Basic equations

We consider a system composed of N identical molecules, modelled as spherical Brownian particles of radius R, mass M and a net number of electric charges Z, moving in a fluid with viscosity η at a fixed temperature T, interacting through a pairwise potential $U(r)$ which depends only on the distance r between their centres.
Under the assumption that the friction exerted by the fluid environment on the particles is described by Stokes' law, the dynamics of the system is given by N coupled Langevin equations

[Gar10]:

$$M\frac{d^2\boldsymbol{r}_i}{dt^2} = -\gamma\frac{d\boldsymbol{r}_i}{dt} - \sum_{j=1,j\neq i}^{N} \boldsymbol{\nabla}_{\boldsymbol{r}_i} U\left(|\boldsymbol{r}_i - \boldsymbol{r}_j|\right) + \\ + \sqrt{2\gamma k_B T}\boldsymbol{\xi}_i(t) \qquad \text{for } i = 1, ..., N \tag{6.1}$$

where $\boldsymbol{r}_i$ is the coordinate of the center of i-th particle, $\gamma = 6\pi\eta R$ is the friction coefficient and k_B is the Boltzmann constant. The stochastic displacements are uncorrelated so that $\boldsymbol{\xi}(t) = (\boldsymbol{\xi}_1, ..., \boldsymbol{\xi}_N)$ is a $3N$-dimensional random process modelling the fluctuating force due to the collisions with water molecules, usually represented as a Gaussian white noise process satisfying:

$$\begin{cases} \langle \xi^\alpha(t)\rangle_\xi = 0 \\ \\ \langle \xi_i^\alpha(t)\xi_k^\beta(t')\rangle_\xi = \delta^{\alpha\beta}\delta_{ik}\delta(t-t') \end{cases} \tag{6.2}$$

where $\alpha, \beta = x, y, z$ are the Cartesian components of $\boldsymbol{\xi}_i$'s and $\langle\cdot\rangle_\xi$ stands for the average over many realizations of the noise process. As the random process is stationary the average over different realizations of the noise is equivalent to a time average

$$\langle f(\boldsymbol{\xi})\rangle_\xi = \lim_{t\to+\infty}\frac{1}{t}\int_0^t f(\boldsymbol{\xi}(\tau))\mathrm{d}\tau = \lim_{t\to+\infty}\langle f(\boldsymbol{\xi}(t))\rangle_t \tag{6.3}$$

Considering times much larger than the relaxation time $\tau_r = M/\gamma$, we can neglect inertial effects obtaining the overdamped limit for Eqs. (6.1):

$$\gamma\frac{d\boldsymbol{r}_i}{dt} = -\sum_{j=1,j\neq i}^{N} \boldsymbol{\nabla}_{\boldsymbol{r}_i} U\left(|\boldsymbol{r}_i - \boldsymbol{r}_j|\right) + \\ + \sqrt{2\gamma k_B T}\boldsymbol{\xi}_i(t) \qquad i = 1, ..., N \tag{6.4}$$

In systems like the one we are interested in (involving protein or nucleid acids in aqueous medium) τ_r is negligible compared with the characteristic time scales for experimental observations [1], so we can assume that the dynamics for such systems is described by Eqs.(6.4).
As the deterministic interactions are in general non linear, we are dealing with a system of first order Stochastic Differential Equations (SDEs) which describes a randomly perturbed nonlinear N-body dynamical system with an expected complex (chaotic) dynamics since the integrability is exceptional. For this reason, we undertake the numerical integration of Eqs.(6.4). We remark that Eqs.(6.4) can be considered as a Lagrangian description of a system whose Eulerian description is given by a Fokker-Planck equation for the N-body probability distribution

[1] I.e. for a biomolecule with a hydrodynamic radius $R = 2\times10^{-3}\mu$m and mass $M = 15K$Da in pure water at 300K, the relaxation time τ_r is in the order of $10^{-6}\mu$s.

$P_N(\boldsymbol{r}_1, ...\boldsymbol{r}_N, t)$ [**?**] of the form:

$$\frac{\partial P_N}{\partial t} = \gamma \sum_{i=1}^{N} \boldsymbol{\nabla}_{\boldsymbol{r}_i} \cdot \left(D_B \boldsymbol{\nabla}_{\boldsymbol{r}_i} P_N + P_N \frac{\boldsymbol{\nabla}_{\boldsymbol{r}_i} U(\boldsymbol{r}_1, ..., \boldsymbol{r}_n)}{\gamma} \right) \tag{6.5}$$

where $D_B = k_B T/\gamma$ is the Brownian diffusion coefficient and $U(\boldsymbol{r}_1, ..., \boldsymbol{r}_n) = \sum_{i=1}^{N} \sum_{j>i} U(|\boldsymbol{r}_i - \boldsymbol{r}_j|)$ is the total interaction energy. It is well known that Gibbs configurational distribution $P_N^{eq} = P_N^{eq}(\boldsymbol{r}_1, ..., \boldsymbol{r}_N)$ is the stationary solution of Eq.(6.5) which also minimizes free energy [**?**]:

$$P_N^{eq} = \frac{1}{Z} \exp\left[-\beta U(\boldsymbol{r}_1, ..., \boldsymbol{r}_n)\right] \tag{6.6}$$

where $\beta = 1/k_B T$ and

$$Z = \int \exp\left[-\beta U(\boldsymbol{r}_1, ..., \boldsymbol{r}_n)\right] \prod_{i=1}^{N} \mathrm{d}\boldsymbol{r}_i \tag{6.7}$$

The distribution of Eq.(6.6) defines an equilibrium measure μ^{eq}

$$\mu^{eq}(f(\boldsymbol{r}_i)) = \int f(\boldsymbol{r}_i) P_N^{eq}(\boldsymbol{r}_i) \prod_{i=1}^{N} \mathrm{d}\boldsymbol{r}_i \tag{6.8}$$

which is invariant respect to the flow defined by Eqs.(6.4). As we are interested especially in the behaviour of systems described by Eqs. (6.4) in the limit $t \to +\infty$, we assume that the system thermalizes without any dependence on initial conditions, *i.e.* for every initial configuration $\{\boldsymbol{r}_i(0)\}_{i=1,..N}$ it exists a time $\tilde{t}$ such as $P_N(t) \simeq P_N^{eq}$ for $t > \tilde{t}$.

6.2.2 Model potentials

The explicit forms of the pairwise potential $U(|\boldsymbol{r}|)$ used in our simulations have been the following. The first case that we considered is the electrostatic interaction among identical molecules in electrolytic solution; this is described by the Debye-Hückel potential [AR76]:

$$U_{\text{Debye}}(\boldsymbol{r}) = \frac{(Ze)^2}{\varepsilon |\boldsymbol{r}|} \cdot \frac{e^{-\frac{2R}{\lambda_D}\left(\frac{|\boldsymbol{r}|}{2R} - 1\right)}}{(1 + R/\lambda_D)^2} \tag{6.9}$$

where λ_D is the Debye length of the electrolytic solution, R is the molecular radius, e is the elementary charge and ε is the static dielectric constant of the medium. As water is ubiquitous in microscopic biological systems, we put $\varepsilon = \varepsilon_{water} \simeq 80$, *i.e.* its static value at room temperature. Coulomb screening is an essential feature of biological systems which shortens the range of electrostatic interactions due to small ions freely moving in the environment. In order to study how the diffusion and dynamical properties of the system change by varying the spatial range of the interactions, we consider different values for λ_D and, in the ideal case of $\lambda_D \to +\infty$, we

adopt the pure Coulomb potential for charged particles in a dielectric medium:

$$U_{\text{Coul}}(\boldsymbol{r}) = \frac{(Ze)^2}{\varepsilon|\boldsymbol{r}|} \quad . \tag{6.10}$$

The second case concerns the long-range attractive dipolar potential predicted by the classical electrodynamics among biomolecules*out-of-thermal-equilibrium* (see chapter 3 for more details). This, in regularized form, reads as

$$U_{\text{Dipolar}}(\boldsymbol{r}) = -\frac{c}{|\boldsymbol{r}|^3 + \alpha} \tag{6.11}$$

where c is a positive parameter and α is a parameter that prevents $U(r)$ from becoming singular. This potential describes both an attractive electrostatic and an attractive electrodynamic dipole-dipole interaction. In describing a system with a strong Debye shielding, the use of the potential of Eq.(6.11) is equivalent to the implicit assumption that this potential is of *electrodynamic* origin. The parameter α flattens $U(r)$ at short distances when these are comparable with the radius R of the molecules. In fact, when r is small, higher multipolar moments could play a role and, in principle, this would lead to the description of the interaction among complex bodies whose charge distributions should be taken into account[Sto08].

Here it is assumed that the net result of these interactions (which can be attractive as well as repulsive), occurring when the molecules are close one to the other, is zero. The softened potential Eq.(6.11) solves this problem. The parameter α is fixed by the condition that the second derivative of U (where the force intensity reaches its maximal value) vanishes, that is $\alpha = 2r^3$, at $\boldsymbol{r} = 0.1\mu$m.
The value of the coefficient c, which controls the force intensity, has been determined by the requirement that $U(\boldsymbol{r})$, at the same value $\boldsymbol{r} = 0.1\mu$m, is equal to a given fraction of $-k_BT$, whence $U(\boldsymbol{r} = 0.1\ \mu\text{m}) = -k_BT/10$. A-priori we could think that, in order to have some observable effect, deterministic forces should overcome the average thermal energy per degree of freedom. However we observed that this is not the case: for example with $U(\boldsymbol{r} = 0.1\ \mu\text{m}) = -3k_BT$ we always found a vanishing D. This happens because deterministic forces keep almost the same directions on time scales for which random forces (that mimic water molecules collisions) incoherently change much more their directions. The relevant physical consequence is that interaction potentials definitely weaker than k_BT can have sizeable effects. That the choice $U(\boldsymbol{r} = 0.1\ \mu\text{m}) = -k_BT/10$ is realistic for biomolecules is supported by quantitative estimates that can be found in [**?**].

6.2.3 Numerical algorithms

We have numerically studied systems of N molecules confined in a cubic volume of size L. To get rid of spurious boundary effects, periodic boundary conditions (PBC) have been assumed which implies the existence of an infinite number of replicas/images throughout the space. As we are interested in studying dynamical properties and diffusive behaviour of different concen-

trations of molecules, we fixed the number of molecules N and varied the average intermolecular distance $\langle d \rangle$ according to the relation

$$L = \sqrt[3]{N}\langle d \rangle \tag{6.12}$$

In presence of long-range interactions and PBC, each molecule contained in the previously mentioned box interacts with all the molecules contained in the above mentioned images/replicas, that is, the pairwise potential $U(\boldsymbol{r}_i, \boldsymbol{r}_j) = U(|\boldsymbol{r}_i - \boldsymbol{r}_j)|$ in Eqs. (6.1) and (6.4) has to be replaced by an effective potential $U^{\text{eff}}(\boldsymbol{r}_i, \boldsymbol{r}_j)$ of the form:

$$U^{\text{eff}}(\boldsymbol{r}_i, \boldsymbol{r}_j) = \sum_{\boldsymbol{k}\in\mathbb{Z}^3} U(|\boldsymbol{r}_i - \boldsymbol{r}_j + \boldsymbol{k}L|) \tag{6.13}$$

where $\mathbb{Z}^3$ is the space of 3-dimensional integer vectors. In order to compute the force $\boldsymbol{F}_j(\boldsymbol{r}_i)$ on the i-th particle due to the j-th particles and all its replicas, we rearrange the terms of the sum in Eq. (7.9), so that

$$\begin{aligned} \boldsymbol{F}_j(\boldsymbol{r}_i) = -\boldsymbol{\nabla}_{\boldsymbol{x}_i} U(|\boldsymbol{x}_i - \tilde{\boldsymbol{r}}_j|) + \\ + \boldsymbol{\nabla}_{\boldsymbol{x}_i} \sum_{\boldsymbol{k}\in\mathbb{Z}^3, \boldsymbol{k}\neq\boldsymbol{0}} U(|\boldsymbol{x}_i - \tilde{\boldsymbol{r}}_j + \boldsymbol{k}L|) \end{aligned} \tag{6.14}$$

where $\boldsymbol{x}_i$ is the i-th particle image position into the reference box and $\tilde{\boldsymbol{r}}_j$ is the nearest image of j-th particle, that is

$$|\boldsymbol{x}_i - \tilde{\boldsymbol{r}}_j| = |\boldsymbol{r}_{i,j}| = \min_{\boldsymbol{k}\in\mathbb{Z}^3} |\boldsymbol{x}_i - \boldsymbol{r}_j + \boldsymbol{k}L| < \frac{L\sqrt{3}}{2} = \lambda_{NN} \tag{6.15}$$

It is clear by Eqs. (6.14) and (6.15) that short and long-range interactions (in the sense specified in the Introduction) have to be managed in two different ways. For short range interactions it is always possible to define a cutoff length scale λ_{cut} such that the effects of the interactions beyond this distance are negligible. In the systems we have studied by means of numerical simulations, the Debye electrostatic potential is a short range potential with a cutoff scale of the order of some units of the Debye length λ_D. As for each case considered it is $\lambda_{NN} > 30\lambda_D$, the second term on the right-hand side of Eq.(6.14) has been neglected in numerical computations. For long-range interactions (*i.e.* Coulomb potential Eq.(7.15) and dipole-dipole electrodynamic potential Eq.(6.11)), it is not possible to define a cutoff length scale λ_{cut} so that, in principle, the infinite sum in Eq.(6.14) should be considered. A classical way to account for long-range interactions resorts to the so called Ewald summation [AT89]. In the subsequent Section we describe a more recent and practical method replacing Ewald's one - known as Isotropic Periodic Sum (IPS). The equations of motion (6.4) were numerically solved using the Euler-Heun algorithm [BLL07], a second order predictor-corrector scheme. The position $\boldsymbol{r}_{i,n}$ of the i-th particle at time $t_n = t_0 + n\Delta t$, t_0 being the initial time, is obtained by:

$$\boldsymbol{r}_{i,n} = \boldsymbol{r}_{i,n-1} + \frac{1}{2\gamma}\Big[\boldsymbol{F}(\boldsymbol{r}_{i,n-1}) + \boldsymbol{F}(\tilde{\boldsymbol{r}}_{i,n})\Big]\Delta t + \sqrt{\frac{2kT}{\gamma}}\boldsymbol{\xi}_{i,n-1} \tag{6.16}$$

where $\boldsymbol{F}$ is the resultant of the forces acting on the i-th particle, and $\tilde{\boldsymbol{r}}_{i,n}$ is calculated with the Euler predictor by:

$$\tilde{\boldsymbol{r}}_{i,n} = \boldsymbol{r}_{i,n-1} + \frac{1}{\gamma}\boldsymbol{F}(\boldsymbol{r}_{i,n-1})\Delta t + \sqrt{\frac{2kT}{\gamma}}\boldsymbol{\xi}_{i,n-1} \tag{6.17}$$

The initial position of each particle is randomly assigned at t_0 using a uniform probability distribution in a cubic box of edge L.

IPS correction to long-range potentials

Because of the long-range nature of Coulomb and dipolar potentials (described by Eqs.(7.15) and (6.11), respectively) the force acting on each particle is given by the sum of the forces exerted by all the particles in the box and by the particles belonging to the images. For the computation of these forces, we used the IPS method [WB05] [WB08], a cutoff algorithm based on a statistical description of the images isotropically and periodically distributed in space. Assuming that the system is homogeneous on a length scale R_c, we can define an effective pairwise IPS potential $U^{IPS} = U^{IPS}(|\boldsymbol{r}_{i,j}|, R_c)$ which takes into account the sum of pair interactions within the local region and with the images of this one:

$$U^{IPS}(|\boldsymbol{r}_{i,j}|, R_c) = \begin{cases} U(|\boldsymbol{r}_{i,j}|) + \phi(|\boldsymbol{r}_{i,j}|, R_c), & |\boldsymbol{r}_{i,j}| \leq R_c \\ \\ 0, & |\boldsymbol{r}_{i,j}| > R_c \end{cases} \tag{6.18}$$

where $\phi(|\boldsymbol{r}_{i,j}|, R_c)$ is a correction to the potential obtained by computing the total contribution of the interactions with the particle images beyond the cutoff radius R_c [WB05] [WB08]. For the Coulomb potential of Eq.(7.15), we obtained an analytical expression for the IPS correction $\phi_{\text{Coul}}(\boldsymbol{r}_{i,j}, R_c)$. For computational reasons this has been approximated by a polynomial of degree seven in $x = |\boldsymbol{r}_{i,j}|/R_c$ with x in the interval $(0; 1]$:

$$\begin{aligned} \phi_{\text{Coul}}(x) = &- 9.13636 \times 10^{-7} + 0.000100298x + \\ &+ 0.298588x^2 + 0.0151595x^3 + \\ &+ 0.00881283x^4 + 0.10849x^5 + \\ &- 0.0930264x^6 + 0.0482434x^7 \end{aligned} \tag{6.19}$$

For the regularized dipole potential of Eq.(6.11) it is not possible to compute analytically the IPS correction. Nevertheless, since the regularization constant α in (6.11) could be negligible with respect to R_c^3, so that $\alpha/R_c^3 \ll 1$, we will assume that the dipolar potential has the form $U_{\text{Dipolar}}(r) \simeq c/r^3$ for $r \geq R_c$. Thus, we can compute the exact IPS correction $\phi_{\text{Dipolar}}(|\boldsymbol{r}_{i,j}|, R_c)$,

and, approximating this by means of a polynomial, we obtain:

$$\begin{aligned}\phi^{IPS}_{\text{Dipolar}}(x) = &- 3.34576 \times 10^{-6} + 0.000199865x + \\ &+ 0.936254x^2 + 0.0259481x^3 + \\ &+ 0.0971465x^4 + 0.184721x^5 + \\ &- 0.146205x^6 + 0.0877732x^7\end{aligned} \tag{6.20}$$

We have chosen $R_c = L/2$ under the hypothesis that on this scale the system is homogeneous.

6.2.4 Long-time diffusion coefficient

We aim at assessing the experimental detectability of long-range interactions between biomolecules taking into account quantities accessible by means of standard experimental techniques. A valid approach to do so is the study of transport properties. For this reason, in our simulations we chose the long-time diffusion coefficient D as main observable of the system described by Eqs. (6.4). This coefficient is defined, consistently with Einstein's relation [AT89], as:

$$D = \lim_{t \to +\infty} \frac{\langle |\Delta \boldsymbol{r}_i(t)|^2 \rangle}{6t} \tag{6.21}$$

$\Delta \mathbf{r}_i(t) = \boldsymbol{r}_i(t) - \boldsymbol{r}_i(0)$ being the total displacement of a particle in space and $\langle a_i \rangle = 1/N \sum_{i=1}^{N} a_i$, the average over the particle set. We remark that in our system the displacements $\Delta \boldsymbol{r}_i(t)$ are not mutually independent due to the interaction potential $U(|\boldsymbol{r}_i - \boldsymbol{r}_j|)$ in Eqs. (6.4) which establishes a coupling between different particles; in that case, the average over particles index concerns correlated stochastic variables. Nevertheless, as our system is non-linear with more than three degrees of freedom, it is expected to be chaotic [**?**] so that, in this case, the statistical independence of particle motions is recovered. Moreover, when a chaotic diffusion gives $\langle |\Delta \boldsymbol{r}_i(t)|^2 \rangle \propto t$ (which is the case of the models considered in the present work), the diffusion coefficient D is readily computed through a linear regression of $\langle |\Delta \boldsymbol{r}_i(t)|^2 \rangle$ expressed as a function of time. In what follows we refer to $\langle |\Delta \boldsymbol{r}_i(t)|^2 \rangle$ as Mean Square Displacement(MSD).

6.2.5 Self-diffusion coefficient for interacting particles

In this Section, we derive a formula which corrects the Brownian diffusion coefficient by taking into account molecular interactions described by $U(r)$ in Eqs.(6.1). Following the classical derivation given by Langevin, we rewrite Eqs.(6.1) in terms of the displacement of each particle with respect to its initial position: $\Delta \boldsymbol{r}_i = \boldsymbol{r}_i(t) - \boldsymbol{r}_i(0)$

$$\begin{aligned}M \frac{\mathrm{d}^2 \Delta \mathbf{r}_i}{\mathrm{d}t^2} = &- \gamma \frac{\mathrm{d}\Delta \boldsymbol{r}_i}{\mathrm{d}t} - \sum_{j=1}^{N} \nabla_{\boldsymbol{r}_i} U(\boldsymbol{r}_i, \boldsymbol{r}_j) + \\ &+ \sqrt{2\gamma k_B T} \boldsymbol{\xi}_i(t) \qquad \text{for } i = 1, ..., N\end{aligned} \tag{6.22}$$

since $\mathrm{d}^n\mathbf{r}_i/\mathrm{d}t^n = \mathrm{d}^n\Delta\mathbf{r}_i/\mathrm{d}t^n$. Taking the scalar product with $\Delta\boldsymbol{r}_i$ of both sides, we obtain:

$$\begin{aligned}&\frac{1}{2}M\frac{\mathrm{d}^2|\Delta\boldsymbol{r}_i|^2}{\mathrm{d}t^2} - Mv_i^2 = -\frac{\gamma}{2}\frac{\mathrm{d}|\Delta\boldsymbol{r}_i^2|}{\mathrm{d}t}+\\&-\Delta\boldsymbol{r}_i\cdot\sum_{j\neq i}^{N}\nabla_{\boldsymbol{r}_i}U(\boldsymbol{r}_i,\boldsymbol{r}_j)+\sqrt{2\gamma_A k_B T}\Delta\boldsymbol{r}_i\cdot\boldsymbol{\xi}_i(t)\\&\qquad\text{for } i=1,...,N\end{aligned} \tag{6.23}$$

where $v_i^2 = |\mathrm{d}\Delta\boldsymbol{r}_i/\mathrm{d}t|^2 = |\mathrm{d}\boldsymbol{r}_i/\mathrm{d}t|^2$. Introducing the time derivative of the square module of the total displacement $z_i = \mathrm{d}|\Delta\boldsymbol{r}_i|^2/\mathrm{d}t$, we obtain

$$\begin{aligned}&\frac{1}{2}M\frac{\mathrm{d}z_i}{\mathrm{d}t} - Mv_i^2 = -\frac{\gamma}{2}z_i - \Delta\mathbf{r}_i\cdot\sum_{i\neq j}\nabla_{\mathbf{r}_i}U(\boldsymbol{r}_i,\boldsymbol{r}_j)+\\&\sqrt{2\gamma k_{\mathrm{B}}T}\Delta\boldsymbol{r}_i\cdot\boldsymbol{\xi}_i(t)\qquad\text{for } i=1,...,N\end{aligned} \tag{6.24}$$

According to Eq.(7.18) the self-diffusion coefficient D can be equivalently expressed in terms of z_i as

$$D = \lim_{t\to+\infty}\frac{1}{6t}\int_0^t\frac{\mathrm{d}\langle|\Delta\boldsymbol{r}_i(\tau)|^2\rangle}{\mathrm{d}\tau}\mathrm{d}\tau = \lim_{t\to+\infty}\frac{1}{6}\langle\langle z_i\rangle\rangle \tag{6.25}$$

where $\langle\langle\cdot\rangle\rangle$ indicates a double mean over particles and time. Let us now apply this double averaging to Eqs.(6.24) and remark that $\langle\langle\Delta\boldsymbol{r}_i\cdot\boldsymbol{\xi}_i(t)\rangle\rangle = 0$ because the time average is equivalent to an average over noise realizations (see Eq.(6.3)). Thus we get:

$$\begin{aligned}&\langle\langle z_i\rangle\rangle = -\frac{1}{\gamma}M\left\langle\left\langle\frac{\mathrm{d}z_i}{\mathrm{d}t}\right\rangle\right\rangle+\\&+\frac{2}{\gamma}\left[M\langle\langle v_i^2\rangle\rangle - \langle\langle\Delta\mathbf{r}_i\cdot\sum_{i\neq j}\nabla_{\boldsymbol{r}_i}U(\boldsymbol{r}_i,\boldsymbol{r}_j)\rangle\rangle\right]\end{aligned} \tag{6.26}$$

whose limit for $t\to+\infty$ gives an expression for the diffusion coefficient which explicitly depends on $U(r)$, according to Eq.(6.25). We assume that such a limit is finite for every term on the right hand side in Eq.(6.26) and that:

$$\lim_{t\to+\infty}\left\langle\left\langle\frac{\mathrm{d}z_i}{\mathrm{d}t}\right\rangle\right\rangle = 0 \tag{6.27}$$

which amounts to considering that the motion is diffusive. Since we consider systems at thermodynamic equilibrium, the Equipartition Theorem entails $\lim_{t\to+\infty} M\langle\langle v_i^2\rangle\rangle = 3k_BT$. We thus obtain the following expression for the diffusion coefficient D

$$D = \lim_{t\to+\infty} D_0\left[1 - \frac{\langle\langle\Delta\boldsymbol{r}_i(t)\cdot\sum_{i\neq j}\nabla_{\mathbf{r}_i}U(\boldsymbol{r}_i,\boldsymbol{r}_j)\rangle\rangle}{3k_BT}\right] \tag{6.28}$$

where $D_0 = k_BT/\gamma$ is the Brownian diffusion coefficient.

We remark that the correction term does not depend on initial conditions, as it would appear at a first glance at the equation above. In fact, having assumed thermal equilibrium, the dynamics is self-averaging so that time averages of observables for very long time t (ideally $t\to+\infty$) are

equivalent to an average over initial conditions[2].

For numerical calculations, the potential-dependent term in Eq.(6.28) is computed using:

$$\frac{\Delta D}{D_0} = \frac{D_0 - D_s}{D_0} = \frac{1}{N}\sum_{i=1}^{N}\left(\frac{1}{m}\sum_{k=1}^{m}\Delta \boldsymbol{r}_i(k\Delta t)\cdot \boldsymbol{F}_i(k\Delta t)\right) \tag{6.29}$$

where $\Delta \boldsymbol{r}_i(k\Delta t) = \boldsymbol{r}_i(k\Delta t) - \boldsymbol{r}_i(0)$ is the total displacement of the i-th particle at k-th integration step (taking into account PBC according to Eq.(6.14) and possibly IPS corrections) and $\boldsymbol{F}_i(k\Delta t)$ is the resultant force acting on the i-th particle .

6.2.6 Measuring chaos in dynamical systems with noise

Equations (6.4) are a system of non linear differential equations with additive noise. A relevant observable measuring the degree of instability of the dynamics is the Largest Lyapunov Exponent (LLE). The definition and numerical computation of the LLE is standard for noiseless deterministic maps and dynamical systems [BGS76], while it is more debated and controversial for randomly perturbed dynamical systems, the difficulty being due to the non differentiable character of stochastic perturbations [LPV96][GT96][Arn88].
However, note that our system is in principle a smooth dynamical system because the *stochastic* term in Eqs. (6.4) is just a simplified way to represent the *deterministic* (and differentiable) collisional interactions between Brownian solute particles with solvent molecules (water). In other words Eqs.(6.4) are a practical representation of the dynamical system described by the following smooth ODEs:

$$\gamma\frac{d\boldsymbol{r}_i}{dt} = -\sum_{j=1}^{n}\boldsymbol{\nabla}_{\boldsymbol{r}_i}U\left(|\boldsymbol{r}_i - \boldsymbol{r}_j|\right) + \sqrt{2\gamma k_B T}\,\boldsymbol{f}_i(t) \tag{6.30}$$

where $\boldsymbol{f}(t) = (\boldsymbol{f}_1(t), ..., \boldsymbol{f}_N(t))$ is a $3N$-dimensional time-dependent vector of functions representing the effect of collisions of water molecules with Brownian particles on a microscopic scale. If we look at $\boldsymbol{f}(t)$ on a time scale comparable to the characteristic collision time of water molecules with Brownian particles ($\tau_{coll} \sim 1$ps), $\boldsymbol{f}(t)$ is a differentiable function and its Fourier spectrum has a-priori a cut-off frequency. In spite of this, since we study the dynamics on time scales which outnumber τ_{coll} by at least six orders of magnitude, $\boldsymbol{f}(t)$ can be safely approximated by the standard white noise specified by Eqs.(6.2) and (6.3). Each 3-dimensional process $\boldsymbol{f}_i(t)$ would appear as stationary and isotropic on a time scale much larger than and for $\tau_{coll} \to 0$. Such approximation is clearly justified by the fact that for biomolecules in water and typically $\tau_{coll} \ll \tau_r$.
In light of these considerations, the time-average and self-correlation properties of process $\boldsymbol{f}(t)$ have to be compatible with properties Eq.(6.2) for $\tau_{coll} \to 0$. That means that $\mathbf{f}(t)$ has, for

[2] A naive computation, neglecting the effect of PBC, would always give a value of diffusion coefficient that is increased with respect to the Brownian one in the case of repulsive interactions, and decreased in the case of attractive interactions. The presence of infinite replicas due to PBC makes this statement incorrect in our case, as it can be seen using the form of the effective potential in Eq.(7.9).

instance, a null-average process on time scale much larger than τ_{coll} requiring:

$$\begin{cases} |\langle \mathbf{f}_i \rangle_t| \ll \lambda_{\text{diff}} & \text{for} \quad t \gg \tau_{coll} \\ \\ \lim_{t \to +\infty} \langle \mathbf{f}_i \rangle_t = \mathbf{0} & i = 1, ..., 3N \end{cases} \tag{6.31}$$

where $\lambda_{\text{diff}} = \sqrt{k_B T \tau_r / \gamma}$ is a length scale which characterize diffusion.
For what concerns autocorrelation functions $\phi_{ij}^{x_k x_l}(\tau)$ of the process $\mathbf{f}$

$$\phi_{ij}^{x_k x_l}(\tau) = \lim_{t \to +\infty} \frac{1}{t} \int_0^t f_i^{x_k}(\tilde{t} + \tau) f_j^{x_l}(\tilde{t}) \mathrm{d}\tilde{t} \tag{6.32}$$

where i, j are particle indices and x_k, x_j cartesian coordinate ones, we impose:

$$\begin{cases} \phi_{ij}^{x_k x_l}(\tau) \ll 1 & \text{for} \quad \tau > \tau_{coll} \\ \\ \lim_{t \to +\infty} \frac{1}{t} \int_0^t \phi_{ij}^{x_k x_l}(\tau) \mathrm{d}\tau = \delta_{ij} \delta^{x_k, x_l} \end{cases} \tag{6.33}$$

as we are ignoring the hydrodynamical effects which could introduce more complicate correlations for $\mathbf{f}$, *i.e.* both time and space dependent.
The white noise approach is useful for the numerical computation of the dynamics, but the underlying physics is in principle well described by the ODEs system of Eqs.(6.30). Having this in mind, we get rid of the subtleties of defining chaos in randomly perturbed dynamical systems and we resort to standard computational methods [Pet07b]. Deterministic chaos stems from two basic ingredients: stretching and folding of phase space trajectories. In our case the folding of trajectories in phase space is guaranteed by PBC which make phase space compact, while stretching is given by the local instability of the trajectories. Hence their average instability is measured through the usual Largest Lyapunov Exponent λ, defined as:

$$\lambda = \lim_{t \to +\infty} \frac{1}{t} \ln \frac{\|\boldsymbol{\zeta}(t)\|}{\|\boldsymbol{\zeta}(0)\|} \tag{6.34}$$

where $\| \cdot \|$ is the euclidean norm in $\mathbb{R}^{3N}$ and $\boldsymbol{\zeta} = (\zeta_1, ...\zeta_{3N})$ is a 3N-dimensional vector whose time evolution is given by the following tangent dynamics equations:

$$\frac{\mathrm{d}\zeta_i}{\mathrm{d}t} = -\frac{1}{\gamma} \sum_{k=1}^{N} \left. \frac{\partial^2 U}{\partial x_i \partial x_k} \right|_{\boldsymbol{x}(t)} \zeta_k(t) \qquad i = 1, ..., 3N \tag{6.35}$$

Of course, a positive LLE indicates deterministic chaos. Using the above definition we expect that the LLE vanishes in the absence of an interaction potential $U(r)$ in Eqs.(6.30) since the tangent dynamics equations (6.35) becomes trivial. Note that the term $\boldsymbol{f}(t)$ does not contribute to Eqs.(6.35) which means that the precise functional form of "noise" has no influence on the chaotic properties of the system. Besides its theoretical interest, computing LLEs has to do also

with the possibility, at least in principle, of working out these quantities from experimental data. This could provide an additional observable to probe the presence of long-range intermolecular interactions. For numerical computations of the LLE Eq.(6.34) is replaced by:

$$\lambda = \frac{1}{N_{\text{step}}\Delta t} \sum_{m=1}^{N_{\text{step}}} \ln \frac{\|\boldsymbol{\zeta}_m\|}{\|\boldsymbol{\zeta}_{m-1}\|} \tag{6.36}$$

where N_{step} is the total number of integration steps and Δt is the time step. In practice, to compute the time evolution of the tangent vector in Eqs.(6.35) for $N = 1200$ particles (consequently for $3N = 3600$ degrees of freedom) amounts to computing about 6.5 millions of matrix elements of the Hessian of $U(r)$ for each time. This would be a very heavy computational task, thus we resorted to an old algorithm described in the celebrated paper [**?**]. This consists of considering a reference trajectory $\mathbf{x}(t)$ and of computing very short segments of varied trajectories $\tilde{\mathbf{x}}(t)$ issuing very close to this reference trajectory. Details are given in the quoted paper.

6.3 Numerical Results

In the present Section we report the effect of long-distance interactions on the diffusion behavior of a collection of molecules by analysing how D deviates from its Brownian value. The numerical integration of Eqs. (6.4) was performed using the model potentials given in Section 7.3.2, using the integration algorithm with periodic boundary conditions, and the IPS corrections to the interactions both described in Section 6.2.3. The computer code used was written in Fortran90, developed in a parallel computing environment. This program was run on a computer cluster for typical durations of 500 to 1500 hours (total CPU time) for each simulation. The overall CPU time needed for the results reported in this Section amounts to about 200000 CPU hours. All the simulations were performed considering a system of 1200 molecules (since we typically used 120 processors) of radius $R = 0.002\mu$m, at a temperature of 300K, with an integration time step $h = 0.001\mu$s and each computation consisted of $5 - 8 \times 10^6$ steps. In this paper, we use the following system of units: μm for lengths, kDa for masses (1kDa $= 6.0221 \times 10^{-20}$gr) and μs for time.

In our simulations we considered uniform random initial conditions to mimic a typical experimental setup wih a drop of aqueous solution of biomolecules. Then we considered the system in a bona-fide equilibrium state when, by integrating the dynamics, $\langle r^2(t)\rangle$ reached a stable linear time dependence on a millisecond time scale.

The values of the self-diffusion coefficient D have been obtained by means of a least squares fit of the time dependence of the MSD, that is, using the following fitting function:

$$\langle r^2(t)\rangle = b_0 + 6Dt \tag{6.37}$$

where the additive offset b_0 has no physical relevance, but has been included in order to better estimate the long time behavior of the MSD. In the following Sections, the values of D will be plotted normalized by the Brownian diffusion coefficient D_0. This coefficient is known a-

priori and is compared with the numerical outcome obtained for very low concentrations. These values are found to be in very good agreement within typical statistical errors of the order of $1/\sqrt{N} = 1/\sqrt{1200}$. As we will see in the following (see figures 6.2, 6.4, 6.10), the results for $\langle r^2(t)\rangle$ are to an excellent degree of approximation straight lines. Thus, the errors in determining the diffusion coefficient values are tiny, smaller than the size of the symbols referring to D. We will also see that, in addition to the standard source of diffusion represented by the random forces $\sqrt{2\gamma k_B T}\boldsymbol{\xi}_i(t)$, another source of diffusion is given by the intrinsic chaoticity of the particle dynamics stemming from the interparticle interactions. The latter contribution to diffusion does not alter the linear time dependence of the MSD. This circumstance is not new and has been reported in many examples of chaotic diffusion [PVM+88, OP91, OPB85, OC90, CFVP91]. To give a measure of spatial correlation in the simulated system we calculated the radial distribution function $g(r_n)$ defined as:

$$g(r_n) = \frac{1}{N}\sum_{i=1}^{N}\left[\frac{\mathcal{N}_{i,r_n}}{\frac{4\pi}{3}(n^3-(n-1)^3)\rho\delta^3}\right] \quad n = 1, ..., N_{Bin} \tag{6.38}$$

where $\mathcal{N}_{i,r_n}$ represents the number of particles at an "effective" distance $r \in [r_n - \delta; r_n + \delta)$ from the i-th particle (*i.e.* taking into account also different images of the system for PBC), with $\delta = L/(2N_{Bin})$, $r_n = (2n-1)\delta$ and $\rho = N/L^3$. Although the function $g(r_n)$ has a discrete domain, we will refer to it as $g(r)$ for the sake of simplicity and as we set $N_{Bin} = 1000$. We calculated the distance between all pairs of molecules and binned them into an histogram normalized to the density of the system. This function gives a measure of the spatial correlation in the system since it is proportional to the probability of finding a molecule at a given distance r from another one. In addition we have measured the Lyapunov exponent, according to what is given in Section 6.2.6, and the correction to the Brownian value D_0, according to Eq.(6.29).

6.3.1 Excluded volume effects

As we already said, we aim at investigating the different possible sources of deviation from Brownian diffusion, thus we begin with the most simple possibility: excluded volume effects at the foreseen experimental conditions.

We considered hard-spheres with vanishing intermolecular potential, $U = 0$, and modelling impenetrability as follows: whenever two molecules i and j get in touch and interpenetrate at some time t (that is $|\boldsymbol{r}_i(t) - \boldsymbol{r}_j(t)| < 2R$, with R the radius of each molecule) we get back to $t - h$ and redraw the $\boldsymbol{\xi}_i(t)$ until $\boldsymbol{r}_{i,j}(t)$ are such that the impenetrability condition is satisfied. In Figure 6.1 we can see that the excluded volume effects on diffusion coefficient D normalized with the Brownian value D_0 are very small. These results agree with the theoretically predicted values [Yos85] according to which $D = D_0[1 - 2\phi]$ where $\phi = 1/6\pi R^3 n$ and $n = N/L^3$ is the number density.

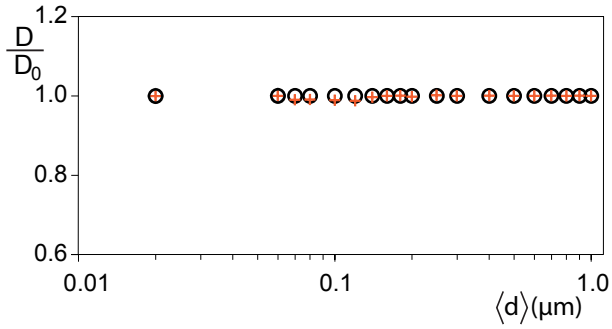

Figure 6.1: Excluded volume simulations. Semi-log plot of the normalized theoretical self diffusion coefficient D/D_0 (open circles) computed according to [Yos85] compared to the outcomes of the standard numerical simulations (crosses) given by [Eqs.(7.18) and (6.37)] versus the average distance between the particles with vanishing intermolecular potential.

6.3.2 Effects of long and short range electrostatic interactions at fixed average intermolecular distance

The next step is obtained by switching on interparticle interactions, keeping fixed all the parameters (temperature, viscosity, average interparticle distance, Debye length) but the number of charges Z. This way, we can vary only the intensity of the interparticle forces measuring the largest Lyapunov exponent and how D deviates from Brownian motion. To begin with, the screened Coulomb potentials defined in Eq.(7.3) have been considered for an average intermolecular distance $\langle d \rangle = 0.04\mu$m and a Debye length $\lambda_D = 0.01\mu$m. In Figure 6.2 and in Figure 6.3, we report the outcomes of these numerical simulations.

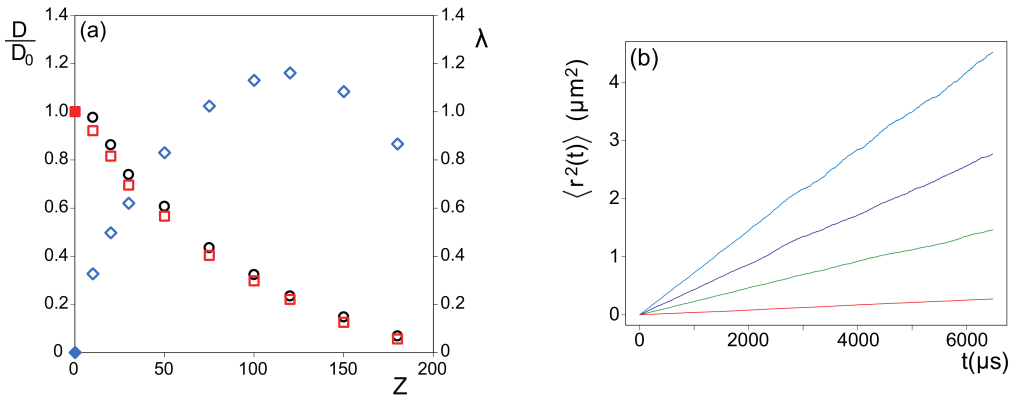

Figure 6.2: (a) Normalized self diffusion coefficient D/D_0 (circles) computed according to [Eq.(6.29)] compared to the outcomes of the standard computation (squares) according to [Eqs.(7.18) and (6.37)] versus the number of charges Z of the particles interacting through Coulomb potential with $\lambda_D = 0.01\mu$m [Eq.(7.3)] at average interparticle distance $\langle d \rangle = 0.04\mu$m. On the second axes we report the largest Lyapunov exponent [Eq.(6.36)] (rhombus). Full symbols represent the corresponding theoretical values for vanishing Z value.(b) Plot of the time evolution of the simulated MSD for different values of charge. The charge Z increases starting from the top line that corresponds at $Z = 10$, passing to $Z = 50$, to $Z = 100$, up to the bottom line corresponding at $Z = 180$.

In Figure 6.2(a) we can see that the stronger the interparticle interaction the larger the deviation from the Brownian diffusion, that is stronger decrease of the diffusion coefficient D. The degree of chaoticity, represented by the largest Lyapunov exponent, is also affected by the strength of the interparticle interaction. At the same time, the time dependence of the MSD remains linear, that is, the chaotic diffusion still follows the Einstein-Fick law [CFVP91], as it can be seen in Figure 6.2(b). The decreasing of the diffusion coefficient occurring in presence of repulsive interactions is due to the fact that the molecules uniformly fill all the accessible volume, thus, since there is no room for a free expansion of the system, the motion of any given molecule is somewhat hindered and slowed down by the surrounding ones. On the contrary, in presence of repulsive forces an increase of diffusion is expected when measured by mutual diffusion coefficient [TP92]. The latter describes the decay of a concentration fluctuation and it is intuitive that under the action of repulsive forces a local higher density of particle diffuses faster than a Brownian diffusion. We can also observe a strikingly good agreement between the values of D obtained through the time dependence of the MSD and by computing the theoretical corrections to Brownian value D_0 due to deterministic forces, according to Equation (6.29). The behavior of the Lyapunov exponents (Figure 6.2(a)) is characterized by an initial increase of the chaoticity of the system with a bending - towards lower values - beginning around $Z = 120$. Such results can be qualitatively understood with the aid of the radial distribution functions $g(r)$ reported in Figure 6.3. The pattern of $g(r)$ shows a transition from a gaseous-like system to more and more spatially correlated systems with increasing Z. The higher Z, the larger the range of spatial ordering as indicated by a larger numbers of peaks displayed by the function $g(r)$ at distance values which are multiples of the average intermolecular distance. This is similar to a transition from a gaseous-like state system to higher spatial ordered systems (like a liquid or possibly a glass).

We can surmise that the behaviour of the LLE is due to the competition between the chaotic dynamics and the spatial ordering. To better elucidate this phenomenology, we have considered the unscreened Coulomb potential.

The results reported in Figures 6.4 and 6.5 have been obtained by means of the Coulomb potential defined in Eqs.(7.15) and (7.17) having kept constant all the parameters (as above with $\langle d \rangle = 0.04\mu$m) with the exception of the number of charges Z.

Likewise to Figure 6.2, we can observe that the stronger the interparticle interaction, the larger the deviation from Brownian diffusion, with a linear time dependence of the MSD for all the charge values used in these simulations, as shown in Figure 6.4(b). The increase of the strength of chaos, measured by Lyapunov exponents, observed between $Z = 10$ and $Z = 50$ (Figure 6.4(a)) is related to the increase of the strength of intermolecular interactions. This corresponds to a gaseous-like state of the system as shown by the first panel of Figure 6.5. In the second panel of the same Figure, the maximum value reached by the LLE, at $Z = 50$, is attained when a sufficient degree of spatial order sets in so that it competes with dynamical chaos of the gaseous-like phase. The strong decrease of the LLE observed from $Z = 75$ is due to a further enhancement of spatial order, as shown by the $g(r)$ in the third panel of Figure 6.5. The fourth panel of the same Figure shows a crystal-like arrangement of the molecules confirmed

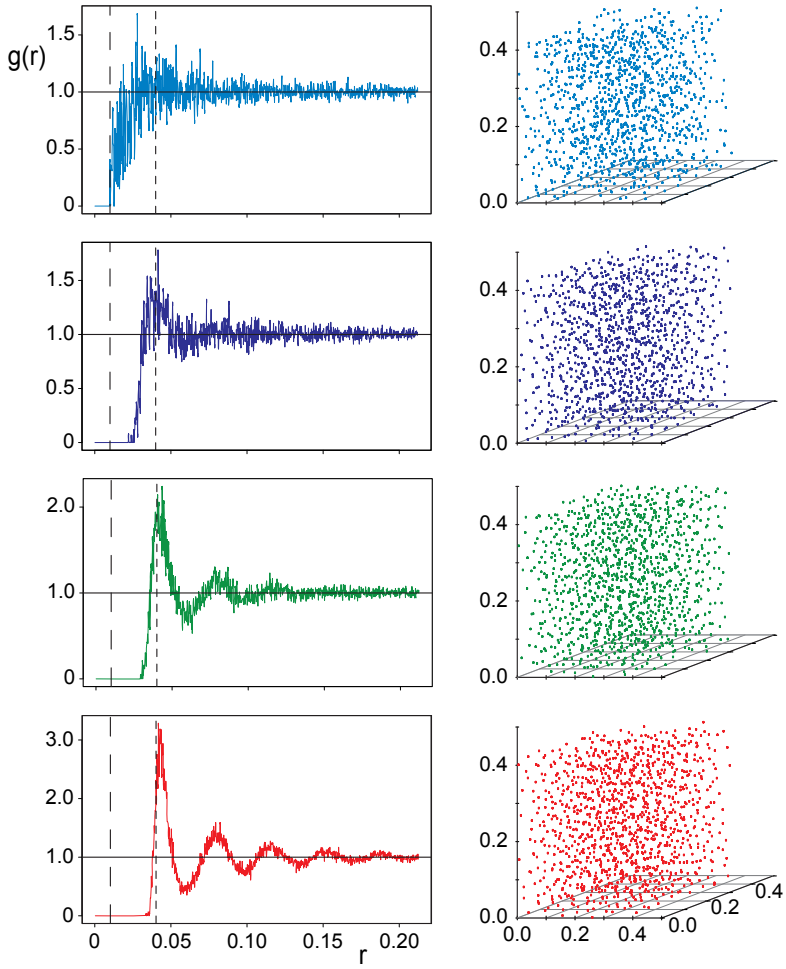

Figure 6.3: Radial distribution function $g(r)$ [Eq.(6.38)] and particles position snapshots at the final simulation time for four charge values of Figure 6.2 starting from the top with $Z = 10$ on the first line, $Z = 50$ on the second line, $Z = 100$ on the third line and $Z = 180$ on the last one. Large dashed black line correspond to $r = \lambda_D = 0.01\mu$m while short dashed black line correspond to the $r = \langle d \rangle = 0.04\mu$m. Full black line show the value $g(r) = 1$. In the left panels the units of r are μm, as well as the units of the snapshots axes to the right.

by the pattern of the function $g(r)$ [**?**]. Moreover for $Z \geq 120$ the LLE drops to values very close to zero with a pattern displaying a seemingly sharp transition. Correspondingly, the diffusion coefficient also drops to zero after a monotonous decrease from its Brownian value at $Z = 0$. Finally, the values of D/D_0 given by Eq.(6.29), reported in Figure 6.4(a), are again in very good agreement with the outcome of the standard computation; a growing discrepancy is observed in the above mentioned transition occurring at $Z = 120$ where the degree of chaoticity is close to vanishing.

6.3.3 Effects of long and short range electrostatic interactions at fixed charge value

Let us now consider the effect of changing the interaction strength resulting from a variation of the average intermolecular distance and a variation of the action radius of electrostatic forces.

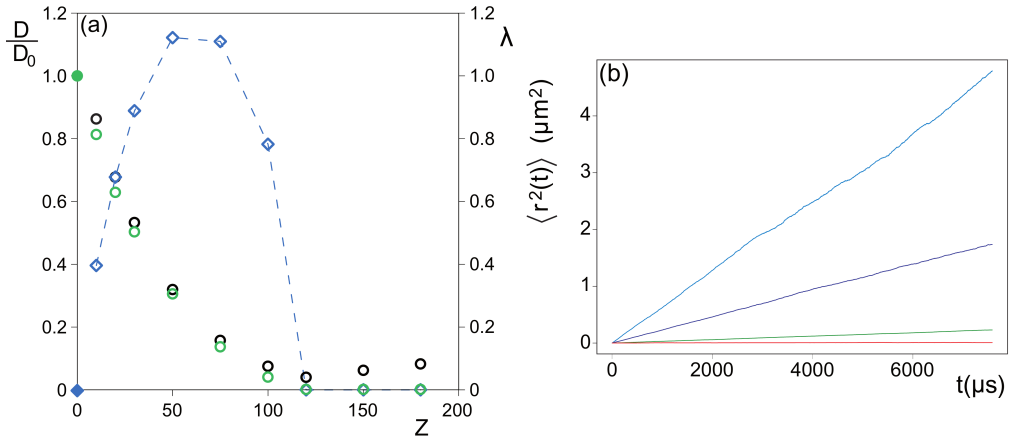

Figure 6.4: (a) Normalized self diffusion coefficient D/D_0 (black circles) computed according to [Eq.(6.29)] compared to the outcomes of the standard computation (grey/green circles) according to [Eqs.(7.18) and (6.37)] versus the number of charges Z of the particles interacting through a pure Coulomb potential [Eq.(7.15)] at average interparticle distance $\langle d \rangle = 0.04\mu$m. On the second axes we report the largest Lyapunov exponent [Eq.(6.36)] (rhombus). Full symbols represent the corresponding theoretical values for vanishing Z value. (b) Plot of the time evolution of the simulated MSD for different values of charge. The charge Z increases starting from the top line that corresponds at $Z = 10$, passing to $Z = 50$, to $Z = 100$, up to the bottom line corresponding at $Z = 180$.

This is obtained by using different Debye lengths ($\lambda_D = 0.001$ and 0.01 μm) for the screened Coulomb potential defined in Eq.(7.3) and by using the Coulomb potential defined in Eqs. (7.15) and (7.17) ($\lambda_D = \infty$), for different charge values ($Z = 10$ and $Z = 100$). The choice of these parameter values is partially inspired, on the one side, by the typical range of values of charges for proteins ($Z = 10$ is a reasonable value for many proteins at physiological pH) and for small fragments of nucleic acids (each pair of nucleotides brings about 2 unbalanced electron charges), and, on the other side, the lowest value $\lambda_D = 0.001$ μm is approximately the Debye length of the cytosol while longer Debye lengths are relevant for prospective in vitro experiments. Let us remark that even though electrostatic attractive interactions play a role in biological contexts, in view of the experimental setups we envisage to detect long-range electrodynamic interactions, the use of *identical particles* is the most favourable to begin with (in fact, the excitation of collective vibrations of identical particles necessarily entails resonance: all of them vibrate with the same frequency spectrum). As a consequence we have considered only repulsive electrostatic interactions.

Figure 6.6 summarizes the dependence of the normalized mean diffusion coefficient as a function of the average distance among the molecules. Different values of λ_D are considered for $Z = 10$ (Fig.6.6 (a)) and $Z = 100$ (Fig.6.6 (b)). We can observe that at low concentrations diffusion reaches its Brownian limit characterized by $D/D_0 \simeq 1$, and the larger the Debye length and the number of charges, the larger the decrease of the diffusion coefficient. It turns out that an appreciable change in the diffusion coefficient shows up for $\lambda_D \geq 0.01\mu$m. The outcomes of numerical computations obtained for $Z = 100$ and $\lambda_D = \infty$ are reported also in Figure 6.7 and compared with the values of the LLE and of the outcomes of the theoretical correction to

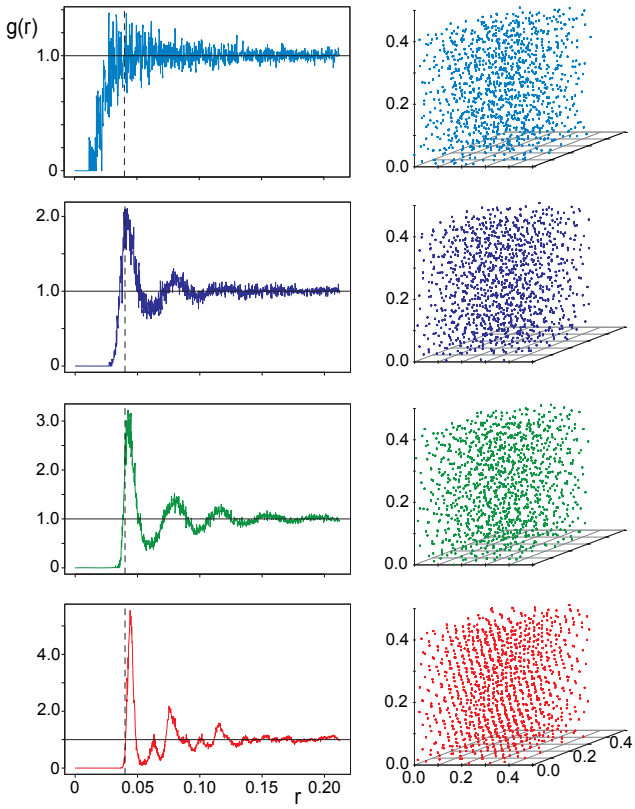

Figure 6.5: Radial distribution function $g(r)$ [Eq.(6.38)] and particles position snapshots at the final simulation time for four charge values of Figure 6.4 starting from the top with $Z = 10$ on the first line, $Z = 50$ on the second line, $Z = 100$ on the third line and $Z = 180$ on the last one. Short dashed black line correspond to the $r = \langle d \rangle = 0.04\mu$m. Full black line show the value $g(r) = 1$. In the left panels the units of r are μm, as well as the units of the snapshots axes to the right.

the Brownian diffusion coefficient ((6.29)). At very high dilutions corresponding to an average interparticle distance larger than 10 μm, the diffusion is Brownian while at shorter interparticle distances the effect of electrostatic interactions is again a decrease of the diffusion coefficient up to a concentration corresponding to $\langle d \rangle = 0.03$ μm where diffusion stops. By resorting to the computation of the radial distribution functions we observe the same phenomenology reported in Figure 6.5, that is, in the case of Brownian diffusion the corresponding radial distribution function closely resembles to that in first panel of Figure 6.5. When diffusion deviates from being purely Brownian the radial distribution shows regular peaks as in the second and third panel of Figure 6.5 and it looks like that in the fourth panel of Figure 6.5 when diffusion stops. At the same time, we observe an increase of the LLE which corresponds to the decrease of D up to the point where D vanishes. When D vanishes, a sudden drop of the LLE is observed to practically zero values. Finally, we observe a very good agreement of the theoretical correction to the Brownian diffusion coefficient except when diffusion stops; this suggests that a developed chaoticity of the dynamics is a requisite for such a computation to be reliable. In other words when the largest Lyapunov exponent becomes exceedingly small the requirement that the dynamics has to be self-averaging is no longer fulfilled.

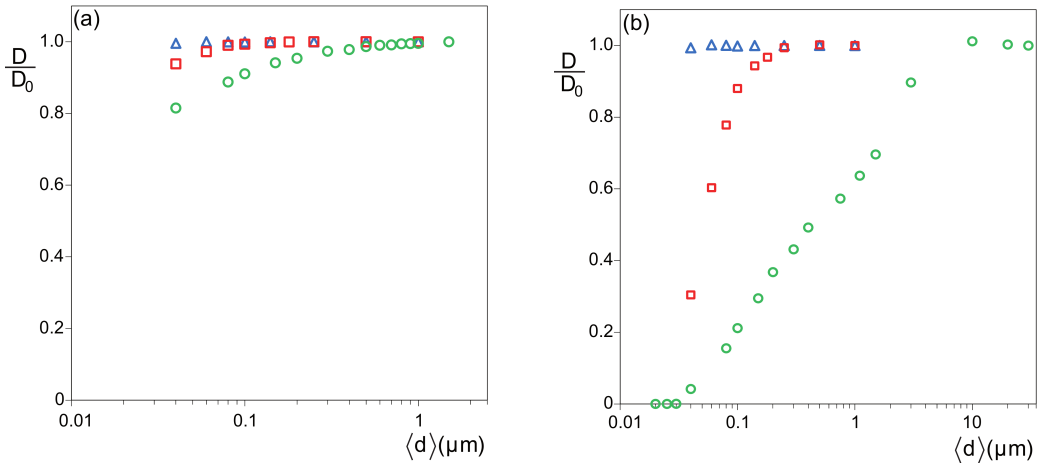

Figure 6.6: Semi-log plot of the normalized self-diffusion coefficient D/D_0 versus the average distance of the particles interacting through Coulomb potentials [Eqs.(7.15) and (7.17)] for different combinations of λ_D values at $Z = 10$ (panel(a)) and $Z = 100$ (panel (b)). The symbols indicate the Debye length values: $\lambda_D = 0.001\mu$m correspond to triangles, $\lambda_D = 0.01\mu$m to squares and $\lambda_D = \infty$ to circles.

6.3.4 Long range attractive dipolar effects

As remarked in the Introduction, we are interested in verifying the experimental detectability of long-range interactions among molecules of biological interest through their diffusive behaviour. In this Section, we focus on the study of diffusive and dynamical properties of the system when both electrostatic Debye potential, described in Eq.(7.3), and attractive dipole-dipole electrodynamic potential, described in Eqs. (6.11) and (6.20), are involved. The choice of considering the simultaneous presence of these two kinds of interactions is motivated by the fact that biomolecules are charged objects with non-vanishing dipolar moments.

The dynamical properties and diffusive behaviour in presence of an attractive interaction are qualitatively different from those observed in the previous sections regarding only the repulsive Coulomb potential. For the sake of clarity, we present and compare the combined presence of Coulomb and dipole-dipole electrodynamic potentials (represented by full symbols) with the presence of only Coulomb potential (represented by open symbols), the latter already presented in the previous Section. The kind of symbol corresponds, as before, to the different Debye length values: triangles correspond to $\lambda_D = 0.001$ μm and squares to $\lambda_D = 0.01$ μm. In Figure 6.8 the numerical outcomes for the normalized diffusion coefficient, D/D_0, are reported as a function of the average intermolecular distance for two charge values, $Z = 10$ (Fig. 6.8(a)) and $Z = 100$ (Fig. 6.8(b)) and different values of the Debye lengths, both in presence and in absence of dipole-dipole electrodynamic potential. At very high dilutions, in a range between $\langle d \rangle = 1\mu m$ and $\langle d \rangle = 0.2\mu m$ the diffusion follows its Brownian limit characterized by $D/D_0 \simeq 1$ for each combination of charge or potential as observed in both panels of the aforementioned figure. Let us resume first the results when only Coulomb potential is involved; in order to observe a significant deviation from the Brownian limit the Debye length must be at least equal to 0.01 μm (open squares) with a more pronounced effect for $Z = 100$ where the deviation from Brownian motion reaches $D/D_0 \simeq 0.3$. To begin with, we switch on the dipolar potential

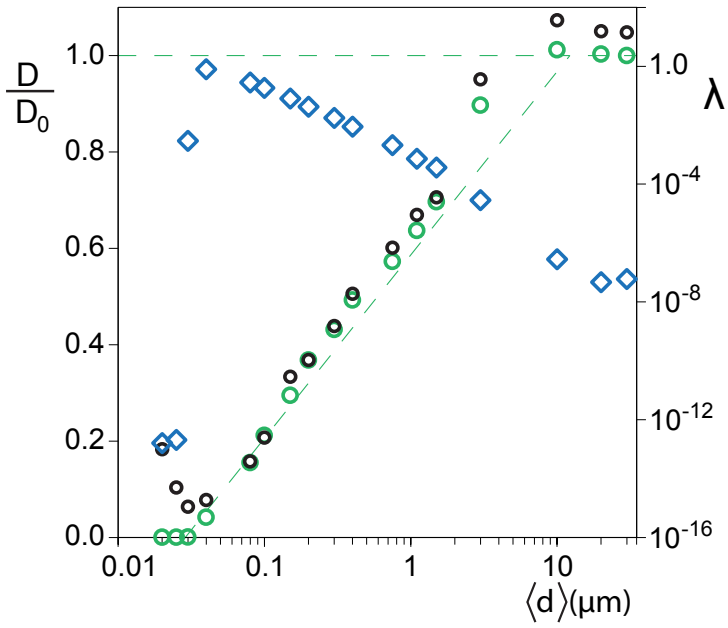

Figure 6.7: Semi-log plot of the normalized self-diffusion coefficient versus the average distance of the particles interacting through Coulomb potential [Eqs.(7.17)] with $Z = 100$. The normalized self diffusion coefficient D/D_0 (black circles) computed according to [Eq.(6.29)] is compared to the outcomes of the standard computation (grey/green circles) according to [Eqs.(7.18) and (6.37)]. On the second axes we report the largest Lyapunov exponent [Eq.(6.36)] (rhombus). The dashed lines are guides to the eye.

focusing on the lower charge value, $Z = 10$ (Fig. 6.8(a)). We can observe a sharp decrease of the normalized diffusion coefficient, with a transition between a diffusive Brownian motion and an absence of diffusion.

These results are independent of the action radius of Coulomb potential, in fact no difference has been observed between the two different Debye length values. The results reported in Figure 6.8(b)) are obtained by switching on the dipolar potential and by increasing the intensity of Coulomb potential (taking $Z = 100$). When the Coulomb interactions is weak ($\lambda_D = 0.001$ μm full triangle), so that the dipolar contribution overcomes it, we can observe the same aforementioned sharp transition characterized by no diffusion.

On the contrary, with a larger Debye length ($\lambda_D = 0.01$ μm full square) the effects of a competition between the two potentials, repulsive and attractive respectively, are observed when the average intermolecular distance is varied. At large average intermolecular distances the particle motions are practically independent one from the other resulting in a Brownian diffusion, while at shorter distances the mutual interactions play an important role. The interplay between the repulsive and attractive interactions leads to a diffusion behaviour dominated by the dipolar interactions in a small range of distances in correspondence of the transition from $D/D_0 \simeq 1$ to $D/D_0 \simeq 0$, as it is observed in Figure 6.8(a). At smaller values of $\langle d \rangle$, the dipolar effect on diffusion is balanced by the presence of short-range Coulomb repulsion, thus preventing the formation of a clustered system. In Fig.6.9, we report the outcomes of numerical computations of D/D_0 *versus* $\langle d \rangle$ obtained in the case of a dominant dipolar potential with respect to the Coulomb one ($Z = 100$ and Debye length $\lambda_D = 0.001$ μm).

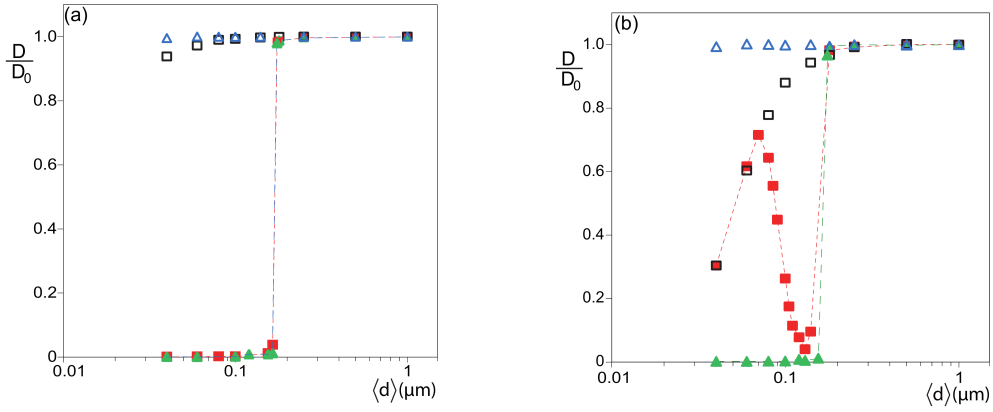

Figure 6.8: Semi-log plot of the normalized self-diffusion coefficient D/D_0 versus the average distance of the particles interacting only through Coulomb potential [Eq.(7.15)] and through Coulomb potential and the attractive dipole-dipole potential [Eq.(6.20)] for different combinations of λ_D values at $Z = 10$ (panel (a)) and $Z = 100$ (panel (b)). The symbol shapes indicate the Debye length values, $\lambda_D = 0.001\mu$m correspond to triangles and $\lambda_D = 0.01\mu$m to squares, while open symbols represent Coulomb potential and full ones the combined action of Coulomb and dipole-dipole potentials.

In the same figure, we add to D/D_0, the values of the LLE and of the outcomes of the theoretical correction to the Brownian diffusion coefficient due to interparticle interactions (Eq. (6.29)). This figure shows a good agreement between the theoretical correction to D_0 and the numerical results. We can also observe that the transition from a diffusive to a non-diffusive behavior goes with a sharp increase of the LLE, indicating a transition from a non-chaotic to a chaotic dynamics. Note that, in the transition region, fluctuating patterns of the LLE and of the theoretical correction to D_0 are found.

While the regular oscillation of D/D_0 versus $\langle d \rangle$ is due to a competition between two forces of opposite sign repulsive electrostatic and attractive dipolar), the oscillation of the Lyapunov exponent below the transition has only a *qualitative* meaning. The clustering transition is reminiscent of a phase transition, implying the well known phenomenon of the critical slowing down of dynamical variables correlation. We can thus surmise that in this region, the dynamics displays long transients to the final clustered configurations, so that memory of the initial conditions could be kept as is confirmed by numerical simulations performed with different initial conditions. However, knowing the exact shape of λ versus $\langle d \rangle$ would not add any relevant information with respect to the aims of the present work.

In Fig.6.10 the radial distribution functions of the particles and the snapshots of their positions are given. These results refer to two average interparticle distances and confirm a transition from a gaseous-like state to a clustered configuration. Summarizing, the diffusion quasi-arrest is always connected to the occurrence of large clusters, as shown by the lower panels in the center and right sides of Figure 6.10. The clustering phenomenon associated with a sudden drop of the diffusion coefficient at some critical average distance among the particles is very sharp (Figure 6.9). This is strongly reminiscent of a *phase transition* due, as usual, to the competition between the entropic driving toward thermal disorder and the determistic forces

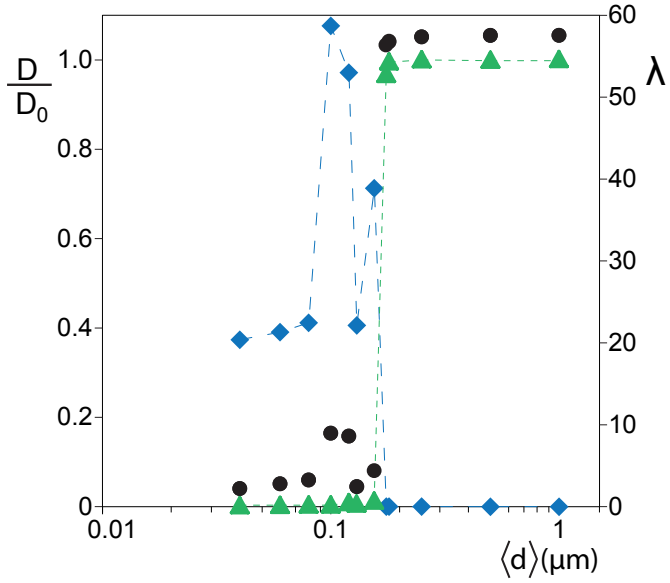

Figure 6.9: Semi-log plot of the normalized self-diffusion coefficient versus the average distance of the particles interacting through Coulomb and dipolar potential [Eqs.(7.15) and (6.20)] with $Z = 100$ and $\lambda_D = 0.001\mu$m. The normalized self-diffusion coefficient D/D_0 (circles) computed according to [Eq.(6.29)] is compared to the outcomes of the standard computation (triangles) according to [Eqs.(7.18) and (6.37)]. On the second axes we report the largest Lyapunov exponent [Eq.(6.36)] (rhombus).

trying to make order in the system. In the clustered phase the particles are confined in definitely smaller space and, in spite of the appearance of chaos due to the deterministic forces that drive the clustering, the particles are not free to move everywhere as in the gaseous phase, thus diffusion is hindered. Finally, let us note that the results presented in the current section indicate a possibility to disentangle the effects of electrostatic and electrodynamic interactions. In fact, by using a sufficiently high ion concentration in prospective experiments, and so weakening the electrostatic forces, only the effects of electrodynamic interactions would be observed.

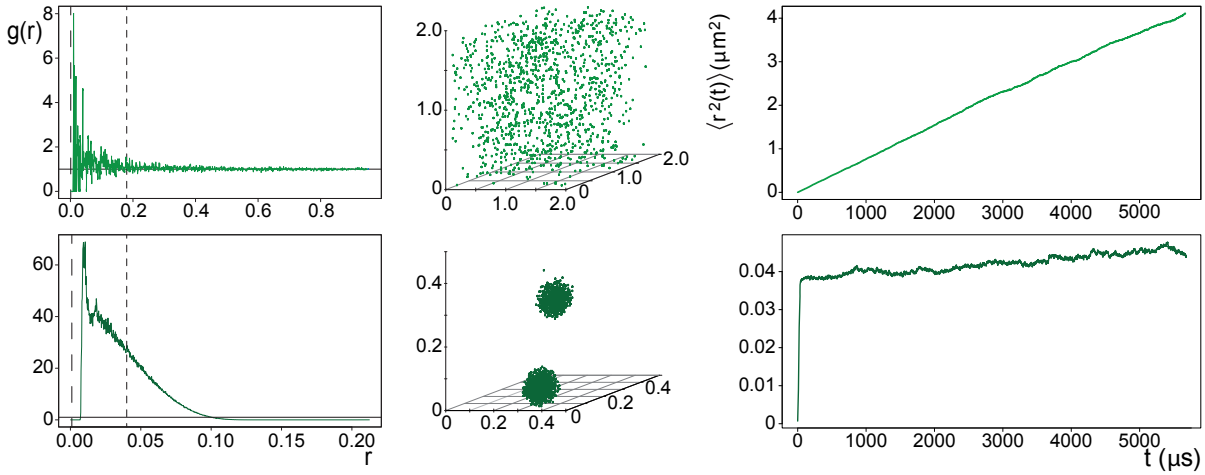

Figure 6.10: Radial distribution function $g(r)$ [Eq.(6.38)], particles position snapshots at the final simulation time and mean square displacement versus time at two average interparticle distance $\langle d \rangle = 0.18\mu$m (first line) and $\langle d \rangle = 0.04\mu$m (second line) for particles of $Z = 100$ interacting with a Coulomb potential [Eq.(7.15) with $\lambda_D = 0.001\mu$m] and with a dipolar potential [Eq.(6.20)]. The large dashed black line corresponds to $r = \lambda_D$ while short dashed black line corresponds to the $r = \langle d \rangle$. The full black line shows the value $g(r) = 1$. In the left-hand panels the units of r are μm, as well as the units of the snapshots axis to the right. In the right-hand panels, the units are μm^2 for the MSD and μs for the time.

6.4 Conclusions and perspectives

In previous sections a work aimed at assessing the experimental possibility of detecting long-range electrodynamic interactions between biomolecules is presented. It consists of a conceptual proof of feasibility of an experimental approach resorting to an actually measurable observable. In particular, this observable is the diffusion coefficient that can be measured by means of several available techniques like pulsed-field gradient nuclear magnetic resonance forced Rayleigh scattering (FRS),Fluorescence Recovery After Photobleaching (FRAP) and Fluorescence Correlation Spectroscopy (FCS) to mention some of them. The long-range electrodynamic forces we are after have been hitherto elusive to observation in spite of many studies on the diffusion behaviour of biomolecules in solution. In order to achieve the above mentioned assessment about experimental detectability of electrodynamic intermolecular interactions, we have performed numerical simulations whose outcomes can be summarized as follows:

1. We have found that, for dilute systems ($\langle d \rangle$ ranging from about 400Å up to 30000Å), the diffusion coefficient is sensitive to all the interactions considered. Starting with a uniform distribution of molecules in all the accessible volume, an interesting phenomenon is observed: the diffusion coefficient decreases independently of the repulsive or attractive nature of the molecular interactions (repulsive Coulomb with and without screening, attractive electrodynamic dipole-dipole).

2. Moreover, we observed that, in the gaseous-like phase, a decrease of the diffusion coeffi-

cient is always accompanied by an increase of chaos. On the contrary, when spatial order sets in, a decrease of the diffusion coefficient is always accompanied by a decrease of chaos. Even though it is well known that no simple relation exists between Lyapunov exponents and transport properties in dynamical systems, the qualitative correspondences observed are consistent with the intuitive idea that both phenomena are related to the intensity of intermolecular interactions.

3. Nice transitional phenomena have been observed: for Coulomb interactions a first transition from purely stochastic diffusion to chaotic plus stochastic diffusion is found; then, at sufficiently high concentrations, a spatial ordering of the molecules is found resembling to a crystal-like structure. For dipole-dipole interactions an abrupt clustering transition is observed, which is strongly reminiscent of an equilibrium phase transition.

4. The simple theoretical model proposed in Section 6.2.5 gives the good values of the diffusion coefficients computed along the dynamics in presence of intermolecular interactions within a few percent of error. This result paves the way - at least in principle - to analytic predictions if the time averages used in this work are replaced by statistical averages Eq.(6.8) worked out with the Boltzmann-Gibbs weight Eq.(6.6) (which is the stationary measure associated with our model equations).

From the experimental point of view, which was the main motivation of the this work work, we conclude that the variations of the diffusion coefficient D with respect to its Brownian value, as well as the patterns of D versus the average interparticle distance $\langle d \rangle$, are such that the practical possibility exists of experimentally tackling the problem of interest by means of, for example, one of the above mentioned techniques.
Let us conclude with a remark about the applicability of the above reported results to two-dimensional systems like, for example, protein diffusion on lipid membranes. The same kind of computations reported above can be performed also in two dimension. But a-priori we expect non-trivial differences between the two and three dimensional cases, for example, the potential $1/r^3$ is long-range in three dimension but short-range in two dimension because in the latter case the exponent 3 is larger than the spatial dimension. Another example of a difference is that in the absence of deterministic interactions a random "walker" in one and two dimension will always almost surely return to the starting point, whereas this is not the case in three dimension because after a theorem due to Polya the probability to return to the origin drops to about 0.34, and this of course affects also the encounter probability of two different objects.

CHAPTER 7 Validation of Fluorescence Correlation Spectroscopy measures for detection of long-range interactions

The present chapter reports about the third and last step of a feasibility study (cfr. [PFN+12] and [NSP+14]) concernng a possible strategy to detect long range electrodynamic forces acting among biomolecules.

7.1 Motivations

The experimental technique envisaged at the end of previous chapter was Fluorescence Correlation Spectroscopy (FCS), a well established experimental technique [MW74, HS07, Els11]. In the present paper we report about this kind of experimental investigation carried on molecules which interact through built-in long range interactions, that is, an electrostatic force field. The interacting molecules (a protein, Lysozyme, and an oppositely charged dye, Alexa488) are solvated in pure water, thus in the absence of Debye screening, and in salted water to confirm that the concentration dependent attenuation of the self diffusion coefficient is due to the electrostatic interparticle interactions. Molecular Dynamics simulations have been also performed, and their results are in excellent agreement with the experimentally observed phenomenology. We conclude that the FCS technique is actually a viable experimental procedure for an assessment of the strength - thus of the potential biological relevance - of resonant electrodynamic intermolecular interactions.

7.2 Experimental measures of self-diffusion coefficient of biomolecules interacting by Fluorescence Correlation Spectroscopy (FCS)

7.2.1 A brief review on FCS

The Fluorescence Correlation Spectroscopy is the experimental technique used to study diffusion of mutual interacting molecules: a brief review on some basic facts on this techniques are presented in what follows[1]. This techniques is applied to investigate diffusion of fluorescent diffusing particles[2] FCS provides a direct measure of a time-domain signal of fluorescence emitted by fluorescent particle traversing a microscopic observation volume. The average time

[1]Concepts and principles of Fluorescence Correlation Spectroscopy (FCS) has been developed by Magde, Elson, and Webb at beginning of ′70s [MEW72],[MEW74],[EM74] and subsequently refined using know-how on Dynamic Light Scattering [BP76] [AP76].

[2]Fluorescence consists in light emission by an atom or a molecule in an excited electronic state. Light emission takes place within 1ns from the radiation absorption (so the creation of the excited state): the emitted light has a lower frequency respect to the absorbed one as a part of the energy is converted in vibrational energy (Stokes shift).

$\langle\tau\rangle$ need for a particle to traverse the volume can be indirectly measured by the analysis of the correlation of fluctuations of the signal. The set-up of FCS is reported in fig.7.1.

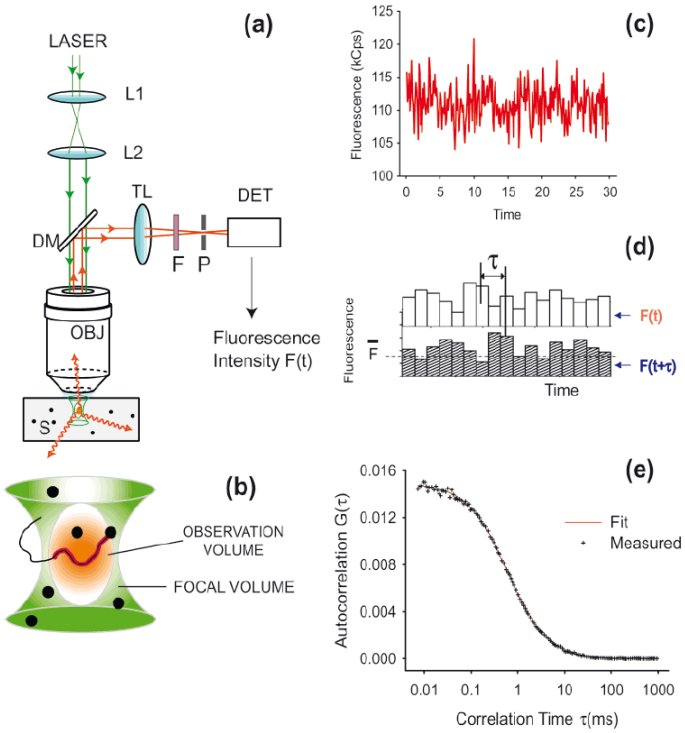

Figure 7.1: FCS set-up.(a) A laser beam is initially dispersed and then focalized by a high numerical aperture microscope objective (OBJ) on a fluorescent sample (S). The epifluorescence is collected by the same objective, reflected by a diachroic (DM), focalized by a tubular lens (TL), filtered (F), and finally detected (DET) after it passed through a confocal opening. (b) Details of the focal volume (green) where the diffusing marked particles (black spot) are observed.(c) Typical detected fluorescence detected signal as a function of time for green rhodamine (RG) at the wavelength $\lambda = 488$ nm. (d) Part of the same signal of fig.(c) The signal is self-correlated at a delayed time (t + τ) to derive the autocorrelation function G(τ). (e) The derived G(τ) allows to derive the average crossing time $\langle\tau\rangle$. (Adapted by [HHHW02]).

The autocorrelation function $G(\tau)$, originated by molecules interacting and diffusing in and out of the observation volume, is defined by

$$G(\tau) = \frac{\langle \delta F(t) \delta F(t+\tau) \rangle}{\langle F(t) \rangle^2}$$

where $\langle F(t) \rangle$ is the average intensity, $\delta F(t)$ the intensity of fluctuations, and the brackets mean ensemble average. The general procedure consists in fitting $G(\tau)$ with the appropriate mathematical model describing the characteristics of the system under study. The analytical form of the autocorrelation function (ACF) for a single molecular species, assuming a three-dimensional Gaussian profile of the excitation beam accounting for diffusion [MW74] and a triplet state of the dye [WMR95], is obtained under the assumption that diffusion driven by random hits of water molecules and protein-dye dynamics driven by electrostatic forces are

independent processes:

$$G(\tau) = 1 + \frac{1}{N} \frac{1 + n_T \exp\left(-\frac{\tau}{\tau_T}\right)}{\left(1 + \frac{\tau}{\tau_D}\right)\sqrt{1 + s^2 \frac{\tau}{\tau_D}}} \ . \tag{7.1}$$

Here N stands for the number of molecules in the FCS observation volume, τ_D is the diffusion time through this volume, τ_T the triplet lifetime, $n_T = Tr/(1 - Tr)$, with Tr the fraction of molecules in the triplet state. The dimensionless parameter s, called structure parameter, describes the spatial properties of the detection volume. It is given by $s = \omega_{x,y}/\omega_z$, where the parameter ω_z is related to the length of the detection volume along the optical axis, and the radial waist $\omega_{x,y}$ is related to the radius of its orthogonal section. The diffusion coefficient D is expressed as a function of the radial waist $\omega_{x,y}$, and of the diffusion time τ_D by:

$$D = \omega_{x,y}^2/4\tau_D \ . \tag{7.2}$$

7.2.2 How characterize long-range interaction with FCS experiments

In the present Section we report about the effect of electrostatic long distance intermolecular interactions on the diffusion behaviour of oppositely charged molecules. Molecular diffusion is detected using FCS.

The interacting molecules considered in the present study are Lysozyme, a small globular protein of 14307 KDa [Can63, Jol69] keeping a net positive charge for all pH values up to its isoelectric point, which is around pH = 11.35 [WD51], and Alexa Fluor 488 dye (hereinafter AF488) a very bright anionic fluorophore. FCS is a well established spectroscopic technique that enables a real time investigation of diffusion processes through a statistical analysis of the fluctuating fluorescence signal detected [MW74, HS07, Els11, RE12, HHHW02]. Self diffusion is affected by any interaction among the diffusing species, repulsive or attractive, that produce an attenuation depending on the interparticle interaction; the stronger the interaction the larger the deviation from Brownian diffusion [NSP+14]. The experimentally accessible parameters to implement this study are the average intermolecular distance $\langle d \rangle$ and the ionic strength of the electrolytic solution used, as already discussed in [NSP+14]. The average intermolecular distance among molecules changes with their concentration as $\langle d \rangle = C^{-1/3}$, where C is the total number of molecules per reaction volume. The electrostatic interaction among the molecules in electrolytic solution is described by the Debye-Hückel potential (see the previous chapter):

$$U_{\text{Debye}}(\mathbf{r}) = \frac{Z_1 Z_2 (e)^2}{\varepsilon_r |\mathbf{r}|} \cdot \frac{\exp\left[-\frac{2R}{\lambda_D}\left(\frac{|\boldsymbol{r}|}{2R} - 1\right)\right]}{(1 + R/\lambda_D)^2} \ , \tag{7.3}$$

where λ_D is the Debye screening length of the electrolytic solution, R is the molecular radius, e is the elementary charge and ε_r is the static dielectric constant of the medium. For a monovalent electrolyte, like NaCl which has been used throughout this study, the Debye length in Eq.(7.3)

reduces to:

$$\lambda_D = \sqrt{\frac{\varepsilon_r \varepsilon_0 k_B T}{2 N_A e^2 I}} \ . \tag{7.4}$$

where ε_0 is the vacuum permittivity, k_B is the Boltzmann constant, N_A is the Avogadro constant and I is the ionic strength. Debye screening-due to small ions freely moving in the environment-is an essential feature of biological systems because it shortens the range of electrostatic interactions. In the limiting case of $\lambda_D \to +\infty$, charged particles in electrolytic solution are submitted to a pure Coulomb potential given by:

$$U_{\text{Coul}}(\boldsymbol{r}) = \frac{Z_1 Z_2 (e)^2}{\varepsilon_r |\boldsymbol{r}|} \ , \tag{7.5}$$

that is, the Debye-Hückel short-range potential turns to a long-range one. By long-range interaction we mean an interaction potential falling off with the interparticle distance r as $1/r^\nu$ with $\nu \leq d$, d being the spatial dimension of the system.

7.2.3 FCS results

The main outcome of FCS measurements on a solution of oppositely charged molecules is the average time τ_D taken by a molecule of AF488 to cross the section of some observation volume in presence of different concentrations of Lysozyme. The measure of τ_D gives access to physical quantities as the diffusion coefficient D (Eq. (7.2)) and the hydrodynamic radius R_H (Eq.(**??**)). This study has been performed for different average values of the intermolecular interaction strength. The latter depends on the average intermolecular distance $\langle d \rangle$, and, possibly, on a variation of the Debye screening length. The average distance between any two interacting molecules is given by

$$\langle d \rangle = (C_{AF488} + C_{Lys})^{-1/3} \ , \tag{7.6}$$

where the concentration of the AF488 dye has been kept constant and equal to 1 nM, while the Lysozyme concentration covered a range between 0 and 0.69 mM (9.86 mg/ml).

In Figure 7.2 some typical outcomes of the FCS measurements are displayed. These are the autocorrelation functions (ACFs) of fluorescence intensity fluctuations (for graphical reasons the normalized versions are displayed). Then the experimental ACFs are fitted by means of the analytic expression in Eq.(7.1). Out of these measurements and fittings one obtains the diffusion times τ_D , and hence the values of the diffusion coefficient D, at different values of $\langle d \rangle$. When the Lysozyme concentration is zero the solution contains only 1nM of AF488 corresponding to an average intermolecular distance of 11841.8Å. The diffusion coefficient of the dye in the absence of Lysozyme is used as the infinite dilution value D_0 of AF488. Then the average protein-dye distance is varied by varying the Lysozyme concentration. In order to change the action range of electrostatic interactions we chose five different NaCl concentrations: $0, 20, 50, 100, 150$ mM. The 0 mM concentration of NaCl implies that the molecules are solvated in pure water and submitted to a pure Coulombic potential (Eq.(7.5)), while the additions of salt in solution screens the electrostatic interaction between charged molecules (Eq.(7.3)). The Debye screening lengths for NaCl salt contents of $20, 50, 100$ and 150 mM, are equal to 21.4Å,

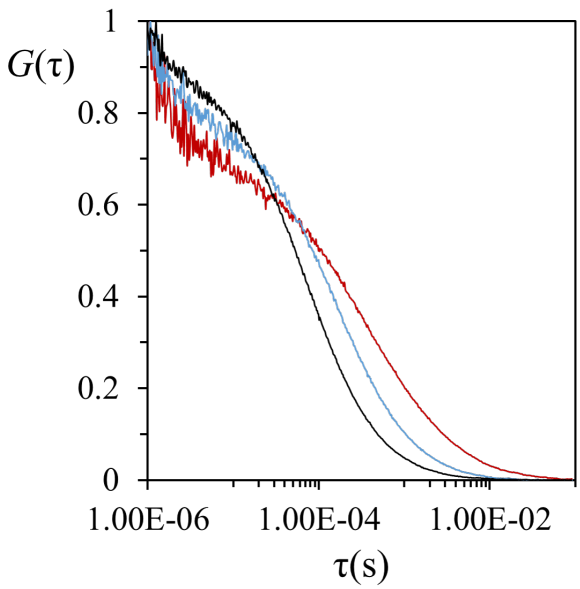

Figure 7.2: Semilog plot of the normalized autocorrelation function of fluorescence fluctuations, defined in Eq.(7.1), obtained at $\langle d \rangle = 240$Å (red line), at $\langle d \rangle = 920$Å (blue line), and at $\langle d \rangle = 4200$Å (black line).

13.6Å, 9.6Å and 7.8Å (Eq.(7.4) for a temperature of 30°C), respectively.

As several experiments have been performed on different days - so that the outcomes of the measures can be affected by even minor FCS setup modifications - the values of the measured diffusion coefficient D are normalized to the infinite dilution value D_0, which is determined anew each time a new experiment is performed, and which corresponds to Brownian diffusion of the dye molecules.

In Figure 7.3(a) we can observe that at low concentrations of Lysozyme, corresponding to an average interparticle distance larger than approximately 2000Å, the diffusion of the dye molecules is Brownian, that is, $D/D_0 \simeq 1$, where $D/D_0 = \tau_{D_0}/\tau_D$ (see Eq.(7.2)). By increasing the Lysozyme concentration, a marked drop of the normalized diffusion coefficient is observed. A rough estimate of the distance at which the electrostatic interaction energy of Eq.(7.5) - written for two molecules - equals the average thermal noise energy of $3k_BT/2$ gives a distance of $\sim$ 2500Å between a Lysozyme molecule and a dye molecule. Below this value of the intermolecular distance, a sizeable effect of the electrostatic interaction is expected. As a matter of fact, this is in very good agreement with the observed average distance at which D/D_0 starts bending. The patterns of the ACFs reported in Figure 7.2 are well fitted by the single species function in Eq.(7.1) even though a-priori a two-species ACF [**?**] could seem to better take into account the presence of two subpopulations, one of complexed dye molecules with proteins, and the other of freely moving dye molecules. However, we have to think of a more complex dynamical situation. When the concentration of protein molecules is such that D/D_0 starts bending, the non-complexed dye molecules are subjected to an electrostatic attraction in every direction exerted by the surrounding protein molecules, this situation of "frustration" slows down their diffusion [NSP+14]. Then we have to think of the possible formation of temporary/"flickering" bound states between the protein and the dye molecules. In fact, the thermal fluctuations,

due to the collisions with the surrounding water molecules, continuously tend to destroy the bound states. The larger the concentration of Lysozyme, the more frequent presumably is the formation of temporary bound states Lysozyme-AF488, thus resulting in a lowering of the value of the diffusion coefficient. Of course the existence of a subpopulation of permanently bounded states Lysozyme-AF488 is not excluded, and also these complexes necessarily contribute to reduce the diffusion coefficient. In view of the just depicted dynamical scenario, we report in what follows the data corresponding to the whole dye population obtained by fitting the ACFs with the function in Eq. (7.1).

As the Lysozyme concentration is increased the average distance between the proteins and the dyes is reduced, and the electrostatic interaction between these oppositely charged molecules is strengthened. This results in an increasing fraction of temporarily bounded pairs of proteins and dye molecules, so species with different diffusion coefficients are detected by the FCS apparatus which thus averages the corresponding values of τ_D. This provides a natural explanation of the physical origin of the observed pattern of the diffusion coefficient displayed in Figure 7.3(b). Let us remark that investigating the details of the clustering process is far beyond the aim of the present work, which is to validate the FCS technique to detect intermolecular long-range interactions.

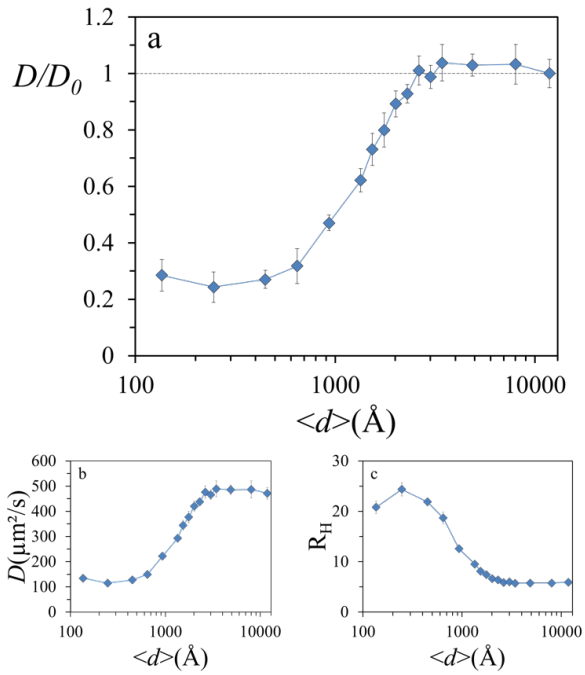

Figure 7.3: Semilog plot of the normalized diffusion coefficients D/D_0 of AF488 as a function of the distance in Å between proteins and dyes (a); semilog plot of the diffusion coefficient D for a single experiment with 0mM of NaCl in solution (b); semilog plot of hydrodynamic radius (c) of AF488 (1nM) versus the average distance between all the molecules in pure water.

As a cross check we observe that the diffusion coefficient D measured at the lowest values of the intermolecular distances has to correspond to the condition where all the molecules of AF488 are bounded to the Lysozyme molecules for most of the time, thus in this case D must approximately equal the value of the Lysozyme diffusion coefficient (apart from a

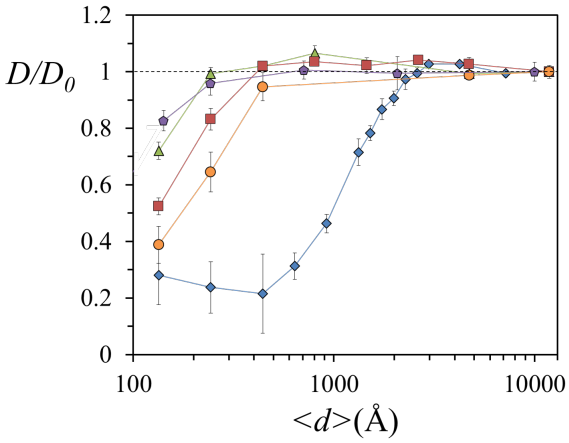

Figure 7.4: Semilog plot of the normalized diffusion coefficients D/D_0 at different concentrations of NaCl in solution: 0mM (blue diamonds), 20mM (orange dots), 50mM (red squares), 100mM (purple rectangles) and 150mM (green triangles); smaller symbols are used to refer to different experiments.

small difference due to a slightly modified Stokes radius). Therefore, the diffusion coefficient of Lysozyme molecules chemically labelled with AF488 has been measured. The value obtained is $D_{Lys} = 166.55 \pm 1\mu\text{m}^2/\text{s}$ which is in fairly good agreement with that one corresponding to the lowest intermolecular distance in Figure 7.3(b).

The above given natural explanation of the result displayed in Figure 7.3(a) can be further and nicely confirmed by acting on the effective range of the the intermolecular interaction potential according to Eq.(7.3). The range of the potential is controlled by the Debye screening length λ_D, which depends on the concentration of freely moving ions in the electrolytic solution. This is practically realised by adding to the watery solution of proteins and dyes different concentrations of sodium chloride. The effect of this action on λ_D is shown in Figure 7.4. The different patterns of $D(\langle d \rangle)$ are consistently showing that the higher the ionic strength (that is the shorter λ_D) the shorter the distance $\langle d \rangle$ at which D deviates from a Brownian value.

7.3 Numerical results for validation of the experimental tehcnique

Numerical simulations of molecular dynamics have been performed to strengthen the interpretation of numerical results presented in previous chapter: i.e., the fingerprint of long-range (attractive, in this case) interactions is sharp, transitional-like drop of diffusion coefficient of the dye particles.

New numerical simulation are required as in this case the system is constituted by *two different molecular species* (dyes and the lysozime molecules) while, in the simulation presented in the previous chapter only one molecular specie has been considered. Moreover, as in this case electrostatic forces can be also attractive, the highly non-trivial problem of represent the excluded volume of the spherical particles has to be considered.

7.3.1 Basic dynamical equations

We have numerically studied systems of two populations of molecules confined in a cubic volume of size L. The number of particles for each type is fixed: N_A is the number of A-type particles (Lysozyme molecules), and N_B is the number of B-type particles (AF488 molecules). To avoid spurious boundary effects, periodic boundary conditions (PBC) have been assumed, which is equivalent to the existence of an infinite number of images/replicas throughout the space. In order to study diffusion at different concentrations, the numbers of molecules N_A and N_B are kept fixed, and the average intermolecular distance $\langle d \rangle$ among the molecules of type A and B is then controlled according to the relation

$$L = \sqrt[3]{N_A + N_B}\, \langle d \rangle \ . \tag{7.7}$$

We remark that such a choice is not entirely equivalent to the experimental situation described in the previous paragraphs where the dye (AF488) concentration was fixed; in fact, in molecular dynamics simulations (MDS) both the concentration of Lysozyme and dye change with $\langle d \rangle$, the ratio of concentrations being constant. This choice is justified by the fact that in real experiments N_A/N_B varies in a range $[1 - 5 \times 10^5]$; fixing $N_B = 50$, the experimental situation would correspond to taking N_A in a range $[1 - 2.5 \times 10^6]$, which is very highly demanding for computation. In MDS the ratio N_A/N_B has been chosen as large as possible ($N_A/N_B = 10$ in our case) to avoid that dye molecules (AF488) dynamics could significantly affect the biomolecules (Lysozyme) dynamics.

In the presence of long-range interactions and PBC, each molecule contained in the previously mentioned box interacts with all the molecules contained in the above mentioned images/replicas, that is, the pairwise potential

$$U_{kl}(r_{i_k j_l}) = U(|\boldsymbol{r}_{i_k} - \boldsymbol{r}_{j_l}|) \tag{7.8}$$

in Eq. (6.4) has to be replaced by an effective potential $U_{kl}^{\text{eff}}(r_{i_k j_l})$ of the form:

$$U_{kl}^{\text{eff}}(r_{i_k j_l}) = \sum_{\boldsymbol{n} \in \mathbb{Z}^3} U(|\boldsymbol{r}_{i_k} - \boldsymbol{r}_{j_l} + \boldsymbol{n}L|) \ , \tag{7.9}$$

where $\mathbb{Z}^3$ is the space of 3-dimensional integer vectors.

It is clear that short and long-range interactions (in the sense specified in the Introduction) have to be managed in two different ways. For short range interactions it is always possible to define a cutoff length scale λ_{cut} such that the effects of the interactions beyond this distance are negligible. In the systems we have studied by means of numerical simulations, the Debye electrostatic potential is a short range potential with a cutoff scale of the order of some units of the Debye length λ_D. For long-range interactions as the Coulomb potential Eq.(7.15), it is not possible to define a cutoff length scale λ_{cut} so that, in principle, an infinite sum should be considered. A classical way to account for long-range interactions resorts to the so called Ewald summation [AT89]. In the following Section we describe a more recent and practical

method - replacing Ewald's one - known as Isotropic Periodic Sum (IPS). The equations of motion (6.4) were numerically solved using a second order Euler-Heun algorithm [BLL07],that is, a predictor-corrector scheme.

The initial position of each particle is randomly assigned at t_0 using a uniform probability distribution in a cubic box of edge L.

7.3.2 Model potential

The interactions among the molecules are linear combinations of pairwise potentials regularized as follows:

$$U_{kl}(r_{i_k j_l}) = \begin{cases} U_{SC}(r_{i_k j_l}) & r_{i_k j_l} \leq 1.01\, R_{kl} \\ U_{ElStat}(r_{i_k j_l}) & r_{i_k j_l} > 1.01\, R_{kl} \end{cases} \tag{7.10}$$

where $R_{kl} = R_k + R_l$ is the sum of the two molecular radii, $U_{SC}(r_{i_k j_l})$ is a soft-core potential and $U_{ElStat}(r_{i_k j_l})$ is the Coulomb electrostatic potential. The choice of a soft-core potential is related to the fact that a small fictitious overlap among the interacting molecules is allowed in numerical simulations for computational reasons (that is, to avoid the need of very short integration time steps). The soft-core potential has the form:

$$U_{SC}(r_{i_k j_l}) = A_{SC_{kl}} \exp\left[-\frac{r_{i_k j_l}}{R_{kl}} + 1\right] . \tag{7.11}$$

The parameter related with the potential strength $A_{SC_{kl}}$ has been chosen such that:

$$\Delta r_{SCi_k}(0.95\, R_{kl}) + \Delta r_{SCj_l}(0.95\, R_{kl}) = 0.05\, R_{kl} \ , \tag{7.12}$$

where Δr_{SCi_k} is the drift on the the particle i_k due to the soft-core potential in a discrete time interval Δt:

$$\Delta r_{SCi_k}(r_{i_k j_l}) = \frac{\Delta t}{\gamma_k} \left| \frac{\mathrm{d}U_{SC}(r_{i_k j_l})}{\mathrm{d}r} \right| . \tag{7.13}$$

This yields the following expression for $A_{SC_{kl}}$:

$$A_{SC_{kl}} = 0.05\, \exp\left[-0.05\right] \frac{R_{kl}^2}{\Delta t} \left(\frac{1}{\gamma_k} + \frac{1}{\gamma_l} \right)^{-1} . \tag{7.14}$$

The electrostatic Coulomb potential $U_{ElStat}(r_{i_k j_l})$, describing the experimental condition where no salt is dissolved in solution, is:

$$U_{\mathrm{Coul}}(r_{i_k j_l}) = \frac{Z_k\, Z_l\, e^2}{\varepsilon\, r_{i_k j_l}} \ , \tag{7.15}$$

where e is the elementary charge and ε is the electric permittivity of the medium, for which the static value at room temperature is $\varepsilon = \varepsilon_{water} \simeq 80$.

IPS correction to long-range potentials

Because of the long-range nature of the Coulomb potential described by Eq.(7.15), the force acting on each particle is given by the sum of the forces exerted by all the particles in the box and by the particles belonging to the images. For the computation of these forces, we used the IPS method [WB05][WB08], a cutoff algorithm based on a statistical description of the images isotropically and periodically distributed in space. Assuming that the system is homogeneous on a length scale R_c, we can define an effective pairwise IPS potential $U^{IPS} = U^{IPS}(|\boldsymbol{r}_{i,j}|, R_c)$ which takes into account the sum of pair interactions within the local region around a particle

$$U^{IPS}(|\boldsymbol{r}_{i,j}|, R_c) = \begin{cases} U(|\boldsymbol{r}_{i,j}|) + \phi(|\boldsymbol{r}_{i,j}|, R_c) \ , & |\boldsymbol{r}_{i,j}| \leq R_c \\ \\ 0 \ , & |\boldsymbol{r}_{i,j}| > R_c \end{cases} \tag{7.16}$$

where $\phi(|\boldsymbol{r}_{i,j}|, R_c)$ is a correction to the potential obtained by computing the total contribution of the interactions with the particle images beyond the cutoff radius R_c[WB05][WB08]. For the Coulomb potential of Eq.(7.15), we obtained an analytical expression for the IPS correction $\phi_{\text{Coul}}(\boldsymbol{r}_{i,j}, R_c)$. For computational reasons this has been approximated by a polynomial of degree seven in $x = |\boldsymbol{r}_{i,j}|/R_c$ with x in the interval $(0; 1]$:

$$\begin{aligned} \phi_{\text{Coul}}(x) = &- 9.13636 \times 10^{-7} + 0.000100298x + \\ &+ 0.298588x^2 + 0.0151595x^3 + \\ &+ 0.00881283x^4 + 0.10849x^5 + \\ &- 0.0930264x^6 + 0.0482434x^7 \end{aligned} \tag{7.17}$$

We have chosen $R_c = L/2$ under the hypothesis that on this scale the system is homogeneous.

7.3.3 Long-time diffusion coefficient

We aim at assessing the experimental detectability of long-range interactions between biomolecules using quantities accessible by means of standard experimental techniques. A meaningful approach to this issue is the study of transport properties. For this reason, in our simulations we chose the long-time diffusion coefficient D as the main observable of the system described by Eqs.(6.4). This coefficient is defined, consistently with Einstein's relation [AT89], as:

$$D = \lim_{t \to +\infty} \frac{\langle |\Delta \boldsymbol{r}_i(t)|^2 \rangle}{6t} \ , \tag{7.18}$$

$\Delta \mathbf{r}_i(t) = \boldsymbol{r}_i(t) - \boldsymbol{r}_i(0)$ being the total displacement of a particle in space and $\langle a_i \rangle = 1/N \sum_{i=1}^{N} a_i$ the average over the particle set. We remark that in our system the displacements $\Delta \boldsymbol{r}_i(t)$ are not mutually independent due to the interaction potential $U(|\boldsymbol{r}_i - \boldsymbol{r}_j|)$ in Eqs.(6.4), which establishes a coupling between different particles; in that case, the average over particles index concerns correlated stochastic variables. Nevertheless, as our system is non-linear with more

than three degrees of freedom, it is expected to be chaotic [**?**] so that, in this case, the statistical independence of particle motions is recovered. Moreover, when a chaotic diffusion gives $\langle|\Delta \boldsymbol{r}_i(t)|^2\rangle \propto t$ (which is the case of the models considered in the present work), the diffusion coefficient D is readily computed through a linear regression of $\langle|\Delta \boldsymbol{r}_i(t)|^2\rangle$ expressed as a function of time. In what follows we refer to $\langle|\Delta \boldsymbol{r}_i(t)|^2\rangle$ as Mean Square Displacement (MSD).

7.3.4 Simulation Parameters

Molecular Dynamics simulations were performed considering a solution with $N_A = 500$ and $N_B = 50$ representing respectively Lysozyme molecules and AF488 molecules. This choice seemed to be a good compromise between the need of a large N_B for a good statistics, a sufficiently large ratio N_A/N_B and the request of a not too high computation time.

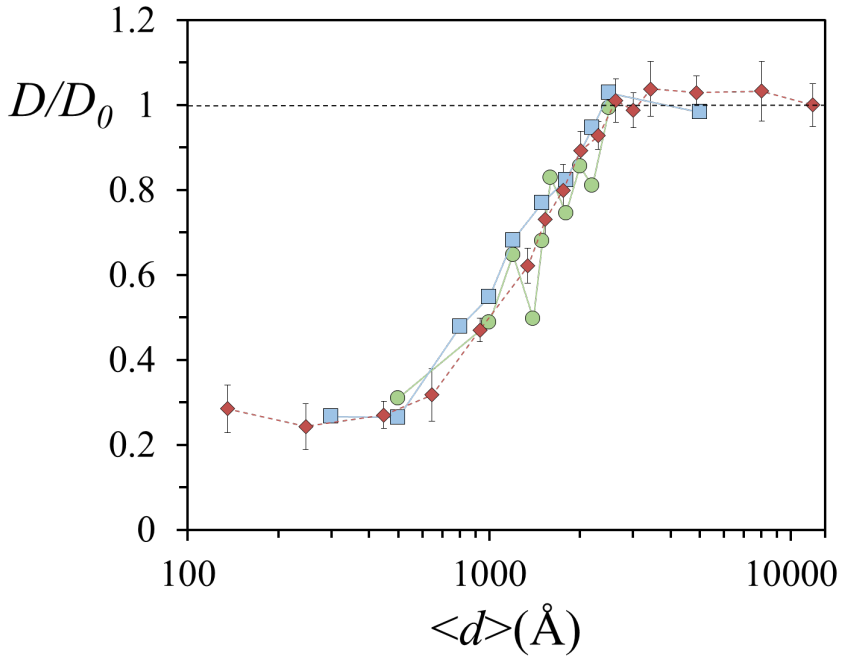

Figure 7.5: Comparison among experimental results and numerical simulations. Semilog plot of the normalized diffusion coefficients D/D_0: experimental values (red diamonds), $N_A = 200$ and $N_B = 20$ (light green circles), $N_A = 500$ and $N_B = 50$ (light blue squares).

The A-type particles, which represent Lysozyme molecules, have a radius $R_A = 2 \times 10^{-3}\,\mu$m and a net electric charge expressed in elementary charge units $Z_A = +10$. The B-type particles, which represent AF488 molecules, have a radius $R_B = 0.5 \times 10^{-3}\,\mu$m and a net electric charge expressed in elementary charge units $Z_B = -2$. The medium where diffusion takes place represents an aqueous solution, so that the viscosity $\eta = 8.90 \times 10^{-4}\text{Pa} \cdot \text{s}^{-1}$ is the water viscosity at $T \simeq 300K$. The relative dielectric permittivity has been taken to be $\varepsilon = 80$ as for pure water.

The time step has been chosen to $\Delta t = 5 \times 10^{-4}\,\mu$s: this choice can allow important overlaps among particles in MDS and does not permit a correct description of excluded volume effects, i.e. the drift due to stochastic forces on dye molecules in a single time steps is comparable

with R_B. Nevertheless the effects we are interested in concern the diffusive behaviour of dyes on larger length and time scales and we considered acceptable such ovelaps. The number of time steps was fixed such that the dynamics was simulated for 5000μs so that for the dye particles $\sqrt{6\,D_0\Delta t} \simeq 4\,\mu\text{m} \gg \langle d \rangle$, where D_0 is the brownian self-diffusion coefficient of the dye molecules, for any considered case. In Figure 7.5 the outcomes of the above described numerical simulations are compared to the experimental results obtained for the same quantity: the diffusion coefficient D, normalized with respect to its Brownian value D_0, as a function of the average interparticle distance $\langle d \rangle$. The numerical outcomes for D quantify the diffusion of the small particles that model the dye molecules. We observe that the choice $N_A = 500$ and $N_B = 50$ yields a less noisy pattern with respect to the choice $N_A = 200$ and $N_B = 20$, what is of course sound. Even though the number of particles considered in numerical simulations is very small with respect to the actual number of molecules in laboratory experiments, a common situation in standard Molecular Dynamics simulations, the agreement among numerical and experimental results is excellent.

7.4 Concluding remarks

The work reported in this chapter concludes a feasibility survey aimed at assessing the adequacy of diffusion studies to detect the activation of electrodynamic intermolecular interactions. Other two works, [PFN+12] and [NSP+14], dealt with this problem from the theoretical and numerical sides, respectively. The present work contains a leap forward in what it provides an experimental assessment of the adequacy of Fluorescence Correlation Spectroscopy to detect intermolecular long range interactions. Even though our ultimate goal is to detect long range *electrodynamic* intermolecular interactions, for the time being we have tested this technique against a system where long range interactions are built-in, that is, a solution of oppositely charged molecules interacting through non-screened electrostatic interactions. As a matter of fact, we have found that FCS is certainly appropriate to detect intermolecular interactions in dilute systems, that is, when the solvated molecules interact at large distances, in the present study up to 2000Å approximately. Furthermore, the excellent quantitative agreement between the experimental outcomes and the corresponding numerical simulations has a twofold relevance. From the one side it confirms that the observed phenomenology, namely, the sudden bending of the diffusion coefficient when the average intermolecular distance is lowered below a critical value, as well as its pattern as a function of the intermolecular distance, are actually due to the electrostatic interaction among the solvated molecules. From the other side this validates the numerical algorithm and approximations adopted, suggesting that this numerical scheme can be safely applied to interpret the readouts of experiments where electrodynamic interactions will be possibly excited.

Conclusions and further perspectives

In this manuscript many different aspects of phase transitions and cooperative phenomena are studied and investigated from different points of view.
In the first part of this manuscript, we investigated the φ^4-model on 2D-lattice elsewhere proposed as counterexample to the Necessity Theorem 1.4.2 which constitutes the conceptual basis of the Topological Theory of phase transitions.
Such an investigation has been motivated mainly by the necessity to save a powerful approach to phase transitions. On the one side it allows to extend the classical theory of phase transitions to small or mesoscopic systems, far from the thermodynamic limit, what makes this theory a powerful theoretical tool also in view of future applications in biophysics. On the other side, the Topological Theory of phase transitions allows to predict, from the topology of equipotential level sets at any finite N, if a system undergoes a phase transition in the thermodynamic limit.
Our numerical and theoretical investigations of the φ^4-model on 2D-lattice suggested that the hypothesis of diffeomorphicity of the equipotential level sets at any finite N is not sufficient to prevent an asymptotic loss of simple connectedness of the equipotential level sets: an additional condition has to be imposed to the vector field generating the diffeomorphism among equipotential level sets to prevent the occurrence of phase transitions in the thermodynamic limit. In this sense, the original "geometrization" of microcanonical thermodynamics, provided in this work, could in principle make easier to construct uniform bounds on this vector field as the derivatives of the microcanonical entropy calculated on a certain level set $\Sigma_{\bar{v}}$ can be expressed as microcanonical averages of some scalar functions associated to the vector field (in particular its divergence and modulus) and of their derivatives. Further more, a method to encode the thermodynamical information on a system in a suitable metric of configuration space, allows to express the derivatives of entropy at any order as functions only of the averages of the mean curvature of the potential level sets and their derivatives with respect to the normal vector field. This insight seems quite promising as the links among global integral geometry and topology are known.
Finally, the application of persistent homology to systems which undergo phase transitions, as illustrated in chapter 2, gives the Topological Theory a computational interest. In fact, this theory is not a mere mathematical speculation on the origin of phase transitions, but it potentially constitutes the theoretical basis for a method that, among other things, allows to study phase transitions in small systems from the computation of the topological properties of configuration space.
The second part of this manuscript has been devoted to present the author's contributions to the ambitious research program aimed at verifying the possibility to electrodynamic long range resonant interactions among biomolecules in acqueous solutions. According to the complex theoretical picture presented in chapter 3, the possibility for biomolecules to exploit this kind

of electrodynamic long-range interactions is strictly dependent on the possibility of inducing collective vibrations of biomolecules. Between the mid of '60s and the '70s, H. Fröhlich developed an heuristic model (that, because of its genericity, has to be considered as a metaphor) that predicts the possibility of canalizing all the vibrational energy of a biomolecule in its lowest frequency vibrational mode when the external energy supply exceeds some threshold value Hitherto the rate equations for the average actions of normal modes have been derived from a *quantum* Hamiltonian system by Wu and Austin. This leads to the conclusion that Fröhlich theory would be a quantum effect: this was the central point which attracted many criticisms that had the consequence of disqualifying this theory as a possible explication of the activation of out-of-equilibrium collective oscillations in biomolecules.

In chapter 4 we show that the Fröhlich-like condensation can exist also in a classical framework. This result makes the "Fröhlich metaphor" more plausible if applied to biomolecules and makes reasonable the experimental search for Fröhlich-like condensation in biomolecules, even in "wet" and "warm" environment, where quantum phenomena are supposed not to take place. Nevertheless, as observed at the end of chapter 4, the Fröhlich-like condensation theory, both in quantum and classical version, is described for an hyper-simplified model whose parameters seem quite hard to estimate for a realistic protein. Moreover, a central point in Fröhlich theory consists of the non-linear interaction of normal modes of the biomolecules with the so called "thermal bath". The original Fröhlich description includes all thermalized degrees of freedom, in particular the surrounding water molecules and other internal vibrational modes of the considered biomolecule. Nevertheless, the problem of describing the interactions of biomolecules undergoing collective oscillations with their surrounding aqueous environment is still an open research field, that has been only partially explored, especially for what concerns the dissipation of vibrational energy.

In chapter 5 a first *experimental* evidence of the activation of collective oscillations of biomolecules in watery solutions and out-of-thermal equilibrium is reported. The importance of this result relies on the fact that it revitalises a research field abandoned for a long time because of major technical difficulties to be overcome in order to perform these measures. Moreover, from the point of view of theoretical physics, also the interpretation of these measures constitutes a real challenge. Despite the fact that our *in vitro* experiments represent a simplified condition with respect to the cellular environment, the presence of water makes really hard a quantitative interpretation of some aspects of the experimental outcomes. In fact, also in this case, the interaction between a biomolecule and its surrounding aqueous environment could play a relevant role.

The theoretical interpretation we provided in chapter 5 explains the main features of the observed spectra: the presence of a protein absorption peak due to light illumination, the value of the frequency for which the absorption peak is observed, the shape of the absorption peak. Any finer analysis of the experimental outcomes cannot leave aside a description of the response of water to electromagnetic radiation in the THz domain. Moreover a deeper understanding of cooperative phenomena of water molecules surrounding a biomolecule is needed to assess the role of hydration molecules in their surmised electrodynamic interaction. For instance, the

presence of a thick layer of organized water around biomolecules (that can be reach the thickness of 2.5nm) can play a decisive role both to amplify the biomolecules electric dipole and to reduce the vibrational energy dissipations of the biomolecule. In this context, further research should address also the fascinating theory proposed by G. Preparata and E. Del Giudice in QED framework on the possibility to induce *coherence domains* in water (see for instance [ABGP95, DGP98, Apo09, DGET09]).

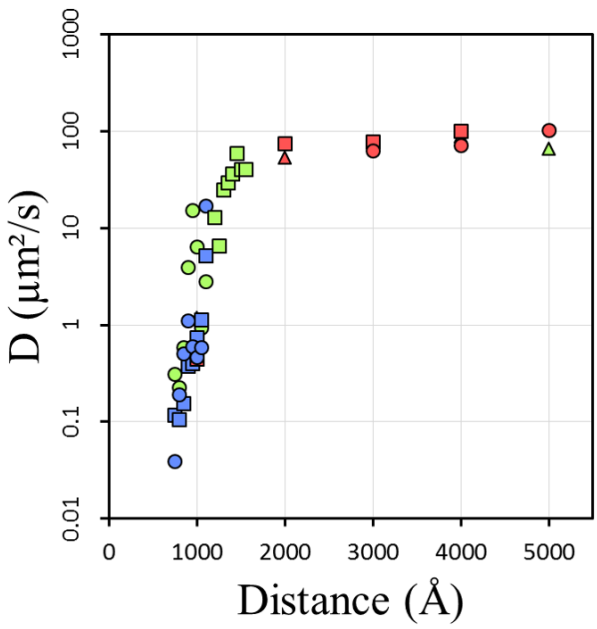

Figure 7.6: Preliminary results of FCS measure of excited BSA self-diffusion coefficient vs. intermolecular average distance. Different colours indicated different measure set.

In chapter 6 and chapter 7 the possibility to recognize the activation of long-range (attractive) interactions through the observation of self-diffusion behaviour has been assessed both by numerical simulation and real FCS experiments. The validation of the experimental method allows to consider the further crucial step: the research of long-range electrodynamic intermolecular interactions among biomolecules when collective oscillations are activated with the same procedure used in the THz experiments so far performed. Preliminary results on the same BSA molecule are reported in Figure 7.6. The results are quite encouraging: a sudden drop of self-diffusion coefficient to lower values is observed for an intermolecular average distance of the order of $\sim 1500\mathring{A}$; a pattern qualitatively very similar to reported in Figure 6.8 for the clustering transition in a system of identical molecules interacting through an attractive potential between oscillating dipoles. If these preliminary results are confirmed by other ongoing experiments, an exciting research field will be opened. A large number of theoretical and experimental issues will be raised for both *in vitro* and prospectively *in vivo* investigations.
About the prospective biological relevance of all the above mentioned results, the excitation of collective vibrations, and thus the activation of long-range attractive forces, would be driven by ATP hydrolysis in living cells. The typical intracellular concentration of ATP molecules is

given around 1 mM implying that a protein molecule in the cell undergoes around 10^6 collisions with ATP molecules per second [AJL+02]. Given the standard free-energy obtained from ATP hydrolysis estimated around 50 kJ.mol^{-1} = 8.306×10^{-13}erg, if we assume that only 1% of the collisions with ATP will provide energy, a power supply of 8.306×10^{-9}erg s^{-1} is potentially available. This is considerably larger than the power supplied to each protein in our THz experiments, thus the condensation mechanism *in vivo* can be considerably faster and more efficient. Adding this long-range electrodynamic selective interactions to the usually considered short-range interactions (chemical bonds, Van der Waals interactions, hydrogen bonds, etc.) would open unpredictable scenarios in our understanding of the functioning of the molecular machinery at work within the living cells. For instance, a quite fascinating study, among the others, would be that of investigating synchronization phenomena in physiological conditions among the biomolecules intervening in some specific biochemical reaction like gene transcription, activation of DNA-polymerase and so on. Finally the presence of phase-locking phenomena could affect the repulsive or attractive nature of biochemical interactions having important consequences at the level of dynamical organization in cellular environment.

A Basic facts of differential geometry and geometric measure theory

A.1 Brief review of Riemannian Geometry

In this appendix we review some concepts concerning the Riemannian Geometry that occurring in the main part of the manuscript. The reader is supposed to be acquainted with very basic notions of differential geometry that we briefly sketch here.

A.1.1 The concept of differentiable manifold

One of the main purpose of the **Differential Geometry** is to extend the applicability of the differential calculus, usually performed on open set of the vector (linear) space $\mathbb{R}^n$, to more general sets. Basically, the definitions and the principal features of the differential calculus are local properties; i.e., they depend only on their behaviour in an arbitrarily small neighbourhood of a point. So, if a set $\mathcal{M}$ is locally as an open set of $\mathbb{R}^n$, we are able to introduce a differential calculus on $\mathcal{M}$.

An n-Smooth Manifold is an abstract set[1] such that a small region around each point of it is done as an open set[2] of $\mathbb{R}^n$ equipped with an additional smooth structure we are going to introduce. A set $\mathcal{M}$ which is locally like the linear space $\mathbb{R}^n$ is called a *topological manifold* of dimension n; here, an inhabitant of $\mathcal{M}$, living a neighbourhood of a given point p, needs exactly n dimensions to describe the surrounding reality. Roughly speaking, the map $\varphi(p) = (x^1(p), \ldots, x^n(p))$ realizes those dimensions on $\mathbb{R}^n$ and the maps $x^1(p), \ldots, x^n(p)$ are called *local coordinates* of $\mathcal{M}$ in p. More formally, given a set $\mathcal{M}$ and $p \in \mathcal{M}$, a chart (U, φ) at p is a bijective map $\varphi : U \to V$, where $U \subset \mathcal{M}$ and V is an open set of $\mathbb{R}^n$. Actually, a chart provides on $U \subset \mathcal{M}$ the coordinates of $\mathbb{R}^n$. In this way, a chart allows one to describe each point of U with a n-tuple of real numbers. Thus, U is the part of $\mathcal{M}$ that is essentially like $\mathbb{R}^n$. Roughly speaking, the chart (U, φ) provides a geographic map to describe $\mathcal{M}$, at least in a small part of it. It is then clear that to describe the whole set $\mathcal{M}$ we need a collection of charts covering all $\mathcal{M}$.

A problem arises when a region of $\mathcal{M}$ is described by different charts: this chance is drawn in Fig. A.1. Consider, for example, two inhabitants of $\mathcal{M}$ living one in a neighbourhood of a point $p \in \mathcal{M}$ and the other in a neighbourhood of a point $q \in \mathcal{M}$. They could display the respective surroundings with two different charts, say (U_1, φ_1), (U_2, φ_2) and so with two different sets of *local coordinates*. Moreover, in case of overlap, i.e. in the region $U = U_1 \cap U_2 \neq \emptyset$, the charts should be (in a suitable sense) equivalent. The equivalence is provided by the compatibility

[1] Here we introduce the concept of the manifold thinking of it as living into no linear space $\mathbb{R}^n$.

[2] This requirement implies that the manifold has the same topology of $\mathbb{R}^n$, at least locally.

condition: $\varphi_1(U)$ and $\varphi_2(U)$ are open sets of $\mathbb{R}^n$ and $\varphi_2 \circ \varphi_1^{-1} : \varphi_1(U) \to \varphi_2(U)$ is a bijective, smooth map with inverse smooth again[3]. The map $\varphi_2 \circ \varphi_1^{-1}$ is called change of coordinates or *transition map*. This map allows U to inherit the structure of the linear space $\mathbb{R}^n$.

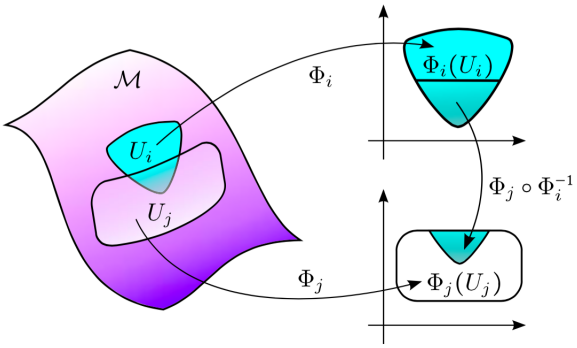

Figure A.1: **The transition map**: the sets $U_i, U_j \subset \mathcal{M}$ have $\Phi_i(U_i)$ and $\Phi_j(U_j)$ as realization into the linear space $\mathbb{R}^2$. The overlap $U_i \cap U_j$ should have the same realization with both Φ_i and Φ_j, as it turns out in the turquoise triangle.

Finally, a natural covering of the set $\mathcal{M}$ is provided by a collection of compatible (each one with each other) charts. In this way all regions of $\mathcal{M}$ can be described by equivalent local coordinates. A collection of compatible charts covering $\mathcal{M}$ is called *atlas*. Moreover, two atlas are compatible if their union is yet an atlas of $\mathcal{M}$. A *differentiable structure* is the maximal (with respect the inclusion) *atlas* $\mathcal{M}$. Thus, a smooth manifold is the pair $(\mathcal{M}, \mathcal{A})$ where $\mathcal{A}$ is a differentiable structure. Trivially, $\mathbb{R}^n$ is a smooth manifold with one chart and local coordinates given by the natural ones.

A.1.2 Tangent and cotangent space

Other extra structures on the manifold $\mathcal{M}$ are possible. The most evident example of manifold with an extra structure is the linear space $\mathbb{R}^n$: it is also a vector space. The canonical scalar product allows to introduce a metric structure on $\mathbb{R}^n$: we can measure the length of the tangent vectors, the length of the curves and the distance between two different points. Now we want introduce a metric structure also on $\mathcal{M}$. Doing that we obviously need a structure of vector space associated with $\mathcal{M}$. We know that a small region is like an open set[4] $U \subset \mathbb{R}^n$, but as matter of fact we can not add two different points p and q in $\mathcal{M}$. The associated structure of vector space is given by the definition of the **tangent space** of $\mathcal{M}$ at a given point $p \in \mathcal{M}$. Thus, at any point p we have a vector structure and so a scalar product. Then, roughly speaking, we can consider a metric structure on $\mathcal{M}$ as the union of all scalar product on any tangent space as p varies on $\mathcal{M}$. Let us see first what is a tangent vector of $\mathcal{M}$ at p and then which is the structure of the tangent space. Consider another mathematical object with one dimension, the *curve*, different from the *line*[5]. More formally, a smooth *curve* is a smooth map $\sigma : I \to \mathbb{R}^n$,

[3]This is properly the definition of a *diffeomorphism*.

[4]This means, the small region of $\mathcal{M}$ has the same topology of $\mathbb{R}^n$.

[5]The number eight drawn in a $\mathbb{R}^2$ is a *curve*, but not a *line*. In fact, any small region around the auto-intersection point is a cross, but not a straight line, as request from the definition of the *line*.

where $I \subset \mathbb{R}$ is an interval. Given $p \in \mathcal{M}$, we can realize a small region around p as an open set $U \subset \mathbb{R}^n$ and perform the derivative of any differentiable function defined on it. A *tangent vector* of $\mathcal{M}$ at p is the one $\sigma'(0)$, where $\sigma : (-\delta, \delta) \to \mathcal{M}$ is a curve inside the small region around p and such that $\sigma(0) = p$: see Fig. A.2 for a major understanding of the concept. The collection of all tangent vectors of $\mathcal{M}$ at p is the tangent space $T_p\mathcal{M}$ of $\mathcal{M}$ at p. In general,

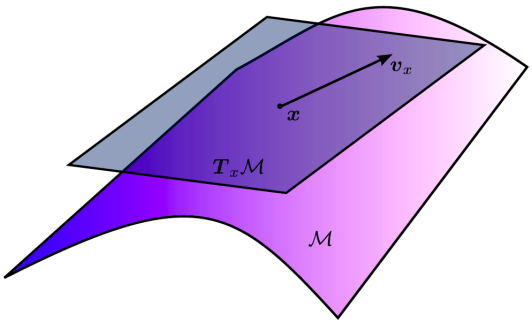

Figure A.2: **The tangent space of $\mathcal{M}$ at x**: the vector v_x is the tangent vector of a suitable curve $\sigma(t)$ living in a small region of $\mathcal{M}$, such that $\sigma(0) = x$.

given an n-dimensional smooth manifold $\mathcal{M}$ and a point $p \in \mathcal{M}$, the tangent space $T_p\mathcal{M}$ of $\mathcal{M}$ at p is a vector space which could be identified with the set of the partial derivatives. So, let (U, φ) be the chart providing the realization of the small region around p as an open set of $\mathbb{R}^n$, a basis of $T_p\mathcal{M}$ is given by $\mathcal{B} = \{\boldsymbol{\partial}_1, \ldots, \boldsymbol{\partial}_n\}$, where $\boldsymbol{\partial}_i = \dfrac{\partial}{\partial x^i}$ and $\{x^i\}_{i=1}^n$ is the set of local coordinates.

The vector space structure $T_p\mathcal{M}$ naturally allows to define a dual vector space, the so called **cotangent space** $T_p^*\mathcal{M}$, such that every; namely if $\theta \in T_p^*\mathcal{M}$ and $\boldsymbol{X} \in T_p\mathcal{M}$ then $\theta_p(\boldsymbol{X}) \in \mathbb{R}$. In particular, if $\mathcal{B}^* = \{dx_p^1, \ldots, dx_p^n\}$ is a basis of $T_p^*\mathcal{M}$ then $dx_p^i(\partial_j) = \delta_{ij}$[6]

This two vector space allow to construct a *tensor space* of rank (r, s), a multilinear map of the form

$$\mathcal{T}^{(r)}_{(s),p} = \otimes_r T_p\mathcal{M} \otimes_s T_p^*\mathcal{M} \tag{A.1}$$

an element $t \in \mathcal{T}^{(r)}_{(s),p}$ that in local components read

$$t = t^{i_1 \ldots i_r}_{j_1 \ldots j_s} \boldsymbol{\partial}_{i_1} \otimes \boldsymbol{\partial}_{i_r} \otimes \mathrm{d}x_p^{j_1} \otimes \mathrm{d}x_p^{j_s} \,. \tag{A.2}$$

Fundamental operation on the tensor and their multilinear algebra are

- the *linear combination of two tensor* that in coordinates reads $(\alpha x + \beta y)^{i_1 \ldots i_r}_{j_1 \ldots j_s} = \alpha x^{i_1 \ldots i_r}_{j_1 \ldots j_s} + \beta y^{i_1 \ldots i_r}_{j_1 \ldots j_s}$ where $\alpha, \beta \in \mathbb{R}$;
- let $1 \leq \lambda \leq r$ and $1 \leq \mu \leq s$ and $x \in \mathcal{T}^{(r)}_{(s),p}$ then its *tensor contraction* $C_{\lambda\mu}(x) \in \mathcal{T}^{(r-1)}_{(s-1),p}$ reads in coordinate $(C_{\lambda\mu}(x))^{i_1 \ldots i_r}_{j_1 \ldots j_s} = x^{i_1 \ldots i_{\lambda-1} k i_{\lambda+1} \ldots i_r}_{j_1 \ldots j_{\mu-1} k j_{\mu+1} \ldots j_s}$
- the *tensor product* of two tensor $x \in x \in \mathcal{T}^{(r_1)}_{(s_1),p}$ and $x \in \mathcal{T}^{(r_2)}_{(s_2),p}$ whose action in coordinates

[6] $\mathcal{B}^*$ is the dual basis of $\mathcal{B}$ and the Kronecher symbol δ_{ij} is defined as $\delta_{ij} = 1$ if $i = j$, otherwise it is zero.

reads

$$(x \otimes y)^{i_1 \dots i_{r_1+r_2}}_{j_1 \dots j_{s_1+s_2}} = {}^{i_1 \dots i_{r_1}}_{j_1 \dots j_{s_1}} \cdot y^{i_{r_1+1} \dots i_{r_1+r_2}}_{j_{s_1+1} \dots j_{s_1+s_2}} \tag{A.3}$$

this operation satisfies associative and distributive laws;

- the *index permutation* σ that can be applied to tensors of rank $(r, 0)$ (multivector) or $(0, s)$ (multiform); for instance, in the latest case we have that $(\sigma(x))_{j_1 \dots j_s} = x_{j_{\sigma 1} \dots j_{\sigma s}}$. If we define the sign of a permutation as

$$\mathrm{sgn}\sigma = \begin{cases} +1 & \text{even permutations} \\ -1 & \text{odd permutations} \end{cases} \tag{A.4}$$

we can introduce the *symmetrazing map* S_s and the *alternating* map A_s of a multiform $x \in \mathcal{T}^{(0)}_{(s),p}$

$$A_s(x) = \frac{1}{s!} \sum_{\sigma \in \mathcal{S}(s)} \mathrm{sgn}\sigma \cdot \sigma x S_s(x) = \frac{1}{s!} \sum_{\sigma \in \mathcal{S}(s)} \sigma x \ . \tag{A.5}$$

The alternating map allows to define an *exterior (wedge) product* of an s-form η and an k-form ρ as

$$\eta \wedge \rho = A_{s+k}(\eta \otimes \rho) \tag{A.6}$$

with associative law, distributive law respect to sum and anticommutative law, i.e. $\rho \wedge \theta = (-1)^{ks} \theta \wedge \rho$. The local space of k-forms will be indicated in what follows with Λ^k_p.

A.2 Tensor fields, derivations, connections and curvatures

The vector (or tensor) space introduced in the previous section are defined point-wise; the next step to enrich the structure of a differential manifolds consists in extend such structures to the whole manifold. A very simple way to realise this consists in taking the disjoint union $T\mathcal{M}$ of all $T_p\mathcal{M}$ with respect $p \in \mathcal{M}$: this is called the *tangent bundle*. Analogously the disjoint union $T^*\mathcal{M}$ of all $T^*_p\mathcal{M}$ with respect $p \in \mathcal{M}$ is called the *cotangent bundle*. Thus, a tangent (co-tangent) bundle is a vectorial over structure upon the manifold; more in general the disjoint union of the tensor in each point $p \in \mathcal{M}$ of a riemanian manifold constitute the so called *tensor bundle*. In Fig. A.3 the columns represent the vector spaces built upon the flat manifold $\mathbb{R}^2$: each column correspond to one tangent space, called *fiber* of the tangent bundle while the flat manifold is the *base* of the bundle More in general the fiber can be constituted by an arbitrary vector space V (as a space of tangent vector, covector, tensor spaces obtained as tensor product of them) and the *vector bundle* associated has the *local* structure of the Cartesian product of the manifold and the vector space: when this properties holds also globally the bundle is *trivial*. An application with associate at each point p of the base $\mathcal{M}$ a vector in the corresponding fiber $V_p\mathcal{M}$ is a *section* of the fiber bundle. A *vector field* over a manifold $\mathcal{M}$ can be regarded as a section in some vector bundle $V\mathcal{M}$, as for instance the tangent bundle $T\mathcal{M}$.
In this case a vector field $\mathbf{X} \in \mathcal{T}_f\mathcal{M}$ that takes the value $\mathbf{X}(p) = X^i(p)\boldsymbol{\partial}_i$ in $p \in \mathcal{M}$ can be

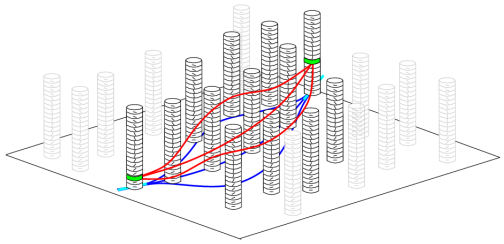

Figure A.3: **The tangent bundle**: the columns represent the tangent spaces, called, in general, fibers of bundle. The blue lines are curves on the manifold, while the red lines are indicated as the sections of the tangent bundle upon the blue curve.

locally regarded as the tangent vector field of a curve $\gamma(t) \in \mathcal{M}$ with $\gamma(0) = p$ and $\dot{\gamma}(0) = \mathbf{X}(p)$. The tangent bundle structure allows to introduce the operation of **tensor derivation**[7] $\mathcal{D}\mathcal{T}_s^{(r)} \to \mathcal{T}_s^{(r)}$ that in general have to satisfy the the following properties:

- Commutes with contractions, i.e. if $A \in \mathcal{T}_s^{(r)}$, $\{V_j\}_{j=1,\dots,s} \in T$ and $\{\alpha_i\}_{i=1,\dots,s}$

$$\begin{aligned}
&\mathcal{D}A(\theta_1,\dots,\theta_i,\dots,\theta_r,V_1,\dots,V_j,\dots,V_s) = (\mathcal{D}A)(\theta_1,\dots,\theta_i,\dots,\theta_r,V_1,\dots,V_j,\dots,V_s)+\\
&+\sum_{i=0}^{r} A(\theta_1,\dots,\mathcal{D}\theta_i,\dots,\theta_r,V_1,\dots,V_j,\dots,V_s)+\\
&+\sum_{j=1}^{s} A(\theta_1,\dots,\theta_i,\dots,\theta_r,V_1,\dots,\mathcal{D}V_j,\dots,V_s)
\end{aligned} \tag{A.7}$$

- satisfy a Leibniz law with respect to tensor product, i.e. $\mathcal{D}(A \otimes B) = \mathcal{D}A \otimes B + A \otimes \mathcal{D}B$.

From this two properties is follows that the action of a derivation is specified by its action over function and vector field. The **Lie derivative** $\mathcal{L}_{\boldsymbol{X}}$ with respect to a vector field $\mathbf{X}$ generalize the concept of derivation along a curve: it measure the local rate of change of a tensor field along a curve whose tangent vector is $\mathbf{X}$. Its action over functions f and vector fields $Y \in T\mathcal{M}$ is given by:

$$\mathcal{L}_{\mathbf{X}} f := \mathbf{X}(f) = X^i \partial_i f \qquad \mathcal{L}_{\mathbf{X}} \mathbf{Y} = [\mathbf{X}, \mathbf{Y}] = \left(X^j \partial_j Y^i - Y^j \partial_j X^i\right) \boldsymbol{\partial}_i \tag{A.8}$$

and consequently its action on one form is given by $\mathcal{L}_{\mathbf{X}}(\theta) = (\mathcal{L}_{\mathbf{X}}\theta)_i \, \mathrm{d}x^i = X^i \partial_i \theta_j + \theta_j \partial_i X^i$. We notice that to calculate the values of the derivative of a tensor with respect to a vector field $\mathbf{X}$ in a point p it is not sufficient to know its point-wise value but it is required its local value for the presence of its derivatives[8]. Moreover this derivation cannot be applied to a general vector bundle constructed over $\mathcal{M}$. For this latest case is required to introduce the concept of **connection** over a vector bundle. Let be $\Gamma(E)$ the set of all sections over a q-dimensional vector bundle E with base $\mathcal{M}$ and fibre V ; then a connection ∇ over this vector bundle is a map $\nabla : \Gamma(E) \to \Gamma(T * \mathcal{M} \otimes E)$ such that

[7] The function over a manifold can be regarded as a tensor bundle of $(0,0)$-rank

[8] The only case where the point-wise information of $\mathbf{X}$ is sufficient is when it is applied to functions

- the connection of a sum of sections is the sum of the connections of each section, i.e. $s_1, s_2 \in \Gamma(E)$ it follows that $\nabla(s_1 + s_2) = \nabla s_1 + \nabla s_2$;
- if f is a function over $\mathcal{M}$ and $s \in \Gamma(E)$ then $\nabla(fs) = \mathrm{d}f \otimes s + f\nabla s$ where $\mathrm{d}f = \partial_i f \mathrm{d}x^i$ is the differential of the function.

When the connection ∇s is contracted with a vector field $\mathbf{X} \in T\mathcal{M}$ is called **covariant derivative** of s with respect to $\mathbf{X}$ and it is indicated with $\nabla_{\mathbf{X}} s$. The action of the connection is characterized by matrix valued 1-form, called *connection form* θ: if $\mathbf{s} = s^\alpha \mathbf{e}_\alpha$ is a section in vector bundle V whose local basis is $\{\mathbf{e}_\alpha\}_{\alpha=1,\dots,q}$

$$\nabla s = \mathrm{d}s^\alpha \otimes \mathbf{e}_\alpha + s^\beta \theta^\alpha_\beta \mathbf{e}_\alpha = \left(\partial_i s^\alpha + s^\beta \theta^\alpha_{\beta;i}\right) \mathrm{d}x^i \otimes \mathbf{e}_\alpha \,. \tag{A.9}$$

Covariant derivative with respect to $\mathbf{X} = X^i \boldsymbol{\partial}_i$ on a tensor bundle $\mathcal{T}^{(r)}_{(s)}\mathcal{M}$ acts like a derivation; it follows that also in this case it is uniquely defined by its action on function and vectors

$$\nabla_{\mathbf{X}} f = X^i \partial_i f \qquad \nabla_{\mathbf{X}} \mathbf{Y} = X^j \left(\partial_j Y^i + Y^k \theta^i_{k;j}\right) \boldsymbol{\partial}_i \tag{A.10}$$

and consequently, in the case of the covariant derivative with respect to $\mathbf{X}$ of a general tensor $t = t^{i_1 \dots i_s}_{j_1 \dots j_r} \boldsymbol{\partial}_{i_1} \otimes \dots \boldsymbol{\partial}_{i_s} \otimes \mathrm{d}x^{j_1} \otimes \dots \mathrm{d}x^{j_r}$ it is given by

$$(\nabla_{\mathbf{X}} t)^{i_1 \dots i_s}_{j_1 \dots j_r} = X^k \left(\partial_k t^{i_1 \dots i_s}_{j_1 \dots j_r} + \sum_{l=1}^{r} \theta^{i_l}_{i_m;k} t^{i_1 \dots i_m \dots i_s}_{j_1 \dots j_r} - \sum_{l=1}^{s} \theta^{j_m}_{j_l;k} t^{i_1 \dots i_m \dots i_s}_{j_1 \dots j_r} \right) \tag{A.11}$$

For connections on the tangent bundle, the **torsion** $(2,1)$-rank tensor is defined as

$$\mathrm{Tor}(\mathbf{X}, \mathbf{Y}) = \nabla_{\mathbf{X}} \mathbf{Y} - \nabla_{\mathbf{Y}} \mathbf{X} - [\mathbf{X}, \mathbf{Y}] \tag{A.12}$$

and in components reads

$$\mathrm{Tor}^k_{ij} = \theta^k_{i;j} - \theta^k_{j;i} - ([\boldsymbol{\partial}_i, \boldsymbol{\partial}_j])^k \,. \tag{A.13}$$

In general $\nabla_{\mathbf{X}} \nabla_{\mathbf{Y}} \neq \nabla_{\mathbf{Y}} \nabla_{\mathbf{X}}$ a measure of the difference between these derivatives is the **curvature** R of the connection, i.e.

$$R(\mathbf{X}, \mathbf{Y}) = \nabla_{\mathbf{X}} \nabla_{\mathbf{Y}} - \nabla_{\mathbf{Y}} \nabla_{\mathbf{X}} - \nabla_{[\mathbf{X}, \mathbf{Y}]} \tag{A.14}$$

A.3 Differential forms, exterior differentiations, integration of forms

Let us indicate with $A^k(\mathcal{M})$ the tensor bundle constructed over the manifold $\mathcal{M}$ as a disjoint union of the k-form spaces Λ^k_p. For the n-dimensional manifold $\mathcal{M}$ the space $A(\mathcal{M}) = \sum_{k=0}^{n} A^k(\mathcal{M})$ is a graded algebra as with respect to the operation of sum $+$ and wedge product $\wedge$ of differential forms, meaning that $A(\mathcal{M})$ is a direct sum of a sequence of a vector spaces, and the product $\wedge$ defines a map $\wedge : A^r(\mathcal{M}) + A^s(\mathcal{M}) \to A^{r+s}(\mathcal{M})$ where $A^{r+s}(\mathcal{M})$ is zero when $r + s > n$. The

exterior derivative d is a derivation introduced on $A(\mathcal{M})$ such that $\mathrm{d}(A^k(\mathcal{M})) \subset A^{k+1}(\mathcal{M})$ such that for any $\alpha, \beta \in A(\mathcal{M})$:

- $\mathrm{d}(\alpha + \beta) = \mathrm{d}\alpha + \mathrm{d}\beta$;
- if $\alpha \in A^r(\mathcal{M})$ then $\mathrm{d}(\alpha \wedge \beta) = \mathrm{d}\alpha \wedge \beta + (-1)^r \alpha \wedge \mathrm{d}\beta$;
- if f is a smooth function $\mathcal{M}$ (i.e. $f \in A^0(\mathcal{M})$), where $\mathrm{d}f = \partial_i f \mathrm{d}x^i$
- if f is a smooth function $\mathcal{M}$ then $\mathrm{d}(\mathrm{d}f) = 0$.

The exterior differentiation of a differential k-form $\alpha \in A^k(\mathcal{M})$ is given by

$$\begin{aligned}(\mathrm{d}\alpha)(\mathbf{X}_1, \ldots, \mathbf{X}_{k+1}) &= \sum_{i=1}^{k+1} (-1)^{i+1} \mathbf{X}_i \left(\alpha(\mathbf{X}_1, \ldots, \mathbf{X}_{i-1}, \mathbf{X}_{i+1}, \ldots \mathbf{X}_{k+1})\right) + \\ &+ \sum_{1 \le i < j \le k+1} (-1)^{i+j} \alpha([\mathbf{X}_i, \mathbf{X}_j], \mathbf{X}_1, \ldots \mathbf{X}_{i-1} \mathbf{X}_{i+1} \ldots \mathbf{X}_{j-1} \mathbf{X}_{j+1} \ldots \mathbf{X}_{k+1})\end{aligned} \tag{A.15}$$

The *Poincare's Lemma* states that $\mathrm{d}^2\alpha = 0$ for all $\alpha \in A(\mathcal{M})$. The space $A(\mathcal{M})$ endowed with the differential d is called a complex. In any subspace $A^k(\mathcal{M})$ two subspaces can be identified:

- the space $Z^k(\mathcal{M})$ of all k-forms α that are *closed*, so $\mathrm{d}\alpha = 0$, (also called *cocycles*)
- the space $B^k(\mathcal{M})$ of all k-forms α that are *exact*, so that exist $\beta \in C^{k-1}(\mathcal{M})$ such that $\mathrm{d}\beta = \alpha$, (also called *coboundaries*).

The cohomology space $H^k(\mathcal{M}; \mathbb{R})$ is defined as

$$H^k(\mathcal{M}; \mathbb{R}) = Z^k(\mathcal{M}) / B^k(\mathcal{M}) \tag{A.16}$$

and an element $[\omega]$ in this space is the *equivalence class* of k-forms that differ among them for an exact form, i.e. $[\omega_1] = [\omega_2]$ if $\omega_1 - \omega_2 = \mathrm{d}phi$. From the definition of differential k-form it follows that $H^k(\mathcal{M}, \mathbb{R}) = 0$ if $k > n$.
The **De Rham cohomology space** $H^*(\mathcal{M}; \mathbb{R})$ is a graded space obtained as the direct sum of the k-dimensional cohomology spaces:

$$H^*(\mathcal{M}, \mathbb{R}) = \otimes_{k \ge 0} H^k(\mathcal{M}; \mathbb{R}) \,. \tag{A.17}$$

and it is a multiplication ring with the the addition $[\omega_1] + [\omega_2] = [\omega_1 + \omega_2]$ and the multiplication $[\omega_1] \smile [\omega_2] = [\omega_1 \wedge \omega_2]$. Moreover if $f : \mathcal{M}^n \to \mathcal{N}^k$ is a smooth map the pullback[9] $f^* : A^p(\mathcal{N}^k) \to A^k(\mathcal{M}^n)$ is a *homomorphism induced by the mapping* among cohomology rings, i.e. $f^* : H^*(\mathcal{N}^k; \mathbb{R}) \to H^*(\mathcal{M}^k; \mathbb{R})$ with $f^*[\omega] = [f^*\omega]$.
Two smooth mapping $f_0 : \mathcal{M}^n \to \mathcal{N}^k$ and $f_1 : \mathcal{M}^n \to \mathcal{N}^k$ are smoothly homotopic if there is a

[9] Let be $h : \mathcal{N} \to \mathcal{M}$ an application between two manifolds, and let $f : \mathcal{M} \to \mathbb{R}$ be a function over $\mathcal{M}$, then the **pullback** of a function is defined as the function $(h^* f) : \mathcal{N} \to \mathbb{R}$ s.t. $(h^* f) = f \circ h$. The wedge product and exterior differentiation commutates with the pullback of forms, i.e. $h^*(\omega_1 \wedge \omega_2) = h^*\omega_1 \wedge h * \omega_2$ and $\mathrm{d}(h^* f) = h^* \mathrm{d}\omega$.

smooth *homotopy* mapping $F : \mathcal{M}^n \times [0,1] \to \mathcal{N}^k$ such that $F(x,k) = f_k(x)$ with $k = 0,1$. In this case the action of the homomorphism of cohomology rings $f_0^* : H^*(\mathcal{N}^k;\mathbb{R}) \to H^*(\mathcal{M}^n;\mathbb{R})$ and $f_1^* : H^*(\mathcal{N}^k;\mathbb{R}) \to H^*(\mathcal{M}^n;\mathbb{R})$ coincides. Two manifolds $\mathcal{M}^n$ and $\mathcal{N}^n$ are said to be *homotopically equivalent* if there exists two mappings $f : \mathcal{M}^n \to \mathcal{N}^k$ and $g : \mathcal{N}^k \to \mathcal{M}^n$ such that fg and gf are homotopic to the identity. It can be proved that two homotopically equivalent manifolds have isomorphic cohomology groups.
The integration of exterior derivatives allows to connect local and global properties of a manifold. The first step consists in defining an **orientable manifold** as n-dimensional manifold $\mathcal{M}$ where there exists a continuous and nonvanishing exterior differential n-form; two differential n-forms which differ everywhere by a function factor which is always positive define an *orientation*. Let us suppose that $\mathcal{M}$ is a manifold oriented by a differential n-form ω, then a chart (U,x) is *compatible* if ω and $\mathrm{d}x^1 \wedge \ldots \wedge \mathrm{d}x^n$ define the same orientation.
The main results that allows to define the integration over a manifold is the **Partition of Unity Theorem**: suppose Σ is an open covering of a smooth manifold $\mathcal{M}$. Then there exists a family of smooth functions $\{g_\alpha\}$ on $\mathcal{M}$ satisfying the following conditions:

- $0 \leq g_\alpha \leq 1$ and the supp$g_\alpha = \{p \in \mathcal{M} | g_\alpha(p) \neq 0\}$ is compact for each α. Moreover, there exists an open set $W_i \in \Sigma$ such that $g_\alpha \subset W_i$;
- For each point $p \in \mathcal{M}$ there is a neighbourhood U that intersects suppg_α for only a finite number of α
- $\sum_\alpha g_\alpha = 1$.

The **integral** of a differential m-form ω is defined as

$$\int_{\mathcal{M}} \omega = \sum_\alpha \int_{W_i} g_{alpha}\omega \tag{A.18}$$

where in a local coordinate system $g_{alpha}\omega = f(x^1,\ldots,x^n)\mathrm{d}x^1 \wedge \ldots \wedge \mathrm{d}x^n$ so that $\int_{W_i} g_{alpha}\omega = \int_{W_i} f(x^1,\ldots,x^n)\mathrm{d}x^1 \ldots \mathrm{d}x^n$. Let us suppose that $h : \mathcal{N} \to \mathcal{M}$ is the imbedding of a k-dimensional submanifold in the n-dimensional ambient manifold $\mathcal{M}$. Then the integral of the differential k-form $h^*\omega$ over $\mathcal{N}$ is defined as

$$\int_{h(\mathcal{N})} \omega = \int_{\mathcal{N}} h^*\omega \ . \tag{A.19}$$

A very relevant result in integration theory of differential forms is the **Stokes Theorem**: let ω be a $(n-1)$-form and $D \subseteq \mathcal{M}$ and with a smooth or piecewise smooth boundary ∂D then

$$\int_{\partial D} \omega = \int_D \mathrm{d}\omega \ . \tag{A.20}$$

This formula has its importance as it allows to characterize the topology of a certain domain D over a manifold $\mathcal{M}$ as it establishes a duality (Poincar duality) among the boundary operator

∂ and the coboundary operator (i.e. the exterior differentiation) d on forms. This result can be expressed

$$\int_{\partial D} \omega = (\partial D, \omega) = (D, \mathrm{d}\omega) = \int_D \mathrm{d}\omega \tag{A.21}$$

which represents the link between homology, the rigorous mathematical way to classify the manifolds with respect to their "holes", and the De Rham cohomology of differential forms on manifolds.

A geometric *cycle* on a manifold $\mathcal{M}^n$ is a pair $(\mathcal{N}^k, f)$ consisting of a smooth mapping $f : \mathcal{N}^k \to \mathcal{M}^n$. If there is an orientation on the manifold $\mathcal{N}^k$, then such a cycle will be said to be oriented. Any closed k-form ω on a manifold $\mathcal{M}^n$ specifies a function on the set of all k-dimensional cycles $z = (\mathcal{N}^k, f)$ by the formula

$$\langle \omega, z \rangle = \int_{N_k} f^* \omega \,. \tag{A.22}$$

It can be proved that the value of $\langle \omega, z \rangle$ depends only by the cohomology group $[\omega]$.

Let $A_p(\mathcal{M})$ the space generated by all the oriented p-cycle over the field $\mathbb{R}$. For each element z of this space we can define the integral of a closed p-form ω over z. Namely let $z = \lambda_1 z_1 + \ldots + \lambda_k z_k$ where $\lambda_i \in \mathbb{R}$ and $z_i = (\mathcal{N}_i^p, f_i)$ are ordinary cycles. Then

$$\langle \omega, z \rangle = \sum_i \lambda_i \langle \omega, z_i \rangle = \sum_i \lambda_i \int_{\mathcal{N}_i} f_i^* \omega \tag{A.23}$$

Let $B_p(\mathcal{M}) \subset A_p(\mathcal{M})$ be the subspace that consist of the cycles such that the integral of all closed p-forms over these cycles vanish. The quotient space

$$H_p(\mathcal{M}^p; \mathbb{R}) = A_p(\mathcal{M}^n)/B_p(\mathcal{M}^n) \tag{A.24}$$

is called the real p-dimensional homology group of the manifold $\mathcal{M}^n$. The homology space is dual to the cohomology group $H^p(\mathcal{M}^p; \mathbb{R})$ and for any nonzero element $[\omega] \in H^p(\mathcal{M}^p; \mathbb{R})$ the linear functional

$$\langle [\omega], [z] \rangle = \langle \omega, z \rangle \qquad z \in H_p(\mathcal{M}^p; \mathbb{R}) \,. \tag{A.25}$$

For compact manifolds all the cohomology groups are finite-dimensional and their dimensions are called *Betti numbers* $b_p(\mathcal{M}) = \mathrm{dim} H_p(\mathcal{M}^p; \mathbb{R}) = \mathrm{dim} H^p(\mathcal{M}^p; \mathbb{R})$ and are topological invariants. The alternating sum of the Betti numbers is the *Euler characteristics* $\chi(\mathcal{M}) = \sum_{i=0}^{n} (-1)^i \, b_i(\mathcal{M})$; as for a compact n-dimensional connected manifold without boundaries the Poincare duality implies $H^{n-k}(\mathcal{M}^p; \mathbb{R}) = H^k(\mathcal{M}^p; \mathbb{R})$ it follows that for odd-dimensional manifolds the Euler characteristic vanishes $\chi(\mathcal{M}^{2n+1}) = 0$.

A.4 Riemannian structure

Thanks to the vector structure, a scalar product, can be defined on $T_p\mathcal{M}$ as $g_p : T_p\mathcal{M} \times T_p\mathcal{M} \to \mathbb{R}$. This is a way to associate a *real* number to any pair $(\mathbf{X}_p, \mathbf{Y}_p)$ of tangent vectors. This product inherits all the features of the canonical scalar product on the linear space $\mathbb{R}^n$; in

particular $\|\mathbf{X}_p\|^2_{g_p} = g_p(\mathbf{X}_p, \mathbf{X}_p) > 0$ for all tangent vector $\mathbf{X}_p$ and $g_p(\mathbf{X}_p, \mathbf{Y}_p) = 0$, if and only if one of the tangent vectors X_p or Y_p is null.
The Riemannian structure allows to define the *gradient* $\mathbf{grad}_g f$ of a function f on $\mathcal{M}$ as the vector field with the property

$$g(\mathbf{grad}_g f, \mathbf{Y}) = \mathbf{Y}(f) = Y^i \partial_i f \,. \tag{A.26}$$

and the *divergence* of a vector field $\mathbf{X}$ as

$$(\mathrm{div}_g \mathbf{X}) = \sum_{j=1}^{N} \mathrm{d}x^j \left(\nabla_{\boldsymbol{\partial}_j} \mathbf{X}\right) \,. \tag{A.27}$$

If this properties holds for every point $p \in \mathcal{M}$ for the tensor field $(0,2)$-rank $g = g_{ij}\mathrm{d}x^i \otimes \mathrm{d}x^j$ such a tensor is a **metric tensor field** that defines a **Riemannian structure** over the manifold $\mathcal{M}$.
The definition of a metric tensor allows to define the length of a curve $c(t) : [a,b] \to \mathbb{R}$ as

$$L(c) = \int_a^b \|\dot{\mathbf{c}}(t)\|^2 \mathrm{d}t \,. \tag{A.28}$$

and the volume form dVol_g

$$\mathrm{dVol}_g = |\mathrm{det} g_{ij}|^{1/2} \mathrm{d}x^1 \wedge \ldots \wedge \mathrm{d}x^N \,. \tag{A.29}$$

The inverse of g_{ij} is given by the g^{kl} matrix with $g_{ij}g^{jk} = \delta_i^k$; this two matrices allows to define the raising and lowering of indices of a tensor, i.e.

$$g_{ki_l} t^{i_1 \ldots i_l \ldots i_r}{}_{j_1 \ldots j_r} = t^{i_1 \ldots i_{l-1}}{}_k{}^{i_{l+1} \ldots i_r}{}_{j_1 \ldots j_r} \qquad g^{kj_l} t^{i_1 \ldots i_r}{}_{j_1 \ldots j_l \ldots j_r} = t^{i_1 \ldots i_r}{}_{j_1 \ldots j_{l-1}}{}^k{}_{j_{l+1} \ldots j_r} \tag{A.30}$$

This allows to define the *metric-dependent trace of a* $(0,2)$*-rank tensor* $A = A_{ij}\mathrm{d}x^i \otimes \mathrm{d}x^j$ as:

$$\mathrm{Tr}^g(A) = g^{ij} A_{ij} = A^i{}_i \,. \tag{A.31}$$

The Riemannian structure puts some constraints on the definition of a connection on the tangent and tensor bundles over a given manifold; in particular, a **Levi-Civita connection** is *compatible with the metric*, that means

$$(\nabla_{\mathbf{X}} g)_{ij} = X^k \partial_k g_{ij} - \theta^l_{i;k} g_{lj} - \theta^l_{j;k} g_{il} \tag{A.32}$$

and *torsion free*, i.e. $\mathrm{Tor} = 0$. In this case the components of the matrix-valued connection form are expressed by the *Christoffel symbol* $\Gamma^k_{ij} = \theta^k_{j;i}$. It can be proved that the for a given metric g over $\mathcal{M}$ a unique Levi-Civita is defined.
The Christoffel symbol can be expressed as a function of derivatives of the components of the

metric tensor

$$\Gamma^i_{jk} = \frac{1}{2} g^{il} \left(\partial_j g_{lk} + \partial_k g_{jk} - \partial_l g_{jk} \right) . \tag{A.33}$$

The curvature tensor for a Levi-Civita connection specified by the symbols Γ^i_{jk} is the **Riemann curvature tensor** that in components reads:

$$R^i_{jkl} = \partial_l \Gamma^i_{jk} - \partial_j \Gamma^i_{kl} + \Gamma^m_{jk} \Gamma^i_{ml} - \Gamma^m_{jl} \Gamma^i_{mk} \tag{A.34}$$

and whose completely covariant version is the tensor $R_{ijkl} = g_{mi} R^i_{jkl}$ with basic symmetries:

$$R_{ijkl} = -R_{jikl} = -R_{ijlk} = R_{klij} . \tag{A.35}$$

In order to give a geometrical interpretation of Riemann curvature, let us introduce the concept *geodesic curve* as the shortest smooth curve that connects two points on a Riemannian manifold; a variational formulation of this condition for a geodesic $\gamma = (x^1(t) \dots x^N(t)))$ is given by:

$$\Delta_{\dot{\gamma}} \dot{\gamma} = 0 \quad \Rightarrow \quad \ddot{x}^i + \Gamma^i_{kj} \ddot{x}^j \ddot{x}^k . \tag{A.36}$$

Now let us consider a smooth one parameter family of geodesic γ_τ with $\gamma_0(t) = \gamma(t)$ than the *Jacobi vector field* $\mathbf{J}$ along the geodesic $\gamma(t)$ is defined as

$$\mathbf{J} = \partial \gamma_\tau(t) \Big|_{\tau=0} \tag{A.37}$$

The Riemann curvature tensor gives a measure of the local geodesic spread. The evolution of the Jacobi field along a given geodesic is described by the *Jacobi-Levi-Civita equation.* Let us suppose that along the geodesic it is consider a orthonormal frame $\{\mathbf{e}_i\}_{i=1,\dots,N}$ in $T_{\gamma(t)}\mathcal{M}$, parallel transported all along $\Delta \mathbf{e}_i = 0$ and with $\mathbf{e}_1 = \dot{\gamma}/\|\dot{\gamma}\|_g$ than if the jacobi vector field is expressed $\boldsymbol{J} = y^i \mathbf{e}_i$ the Jacobi Levi Civita for the geodesic spread reads

$$\ddot{y}^k + \|\dot{\gamma}\|_g^2 \mathrm{R}^k_{1j1} y^j = 0 . \tag{A.38}$$

The contraction $C_{1,2}(R)$ of the Riemann curvature tensor is the **Ricci curvature tensor**

$$\mathrm{Ric}_{ij} = R^k_{ikj} = \partial_l \Gamma^l_{ji} - \partial_j \Gamma^l_{li} + \Gamma^l_{lk} \Gamma^k_{ji} - \Gamma^l_{jk} \Gamma^k_{il} . \tag{A.39}$$

For a given metric g the Ricci curvature gives a local measure of the difference between the volume form with respect to an euclidean metric $g_{\mathbb{E}}$, i.e. if in a certain point $g_{ij} = \delta_{ij} + o\left(\|\mathbf{X}\|_g^2\right)$ with $\mathbf{X} = X^i \boldsymbol{\partial}_i$

$$\mathrm{dVol}_g = \mathrm{dVol}_{g_{\mathbb{E}}} \left(1 - \frac{1}{6} \mathrm{Ric}_{jk} X^k X^j + o\left(\|\mathbf{X}\|_g^3\right) \right) \tag{A.40}$$

so in the directions $\mathbf{X}$ such that $\mathrm{Ric}(\boldsymbol{X}, \boldsymbol{X})$ is positive the volume is contracted with respect to the Euclidean volume.

The metric-dependent trace of the Ricci curvature tensor is the **Scalar curvature** $\mathcal{R} = \mathrm{Tr}^g \mathrm{Ric} = g^{ij} \mathrm{Ric}_{ij}$.

A.5 Riemmanian geometry of codimension one submanifolds (regular level sets)

Let $(\mathcal{M}, \bar{g})$ be a N-dimensional Riemannian manifold whose Levi-Civita commection is $\overline{\nabla}$. A **regular Submanifold** of dimension K is a subset Σ such that for every point $p \in \Sigma$ such that for a certain chart (U, x) over $\mathcal{M}$ it holds $x\,(U \cap Sigma) = x(U) \cup \mathbb{R}^K \times \{c\}$ for some $c \in \mathbb{R}^{N-K}$, that means that exists a chart over $\mathcal{M}$ such that for its restriction over Σ there are $N-K$ fixed components. In particular, the set defined as a locus that in a chart (U, x) reads $\Sigma = \{p \in \mathcal{M} | f_A(x^1(p), ..., x_N(p))\} = 0 \qquad$ for $A = 1, ..., L$ it is a K-dimensional level sets (with $K \leq L$) if the rank of the Jacobian $\partial_i f_A$ is K.
The equipotential level sets discussed in the first part of this manuscript are an example of regular submanifold without boundaries in absence of critical point of potential energy. Moreover in this specific case, we have a local **regular foliation** $\mathcal{F}$ of the configuration space, namely when the ambient manifolds can be regarded as the disjoint union of connected regular submanifolds $\Sigma_{\mathbf{a} \in \mathbb{R}^{N-K}}$ called *leaves* of dimension K (and co-dimension $N-K$) such that in a neighbourhood of any point of the ambient space exists a chart (U, x) such where the coordinate can be expressed in the form $(a^1, ..., a^{N-K}, x^1, ..., x^K)$. In what follows we consider level sets of one single function so that $K = N - 1$.
As we supposed that the ambient space has a Riemannian structure, each leaf inherits a metric structure, the so called **First Fundamental Form** $\mathrm{I} : T_p\Sigma \times T_p\Sigma \to \mathbb{R}$ defined over a regular submanifold of co-dimension one

$$\mathrm{I}_\Sigma(\mathbf{X}, \mathbf{Y}) :\equiv \bar{g}(\mathbf{X}, \mathbf{Y}) \qquad \mathbf{X}, \mathbf{Y} \in T_p\Sigma \tag{A.41}$$

and it coincides with the restriction of metric tensor $\bar{g}$ on the immersed co-dimension one submanifold Σ. This allows to define a Levi-Civita connection ∇ over the regular submanifold. In order to introduce a more suitable notation for a fixed Σ, we will use in what follows $g = \mathrm{I}$.
Moreover, for a co-dimension one regular submanifold Σ in a ambient space $\mathcal{M}$ it is possible to define a **normal vector field** as the vector field $\boldsymbol{\nu} \neq \mathbf{0}$ such that $\bar{g}(\boldsymbol{\nu}, \mathbf{X}) = 0$ for every $\mathbf{X} \in T_p\Sigma$.
The rate of (covariant) variation of the normal vector field in a direction tangent to the submanifolds defines is intuitively related with the concept of curvature for a immersed submanifold. This is can be formalized as follows. First of all let us consider the **Weingarten operator or Shape Operator** $W_{\boldsymbol{\nu}_p} : T_p\Sigma \to T_p\Sigma$:

$$W_{\boldsymbol{\nu}_p}(X) :\equiv \overline{\nabla}_{\mathbf{X}} \boldsymbol{\nu}\big|_p \qquad \mathbf{X} \in T_p\Sigma \quad . \tag{A.42}$$

This operator can be regarded as $(1,1)$-rank tensor field over he submanifold tangent space; the induced metric structure over the submanifold allows to construct a $(0,2)$-rank tensor field over this submanifold called **Second Fundamental Form** $\mathrm{II}_\Sigma : T_p\Sigma \times T_p\Sigma \to \mathbb{R}$

$$\mathrm{II}_\Sigma(\mathbf{X}, \mathbf{Y}) = \bar{g}(W_\nu(\mathbf{X}), \mathbf{Y}) = \bar{g}(\nabla_{\mathbf{X}} \boldsymbol{\nu}, \mathbf{Y}) = -\bar{g}(\boldsymbol{\nu}, \nabla_{\mathbf{X}} \mathbf{Y}) \qquad \mathbf{X}, \mathbf{Y} \in T_p\Sigma \tag{A.43}$$

The second fundamental form is symmetric in its arguments as:

$$\begin{aligned}\mathrm{II}(\mathbf{X},\mathbf{Y}) &= \bar{g}(\overline{\nabla}_{\mathbf{X}}\boldsymbol{\nu},\mathbf{Y}) = -\bar{g}(\boldsymbol{\nu},\overline{\nabla}_{\mathbf{X}}\mathbf{Y}) = -\bar{g}(\boldsymbol{\nu},\overline{\nabla}_{\mathbf{Y}}\mathbf{X}) - \bar{g}(\boldsymbol{\nu},[\mathbf{X},\mathbf{Y}]) = \\ &= \bar{g}(\overline{\nabla}_{\mathbf{Y}}\boldsymbol{\nu},\mathbf{X}) = \mathrm{II}(\mathbf{Y},\mathbf{X}) \qquad \mathbf{X},\mathbf{Y}\in T_p\Sigma\end{aligned} \tag{A.44}$$

The eigenvalues $(\lambda_1,...,\lambda_n)$ of the Weingarten operator are called **principal curvatures** and the metric-dependent trace of shape operator is called **mean curvature**:

$$h_{\Sigma,\bar{g}} = \frac{\sum_{i=1}^{N-1}\lambda_{i,\bar{g}}}{N-1} = \frac{\mathrm{Tr}^g(\mathrm{II})}{N-1} = \frac{\tau_{1,\bar{g}}}{N-1} \tag{A.45}$$

We derive a formula for the variation of mean curvature along the normal direction, in a coordinate system $(x^0,x^1,...,x^{N-1})$, where $\boldsymbol{\partial}_0=\boldsymbol{\nu}$, for a co-dimension one regular foliation

$$\mathcal{L}_{\boldsymbol{\nu}}(\tau_{1,\bar{g}}) = \overline{\nabla}_{\boldsymbol{\nu}}\left(g^{ij}\mathrm{II}_{ij}\right) = \mathcal{L}_{\boldsymbol{\nu}}(g^{ij})\mathrm{II}_{ij} + g^{ij}\mathcal{L}_{\boldsymbol{\nu}}\left(\mathrm{II}_{ij}\right) \qquad i,j=1,...,N-1 \tag{A.46}$$

We note that

$$\mathcal{L}_{\boldsymbol{\nu}}\left(g^{ij}g_{jk}\right) = 0 \tag{A.47}$$

from what follows

$$\mathcal{L}_{\boldsymbol{\nu}}g^{ij} = -g^{jk}g^{il}\mathcal{L}_{\boldsymbol{\nu}}(g_{kl})\,. \tag{A.48}$$

The last term can be calculated considering that the action of Lie derivative and covariant differentiation coincide on functions

$$\mathcal{L}_{\boldsymbol{\nu}}(g_{kl}) = \overline{\nabla}_{\boldsymbol{\nu}}\left(\bar{g}(\mathbf{e}_k,\mathbf{e}_l)\right) = 2(\overline{\nabla}^{\bar{g}}_{\boldsymbol{\nu}}\mathbf{e}_k,\mathbf{e}_l) = 2(\overline{\nabla}_{\mathbf{e}_k}\boldsymbol{\nu},\mathbf{e}_l) = 2\mathrm{II}(\mathbf{e}_k,\mathbf{e}_l) = 2\mathrm{II}_{kl} \tag{A.49}$$

so that substituting the last expression in (A.47) we obtain

$$\mathcal{L}_{\boldsymbol{\nu}}g^{ij} = -2\mathrm{II}^{ij} \tag{A.50}$$

and the first term of right-side in eq. (A.46) results

$$\mathcal{L}_{\boldsymbol{\nu}}(g^{ij})\mathrm{II}_{ij} = -2\mathrm{II}^{ij}\mathrm{II}_{ij} = -2(\mathrm{II}^2)^i_i = -2\mathrm{Tr}^g\left(\mathrm{II}^2\right)\left(= -2\sum_{i=1}^{N-1}\lambda^2_{1,\bar{g}} := -2\tau_{2,\bar{g}}\right) \tag{A.51}$$

Let us now consider the Lie derivative of second fundamental form along the normal field.

$$\begin{aligned}\mathcal{L}_{\boldsymbol{\nu}}\mathrm{II}_{ij} &= \mathcal{L}_{\boldsymbol{\nu}}\mathrm{II}(\mathbf{e}_i,\mathbf{e}_j) = \overline{\nabla}_{\boldsymbol{\nu}}\bar{g}(\nabla^{\bar{g}}_{\mathbf{e}_i}\boldsymbol{\nu},\mathbf{e}_j) = \bar{g}(\overline{\nabla}^{\bar{g}}_{\boldsymbol{\nu}}\overline{\nabla}_{\mathbf{e}_i}\boldsymbol{\nu},\mathbf{e}_j) + \bar{g}(\overline{\nabla}_{\mathbf{e}_i}\boldsymbol{\nu},\overline{\nabla}_{\nu}\boldsymbol{e}_j) = \\ &= \bar{g}\left(\bar{R}(\boldsymbol{\nu},\mathbf{e}_i)\boldsymbol{\nu},\mathbf{e}_j\right) + \bar{g}(\overline{\nabla}_{\mathbf{e}_i}\overline{\nabla}_{\boldsymbol{\nu}}\boldsymbol{\nu},\mathbf{e}_j) + \bar{g}([\boldsymbol{\nu},\mathbf{e}_i]\,,\mathbf{e}_j) + \bar{g}(\overline{\nabla}_{\mathbf{e}_i}\boldsymbol{\nu},\overline{\nabla}_{\boldsymbol{\nu}}\mathbf{e}_j)\end{aligned} \tag{A.52}$$

where R is the Riemannian curvature tensor of the ambient space. Under the hypothesis that $\overline{\nabla}_{\boldsymbol{\nu}}\boldsymbol{\nu}=0$ and using the antisymmetrical properties of the Riemann tensor we obtain:

$$\begin{aligned}&\mathcal{L}_{\boldsymbol{\nu}}\mathrm{II}_{ij} = -\bar{g}\left(\bar{R}(\mathbf{e}_i,\boldsymbol{\nu})\boldsymbol{\nu},\mathbf{e}_j\right) + \bar{g}(\overline{\nabla}_{\mathbf{e}_i}\boldsymbol{\nu},\overline{\nabla}_{\mathbf{e}_j}\boldsymbol{\nu}) = -\bar{R}_{j0i0} + \mathrm{W}^k_i\mathrm{W}^l_j\bar{g}(\mathbf{e}_k,\mathbf{e}_l) = \\ &= -\bar{R}_{j0i0} + \mathrm{II}^k_i\mathrm{II}^l_j\bar{g}_{k,l} = -\bar{R}_{j0i0} + \mathrm{II}^k_i\mathrm{II}_{kj}\,.\end{aligned} \tag{A.53}$$

Putting together eqs. (A.47) and (A.53) in eq.(A.46) we obtain

$$\begin{aligned}\mathcal{L}_{\boldsymbol{\nu}}(\tau_{1,\bar{g}}) &= -2\mathrm{II}^{ij}\mathrm{II}_{ij} + g^{ij}\left(-\overline{R}_{j0i0} + \mathrm{II}_i^k\mathrm{II}_{kj}\right) = -\left(\mathrm{II}^{ij}\mathrm{II}_{ij} + \overline{\mathrm{Ric}}_{00}\right) = \\ &= -\mathrm{Tr}^g(\mathrm{II}^2) - \overline{\mathrm{Ric}}(\boldsymbol{\nu},\boldsymbol{\nu}) = -\tau_{2,\bar{g}} - \overline{\mathrm{Ric}}(\boldsymbol{\nu},\boldsymbol{\nu})\end{aligned} \tag{A.54}$$

B Details on the codes used in numerical simulations

In order to investigate the ϕ^4 models described in Eqs.1.45 a code for Montecarlo importance sampling over energy potential level sets has been implemented.

B.1 A MonteCarlo code to explore regular level sets of potential energy

A C code has been realized in order to calculate the weighted averages (2.53) over equipotential level set $\Sigma^N_{N\bar{v}}$. The algorithm consists of a Monte Carlo Metropolis sampling in configuration space over the $\Sigma^N_{N\bar{v}}$ with statistical weight $\chi_N = \|\mathbf{grad}_{\mathbb{R}^N} V_N\|_{\mathbb{R}^N}$. In order to assure that the random configurations explored belong to a energy level set with a fixed potential energy $N\bar{v}$, a reprojection of the point over the chosen $\Sigma^N_{N\bar{v}}$ is performed at any step using the diffeomorphism generated by the vector field $\boldsymbol{\xi}_N$ with a required precision $\delta = \dfrac{\Delta V_N}{V_N} = 10^{-9}$.
More in details, for each simulation a fixed value $\bar{v}$ and a total number of nodes $N = L^2$ has been fixed. The initial configuration $\mathbf{q}(t_0) \in \mathbb{R}^N$ of the system has been chosen such that

$$\begin{cases} V_N(\mathbf{q}(t_0)) = N\bar{v} \\ \sum_{\mathbf{i}\in\Lambda} q_{\mathbf{i}}(t_0) = 0 \qquad \text{(null total magnetization)} \\ q_{(j,k)}(t_0) = -q_{(j,L-k)}(t_0) \quad \forall j,k = 1,...,L \end{cases} \tag{B.1}$$

where V_N takes into the account for periodic boundary condition and the last condition assures a $\mathbb{Z}^2$ symmetrical configuration respect to the central column of the lattice element considered. Analogous condition has been imposed for initial configuration of φ^4-model in $1D$.
In what follows we say that a "configuration $\mathbf{q}$ belongs to $\Sigma^N_{N\bar{v}}$" if $|V_N(\mathbf{q}) - N\bar{v}|/(N\bar{v}) < \delta$.
To move from a configuration $\mathbf{q}(t_i)$ to another $\mathbf{q}(t_{i+1})$ both belonging to $\Sigma^N_{N\bar{v}}$, we use the following procedure. A random vector $\boldsymbol{\eta} \in \mathbb{R}^N$ is extracted with each component η_i uniformly distributed in the interval $[-0.5; 0.5]$ and completely independent from the other. A predicted configuration $\tilde{\mathbf{q}}(t_i + 1)$ is then obtained by

$$\tilde{\mathbf{q}}(t_i) = \mathbf{q}(t_i) + \Delta_q \boldsymbol{\eta} \tag{B.2}$$

with the parameter δ_q regulating the mean module of the displacement in configuration space; in our simulation $\delta_q = 2$. If the new configuration belongs to the fixed level set, then a Metropolis-Hastings acceptance test for the new configuration $\tilde{\mathbf{q}}(t_i + 1)$ using an acceptance probability

$$\rho = \min\{1; \chi(\mathbf{q}(t_i))/\chi(\tilde{\mathbf{q}}(t_i + 1))\}. \tag{B.3}$$

and if the acceptance test successes then $\tilde{\mathbf{q}}(t_i+1)) = \mathbf{q}(t_i+1)$ else $\mathbf{q}(t_i) = \mathbf{q}(t_i+1)$ and the geometric quantities are sampled in $\mathbf{q}(t_i+1)$. Differently, if the configuration obtained by (B.2) does not belong to $\Sigma^N_{N\bar{v}}$ the difference $\Delta V_{Tot} = V_N(\tilde{\mathbf{q}}(t_i+1)) - N\bar{v}$ is calculated and the configuration $\tilde{\mathbf{q}}(t_i+1)$ is reprojected on the fixed level set $\Sigma^N_{N\bar{v}}$ integrating numerically using a second order Heun algorithm the following differential equations

$$\frac{\mathrm{d}x_i}{\mathrm{d}v} = -\chi_N \frac{\partial V_N}{\partial x_i} \tag{B.4}$$

in the interval $v \in [0; \Delta V_{Tot}]$ with initial conditions $\mathbf{x}(0) = \tilde{\mathbf{q}}(t_i+1)$ and discrete steps $\delta_v = \Delta V_{Tot}/10$. If the final configuration belongs to $\Sigma^N_{N\bar{v}}$ then the Metropolis test is performed with $\tilde{\mathbf{q}}(t_i+1)) = \mathbf{x}(\Delta V_{Tot})$, else the reprojection procedure is repeted.

B.2 Derivatives of the Hirsch vector field as function of potential

In the following section we derive explicit formulation of Lie derivatives of one-parameter diffeomorfism vector fiel $\boldsymbol{\xi}$ for a potential V in "critical points-free" region of configuration space $(\mathcal{X}, g_{\mathbb{R}^N}$ endowed with a riemmanian metric. Let $(q_1, ..., q_N)$ be a set of coordinates in configuration space; in what follows we shall refer to ∂_i as the partial derivatives respect to coordinate q_i and (with an abuse of notation respect to the main part of this manuscript) $(\nabla V)_i = (\mathbf{grad}_{\mathbb{R}^N} V)_i = \partial_i V$ and the Hessian $(\mathrm{Hess} V)_{ij} = \partial^2_{ij} V$.
With these chioces the divergence of Hirsch vector field $\zeta = \mathrm{div}_{\mathbb{R}^N} \boldsymbol{\xi}$ reads:

$$\mathrm{div}_{\mathbb{R}^N} \boldsymbol{\xi} = \frac{\Delta V}{\|\nabla V\|^2} - 2\frac{\nabla V \cdot (\mathrm{Hess} V \nabla V)}{\|\nabla V\|^4} \tag{B.5}$$

where $\Delta(\cdot) = \sum_i^N \partial^i \partial_i(\cdot)$ is the Laplacian operator in the Euclidean configuration space and $\|\boldsymbol{X}\|^2 = g_{\mathbb{R}^N}(\boldsymbol{X}, \boldsymbol{X})$ is the Euclidean norm. Consequentely we calculate explicitely higher order Lie derivative of ζ respect to $\boldsymbol{\xi}$ as averages, correlations, and other cumulants of this quantities appears in calculation of microcanonical entropy density. As the Lie derivative operator along the flux generated by vector field $\boldsymbol{\xi}$ is

$$\mathcal{L}_{\boldsymbol{\xi}}(\cdot) = (\boldsymbol{\xi} \cdot \nabla)(\cdot) = \sum_{i=1}^N \frac{\partial^i V}{\|\nabla V\|^2} \partial_i(\cdot) = \frac{\partial^i V}{\|\nabla V\|^2} \tag{B.6}$$

This yields at the first order:

$$\begin{aligned}\mathcal{L}_{\boldsymbol{\xi}}(\zeta) =& \frac{\nabla V \cdot \nabla(\Delta V)}{\|\nabla V\|^4} - 2\frac{(\nabla V \cdot \mathrm{Hess}(V)\nabla V)\Delta V + 2\|\mathrm{Hess} V \nabla V\|^2 + \mathrm{D}^3 V(\nabla V, \nabla V, \nabla V)}{\|\nabla V\|^6} + \\ &+ 8\frac{(\nabla V \cdot \mathrm{Hess} V \nabla V)^2}{\|\nabla V\|^8}\end{aligned} \tag{B.7}$$

at the second order:

$$
\begin{aligned}
\mathcal{L}_{\boldsymbol{\xi}}^{(ii)}(\zeta) =& \frac{\nabla(\Delta V)\cdot(\mathrm{Hess}V\nabla V)+\nabla V\cdot(\mathrm{Hess}(\Delta V)\nabla V)}{\|\nabla V\|^6}+ \\
&-2\Bigg[\frac{\Delta V\mathrm{D}^3V(\nabla V,\nabla V,\nabla V)+2\Delta V\|\mathrm{Hess}V\nabla V\|^2}{\|\nabla V\|^8}+ \\
&+\frac{4(\mathrm{Hess}V\nabla V)\cdot(\mathrm{Hess}V\mathrm{Hess}V\nabla V)}{\|\nabla V\|^8}+ \\
&+\frac{7\mathrm{D}^3V(\mathrm{Hess}V\nabla V,\nabla V,\nabla V)+\mathrm{D}^4V(\nabla V,\nabla V,\nabla V,\nabla V)}{\|\nabla V\|^8+3(\nabla V\cdot\mathrm{Hess}V\nabla V)(\nabla V\cdot\nabla(\Delta V))}\|\nabla V\|^8\Bigg]+ \\
&+\frac{28(\nabla V\mathrm{Hess}V\nabla V)\left[2\|\mathrm{Hess}V\nabla V\|^2+\mathrm{D}^3V(\nabla V,\nabla V,\nabla V)\right]+12(\nabla V\mathrm{Hess}V\nabla V)^2\Delta V}{\|\nabla V\|^{10}}+ \\
&-64\frac{(\nabla V\mathrm{Hess}V\nabla V)^3}{\|\nabla V\|^{12}}
\end{aligned}
\tag{B.8}
$$

at the third order:

$$
\begin{aligned}
\mathcal{L}_{\boldsymbol{\xi}}^{(iii)}(\zeta) = {} & \frac{3\nabla V \cdot \mathrm{Hess}(\Delta V)\mathrm{Hess}V\nabla V + \mathrm{D}^3\Delta V(\nabla V, \nabla V, \nabla V) + \mathrm{D}^3 V(\nabla V, \nabla V, \nabla(\Delta V))}{\|\nabla V\|^8} + \\
& + \frac{\nabla(\Delta V) \cdot \mathrm{Hess}V\mathrm{Hess}V\nabla V}{\|\nabla V\|^8} - 2\Bigg[\frac{4\mathrm{D}^3 V(\nabla V, \nabla V, \nabla V)(\nabla V \cdot \nabla(\Delta V))}{\|\nabla V\|^{10}} + \\
& + \frac{7\mathrm{D}^4 V(\nabla V, \nabla V, \nabla V, \mathrm{Hess}V\nabla V)}{\|\nabla V\|^{10}} + \\
& + \frac{15\mathrm{D}^3 V(\nabla V, \nabla V, \mathrm{Hess}V\mathrm{Hess}V\nabla V) + 7\|\mathrm{D}^3 V(\nabla V, \nabla V)\|^2 + 18\mathrm{D}^3 V(\mathrm{Hess}V\nabla V, \mathrm{Hess}V\nabla V, \nabla V)}{\|\nabla V\|^{10}} + \\
& + \frac{4\mathrm{D}V(\nabla V, \nabla V, \nabla V, \mathrm{Hess}V\nabla V) + \mathrm{D}^5 V(\nabla V, \nabla V, \nabla V, \nabla V, \nabla V) + 8(\nabla V \cdot \nabla(\Delta V))\|\mathrm{Hess}V\nabla V\|^2}{\|\nabla V\|^{10}} + \\
& + \frac{8\|\mathrm{Hess}V\mathrm{Hess}V\nabla V\|^2 + 7\mathrm{D}^3 V(\nabla V, \nabla V, \mathrm{Hess}V\nabla V)\Delta V}{\|\nabla V\|^{10}} + \\
& \frac{\Delta V \mathrm{D}^4 V(\nabla V, \nabla V, \nabla V, \nabla V) + 4\Delta V(\mathrm{Hess}V\nabla V) \cdot \mathrm{Hess}V\mathrm{Hess}V\nabla V}{\|\nabla V\|^{10}} + \\
& + \frac{6(\mathrm{Hess}V \cdot \mathrm{Hess}V\nabla V)(\nabla V \cdot \mathrm{Hess}(\Delta V)\nabla V) + 6(\mathrm{Hess}V \cdot \mathrm{Hess}V\nabla V)(\nabla(\Delta V) \cdot \mathrm{Hess}V\nabla V)}{\|\nabla V\|^{10}}\Bigg] + \\
& + 4\Bigg[\frac{7\left(\mathrm{D}^3 V(\nabla V, \nabla V, \nabla V)\right)^2 + 28\mathrm{D}^3 V(\nabla V, \nabla V, \nabla V)\|\mathrm{Hess}V\nabla V\|^2}{\|\nabla V\|^{12}} + \\
& + \frac{10\Delta V \mathrm{D}^3 V(\nabla V, \nabla V, \nabla V)(\nabla V \cdot \mathrm{Hess}V\nabla V)}{\|\nabla V\|^{12}} + \\
& + \frac{28\|\mathrm{Hess}V\nabla V\|^4 + 20\Delta V\|\mathrm{Hess}V\nabla V\|^2(\nabla V \cdot \mathrm{Hess}V\nabla V)}{\|\nabla V\|^{12}} + \\
& + \frac{(\nabla V \cdot \mathrm{Hess}V\nabla V)[77\mathrm{D}^3 V(\nabla V, \nabla V, \mathrm{Hess}V\nabla V)}{\|\nabla V\|^{12}} + \\
& + \frac{11\mathrm{D}^4 V(\nabla V, \nabla V, \nabla V, \nabla V) + 44(\mathrm{Hess}V\nabla V) \cdot (\mathrm{Hess}V\mathrm{Hess}V\nabla V)}{\|\nabla V\|^{12}} + \\
& + \frac{15(\mathrm{Hess}V \cdot \mathrm{Hess}V\nabla V)(\nabla V \cdot \nabla(\Delta V))]}{\|\nabla V\|^{12}}\Bigg] + \\
& - 8\Bigg[\frac{59\mathrm{D}^3 V(\nabla V, \nabla V, \nabla V)(\nabla V \cdot \mathrm{Hess}V\nabla V)^2}{\|\nabla V\|^{14}} + \\
& + \frac{(\nabla V \cdot \mathrm{Hess}V\nabla V)^2[118\|\mathrm{Hess}V\nabla V\|^2 + 15\Delta V(\nabla V \cdot \mathrm{Hess}V\nabla V)]}{\|\nabla V\|^{14}}\Bigg] + 768\frac{(\nabla V \cdot \mathrm{Hess}V\nabla V)^4}{\|\nabla V\|^{16}}
\end{aligned}
\tag{B.9}
$$

C Basic facts of homololgy

C.1 Simplicial Complexes

We can see a simplicial complex X as a set of polyhedrons (convex hulls of linearly independent points: points, lines, triangles, tetrahedra, and higer dimensional equivalents) in $\mathbb{R}^N$ attached in a good way, i.e., the intersection of two polyhedrons is empty or a face of the two and all the faces of a polyhedron of X is also a polyhedron of X. We can also think of simplicial complexes as abstract sets, with the definition:

Definition C.1.1. *An (abstract) simplicial complex is a non empty family X of finite subsets, called faces, of a vertex set V such that $\sigma \subset \tau \in X$ implies that $\sigma \in X$.*

We assume that the vertex set is finite and totally ordered. A face of $n+1$ vertices is called $n-$face, denoted by $[p_0, \ldots, p_n]$, and n is its dimension. We set, as usual, the dimension of the empty set as -1. The *dimension* of a simplicial complex is the highest dimension of the faces in the complex.

In Figure C.1 the vertices (full circles) represent 0-simplices, segments joining two vertices represent 1-simplices, triangles represent 2-simplices, and the tetrahedron represents a 3-simplex.

C.1.1 Simplicial Homology

Let us fix a field k. In the following, by vector space we intend $k-$vector space. Given a simplicial complex X of dimension d, for any n such that $0 \leq n \leq d$ consider the vector space $\mathrm{C}_n := \mathrm{C}_n(X)$ of all the linear combinations of n-faces of X with coefficients in k. Elements in C_n are called *n-chains*.

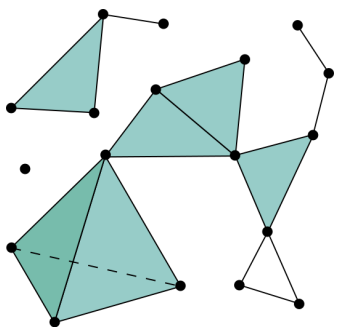

Figure C.1: (Color online) A graphic representation of a simplicial complex

The *boundary* operators are the linear maps sending a n-face to the alternate sum of its $(n-1)$-faces, i.e.,

$$\partial_n : \mathrm{C}_n \longrightarrow \mathrm{C}_{n-1} \tag{C.1}$$

$$[p_0, \ldots, p_n] \rightarrow \sum_{j=0}^{n} (-1)^i [p_0, \ldots, p_{j-1}, p_{j+1}, \ldots, p_n]. \tag{C.2}$$

They share the property $\partial_{n-1} \circ \partial_n = 0$. The nullspace $\ker \partial_n = \{c \in \mathrm{C}_n | \partial_n c = 0\}$, that is, the subspace of C_n containing only the *n-chains* without boundary, is called the vector space of *n-cycles* and denoted by $\mathrm{Z}_n := \mathrm{Z}_n(X)$, with by convention $\mathrm{Z}_0 = \emptyset$. The subspace $\mathrm{Im}\, \partial_{n+1}$ of C_n, is called the vector space of *n-boundaries* and denoted by $\mathrm{B}_n := \mathrm{B}_n(X)$, with by convention $\mathrm{B}_d = \emptyset$. The property $\partial_{n-1} \circ \partial_n = 0$ is then equivalent to $\mathrm{B}_n \subseteq \mathrm{Z}_n$ for all n.

Definition C.1.2. *For $0 \leqslant n \leqslant d$, the $n-$th simplicial homology space of X, with coefficients in k, is the vector space $\mathrm{H}_n := \mathrm{H}_n(X) := \mathrm{Z}_n/\mathrm{B}_n$. We denote by $\beta_n := \beta_n(X)$ the dimension of H_n which is usually called the n-th Betti number of X.*

Let us see two examples. First, let us consider the simplicial complex X consisting of a triangle $[p_1p_2p_3]$ and all its edges and vertices (i.e., $X = \{[p_1p_2p_3], [p_1p_2], [p_1p_3], [p_2p_3], [p_1], [p_2], [p_3]\}$). The boundary of the 2-simplex $[p_1p_2p_3]$ is

$$\partial_2([p_1p_2p_3]) = [p_2p_3] - [p_1p_3] + [p_1p_2] \tag{C.3}$$

that is a one-chain whose boundary is

$$\begin{aligned} \partial_1(\quad [p_2p_3] - [p_1p_3] + [p_1p_2]) &= [p_3] - [p_2] + \\ &+ [p_1] - [p_3] + [p_2] - [p_1] = 0. \end{aligned} \tag{C.4}$$

Therefore $Z_1 = B_1$ is the vector space generated by $[p_2p_3] - [p_1p_3] + [p_1p_2]$, so $H_1 = \emptyset$ and $\beta_1 = 0$.

After let us consider the simplicial complex X' consisting of all the edges and vertices of the triangle but without the face $[p_1p_2p_3]$ (i.e., $X' = X/[p_1p_2p_3]$). Therefore Z_1' is generated by $[p_2p_3]-[p_1p_3]+[p_1p_2]$ whereas $B_1' = \emptyset$. So $H_1' = Z_1'$ and $\beta_1' = 1$. Comparing the two examples, we see that by eliminating the two-face from X (roughly speaking, punching hole in the triangle) a generator of H_1 is created. In conclusion, the homology spaces characterize the presence of holes in simplicial complexes. Indeed, the 0-th Betti number is the number of connected components of X, the first Betti number is the number of generators of two dimensional (poligonal) holes, the third Betti number is the number of generator of three dimensional holes (convex polyhedron), etc.

C.1.2 Persistent Homology

The starting point in persistent homology is a filtration. As in [CZ05], we call a simplicial complex X filtered if we are given a family of subspaces $\{X_v\}$ parametrized by $\mathbb{N}$, such that

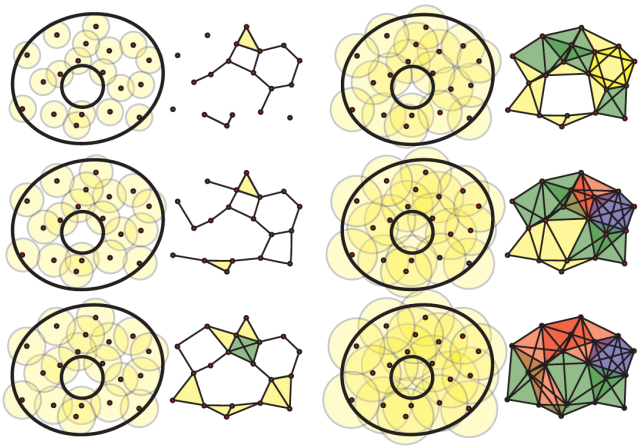

Figure C.2: (Color online) Rips Complex Filtration. Reproduced with owner's permission from: Ghrist, Robert. "Barcodes: the persistent topology of data." Bulletin of the American Mathematical Society 45.1 (2008): 61-75.

$X_v \subseteq X_w$ whenever $v \leq w$ and X_v is a simplicial complex. The family $\{X_v\}$ is called a *filtration*.

There are many ways to construct a filtration from a point cloud or a network. The most popular filtration for data analysis is the *Rips-Vietoris filtration* [CZ05].

The Rips-Vietoris complex is a simplicial complex associated to a set of points in a metric space in the following way: every point p is the center of a radius ρ ball $D(p, \rho)$ and $n+1$ points $\{p_0, \ldots, p_n\}$ determine a $n-$face in the Rips-Vietoris complex if the corresponding radius ρ balls intersect two by two, i.e $D(p_i, \rho) \cap D(p_j, \rho) \neq \emptyset$ for all $i \neq j \in \{0 \ldots n\}$. Clearly the Rips-Vietoris complex depends on the parameter ρ and if $\rho_1 < \rho_2$ the complex with ρ_1 radius balls is contained in the complex with ρ_2 radius balls. To the growth of ρ we obtain an increasing sequence of simplicial complexes, a filtration, the Rips-Vietoris filtration. In this context persistent topological features of the filtration are considered as features of the point cloud. Figure C.2 pictorially represents a Rips-Vietoris filtration: given a point cloud, it is shown that simplicial complexes of increasing complexity are found by increasing the radii of the balls centered at the points of the cloud.

The following basic properties of the algebraic structure of persistent homology hold:

Proposition C.1.1. *Let X and Y be two simplicial complexes, a simplicial map $f : X \to Y$ is a map sending vertices of X to vertices of Y and faces of X to faces of Y. Then f determines a linear map between the homology groups $H_i(f) : H_i(X) \to H_i(Y)$ for all i.*

From which it makes sense the following.

Definition C.1.3. *The persistent homology module of a filtration is given by the direct sum of the homology groups of the simplicial complexes $H_n(X_v)$ and the linear maps $i_{v,w} : H_n(X_v) \to H_n(X_w)$ induced in homology by the inclusions $X_v \hookrightarrow X_w$ for all $v \leq w$.*

Following [CZ05], this system is called a module because the direct sum of vector spaces $H_n = \oplus_v H_n(X_v)$ has a $k[x]-$module structure via an algebraic action given by $x \cdot m := i_{v,v+1}(m)$ for $m \in H_n(X_v)$. The linear maps $i_{v,v+1}$ are not always injective. A persistent homology

generator is a generator of H_n as $k[x]-$module, i.e an element $g \in H_n(X_v)$ such that there is no $h \in H_n(X_w)$ for $w < v$ with the property that $x^{v-w}h = g$. By the structure theorem on modules over principal ideal domains, the isomorphism class of a $k[x]-$module is completely determined by the degree of each generator g (birth of the generator β_g) and the degree in which the generator is annihilated by the module action (death of the generator δ_g). The persistence (lifetime) of a generator is measured by $p_g := \delta_g - \beta_g$.

Persistent homology modules can be computed using libraries like *javaPlex* (Java) or *Dionysus* (C++), which are both available from the Stanford's CompTop group website (http://comptop.stanford.edu/).

Bibliography

[ABGP95] Raffaella Arani, Ivan Bono, Emilio Del Giudice, and Giuliano Preparata. Qed coherence and the thermodynamics of water. International Journal of Modern Physics B, 9(15):1813–1841, 1995.

[AD68] G Adam and M Delbrück. Reduction of dimensionality in biological diffusion processes. Structural chemistry and molecular biology, 198, 1968.

[AJL+02] Bruce Alberts, Alexander Johnson, Julian Lewis, Martin Raff, Keith Roberts, and Peter Walter. Energy conversion: mitochondria and chloroplasts. 2002.

[AN07] John M Alongi and Gail Susan Nelson. Recurrence and topology, volume 85. American Mathematical Soc., 2007.

[AP76] SR Aragon and R Pecora. Fluorescence correlation spectroscopy as a probe of molecular dynamics. The Journal of Chemical Physics, 64(4):1791–1803, 1976.

[Apo09] M Apostol. Coherence domains in matter interacting with radiation. Physics Letters A, 373(3):379–384, 2009.

[AR76] John L Anderson and C Christopher Reed. Diffusion of spherical macromolecules at finite concentration. The Journal of Chemical Physics, 64(8):3240–3250, 1976.

[AR95] M. Antoni and S. Ruffo. Phys. Rev. E, 52:2361, 1995.

[Arn88] Ludwig Arnold. Lyapunov exponents of nonlinear stochastic systems. In Nonlinear Stochastic Dynamic Engineering Systems, pages 181–201. Springer, 1988.

[AT89] M.P. Allen and D.J. Tildesley. Computer Simulation of Liquids. Oxford Science Publ. Clarendon Press, 1989.

[Bac14a] M Bachmann. Novel concepts for the systematic statistical analysis of phase transitions in finite systems. In Journal of Physics: Conference Series, volume 487, page 012013. IOP Publishing, 2014.

[Bac14b] Michael Bachmann. Thermodynamics and statistical mechanics of macromolecular systems. Cambridge University Press, 2014.

[Bar81] Mary D Barkley. Salt dependence of the kinetics of the lac repressor-operator interaction: role of nonoperator deoxyribonucleic acid (dna) in the association reaction. Biochemistry, 20(13):3833–3842, 1981.

[Bas94] Sergey I Bastrukov. Low-frequency elastic response of a spherical particle. Physical Review E, 49(4):3166, 1994.

[Bay03] Vincent Bayle. Propriétés de concavité du profil isopérimétrique et applications. PhD thesis, Université Joseph-Fourier-Grenoble I, 2003.

[Bes07] Arthur L Besse. Einstein manifolds. Springer Science & Business Media, 2007.

[BGS76] Giancarlo Benettin, Luigi Galgani, and Jean-Marie Strelcyn. Kolmogorov entropy and numerical experiments. Physical Review A, 14(6):2338, 1976.

[BLL07] Kevin Burrage, Ian Lenane, and Grant Lythe. Numerical methods for second-order stochastic differential equations. SIAM Journal on Scientific Computing, 29(1):245–264, 2007.

[Bol99] H Bolterauer. Elementary arguments that the wu–austin hamiltonian has no finite ground state (the search for a microscopic foundation of fröhlichs theory). Bioelectrochemistry and bioenergetics, 48(2):301–304, 1999.

[BP76] Bruce J Berne and Robert Pecora. Dynamic light scattering: with applications to chemistry, biology, and physics. Courier Corporation, 1976.

[BPH05] H Behringer, M Pleimling, and A Hüller. Finite-size behaviour of the microcanonical specific heat. Journal of Physics A: Mathematical and General, 38(5):973, 2005.

[Can63] Robert E Canfield. The amino acid sequence of egg white lysozyme. Journal of Biological Chemistry, 238(8):2698–2707, 1963.

[Car09] G Carlsson. Topology and data. B. Am. Math. Soc., 46(2):255–308, 2009.

[Cas95a] L. Casetti. Physica Scripta 51, 29, 1995.

[Cas95b] Lapo Casetti. Efficient symplectic algorithms for numerical simulations of hamiltonian flows. Physica scripta, 51(1):29, 1995.

[CCC+98a] L. Caiani, L. Casetti, C. Clementi, G. Pettini, M. Pettini, and R. Gatto. Geometry of dynamics and phase transitions in classical lattice ϕ^4 theories. Phys.Rev. E, 57:3886, 1998.

[CCC+98b] Lando Caiani, Lapo Casetti, Cecilia Clementi, Giulio Pettini, Marco Pettini, and Raoul Gatto. Geometry of dynamics and phase transitions in classical lattice φ 4 theories. Physical Review E, 57(4):3886, 1998.

[CCP98] Lando Caiani, Lapo Casetti, and Marco Pettini. Hamiltonian dynamics of the two-dimensional lattice. Journal of Physics A: Mathematical and General, 31(15):3357, 1998.

[CDFR14] Alessandro Campa, Thierry Dauxois, Duccio Fanelli, and Stefano Ruffo. Physics of long-range interacting systems. OUP Oxford, 2014.

[CDR09] A. Campa, T. Dauxois, and S. Ruffo. Statistical mechanics and dynamics of solvable models with long-range interactions. Phys. Rep., 480(3–6):57–159, 2009.

[CFVP91] Andrea Crisanti, Massimo Falcioni, Angelo Vulpiani, and Giovanni Paladin. Lagrangian chaos: transport, mixing and diffusion in fluids. La Rivista del Nuovo Cimento (1978-1999), 14(12):1–80, 1991.

[CHH+06] Ivan Corwin, Neil Hoffman, Stephanie Hurder, Vojislav Šešum, and Ya Xu. Differential geometry of manifolds with density. Rose-Hulman Und. Math. J, 7(1):2, 2006.

[Cho83] Kuo-Chen Chou. Low-frequency vibrations of helical structures in protein molecules. Biochemical Journal, 209(3):573–580, 1983.

[Cho84] Kuo-Chen Chou. Biological functions of low-frequency vibrations (phonons). iii. helical structures and microenvironment. Biophysical journal, 45(5):881, 1984.

[CHT97] Leonor Cruzeiro-Hansson and Shozo Takeno. Davydov model: The quantum, mixed quantum-classical, and full classical systems. Physical Review E, 56(1):894, 1997.

[CKY+07] Jing-Yin Chen, JR Knab, Shuji Ye, Yunfen He, and AG Markelz. Terahertz dielectric assay of solution phase protein binding. Applied physics letters, 90(24):243901, 2007.

[CP48] HBG Casimir and D Polder. The influence of retardation on the london-van der waals forces. Physical Review, 73(4):360, 1948.

[CPC00] L. Casetti, M. Pettini, and E. G. D. Cohen. Phys. Rep., 337:237341, 2000.

[CPC03] L. Casetti, M. Pettini, and E. G. D. Cohen. J. Stat. Phys., 111:1091, 2003.

[CPV15] Luca Cerino, Andrea Puglisi, and Angelo Vulpiani. A consistent description of fluctuations requires negative temperatures. Journal of Statistical Mechanics: Theory and Experiment, 2015(12):P12002, 2015.

[CZ90] Antonio Coniglio and Marco Zannetti. Renormalization group for growth kinetics in the large-n limit. Physical Review B, 42(10):6873, 1990.

[CZ05] G Carlsson and A Zomorodian. Persistent homology - a survey. Discrete Comput. Geom, 33(2):249–274, 2005.

[Dav73] AS Davydov. The theory of contraction of proteins under their excitation. Journal of Theoretical Biology, 38(3):559–569, 1973.

[Dav77] Alexander S Davydov. Solitons and energy transfer along protein molecules. Journal of theoretical biology, 66(2):379–387, 1977.

[Deb21] Petrus Josephus Wilhelmus Debye. Molekularkräfte und ihre elektrische deutung. Hirzel, 1921.

[DGDMV85] E Del Giudice, S Doglia, M Milani, and G Vitiello. A quantum field theoretical approach to the collective behaviour of biological systems. Nuclear Physics B, 251:375–400, 1985.

[DGET09] E Del Giudice, V Elia, and A Tedeschi. The role of water in the living organisms. Neural Network World, 19(4):355, 2009.

[DGP98] E Del Giudice and G Preparata. A new qed picture of water: understanding a few fascinating phenomena. In Macroscopic quantum coherence. Proceedings of the international conference, 1998.

[DH23] P Debye and E Hückel. De la theorie des electrolytes. i. abaissement du point de congelation et phenomenes associes. Physikalische Zeitschrift, 24(9):185–206, 1923.

[DS93] Michael Dyakonov and Michael Shur. Shallow water analogy for a ballistic field effect transistor: New mechanism of plasma wave generation by dc current. Physical review letters, 71(15):2465, 1993.

[DSG07] V. De Silva and R. Ghrist. Coverage in sensor networks via persistent homology. Algebraic and Geometric Topology 7, page 339358, 2007.

[EL30] R Eisenschitz and F London. Über das verhältnis der van der waalsschen kräfte zu den homöopolaren bindungskräften. Zeitschrift für Physik, 60(7-8):491–527, 1930.

[ELA02] H. Edelsbrunner, D. Letscher, and A.Zomorodian. Topological persistence and simplification. Discrete Comput. Geom., 28:511533, 2002.

[Ell07] WJ Ellison. Permittivity of pure water, at standard atmospheric pressure, over the frequency range 0–25 thz and the temperature range 0–100 c. J. Phys. Chem. Ref. Data, 36(1):1–18, 2007.

[Ell12] Richard Steven Ellis. Entropy, large deviations, and statistical mechanics, volume 271. Springer Science & Business Media, 2012.

[Els11] Elliot L. Elson. Fluorescence correlation spectroscopy: Past, present, future. Biophysical Journal, 101:2855 – 2870, December 2011.

[EM74] Elliot L Elson and Douglas Magde. Fluorescence correlation spectroscopy. i. conceptual basis and theory. Biopolymers, 13(1):1–27, 1974.

[Fed14] H. Federer. Geometric Measure Theory. Classics in Mathematics. Springer Berlin Heidelberg, 2014.

[Fra11] Roberto Franzosi. Microcanonical entropy and dynamical measure of temperature for systems with two first integrals. Journal of Statistical Physics, 143(4):824–830, 2011.

[Frö68] Herbert Fröhlich. Long-range coherence and energy storage in biological systems. International Journal of Quantum Chemistry, 2(5):641–649, 1968.

[Frö72] H Fröhlich. Selective long range dispersion forces between large systems. Physics Letters A, 39(2):153–154, 1972.

[Frö77] H Fröhlich. Long-range coherence in biological systems. La Rivista del Nuovo Cimento (1971-1977), 7(3):399–418, 1977.

[Fro78] Herbert Frohlich. Coherent electric vibrations in biological systems and the cancer problem. IEEE Transactions on Microwave Theory and Techniques, 26(8):613–618, 1978.

[Frö80] H Fröhlich. The biological effects of microwaves and related questions. Advances in electronics and electron physics, 53:85–152, 1980.

[Gar10] C. Gardiner. Stochastic Methods: A Handbook for the Natural and Social Sciences. Springer Series in Synergetics. Springer Berlin Heidelberg, 2010.

[GH10] J. Gamble and G. Heo. Exploring uses of persistent homology for statistical analysis of landmark-based shape data. J. Multivar. Analysis, 101:21842199, 2010.

[Ghr08] R Ghrist. Barcodes: The persistent topology of data. B. AM. Math. Soc., 45(61), 2008.

[GK05] DHE Gross and JF Kenney. The microcanonical thermodynamics of finite systems: The microscopic origin of condensation and phase separations, and the conditions for heat flow from lower to higher temperatures. The Journal of chemical physics, 122(22):224111, 2005.

[Gla63] Roy J Glauber. Coherent and incoherent states of the radiation field. Physical Review, 131(6):2766, 1963.

[Glu64] E Glueckauf. Bulk dielectric constant of aqueous electrolyte solutions. Transactions of the Faraday Society, 60:1637–1645, 1964.

[Gro01] Dieter HE Gross. Microcanonical thermodynamics: Phase transitions in small systems, volume 66. World Scientific, 2001.

[GT96] Axel Grorud and Denis Talay. Approximation of lyapunov exponents of nonlinear stochastic differential equations. SIAM Journal on Applied Mathematics, 56(2):627–650, 1996.

[Ham37] HC Hamaker. The londonvan der waals attraction between spherical particles. physica, 4(10):1058–1072, 1937.

[HCK+11] Yunfen He, J-Y Chen, Joseph R Knab, Wenjun Zheng, and Andrea G Markelz. Evidence of protein collective motions on the picosecond timescale. Biophysical journal, 100(4):1058–1065, 2011.

[HHHW02] Samuel T Hess, Shaohui Huang, Ahmed A Heikal, and Watt W Webb. Biological and chemical applications of fluorescence correlation spectroscopy: a review. Biochemistry, 41(3):697–705, 2002.

[Hil93] R Hilfer. Classification theory for anequilibrium phase transitions. Physical Review E, 48(4):2466, 1993.

[Hir97] M.W. Hirsch. Differential Topology. Graduate Texts in Mathematics. Springer New York, 1997.

[HP96] Stuart Hameroff and Roger Penrose. Orchestrated reduction of quantum coherence in brain microtubules: A model for consciousness. Mathematics and computers in simulation, 40(3):453–480, 1996.

[HP14] Stuart Hameroff and Roger Penrose. Consciousness in the universe: A review of the orch ortheory. Physics of life reviews, 11(1):39–78, 2014.

[HS07] E. Haustein and P. Schwille. Fluorescence correlation spectroscopy: Novel variations of an established technique. Annu. Rev. Biophys. Biomol. Struct., 36:151–169, 2007.

[Isr15] J.N. Israelachvili. Intermolecular and Surface Forces. Intermolecular and Surface Forces. Elsevier Science, 2015.

[Jac07] J D Jackson. CLASSICAL ELECTRODYNAMICS, 3RD ED. Wiley India Pvt. Limited, 2007.

[Jol69] P Jolles. Lysozymes: a chapter of molecular biology. Angewandte Chemie International Edition in English, 8(4):227–239, 1969.

[JRdXOG92] G. Ruderman J. R. de Xammar Oro and J. R. Grigera. Threshold frequency for the ionic screening of electric fields in electrolyte solutions. Journal of the Chemical Society, Faraday Transactions, 88(5):699–703, 1992.

[JRdXOG08] G. Ruderman J. R. de Xammar Oro and J. R. Grigera. Electrodynamics of interactions in electrolyte media. possible consequences in biological functions. Biophysics, 53(3):195–198, 2008.

[JS10] Hans-Rudolf Jauslin and Dominique Sugny. Dynamics of mixed classical-quantum systems, geometric quantization and coherent states. Mathematical Horizons for Quantum Physics, 20:65, 2010.

[KCHM07] Joseph R Knab, Jing-Yin Chen, Yunfen He, and Andrea G Markelz. Terahertz measurements of protein relaxational dynamics. Proceedings of the IEEE, 95(8):1605–1610, 2007.

[KCM06] Joseph Knab, Jing-Yin Chen, and Andrea Markelz. Hydration dependence of conformational dielectric relaxation of lysozyme. Biophysical journal, 90(7):2576–2581, 2006.

[KDT+07] Eilon D Kirson, Vladimír Dbalỳ, František Tovaryš, Josef Vymazal, Jean F Soustiel, Aviran Itzhaki, Daniel Mordechovich, Shirley Steinberg-Shapira, Zoya Gurvich, Rosa Schneiderman, et al. Alternating electric fields arrest cell proliferation in animal tumor models and human brain tumors. Proceedings of the National Academy of Sciences, 104(24):10152–10157, 2007.

[Kei95] Fritz Keilmann. Fir microscopy. Infrared Physics & Technology, 36(1):217–224, 1995.

[Kit04] C. Kittel. Introduction to Solid State Physics. Wiley, 2004.

[KKD+02] W Knap, V Kachorovskii, Y Deng, S Rumyantsev, J-Q Lü, R Gaska, MS Shur, Grigory Simin, X Hu, M Asif Khan, et al. Nonresonant detection of terahertz radiation in field effect transistors. Journal of Applied Physics, 91(11):9346–9353, 2002.

[KM11] Michael Kastner and Dhagash Mehta. Phase transitions detached from stationary points of the energy landscape. Phys. Rev. Lett., 107:160602, Oct 2011.

[Kol] Sergiĭ Kolyada. Some aspects of topological transitivitya survey.

[Kra08] P Kramer. A review of the time-dependent variational principle. In Journal of Physics: Conference Series, volume 99, page 012009. IOP Publishing, 2008.

[KS80] P Kramer and M Saraceno. Geometry of the time-dependent variational principle in quantum mechanics. In Group Theoretical Methods in Physics, pages 112–121. Springer, 1980.

[Lau89] Peter Laurence. On the convexity of geometric functional of level for solutions of certain elliptic partial differential equations. Zeitschrift fr angewandte Mathematik und Physik ZAMP, 40(2):258–284, 1989.

[Led05] Michel Ledoux. The concentration of measure phenomenon. Number 89. American Mathematical Soc., 2005.

[Lee09] Jeffrey M Lee. Manifolds and differential geometry, volume 107. American Mathematical Society Providence, 2009.

[Li93] Peter Li. Lecture notes on geometric analysis, volume 6. Citeseer, 1993.

[Lod08] H. Lodish. Molecular Cell Biology. W. H. Freeman, 2008.

[Lon37] Fritz London. The general theory of molecular forces. Trans. Faraday Soc., 33:8b–26, 1937.

[LPV96] Vittorio Loreto, Giovanni Paladin, and Angelo Vulpiani. Concept of complexity in random dynamical systems. Physical Review E, 53(3):2087, 1996.

[LRW+15] Ida V Lundholm, Helena Rodilla, Weixiao Y Wahlgren, Annette Duelli, Gleb Bourenkov, Josip Vukusic, Ran Friedman, Jan Stake, Thomas Schneider, and Gergely Katona. Terahertz radiation induces non-thermal structural changes associated with fröhlich condensation in a protein crystal. Structural dynamics, 2(5):054702, 2015.

[MA92] R. I. McLachlan and P. Atela. The accuracy of symplectic integrators. Nonlinearity, 5(2):541, 1992.

[Max54] James Clerk Maxwell. Electricity and magnetism. 1954.

[MEW72] Douglas Magde, Elliot Elson, and Watt W Webb. Thermodynamic fluctuations in a reacting systemmeasurement by fluorescence correlation spectroscopy. Physical Review Letters, 29(11):705, 1972.

[MEW74] Douglas Magde, Elliot L Elson, and Watt W Webb. Fluorescence correlation spectroscopy. ii. an experimental realization. Biopolymers, 13(1):29–61, 1974.

[MHK12] Dhagash Mehta, Jonathan D. Hauenstein, and Michael Kastner. Energy-landscape analysis of the two-dimensional nearest-neighbor φ^4 model. Phys. Rev. E, 85:061103, Jun 2012.

[Mil63] J. Milnor. Morse theory. Ann. Math. Studies 51 (Princeton University Press, Princeton), 1963.

[Mor05] Frank Morgan. Manifolds with density. Notices of the AMS, pages 853–858, 2005.

[MS07] Efstratios Mylonas and Dmitri I Svergun. Accuracy of molecular mass determination of proteins in solution by small-angle x-ray scattering. Applied Crystallography, 40(s1):s245–s249, 2007.

[MW74] Elson E. L. Magde, D. and W. W. Webb. Fluorescence correlation spectroscopy. ii. an experimental realization. Biopolymers, 13:29–61, 1974.

[MWHB02] Andrea Markelz, Scott Whitmire, Jay Hillebrecht, and Robert Birge. Thz time domain spectroscopy of biomolecular conformational modes. Physics in medicine and biology, 47(21):3797, 2002.

[Nic]

[NMT+09] P Nouvel, H Marinchio, J Torres, C Palermo, D Gasquet, L Chusseau, L Varani, P Shiktorov, E Starikov, and V Gružinskis. Terahertz spectroscopy of plasma waves in high electron mobility transistors. Journal of Applied Physics, 106(1):013717, 2009.

[NSP+14] Ilaria Nardecchia, Lionel Spinelli, Jordane Preto, Matteo Gori, Elena Floriani, Sebastien Jaeger, Pierre Ferrier, and Marco Pettini. Experimental detection of long-distance interactions between biomolecules through their diffusion behavior: Numerical study. Physical Review E, 90(2):022703, 2014.

[NSW08] P. Niyogi, S. Smale, and S. Weinberger. Finding the homology of submanifolds with high confidence from random samples. Discrete and Computational Geometry, 39:419–441, 2008.

[OC90] AR Osborne and R Caponio. Fractal trajectories and anomalous diffusion for chaotic particle motions in 2d turbulence. Physical review letters, 64(15):1733, 1990.

[OP91] Maurizio Ottaviani and Marco Pettini. Turbulent diffusion of test particles in strongly magnetized plasmas. International Journal of Modern Physics B, 5(08):1243–1262, 1991.

[OPB85] AR Osborne, A Provenzale, and L Bergamasco. A comparison between the cnoidal wave and an approximate periodic solution to the korteweg-de vries equation. Il Nuovo Cimento C, 8(1):26–38, 1985.

[Par73] VA Parsegian. Long-range physical forces in the biological milieu. Annual review of biophysics and bioengineering, 2(1):221–255, 1973.

[Pet07a] M. Pettini. Geometry and Topology in Hamiltonian Dynamics and Statistical Mechanics. IAM Series n. 33. Springer-Verlag New York, 2007.

[Pet07b] Marco Pettini. Geometry and topology in Hamiltonian dynamics and statistical mechanics, volume 33. Springer Science & Business Media, 2007.

[PET+14] G. Petri, P Expert, F Turkheimer, R Carhart-Harris, D Nutt, P J Hellyer, and F Vaccarino. Homological scaffolds of brain functional networks. Journal of The Royal Society Interface, 11(101):20140873–20140873, December 2014.

[PFN+12] Jordane Preto, Elena Floriani, Ilaria Nardecchia, Pierre Ferrier, and Marco Pettini. Experimental assessment of the contribution of electrodynamic interactions to long-distance recruitment of biomolecular partners: Theoretical basis. Phys. Rev. E, 85:041904, Apr 2012.

[PNE+13] Stefania Perticaroli, Jonathan D Nickels, Georg Ehlers, Hugh O'Neill, Qui Zhang, and Alexei P Sokolov. Secondary structure and rigidity in model proteins. Soft Matter, 9(40):9548–9556, 2013.

[PPT15] Jordane Preto, Marco Pettini, and Jack A Tuszynski. Possible role of electrodynamic interactions in long-distance biomolecular recognition. Physical Review E, 91(5):052710, 2015.

[Pre12] Jordane Preto. Semi-classical statistical approach to fr\" ohlich condensation theory. arXiv preprint arXiv:1203.2006, 2012.

[Pre13] Jordane Preto. PhD thesis, University of Marseille, 2013.

[PSY+15] Nikita Penkov, Nikolay Shvirst, Valery Yashin, Eugeny Fesenko Jr, and Eugeny Fesenko. Terahertz spectroscopy applied for investigation of water structure. The Journal of Physical Chemistry B, 119(39):12664–12670, 2015.

[PVM+88] Marco Pettini, Angelo Vulpiani, Jacques H Misguich, Michel De Leener, John Orban, and Radu Balescu. Chaotic diffusion across a magnetic field in a model of electrostatic turbulent plasma. Physical Review A, 38(1):344, 1988.

[PW13] J. Pokorny and T.M. Wu. Biophysical Aspects of Coherence and Biological Order. Springer Berlin Heidelberg, 2013.

[RE12] Rudolf Rigler and Elliot S Elson. Fluorescence correlation spectroscopy: theory and applications, volume 65. Springer Science & Business Media, 2012.

[RMM+09] Jeffrey R Reimers, Laura K McKemmish, Ross H McKenzie, Alan E Mark, and Noel S Hush. Weak, strong, and coherent regimes of fröhlich condensation and their applications to terahertz medicine and quantum consciousness. Proceedings of the National Academy of Sciences, 106(11):4219–4224, 2009.

[Rue99] D. Ruelle. Statistical Mechanics: Rigorous Results. World Scientific, 1999.

[Rug97] Hans Henrik Rugh. Dynamical approach to temperature. Physical review letters, 78(5):772, 1997.

[Rug98] Hans Henrik Rugh. A geometric, dynamical approach to thermodynamics. Journal of Physics A: Mathematical and General, 31(38):7761, 1998.

[Rug01] Hans Henrik Rugh. Microthermodynamic formalism. Physical Review E, 64(5):055101, 2001.

[Sco92] Alwyn Scott. Davydov's soliton. Physics Reports, 217(1):1–67, 1992.

[SDD15] Oleksandr Sushko, Rostyslav Dubrovka, and Robert S Donnan. Sub-terahertz spectroscopy reveals that proteins influence the properties of water at greater distances than previously detected. The Journal of chemical physics, 142(5):055101, 2015.

[Sim09] Elie Simo. Jacobian elliptic solitons in inhomogeneous alpha-helical proteins. Physica Scripta, 80(4):045801, 2009.

[SML05] J. Silva, J. S. Marques, and J. M. Lemos. Sparse multidimensional scaling using landmark points. Conference: Neural Information Processing Systems-NIPS, 2005.

[SSLB11] Stefan Schnabel, Daniel T Seaton, David P Landau, and Michael Bachmann. Microcanonical entropy inflection points: Key to systematic understanding of transitions in finite systems. Physical Review E, 84(1):011127, 2011.

[Sto08] Anthony J. Stone. Intermolecular potentials. Science, 321(5890):787–789, Aug 2008.

[TNC+95] JA Tuszyński, MLA Nip, PL Christiansen, M Rose, and Ole Bang. Exciton self-trapping in the ginzburg–landau framework. Physica Scripta, 51(4):423, 1995.

[Tou15] Hugo Touchette. Equivalence and nonequivalence of ensembles: Thermodynamic, macrostate, and measure levels. Journal of Statistical Physics, 159(5):987–1016, 2015.

[TP92] Mark A. Tracy and R. Pecora. Synthesis, characterization, and dynamics of a rod/sphere composite liquid. Macromolecules, 25(1):337–349, Jan 1992.

[vHB89] Peter H von Hippel and OG Berg. Facilitated target location in biological systems. Journal of Biological Chemistry, 264(2):675–678, 1989.

[WA77] TM Wu and Steven Austin. Bose condensation in biosystems. Physics Letters A, 64(1):151–152, 1977.

[WA78a] TM Wu and Steven Austin. Bose-einstein condensation in biological systems. Journal of theoretical biology, 71(2):209–214, 1978.

[WA78b] TM Wu and Steven Austin. Cooperative behavior in biological systems. Physics Letters A, 65(1):74–76, 1978.

[WA81] TM Wu and Steven J Austin. Fröhlich's model of bose condensation in biological systems. Journal of Biological Physics, 9(2):97–107, 1981.

[WB05] Xiongwu Wu and Bernard R Brooks. Isotropic periodic sum: A method for the calculation of long-range interactions. The Journal of chemical physics, 122(4):044107, 2005.

[WB08] Xiongwu Wu and Bernard R Brooks. Using the isotropic periodic sum method to calculate long-range interactions of heterogeneous systems. The Journal of chemical physics, 129(15):154115, 2008.

[WD51] LR Wetter and HFr Deutsch. Immunological studies on egg white proteins iv. immunochemical and physical studies of lysozyme. Journal of Biological Chemistry, 192(1):237–242, 1951.

[WKLS90] Xiao-Zhong Wu, Leo Kadanoff, Albert Libchaber, and Masaki Sano. Frequency power spectrum of temperature fluctuations in free convection. Physical review letters, 64(18):2140, 1990.

[WMR95] Jerker Widengren, Uelo Mets, and Rudolf Rigler. Fluorescence correlation spectroscopy of triplet states in solution: a theoretical and experimental study. The Journal of Physical Chemistry, 99(36):13368–13379, 1995.

[Yos85] Nobuo Yoshida. Calculation of the self-diffusion coefficient of interacting brownian particles based on the time-independent smoluchowski equation. The Journal of chemical physics, 83(9):4786–4790, 1985.

[ZG+90] Wei-Min Zhang, Robert Gilmore, et al. Coherent states: theory and some applications. Reviews of Modern Physics, 62(4):867, 1990.

Résumé de la thèse en franais

Les études et les résultats présentés dans ce manuscrit ont pour but de développer une meilleure compréhension des principes à la base de l'auto-organisation dans les systèmes biologiques. De nombreux problèmes de biophysique exigent un moyen de caractériser les phénomènes collectifs également dans les systèmes petits. La théorie topologique des transitions de phase est l'un des approches possibles pour fournir une généralisation de la description des transitions de phase dans les systèmes petits ou mésoscopiques. Cette théorie a été rigoureusement enracinée dans deux théorèmes: un contre exemple à l'un de ces théorèmes a été récemment découvert. La première partie de ce manuscrit est donc consacré à mieux comprendre ce "contre-exemple" pour verifier si et comment la théorie peut tre sauvé. Ce travail peut potentiellement ouvrir la voie à une généralisation de la mme théorie à des cas qui ne sont pas considérés dans la formulation d'origine, comme un presence des interactions à longue portée. Ce dernier cas pourrait tre pertinent pour de nombreux aspects de biophysique; nous mentionnons des interactions intermoléculaires à long portée qui ont été supposés jouer un rle important dans l'organisation de la machinerie biomoléculaire à l'intérieur de la cellule. La précision extraordinaire de cette organisation moléculaire ne semble guère tre le résultat de la diffusion aléatoire seulement. Cela rend le lien conceptuel avec la deuxième partie de ce manuscrit sur la contribution de l'auteur à un projet visant à déterminer si les rencontres de partenaires des réactions biomoléculaires sont activement entranés par des forces attractives et sélectives de nature électrodynamique. L'activation de ces interactions électrodynamiques est théoriquement possible entre des grandes diples oscillants et résonnants dans la gamme de fréquences 0,1-1 THz. Les biomolécules ont des modes dans cette gamme de fréquences attribuée à des oscillations collectives. Mais à l'équilibre les oscillations dipolaires seraient trop petites pour activer des interactions électrodynamiques suffisamment intenses. H. Fröhlich a proposé un modèle heuristique qui prédit la possibilité de canaliser une grande partie de l'énergie vibratoire d'une biomolécule dans ses modes normaux de plus basse fréquence. Dans ce manuscrit les résultats des recherches théoriques, numériques et expérimentales sur la condensation à la Fröhlich sont reportés. En outre, l'auteur de ce manuscrit a participé à la définition conceptuelle et l'interprétation théorique des expériences de spectroscopie THz o une première preuve expérimentale d'un phénomène de condensation à la Fröhlich a été observée pour une protéine en solution aqueuse et hors de l'équilibre thermique. Ceci est une condition préalable à l'activation des oscillations dipolaires géantes qui entranent des interactions électrodynamiques à long portée entre les molécules coresonnantes. Cependant, la question se pose: sont ces forces suffisamment intenses pour entraner l'organisation de la machine biomoléculaire dans la cellule ? pour répondre cette question, il faut concevoir un dispositif expérimental technologiquement réalisable in vitro pour détecter la conséquence directe de l'action des interactions interparticulaires à long portée. Dans cette thèse, on montre que les interactions à longue portée affectent sensiblement les propriétés de diffusion des

molécules en solution. Une empreinte des interactions à long portée pourrait tre un phénomène de "transition" en ce qui concerne le coefficient de diffusion en fonction d'un paramètre de contrle proportionnel à lintensité d'interaction. Une étude de faisabilité (basé sur des simulations de dynamique moléculaire) est reporté pour évaluer cette stratégie expérimentale. Simulations analogues ont été réalisées afin de valider une approche expérimentale visant à trouver une telle empreinte dans les systèmes avec interactions à longue portée.

Abstract of the manuscript

The studies and results reported in this manuscript are aimed to develop a deeper understanding of the principles at the basis of self-organization in biological systems. Many problems in biophysics demand a way to characterize cooperative phenomena also in small systems. The Topological Theory of phase transitions is one of the possible approaches to provide a generalization of description of phase transitions in small or mesoscopic systems. This theory has been rigorously rooted in two theorems that associate topological changes of the equipotential level sets of configuration space with the loss of analyticity of microcanonical entropy. A counterexample to one of these theorems has been recently found. The first part of this manuscript is devoted to investigation of the "counterexample" to understand if and how the theory can be saved. This work can potentially pave the way to a generalization of the same theory to cases not considered in the original formulation, as long-range interactions. This latter case could be of biophysical relevance for many aspects, among the others we mention long-range electrodynamic intermolecular interactions that have been theoretically surmised to play an important role in thermodynamical organization of the biomolecular machinery inside the cell. The extraordinary accuracy of these molecular organization, in fact, hardly seems to be the result of random diffusion only. This makes the conceptual link with the second part of this manuscript reporting on the author's contribution to a project aimed to ascertain whether the encounters of distant cognate partners of biomolecular reactions are actively driven by selective attractive forces of electrodynamic nature. The activation of long-range classical electrodynamic interactions is theoretically possible between large resonant dipoles oscillating in the frequency range $0.1 - 1$ THz. It has been shown that biomolecules have normal modes in this range of frequencies, commonly attributed to collective oscillations. Nevertheless, at equilibrium the associated dipole oscillations due to thermal fluctuations would be too small to be responsible for the activation of sizable long-range electrodynamic interactions. H. Fr"ohlich proposed an heuristic model that predicts the possibility to channel a large part of the vibrational energy of a biomolecule into its lowest frequency normal modes. In this manuscript the results of theoretical, numerical and experimental investigations on Fr"ohlich-like condensation for normal modes of biomolecules are reported. Moreover, the author of this manuscript participated in the conceptual definition and theoretical interpretation of the THz spectroscopy experiments where a first experimental evidence of a Fr"ohlich-like condensation phenomenon has been observed for a protein in watery solution and out of thermal equilibrium. This is a prerequisite for the activation of giant dipole oscillations in biomolecules which entail long-range electrodynamic interactions between coresonant molecules. However, the following question arises: are these forces sufficiently strong to drive the organisation of the biomolecular machinery inside the cell? To answer this question one has to devise a technologically feasible experimental set-up in vitro to detect direct consequence of the action of long-range interparticle interactions. In this thesis

is shown that long-range interactions markedly affect the self-diffusion properties of molecules in solution. A fingerprint of long-range interactions could be a "transitional" phenomenon concerning the self-diffusion coefficient as a function of a control parameter proportional to interaction strength. A feasibility study (based on molecular dynamics simulations) is reported aiming at assessing this experimental strategy. Analogous simulations have been performed to validate an experimental approach aimed at finding such "fingerprint" in systems with built-in long-range interactions.